Mechanistic insights into the HPF1/PARP1 complex



Florian Zobel

St Hugh's College

University of Oxford

A thesis submitted for the degree of

Doctor of Philosophy

word count: 40,469

Trinity 2021

Abstract

ADP-ribosylation is a vital post-translational modification associated with a large range of processes including DNA damage repair, transcription, replication, mitosis, inflammation and cell death. ADP-ribosylation arises through the covalent attachment of ADP-ribose from NAD^+ onto target proteins. The modification strongly varies in size, ranging from a single ADP-ribose unit (MARylation) to large, branched chains (PARylation). In humans, one major family of ADP-ribosyltransferases constituting 17 members are poly-ADP-ribose polymerases (PARPs). Their most prominent member, the nuclear protein PARP1, alone is responsible for the overwhelming majority of ADP-ribosylation in cells. While PARP1 was originally described to modify target substrates on glutamate and aspartate sites, it has become apparent in recent years that the presence of another protein, histone PARylation factor 1 (HPF1), switches its preference to serine target sites. Following this discovery, serine ADP-ribosylation was shown to be the main type of ADP-ribosylation in response to DNA damage. However, how HPF1 engages with PARP1 and is able to change the nature of its catalytic activity has remained unclear. This thesis explores the interaction between HPF1 and PARP1 in human cells, the molecular basis of HPF1/PARP1-catalyzed serine ADP-ribosylation and the consequences of aberrations in both proteins. Crucially, colleagues and I describe the interaction sites on both proteins and show that HPF1 in cells is required for the catalytic completion of PARP1 through a glutamate *finger*. Furthermore, we identify the main sites of PARP1 serine auto-modification and illustrate their significance for PARP inhibitor-resistant PARP1 auto-modification and the release of PARP1 from sites of DNA damage. Finally, we explore in human cells the phenotypic consequences of losing the main PARP1 serine auto-modification sites, the HPF1 catalytic glutamate finger or HPF1-PARP1 interaction. Altogether, these results draw a comprehensive picture of HPF1-PARP1 mechanistic functions and the wider implications of its disruption.

Dedication

To my parents in unending gratitude

Declaration

I declare that this thesis has been composed solely by myself and that it has not been submitted, in whole or in part, in any previous application for a degree. Except where states otherwise by reference or acknowledgement, the work presented is entirely my own.

Florian Zobel

St Hugh's College

Acknowledgements

I would like to first and foremost thank my parents for their unconditional support throughout the entirety of my DPhil course. My gratitude also belongs to my sisters, Isabelle and Theresa, and my grandparents, Elfriede and Franz. I am blessed to have all of them in my life and for them to have so fundamentally impacted my personal growth - not just over the last four years, but since my earliest days.

I am deeply grateful to Zuza, who has been the Luthien to my Beren - to put it in the language of J.R.R. Tolkien - ever since we first met. I draw an indescribable amount of strength from her presence in my life and hope to be repaying in kind.

My thanks go also to my closest friends, who have accompanied me along this journey ever since our first days at St Catherine's College: Roxanna Abhari, Alexander Bucknell, Mikesh Udani, Allison Roth and Kirubin Pillay. I will never forget their unfaltering friendship.

I would like to honour the support I received from my supervisor, Ivan Ahel, not just in navigating my project throughout the course of my DPhil, but also more generally as a mentor. For his commitment I am grateful.

Last, but not least, I would like to express my thanks to the members of the Ahel lab that have helped me with my work, in particular Marcin Suskiewicz and Evgeniia Prokhorova, who I worked with together on two separate publications and some of whose work is also shown in this thesis. I thank Johannes Rack, Marcin Suskiewicz, Evgeniia Prokhorova, Callum Tromans-Coia and Ivan Ahel for proof-reading and commenting on my thesis. Finally, I want to acknowledge the work of our collaborators from Université de Rennes 1 in France, Rebecca Smith, Siham Zentout and Sébastien Huet, whose work from our joint publication earlier this year also features in this thesis.

Contents

Contents **6**

List of Figures **9**

List of Tables **11**

List of Abbreviations **12**

1 Introduction **14**

1.1 ADP-ribosylation 14

1.1.1 Nature and Significance 14

1.1.2 Writers of ADP-ribosylation 16

1.1.3 Readers of ADP-ribosylation 24

1.1.4 Erasers of ADP-ribosylation 29

1.2 DNA repair PARPs 36

1.2.1 PARP1 catalytic activation 36

1.2.2 DNA binding of PARP1 38

1.2.3 PARP1 in DNA damage repair 41

1.2.4 PARP2 in DNA damage repair 47

1.2.5 PARP3 in DNA damage repair 48

1.2.6 PARP1/2 inhibition 48

1.2.7 PARP1/2 and HPF1 51

2 Materials & Methods **53**

2.1 Cell biology 53

2.1.1 Cell lines 53

2.1.2 DNA damage and cell lysis 54

2.1.3 CRISPR Cas9 55

2.1.4 Transfections . . . 56
2.1.5 Recombination in U2OS Flp-In cells . . . 58
2.1.6 Survival assay . . . 59
2.1.7 Cell line storage . . . 60
2.1.8 YFP-tagged protein recruitment to microirradiation sites . . . 60
2.2 Co-IPs and Western Blotting . . . 61
2.2.1 Co-immunoprecipitation . . . 61
2.2.2 Western Blotting . . . 63
2.3 Cloning and mutagenesis PCR . . . 64
2.3.1 E.coli strains . . . 64
2.3.2 Gateway Cloning . . . 64
2.3.3 Site-directed mutagenesis PCR . . . 65
2.3.4 Plasmid propagation . . . 65
2.4 Genotyping . . . 66
2.4.1 Genomic DNA purification . . . 67
2.4.2 Sequencing . . . 67
2.5 Materials . . . 68
2.5.1 Antibodies . . . 68
2.5.2 Buffer solutions and media . . . 68
2.5.3 Expression vectors . . . 72

3 Results **74**

3.1 A system to study cellular ADPr . . . 74
3.1.1 PARP1/HPF1-dependence of ADPr levels in U2OS cells . . . 75
3.1.2 DNA damage induced ADP-ribosylation in 293T and RPE-1 cells . . . 78
3.2 Characterizing HPF1 surface mutants . . . 81
3.2.1 HPF1 ADP-ribosylation sites . . . 81
3.2.2 HPF1 sequence conservation . . . 84
3.2.3 HPF1 in complex with PARP2 ART domain . . . 90
3.3 HPF1 interaction sites on PARP1 . . . 95
3.3.1 Structure of HPF1-PARP1 complex . . . 95
3.3.2 HPF1 interaction sites on PARP1 . . . 97

3.4 PARP1 auto-modification . . . 102
3.4.1 PARP1 auto-modification sites . . . 102
3.4.2 PARP1 auto-modification and PARPi resistance . . . 109
3.4.3 HPF1 expression and PARP inhibitor resistance . . . 114
3.5 PARP1/HPF1 mutant phenotypes . . . 120
3.5.1 The Flp-In T-REx system . . . 120
3.5.2 Stable YFP-PARP1 expression . . . 121
3.5.3 Consequences of impaired PARP1 auto-modification . . . 125
3.5.4 Stable YFP-HPF1 expression . . . 128
3.5.5 Phenotypes of HPF1 mutants . . . 136

4 Discussion **143**
4.1 PARP1/2-HPF1 interaction . . . 143
4.2 HPF1 catalytic residue . . . 144
4.3 PARP1 auto-modification . . . 147
4.4 Clinical relevance . . . 149
4.5 Future directions . . . 150

Bibliography **152**

A Appendix **185**

List of Figures

1.1 Molecular structure of ADP-ribosylation 15
1.2 Ribbon representation of representative ART domains 19
1.3 Domain structures of Clade 1,4 and 5 human PARPs 21
1.4 Recognition sites of PAR-binding domains 27
1.5 Representations of the macroH2A1.1 macrodomain crystal structure 28
1.6 Crystal structures of macroD2 and TARG1 30
1.7 Crystal structures of hARH3 and hARH1 32
1.8 Graphic of inactive PARP1 conformation 37
1.9 Illustration of HD unfolding 38
1.10 Model of SSB-bound PARP1 39
1.11 Model of PARPi function 50

2.1 Vector maps of pDEST YFP and pDEST FLAG CMV 73

3.1 Loss of HPF1 abolishes damage-induced ADPr in U2OS cells 76
3.2 HPF1 transient overexpression restores cellular ADPr 79
3.3 HPF1-PARP1 interaction is vital for cellular ADPr 83
3.4 Sequence alignment of HPF1 orthologues 85
3.5 Conservation map of HPF1 crystal structure surface 86
3.6 Electrostatic map of the HPF1 crystal structure 87
3.7 Residues of the HPF1 conserved corner 88
3.8 HPF1 structure and conserved corner 90
3.9 HPF1-PARP2 ART domain crystal structure 91
3.10 Glutamate and serine ADPr reaction mechanism 93
3.11 Model of DNA-bound HPF1/PARP1 complex 95
3.12 HPF1-bindings sites on PARP1/2 96
3.13 Catalytic inactivation of PARP1 ΔHD drives HPF1 binding 98

3.14 PARP1 C-terminus and H862 are responsible for HPF1 binding 99
3.15 Model showing overlap of Carba-NAD and HPF1 binding in PARP1 100
3.16 PARP1 auto-modification site candidates 103
3.17 PARP1 auto-modification sites 104
3.18 PARP1 auto-modification dependence on serine 106
3.19 PARP1 auto-ADPr status determines dissipation from laser stripes 107
3.20 HPF1 confers auto-ADPr resistance to Olaparib on PARP1 110
3.21 Dependence of PARP1 auto-ADPr inhibition resistance on HPF1 113
3.22 Inhibition-resistant PARP1 auto-ADPr in PARP1 inhibitor titration assay . 114
3.23 PARP1 dissipation from laser-induced damage depends on HPF1 118
3.24 Generation of U2OS Flp-In *PARP1*Δ cells 122
3.25 Complementation of U2OS Flp-In *PARP1*Δ cells 124
3.26 Phenotypic consequences of impaired PARP1 auto-modification 126
3.27 Generation of U2OS Flp-In *HPF1*Δ cells 128
3.28 Complementation of U2OS Flp-In *HPF1*Δ cells 131
3.29 ADPr complementation assay of U2OS Flp-In *HPF1*Δ cells 132
3.30 Doxycycline titration of complemented U2OS Flp-In *HPF1*Δ cells 134
3.31 6-day Olaparib treatment assay of complemented *HPF1*Δ cells 135
3.32 HPF1 catalytic inactivation sensitizes cells to Olaparib 138
3.33 HPF1 E284A shows enhanced recruitment to laser stripes 140

4.1 Structural features of HPF1 E284 and D286 145
4.2 Model of PARP1/HPF1-catalyzed serine ADPr 146

A.1 R239 significance in H3 but not H4 ADPr 185
A.2 ADPr complementation in U2OS Flp-In *HPF1*Δ 186
A.3 Olaparib survival of U2OS Flp-In WT EV1 and *HPF1*Δ WT5 cells 187
A.4 YFP-HPF1 WT, E284A and D286A recruitment to laser-induced damage . 188

List of Tables

2.1 List of commercially available antibodies 68
2.2 List of commercially available plasmids 72

List of Abbreviations

ADPr ADP-ribosylation

ADPRT bacterial ADP-ribosylating toxin

AIF apoptosis-inducing factor

ALC1 amplified in liver cancer 1

APLF polynucleotide-kinase-like factor

ARH ADP-ribose hydrolases

ART ADP-ribosyltransferase

ARTC cholera toxin-like ART

ARTD diphtheria toxin-like ART

BAD benzamide adenine dinucleotide

BER base excision repair

BRCA1 breast cancer 1

BRCA2 Breast cancer type 2

BRCT BRCA1 C-terminus

CAT catalytical domain

DDR DNA dfamage response

DSB double-strand break

dsDNA double-stranded DNA

FHA Forkhead-associated

HD helical domain

HPF1 histone PARylation factor 1

kDA kilodalton

MARylation mono-ADP-ribosylation

MMS methyl methanesulfonate

NER nucleotide excision repair

NHEJ non-homologous end-joining

PARG poly-ADP-ribose glycohydrolase

PARP poly-ADP-ribose polymerase

PARylation poly-ADP-ribosylation

PBZ PAR binding zinc finger

PCNA proliferating cell nuclear antigen

PNKP polynucleotide kinase 3'-phosphatase

PTM post-translational modification

SSB single-strand break

ssDNA single-stranded DNA

TNKS tankyrase

WB Western Blotting

WGR tryptophan-glycine-arginine-rich

WT wildtype

WWE tryptophan-tryptophan-glutamate

XRCC1 X-ray repair cross-complementing protein 1

Introduction

Post-translational modifications (PTM) , which can target both proteins and DNA, strongly increase the versatility of a cell's proteome by modifying the function, localization and stability of their targets. They are incredibly varied in their nature, ranging from amino acid alterations over the attachment of small chemical groups such as methylation or phosphorylation up to the addition of whole proteins such as in SUMOylation and ubiquitylation (Brennan & Barford (2009), Minguez et al. (2012), Wilson (2017)). One such modification, ADP-ribosylation (ADPr) , was first discovered in 1966 and has since lead to the emergence of its own field and the development of a new group of cancer therapeutic drugs (Kraus (2015), Slade (2020)).

1.1 ADP-ribosylation

ADP-ribosylation, i.e. the addition of one or more ADP-ribose units onto a target substrate, can be found in all domains of life and a reversible metabolism of ADP-ribosylation is conserved in all six eukaryotic supergroups, highlighting its significance for eukaryotic survival (Perina et al. (2014)). What exactly this metabolism entails and to which end it operates is outlined below.

1.1.1 Nature and Significance

Similar to ubiquitylation, ADP-ribosylation can occur as a single ADP-ribose unit on one or more sites of a target substrate, so called mono-ADPr or MARylation , or as long chains, referred to as poly-ADPr or PARylation (Figure 1.1). Poly-ADP-ribose chains can reach up almost 200 units in length *in vitro* with branch points on average occurring every 35 residues (Alvarez-Gonzalez et al. (1987), Hayashi et al. (1983)). NAD^+ serves as a substrate for the attachment of ADP-ribose onto target proteins and DNA and RNA,

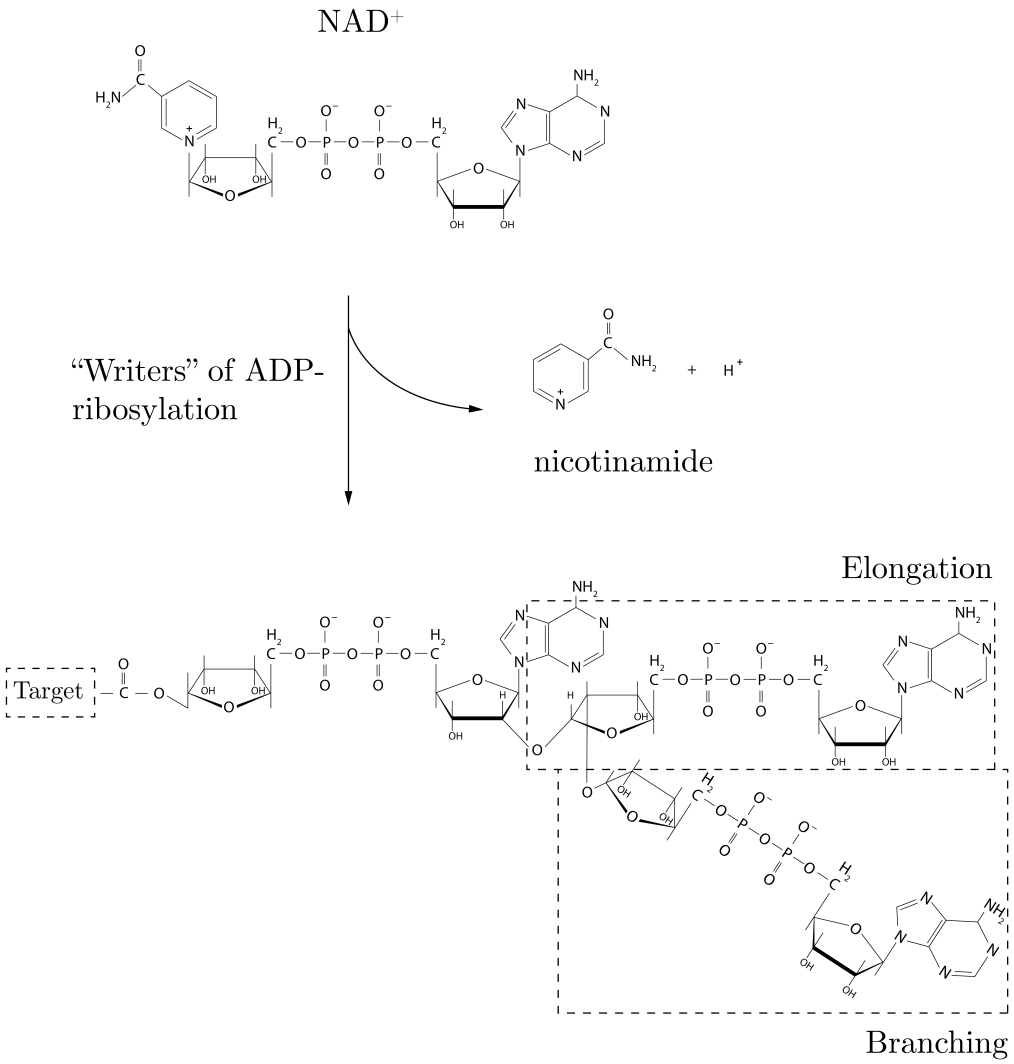


Figure 1.1: *Molecular structure of ADP-ribosylation.* NAD^+ is used as a substrate by writers of ADP-ribosylation to attached one or multiple, consecutive ADP-ribose units onto a target. Consecutive units can be attached in an elongating or branching fashion.

leading to the release of nicotinamide as a by-product (Jankevicius et al. (2016), Munnur & Ahel (2017), Munnur et al. (2019), Schuller et al. (2021)). The initial ADP-ribose unit is attached via a O-, S-, or N-glycosidic bond between the target and the 1" position of the nicotinamide-proximal ribose (distal ribose) following an SN_2 reaction mechanism. Following ADP-ribose units are attached in two different manners, either for elongation or for branching (Figure 1.1). The elongation reaction connects the 2' position of the adenosine-proximal ribose (proximal ribose) belonging to the terminal ADP-ribose unit with the 1" position in the distal ribose of a new NAD^+ molecule, forming a α-1"$\rightarrow$2'-glycosidic bond. The branching reaction on the other hand forms a α-1"$\rightarrow$2"-glycosidic bond between two distal ribose rings (Gibson & Kraus (2012), Malanga & Althaus (2005)). The molecular

structure of PARylation is highlighted in Figure 1.1.

The significance of ADP-ribose in a large number of cellular processes is multifold, including as a scaffold for the localization of APD-ribose-binding proteins, as second messengers, as a modifier of biochemical - catalytic and surface - properties of target proteins, and as indirect contributors to NAD^+ homeostasis. As a result, ADP-ribosylation impacts on cellular DNA damage response, inflammation, transcription, metabolism, mitosis, cell death, mitochondrial function and more (Feldman et al. (2012), Hopp et al. (2021), Huang et al. (2020), Iwata et al. (2016), Luo et al. (2017), Lüscher et al. (2018)). As a result, anomalies in expression or function of proteins catalyzing ADP-ribosylation (*writers*), binding the modification (*readers*) and hydrolyzing it (*erasers*) have been found in a range of cancers and other diseases and are increasingly becoming targets for cancer therapy (Grudem & Hendrickson (2020), Hanzlikova et al. (2020), Schleicher et al. (2018), Slade (2020)).

1.1.2 Writers of ADP-ribosylation

To this date, three independent protein families capable of catalyzing ADPr have been identified: Sirtuins, TM1506 and the superfamily of ADP-ribosyltransferases (ARTs) (Aravind et al. (2015)). While the TM1506 family of proteins has only been defined in bacteria and their function remains obscure, the last decade has seen extensive research on the distribution and characterists of sirtuins and ARTs. Sirtuins have been shown to be conserved across all domains of life with OAADPr (2'-O-acetyl-ADP-ribose)-forming deacetylation being the dominant activity in most members. However, robust ADP-ribosyltransferase activity has also been detected alongside deacetylase activity in eukaryoatic, bacterial and archaeal sirtuins (Aravind et al. (2015), Hawse & Wolberger (2009), Michan & Sinclair (2007), Rack et al. (2015), Simonet et al. (2020)). Similarly, homologues of the ART superfamily have been found in archaea, bacteria as well as all six eukaryotic superfamilies and have even been reported to be present in viruses (Mikolčević et al. (2021), Perina et al. (2014)).

Sirtuins

Sirtuins are a group of proteins named after their yeast founding member silent information regulator 2 (Sir2), which since its discovery has been found to be conserved even in mammals and functions as an epigenetic silencer. At the heart of their catalytic ac-

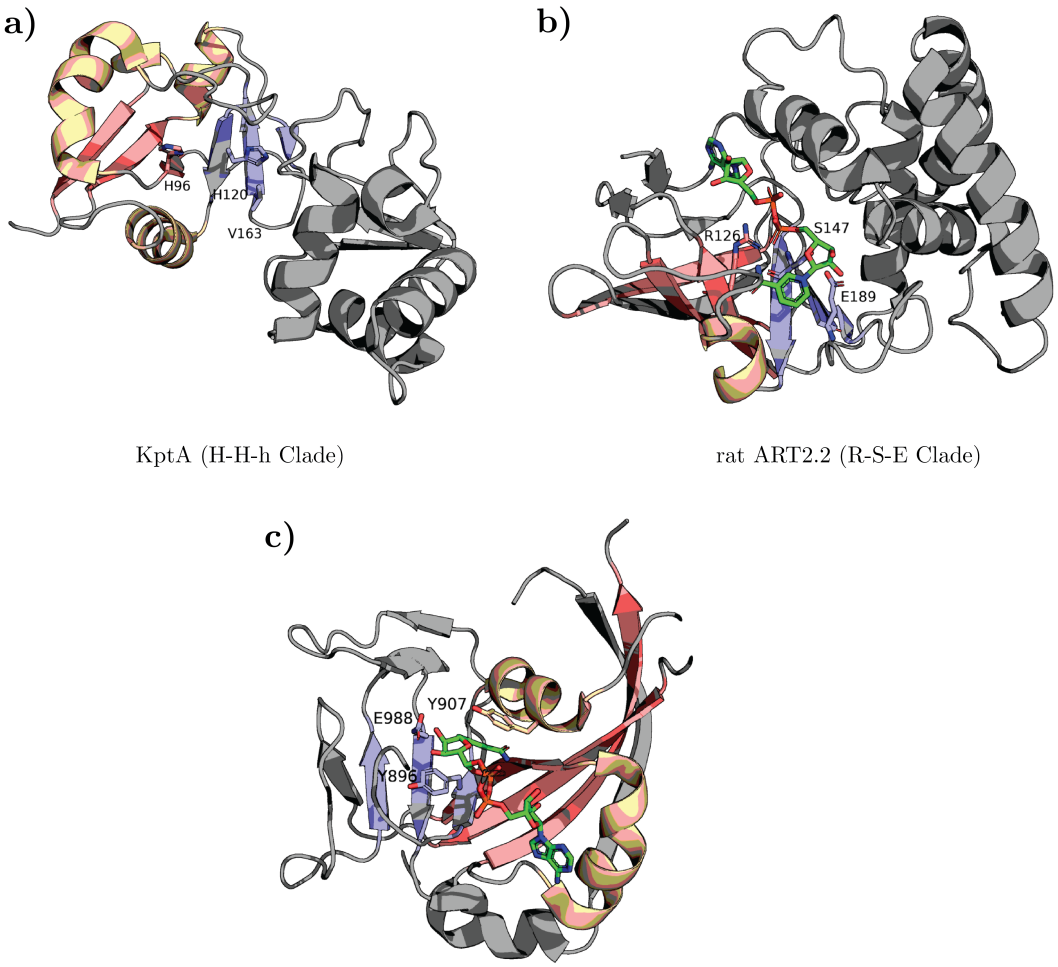
tivity lies a α/β Rossman fold, a super-secondary structure of alternating β-strands and α-helices also referred to as an ADP-binding fold (Hanukoglu (2015)). Different to classical $NAD^+/NADP^+$ binding dehydrogenases, which they resemble, an additional set of conserved residues allows sirtuins to use NAD^+ not just as a redox cofactor, but also a substrate for ADP-ribosyltransferase activity (Aravind et al. (2015)). In mammals, there are seven sirtuin proteins labelled SIRT1-7, which are distributed across different tissues and serve separate functions. Overexpression of Sir2 orthologs in various vertebrate species has been shown to be associated with increased life span, possibly by silencing transcription at the rDNA locus through their histone deacetylase rather than their relatively weak ADP-ribosylation activity. Other roles are equally linked to their deacetylase activity, namely the combined functions of nuclear and mitochondrial sirtuins in metabolism and their implications in aging (Guarente (2018), Hu & Zheng (2018)).

ADP-ribosyltransferases (ARTs)

The most well-studied superfamily of ADP-ribosylation writer proteins are ADP-ribosyltransferases. These proteins have been shown to be able to modify a wide chemical range of substrates, most prominently the carboxyl group of glutamate and aspartate, the hydroxyl group of serine and tyrosine, the thiol group of cysteine and the guanidino group of arginine residues (Aravind et al. (2015)). Depending on the structural nature of the catalytic fold, ARTs can be divided into two groups derived each of a bacterial toxin: cholera toxin-like ARTs (ARTCs) and diphtheria toxin-like ARTs (ARTDs) (Buch-Larsen et al. (2020)). In bacteria, ARTs mostly fulfil the role of both endotoxins and exotoxins. While bacteria of six different phyla contain genes for potential ARTs, only 11 bacterial species have been reported to contain both a potential ADP-ribosyltransferase and an ADP-ribosylhydrolase, suggesting that a substantial proportion of ARTs in bacteria serve bacterial pathogenesis (Lüscher et al. (2018)). Indeed, over 35 bacterial ADP-ribosylating toxins (ADPRTs) have been identified, which can modify a range of different host proteins (G-proteins, actin, small GTPases such as eEF2, etc.) in animals and plants, disrupting signalling pathways and other processes with lethal consequences (Holbourn et al. (2006), Mach (2019), Simon et al. (2014)). For this reason, ADPRTs have emerged as attractive targets in the treatment of microbial infections, particularly in the light of antibiotic resistances to conventional antibiotics (Catara et al. (2019)). Endotoxic toxin/anti-toxin

(TA) systems such as the DarTG system, on the other hand, serve the survival of bacteria (through bacterial persistence, phage defense, etc.) under unfavorable conditions by inhibiting and restoring essential cellular processes (Jankevicius et al. (2016), Lawarée et al. (2020), Zaveri et al. (2020)). Interestingly, ARTs were most likely acquired by eukaryotes from bacteria through horizontal gene transfer (García-Saura et al. (2018)). Although not all ARTs carry catalytic activity, they all share a common α/β core domain (Figure 1.2). It consists of two central three-strandeed β-sheets separated by α-helical elements. The NAD^+ binding pocket is located in the interface of the two β-sheets (Aravind et al. (2015), Bell & Eisenberg (1996)). This ART motif is most clearly visualized in the crystal structures of cholera toxin and diphtheria toxin, but is preserved in all eukaryotic ARTs (Bell & Eisenberg (1996), Merritt et al. (1994), Ruf et al. (1996)). Additionally, eukaryotic ARTDs have acquired an auto-inhibitory helical domain (HD) that suppresses ART catalytic activity in the absence of a specific trigger, further defining the proteins' functions. Together, the HD and ART domain form a combined catalytic (CAT) domain. However, this is addressed in detail in *1.2.1 PARP1 catalytic activation.* Three examples of an ART domain - the conserved ART subdomain of the human PARP1 CAT domain, the structure of rat ecto-ADP-ribosyltransferase 2.2 (ART 2.2) and the structure of *Aeropyrum pernix K1* RNA 2'-phosphotransferase - are shown in Figure 1.2 (Kato-Murayama et al. (2005), Langelier et al. (2018), Ritter et al. (2003)).

According to their catalytic residues, ARTs are classified into three clades: the H-H-h Clade (shown by the example of *Aeropyrum pernix K1* RNA 2'-phosphotransferase in Figure 1.2a), the R-S-E Clade, which characterizes ARTCs (shown by the example of rat ART 2.2 in Figure 1.2b) and the H-Y-E Clade, which belongs to ARTDs (shown by the example of PARP1 in Figure 1.2c). The most rudimentary of the three is the H-H-h Clade, which encompasses the KptA and CC0527 protein families and is represented here by an archaeal KptA in Figure 1.2a. KptA proteins are a group of RNA-processing enzymes and have been shown to ADP-ribosylate RNA (Munir et al. (2018)). In humans, the protein family is represented by tRNA 2'-phosphotransferase 1 (TRPT1), which completes - possibly in a tissue-specific manner - tRNA splicing by transferring a phosphate group from the tRNA splice site onto NAD^+ (Hu et al. (2003)). The functions of proteins belonging to the CC0527 protein family are more obscure. In bacteria, CC0527 family members are speculated to be able to ADP-ribosylate antibiotics as they are often coupled with



KptA (H-H-h Clade)

rat ART2.2 (R-S-E Clade)

ART domain of PARP1 (H-Y-E Clade)

Figure 1.2: *Ribbon representation of representative ART domains.* The conserved β-sheets one and two are colored in *salmon* (β-strands 1, 3 and 6) and *light blue* (β-strands 2, 4 and 5), respectively, and α-helices in *wheat*. **a)** Crystal structure of *Aeropyrum pernix K1* RNA 2'-phosphotransferase. Conserved catalytic residues H96, H120 and V163 identify the protein as belonging to the H-H-h Clade ARTs. **b)** Composite model of rat ecto-ADP-ribosyltransferase 2.2 bound to NAD^+ (PDB: 1OG1 and PDB: 1OG3). Conserved catalytic residues R126, S147 and E189 identify the protein as belonging to the R-S-E Clade ARTCs. **c)** ART domain of human PARP1 bound to the NAD^+ analog benzamide adenine dinucleotide (BAD) (residues 826 - 1012; PDB: 6BHV). Conserved catalytic residues H862, Y907 and E988 identify the protein as belonging to the H-Y-E Clade ARTDs and sit close to the distal ribose of BAD, which simulates the ribose attached to the target amino acid.

antibiotic-detoxifying domains (Aravind et al. (2015)).

The second clade, R-S-E Clade ARTCs, is represented in Figure 1.2b by rat ecto-ADP-ribosyltransferase 2.2 (ART 2.2). In humans this clade counts four members (ARTC1 and

ARTC3-5), of which three (ARTC1, ARTC3 and ARTC4) are membrane-bound and one (ARTC5) is secreted. While ARTC3 and ARTC4 lack the R-S-E motif and are presumed to be catalytically inactive, the motif exhibits mono-ADP-ribosylation activity towards the guanidino group of arginine residues in ARTC1, ARTC2 and ARTC5 (Lüscher et al. (2018)). In mice, ART2.2 leads to the controlled cell death of T lymphocytes by activating the cation channel P2X7 (Laing et al. (2011)).

Substrate specificity is just one feature separating ARTCs from the H-Y-E motif-carrying ARTDs, the activity of which is directed towards other amino acids including serine, glutamate, aspartate and tyrosine. In contrast to ARTCs, ARTDs are capable of catalyzing not only MARylation, but also PARylation. For that reason they are also referred to as poly-ADP-ribose polymerases (PARP) . However, it has recently been agreed that specifically only mammalian members of the ARTD family should be named PARPs and/or tankyrases (TNKS) together with their number in a given species, e.g. human PARP1 (Lüscher et al. (2021)). The ART domain of the latter, which is the most prominent member of human PARPs and is described in detail below, is shown Figure 1.2c. Eukaryotic PARPs can be classified according to six clades: DNA repair PARPs (Clade 1) (see *1.2 DNA repair PARPs*), plant PARPs (Clade 2), undefined heterogeneous group of PARPs (Clade 3), tankyrases (Clade 4) and vault PARPs (Clade 5) (Perina et al. (2014)). The human ARTD family counts 17 member proteins (PARP1-17) with diverse localization and function. Of these, Clade 1 proteins PARP1 and PARP2 as well as Clade 4 PARPs Tankyrase 1 (TNKS1, PARP5a) and Tankyrase 2 (TNKS2, PARP5b) and Clade 5 member PARP4 are capable of PARylation. All other members have either been shown to carry MARylation activity or have not been found to be catalytically active at all.

PARP1, the most extensively studied PARP member, alone is responsible for 85-95% of all PARP activity in different mouse cell lines (Amé et al. (1999), Chen, Kassab, Dantzer & Yu (2018)). The domain structure of this nuclear protein is highlighted in Figure 1.3. In absence of DNA damage, PARP1 shows little inter-domain communication, exhibiting a so-called *beads-on-a-string* conformation, and exists in an auto-inhibited state brought about by its HD (Steffen et al. (2016)). DNA damage sites are recognised by two zinc finger motifs (ZnF1 and 2) in the N-terminal region and a central tryptophan-glycine-arginine-rich (WGR) domain (Eustermann et al. (2011)). Binding to these sites leads to an intramolecular N→C-terminal signal cascade between ZnF1, a third non-DNA-binding

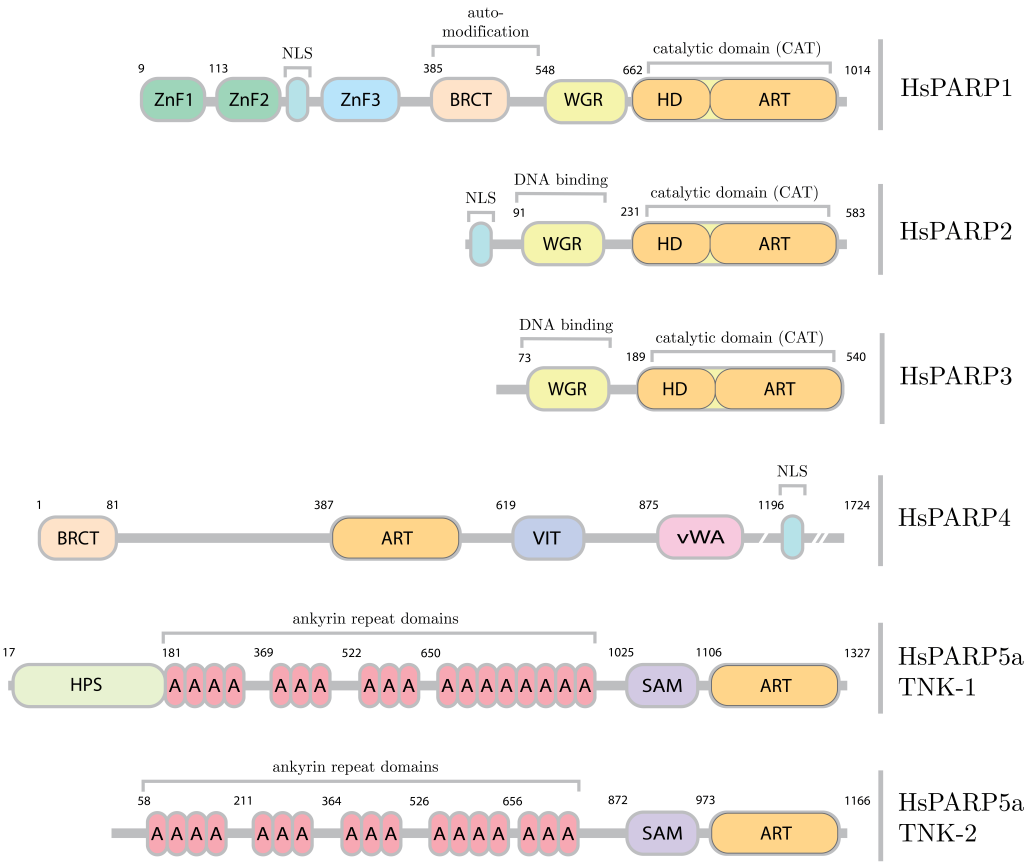


Figure 1.3: *Domain structures of human PARPs from three different clades.* The domain structures are of PARP1-3 (Clade 1), PARP4 (Clade 5) and Tankyrase 1(TNKS1) and Tankyrase 2 (TNKS2) (Clade 4). All six proteins contains the ART domain, also referred to as catalytic (CAT) domain. However, in the nuclear proteins PARP1, PARP2 and PARP3 this domain also comprises auto-inhibitory HD. Further structural elements in the three proteins include DNA binding domains - zinc fingers 1-3 (ZnF1-3) in PARP1 and the tryptophan-glycine-arginine-rich (WGR) domain in PARP1, PARP2 and PARP3. PARP4 carries the vault protein inter-alpha- trypsin (VIT) domain and the Willebrand type A (vWA) domain characteristic of a vault PARP, while Tankyrase 1 and Tankyrase 2 both carry a series of protein-protein interacting ankyrin (A) repeats.

zinc finger motif (ZnF3), the WGR domain and the HD. This triggers dramatic conformational changes resulting in a *compacted* form of PARP1 and unfolding of the HD, releasing auto-inhibition. This was revealed by structural studies showing that the HD achieves catalytic inactivity in PARP1 by physically blocking NAD^+ binding (Dawicki-McKenna et al.

(2015), Langelier et al. (2018)). The studies were confirmed by observations that deletion of the HD creates constitutively active PARP1 (Dawicki-McKenna et al. (2015)). The significance of each of its domains in achieving catalytically active PARP1 is highlighted by the loss or gain of substrate binding in point mutants of domain interface residues between the zinc fingers, WGR domain and HD which do not abrogate DNA binding, such as mutants of PARP1 R78, W79, W318, D45, R591 and L713 (Eustermann et al. (2015), Langelier et al. (2011, 2012), Steffen et al. (2014)). One other domain highlighted in Figure 1.3, the BRCA1 C-terminus (BRCT) fold, upon catalytic activation becomes the target of PARP1 auto-modification by which PARP1 is released from DNA (Eustermann et al. (2015), Loeffler et al. (2011)).

As mentioned above, PARP1 belongs to the DNA repair clade of PARPs and its role in the human DNA damage response will be discussed in depth later. Besides itself, the main targets of PARP1 ADP-ribosylation are histones. Together, their modification achieves: a) chromatin decondensation at sites of DNA damage (through histone ADP-ribosylation), making the surrounding DNA more accessible to repair factors and b) the recruitment of DNA repair factors containing PAR-binding domains (see *1.1.3 Readers of ADP-ribosylation*) (Lebeaupin et al. (2017), Smith et al. (2019)). Similar to PARP1, PARP2 is also recruited to sites of DNA damage, triggering auto-modification and trans-ADP-ribosylation of substrates (Figure 1.3). However, the two proteins have significantly distinct DNA binding affinities depending on the nature of the DNA substrate, illustrating their functional separation in the DNA damage response (DDR) (Bilokapic et al. (2020), Langelier et al. (2012, 2014), Obaji et al. (2018)). The last member of the DNA repair PARPs, PARP3, although similar in domain structure to identical in catalytic domain structure to PARP1 and PARP2 and originally predicted to be capable of catalyzing poly-ADP-ribosylation has so far only been reported to possess mono-ADP-ribosylation activity (Boehler et al. (2011), Rodriguez-Vargas et al. (2019)) (Figure 1.3).

Tankyrase 1 and 2 (TNKS1 and TNKS2, respectively) are involved in several cellular processes, namely telomere maintenance, Wnt signalling and mitosis (Kim (2018)). In contrast to the DNA repair PARPs, they do not carry an inhibitory HD. Rather, their activity is influenced by a large array of protein interactions mediated by their protein-binding domains. These include their multiple ankyrin repeat motifs and sterile alpha motif (SAM)

domain (Figure 1.3). The latter is involved in the oligomerization of tankyrases. One way in which takyrases operate is by controlling the stability of proteins through poly-ADP-ribosylation, marking them for ubiquitylation and subsequent proteosomal degradation (Haikarainen et al. (2014)).

PARP4 is the only member of human vault PARPs (Figure 1.3). While homologues of PARP4 exist in most animals, vault PARPs are not conserved in plants and fungi (Perina et al. (2014)). Originally identified in 1999 as vPARP, PARP4 is the largest of the 17 human PARPs. It is thought to be able to PARylate itself as well as the major vault protein (MVP). Together with PARP4 and telomerase/vault-associated protein (TEP1) and mutliple short untranslated RNAs (vRNAs), 78 copies of MVP form a large ribonucleoprotein (RNP) particle called a vault - a multi-subunit structure of elusive function that is involved in cellular signalling and intracellular transport (Berger et al. (2009), Kickhoefer et al. (1999)).

Members of a group of proteins specific to plants, including Radical-Induced Cell Death 1 (RCD1) and a family of six homologues called Similar To RCD1 (SRO), also contain a PARP-like domain (Figure 1.3). For this reason they are attributed their own clade of plant PARPs (Clade 2). These proteins have been shown to be important for stress adaptation and development in plants. Although they contain an ART domain, RCD1 and SROs are thought to not possess catalytic activity. Rather, they exert their function through interaction with transcription factors (Jaspers et al. (2009, 2010)).

The remaining 11 human PARPs, PARP6-16, belong to Clade 3. While the functions and/or presence of catalytic activity remains obscure in the case of some, the function of a selected few are discussed herein. Sequence alignment has shown that each of these proteins lack the catalytic glutamate, explaining the limitation of their catalytic activity to mono-ADP-ribosylation (Otto et al. (2005)). The above described human PARPs (PARP1-4, TNKS1 and TNKS2) can be separated from PARP6-16 as H-Y-E triad-containing subgroup of human PARPs. Based on amino acid conservation, two other subgroups have been proposed, which both lack the catalytic glutamate: the H-Y-I/L/Y subgroup containing PARP6-8, PARP10-12 and PARP14-16 and the Q/Y-Y-T/V subgroup of PARP9 and PARP13 (Kleine et al. (2008)). The latter subgroup was initially thought to be catalytically inactive, although this has been revised due to findings regarding PARP9. The protein operates in a heterodimer with the E3 ubiquitin ligase DTX3L, which interacts

with STAT1 to stimulate gene expression of interferons and ubiquitylates viral 3C protease as well as histone H2BJ for IGS expression (Zhang et al. (2015)). In addition, as part of the PARP3-DTX3L complex PARP9 is able to retrain E3 function through mono-ADP-ribosylation of ubiquitin at Gly76 (Yang et al. (2017)). In cellular immune response, the two mono-ADP-ribosyltansferases PARP9 and PARP14 act in opposite ways, functioning as pro-inflammatory and anti-inflammatory factor, respectively. These antagonist roles are highlighted in macrophage activation, where PARP14 is able to prevent STAT1 phosphorylation through mono-ADP-ribosylation of phosphorylation site-proximal residues, while PARP9 is able to suppress PARP14 function (Iwata et al. (2016)). A third member, PARP10, is able to modify itself as well as histones (Kleine et al. (2008)). It binds to K63 ubiquitin and subsequently MARylates NEMO, a member of the IKK complex belonging to the NF-κB signalling pathway (Verheugd et al. (2013)). Unsurprisingly, its upregulation is correlated with cellular proliferation and tumorigenesis (Schleicher et al. (2018)).

1.1.3 Readers of ADP-ribosylation

The term readers of ADP-ribosylation encapsulates all proteins, independent of their function, that are able to bind ADP-ribosyl modifications. This group also includes PARPs themselves such as the macro-domain containing *macroPARPs* PARP9, PARP14 and PARP15, the WWE domain-containing PARPs PARP7, PARP11, PARP12, PARP13 and PARP14 and many PARP homologues in other species that have acquired one or another such domain, such as zebrafish PARP2 (Perina et al. (2014)). There exist five classical ADP-ribose binding domains: The PAR binding motif (PBM), the PAR binding zinc finger (PBZ) , macrodomains, tryptophan-tryptophan-glutamate (WWE) domains, and Forkhead-associated (FHA) and BRCT domains (Barkauskaite et al. (2013), Teloni & Altmeyer (2016)) (Figure 1.4).

PBMs

PBMs are characterized by a conserved sequence of hydrophobic residues interspaced by basic residues, the positive charge of which results in electrostatic affinity for negatively charged ADP-ribose instead of binding the molecule through hydrogen bonds. This sequence is usually preceded by a patch of positively charged residues, mostly lysine or

arginine. The motif itself carries the consensus sequence Φx[+]xΦΦ[+][+]ΦΦ[+], where Φ stands for a preference in hydrophobic, [+] in basic/positively charged residues and x signifies the lack of preference for a particular amino acid (Barkauskaite et al. (2013), Pleschke et al. (2000)). The nomenclature used here and in all subsequent motif description is that of the ELM syntax (Aasland et al. (2002)).

PBZ domains

One of the first proteins for which a PBZ domain was described and its structure analyzed was the DNA repair factor aprataxin polynucleotide-kinase-like factor (APLF) , thought to be involved in the non-homologous end-joining (NHEJ) (Ahel et al. (2008), Rulten et al. (2011)). In APLF, the PBZ domain appears as a tandem repeat, similar to the two DNA-binding zinc fingers in the N-terminus of PARP1 (Li et al. (2010)). The zinc ion in the centre of each zinc finger is coordinated by a group of four conserved residues, two cysteines and two histidines. Sequence comparison between species hints at a wider conservation, where each of the cysteine residues is part of a three-amino acid sequence preceded by a conserved arginine, with the consensus sequence being RxxCx[Y/F]GxxCYR[+]xxxHxxx[F/Y]xH. Crystal structure studies of the APLF modules with ligands mimicking PAR indicate that the adenine ring of ADP-ribose stacks with the conserved tyrosine of Cx[Y/F]G and has a weaker edge-face interaction with the tyrosine of CYR[+]. An additional interaction was proposed between the first conserved arginine of CYR[+] and the pyrophosphate of a subsequent ADP-ribose unit, whereby all three interaction points only occur when two ADP-ribose units are connected by an elongating α-1",2'-glycosidic bond making the PBZ motif specific for PAR recognition (Eustermann et al. (2010)) (Figure 1.4).

BRCT and FHA domains

APLF contains one other PAR binding domain, the FHA domain. BRCT and FHA domains are generally regarded as protein-protein interaction domains, such as in the case of p53 binding to the tandem BRCT1 domain of p53-binding protein 1 (53-BP1), or as readers of protein phosphorylation, such as in the case of breast cancer 1 (BRCA1) or polynucleotide kinase 3'-phosphatase (PNKP) (Ali et al. (2009), Clapperton et al. (2004), Derbyshire et al. (2002), Joo et al. (2002), Shiozaki et al. (2004)). However, they have also

been shown to be able to bind PAR (Leung & Glover (2011)) (Figure 1.4). PAR-binding BRCT domains can be found in several DNA damage response factors, namely X-ray repair cross-complementing protein 1 (XRCC1) , DNA Ligase IV and BRCA-1 associated RING domain protein 1 (BARD1) (Teloni & Altmeyer (2016)). Although both domains are listed together here due to their shared functions, their secondary structures differ considerably. The conserved core of BRCT domains consists of a four-stranded β-sheet wedged between one α-helix on one and two α-helices on the other side as confirmed by the crystal structures of the BRCA1 tandem BRCT domain, BRCT6 of TopBP1 and the tandem BRCT repeats of MDC1 (Aasland et al. (2002), Clapperton et al. (2004), Lee et al. (2005)). The FHA domain, on the other hand, forms a β-sandwich of two anti-parallel β-sheets - one consisting of 8 β-strands and one of 3 β-strands - with occasional α-helical elements in the flexible regions between β-strands (Durocher & Jackson (2002), Mahajan et al. (2008)). Two residues have been identified to be essential for ADP-ribose binding in both domains. Mutation of two conserved arginine residues in the FHA domains of PNKP and aprataxin (APTX) triggers loss of PAR and iso-ADP-ribose binding *in vitro*, while mutation of a conserved serine and lysine/arginine residue abolished PAR binding in the BCRT domains of DNA Ligase IV and XRCC1 (Li et al. (2013)).

WWE domains

WWE domains, named after their conserved residues, are found in two groups of proteins: PARPs and HECT or RING containing proteins associated with ubiquitylation (Aravind (2001)). Prominent proteins carrying two WWE domains in tandem are PARP11, PARP14 and the E3 ubiquitin ligases Deltex1 and RNF146. WWE domains occur nearly exclusively in functional-dependent tandems with a single WWE domains comprised of a 2-layer α/β sandwich (Wang et al. (2012)). Not all WWE domain-containing proteins carry the conserved residues required for PAR binding and some members of the family have been described to facilitate protein-protein interactions, for example by binding ankyrin repeats (Teloni & Altmeyer (2016), Zweifel et al. (2005)). In addition, ADP-ribose binding is not a uniform property of WWE domains as RN146 binds iso-ADP-ribose, a substructure of poly-ADP-ribose molecules, while PARP11 can bind mono-ADP-ribosyl modifications (He et al. (2012)) (Figure 1.4). In RNF146, substrate selectivity arises from the presence of four crucial residues (Y109, Y146, Q155 and R165), which form a hydrophobic

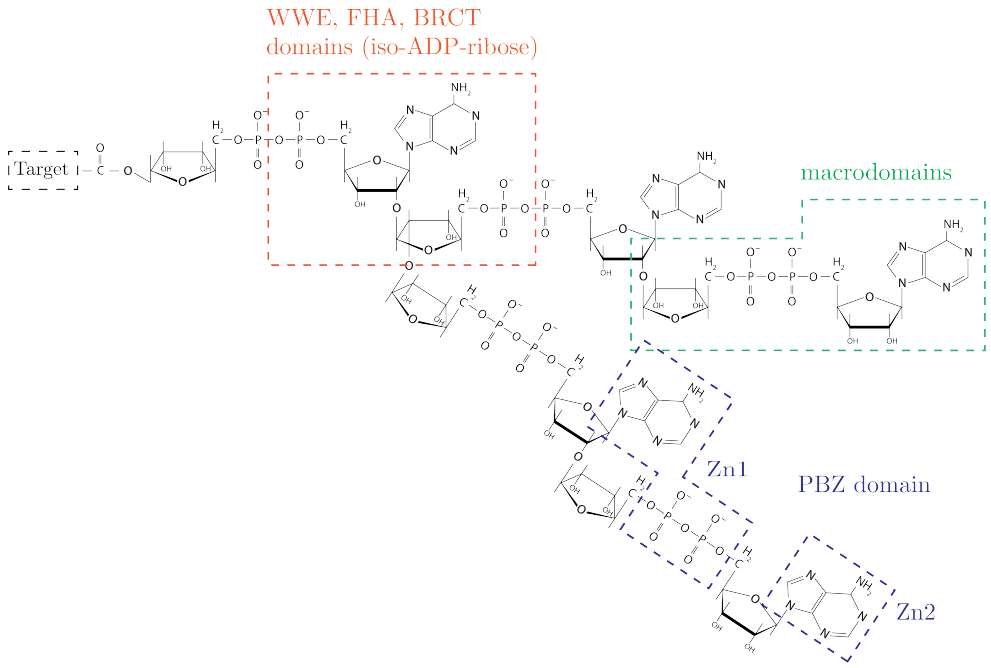


Figure 1.4: *Recognition sites of PAR-binding domains.* ADP-ribosyl modification recognition by two PAR binding zinc finger domains, shown in *blue*, relies on the PAR-specific close proximity of an adenosine ring and pyrophosphate group from neighbouring ADP-ribose units. Iso-ADP-ribose alone or as part of a PAR stucture is recognized by WWE, FHA and BRCT domains, highlighted in *orange*, and macrodomains recognize terminal ADP-ribose bound to another ADP-ribose unit by an *O*-glycosidic bond, shown in *green* (Leung (2014)).

adenosine biding pocket and together with strong electrostatic interactions between the negatively charged ribose-phosphate moieties and positively charges residues on the edge of the β-sheet participate in PAR binding. Y109 interacts with the adenine ring, and Q155 and Y146 with the phosphate groups. Y109 is replaced by a tryptophan in Deltex1 and PARP11, while Q155 and R165 are not conserved in PARP14, which is unable to bind PAR. Besides PAR binding, RNF146 is also a good example of how ADP-ribosylation impacts catalytic activity, with PAR-binding of the WWE domain triggering a conformational change in the RING domain leading to the activation of RNF146 catalytic activity (DaRosa et al. (2015)).

Macrodomains

Macrodomains received their name from the first eukaryotic protein that was discovered to harbour one, rat macroH2A. PARP family member with macrodomains include PARP9 (which can bind PARylated proteins), PARP14 (which binds MARylated pro-

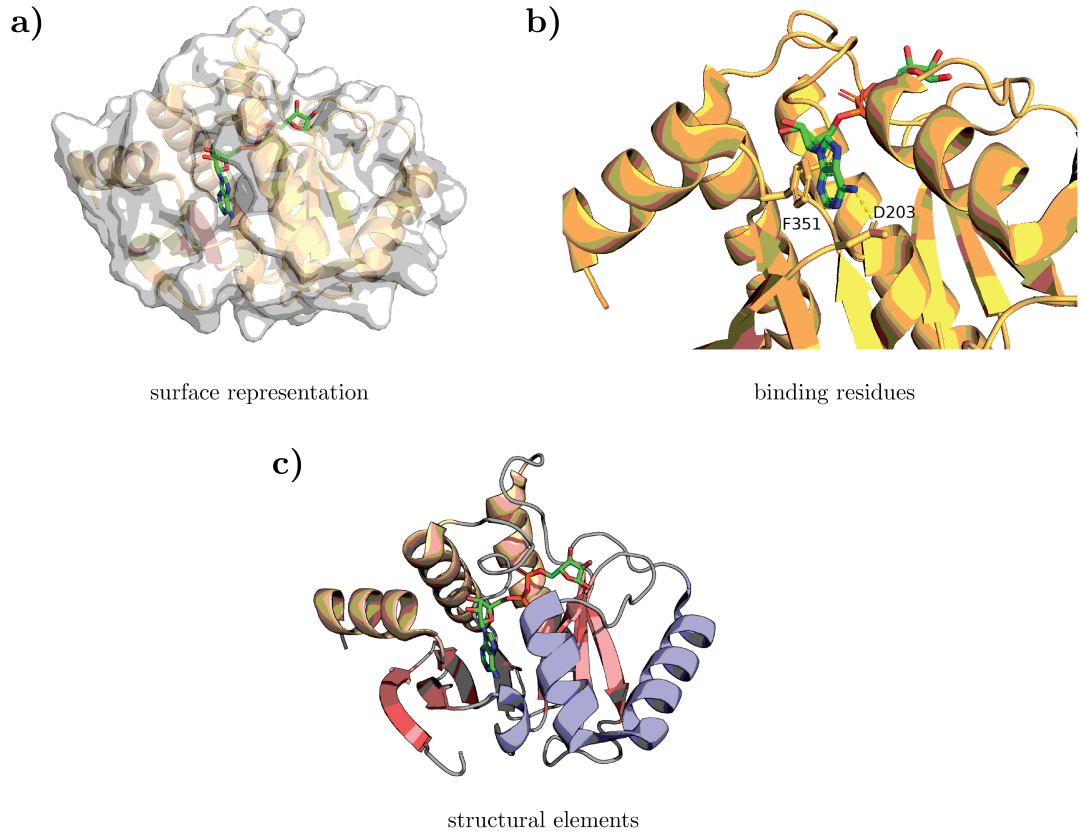


Figure 1.5: *Crystal structure of the macrodomain of human macroH2A1.1, PDB: 3IID.* **(a)** Surface representation of the structure shows ADP-ribose sitting in a groove on top of the mixed β-sheet with loop 1 and loop 2 stretching over the molecule. **b)** The conserved ADP-ribose binding residues aspartate 203 and phenylalanine 531 of the macrodomain interact with adenine of the molecule. **(c)** Ribbon representation of the conserved structural elements of the macrodomain. The seven-stranded β-sheet is colored in *salmon* and the two groups of α-helices at either side of the sheet are colored in *light blue* and in *wheat*.

teins) and PARP15 (Barkauskaite et al. (2015)). Strikingly, and in contrast to the above described PAR binding domains, macrodomains co-evolved together with PARPs and Sirtuins, indicating that they complete ADP-ribose metabolism by removing or transforming PAR signals (Rack et al. (2016)). While the ability to hydrolyse PAR is widespread in macrodomains and will be specifically discussed in *1.1.4 Erasers of ADP-ribosylation*, macrodomains also serve as classical ADP-ribose binding modules (Karras et al. (2005)). They are exemplified here by the macrodomain of human macroH2A1.1, a histone macroH2A1 splice variant (Figure 1.5a). Macrodomains consist of five α-helices and a seven-stranded β-sheet arranged in a 3-layer $\alpha/\beta/\alpha$ sandwich (Figure 1.5c). ADP-ribose is bound in a groove on top of the β-sheet. Similar to other reader domains, the adenine ring of ADP-

ribose stacks with an aromatic amino acid (tyrosine or phenylalanine). Meanwhile, N6 of adenine forms a hydrogen bond with a conserved aspartate (Figure 1.5b). Additional residues at the bottom of the groove and in two loops (loop 1 and loop 2) stretching over ADP-ribose make additional contacts with the pyrophosphate and distal glucose to further stabilise the binding (Rack et al. (2016)) (Figure 1.5a). MacroH2A1.1 is a striking example for the significance of macrodomains in ADP-ribose recognition (Figure 1.5). It recognizes auto-ADP-ribosylated PARP1 and in response triggers increased chromatin density and γ-H2AX levels and inhibits recruitment of the non-homologous end-joining (NHEJ) protein Ku70 (Timinszky et al. (2009)). The macrodomain of another protein involved in chromatin remodelling, amplified in liver cancer 1 (ALC1) , has been shown to be required for its ATPase activity (Gottschalk et al. (2009)).

1.1.4 Erasers of ADP-ribosylation

Erasers of ADP-ribosylation can be split in two families: the ARH and the macrodomain family. While all members of the ARH family are classified as ADP-ribose hydrolases, not all macrodomains possess catalytic activity.

Macrodomains

Similar to ARTs and Sirtuins, macrodomains have be found in all three domains of life, although - like many other systems including ARTs - they appear more regularly and in greater number with increasing complexity of the organism. They can be grouped into six classes: MacroH2A-like, MacroD-type, ALC1-like, PARG-like, Macro2-like and SUD-M-like. Four of these - MacroD-type, MacroH2A-like, ALC1-like and PARG-like - are present in humans. Members of the MacroH2A-like group are generally catalytically inactive, while members of the PARG-like group are associated with PAR hydrolysis and members of the MacroD-type group with MAR hydrolysis. ALC-1-like macrodomains are also mostly catalytically inactive, apart from terminal ADP-ribose protein glycohydrolase (TARG1) (Rack et al. (2016)).

Both MacroD-type macrodomain-containing proteins, MacroD1 and MacroD2, and the ALC1-type protein TARG1 are mono-ADP-ribose hydrolases. However, their reaction mechanism is substantially different. MacroD-type enable hydrolysis of the ADP-ribose chain by hydrogen-bonding the 2” hydroxyl group of the distal ribose in a strained con-

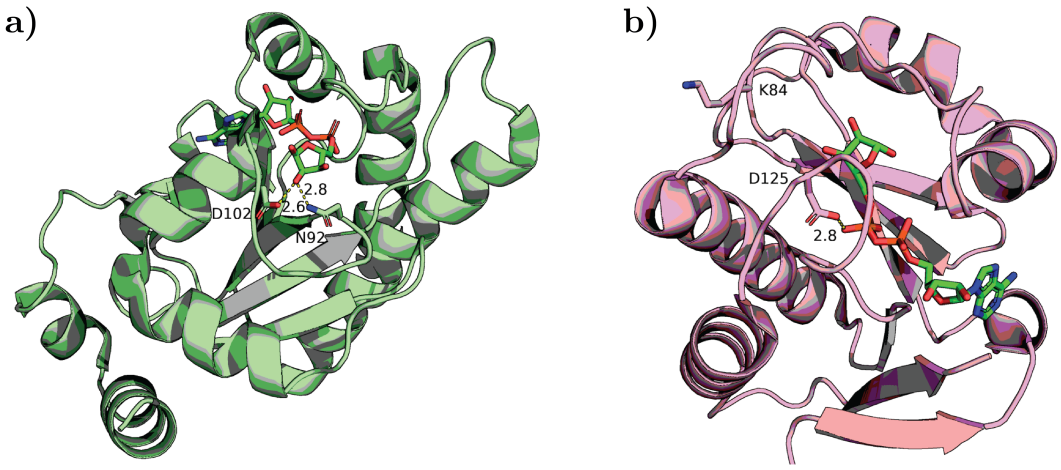


Figure 1.6: *Crystal structures of hMacroD2 and hTARG1.* **(a)** Structure of macroD2 bound to ADP-ribose (PDB: 4IQY). Highlighted are D102 and N92 and their hydrogen bonds with the 2" hydroxyl group of the distal ribose. **b)** Structure of TARG1 bound to ADP-HPD with the catalytic residues K84 and D125 highlighted (PDB: 2L8R). The hydrogen bond between D125 and one of the oxygen atoms of pyrophosphate.

formation through a conserved aspartate residue (Rack et al. (2020)) (Figure 1.6a).This allows the nucleophilic attack on the α-1" position by a water molecule. In some proteins electron withdrawal from the distal ribose ring might also be aided by the coordination of the 2" hydroxyl group through a additional conserved asparagine, although this residue could serve the purpose of protecting the hydroxyl group from a water molecule (Rack et al. (2020)). Figure 1.6a illustrated the conserved aspartate (D102) and asparagine (N92) of human MacroD2 (Jankevicius et al. (2013)). TARG1, on the other hand, uses a lysine residue to form a lysyl-ADP-ribose intermediate, which is subsequently resolved by a catalytic aspartate residue (Figure 1.6b). Additionally, the hydroxyl group of C2" of the proximal ribose remains accessible to subsequent ADP-ribose units, allowing TARG1 to remove both MAR as well as PAR from a target proteins (Rack et al. (2016)). The catalytic lysine (K84) and aspartate (D125) of human TARG1 are highlighted in Figure 1.6b. Despite their different reaction mechanisms all three proteins cleave the same type of ADPr, removing mono/poly-ADP-ribose from acidic (glutamate and aspartate) residues (Jankevicius et al. (2013), Rosenthal et al. (2013), Sharifi et al. (2013)). Poly-ADP-ribose glycohydrolase (PARG) , the namesake of the PARG-like group of macrodomains, is the only type of macrodomain-containing protein to be able to cleave within PAR chains. In contrast to MacroD1, MacroD2 and TARG1, a catalytic glutamate forms an oxocarbe-

nium intermediate of the terminal (*n*) ADP-ribose unit by protonating the C2' OH-group of adenine-proximal ribose of the (*n-1*) ADP-ribose unit, cleaving the α-2,1-glycosidic bond. Subsequently, a water molecule located in close proximity is activated by the same (now de-protonated) glutamate and carries out a nucleophilic attack on C5" of the adenine-distal ribose of the terminal (*n*) ADP-ribose unit, leading to the release of ADP-β-ribose and (*n-1*) PAR (Kim et al. (2012), Slade et al. (2011), Tucker et al. (2012)). While this reaction mechanism describes the exo-glycohydrolase activity of PARG, it also possesses endo-glycohydrolase activity (Barkauskaite et al. (2013), Tucker et al. (2012)). However, PARG is not able to remove the intial ADP-ribose unit attached to the target protein, relying on MacroD1, MacroD2, TARG1 and members of the ARH family to catalyze its hydrolysis.

MacroD1 and MacroD2 have both been implicated in a series of vital cellular pathways. MacroD1 stimulates NF-κB activity, negatively regulates the insulin pathway and acts as a co-factor of the ERα and androgen receptor, while MacroD2 has been shown to act in response to DNA double strand breaks and in WNT-signalling. Unsurprisingly, aberrations in the gene locus of MacroD1 and MacroD2 have been associated with various cancers and - in the case of MacroD2 - also disorders such as schizophrenia and autism (Rack et al. (2020)). Both proteins are generally present in the nucleus, although MacroD1 has been shown to also appear in the cytosol and in mitochondria, where its role remains elusive (Agnew et al. (2018), Rack et al. (2020)). TARG1, which is also a nuclear protein, has found to be mutated in patients with severe neurodegeneration and could act in PAR-driven cell death (parthanatos) by releasing PAR catalyzed by PARP1 in response to DNA damage (Sharifi et al. (2013)). Parthanatos arises from PARP1 overactivation and excessive PAR formation, which in neurons occurs in response to the generation of DNA damage-inducing oxidants (Robinson et al. (2019)). Following cleavage of PAR by TARG1, the chains are translocated to mitochondria and trigger the release of apoptosis-inducing factor (AIF) from the intermembrane space. Finally, AIF travels to the nucleus, where it causes chromatolysis (Fatokun et al. (2014), Robinson et al. (2019)). PARG possesses stronger catalytic activity than TARG1 and is the main actor in poly-ADP-ribosylation reversal. It mainly degrades PAR chains through its exoglycoside activity, preventing NAD^+ depletion, DNA repair defects and replication stress (Gravells et al. (2017), Houl et al. (2019), Shirai et al. (2013)). Consequently, the lack of PARG is lethal in mouse

embryos (O'Sullivan et al. (2019)).

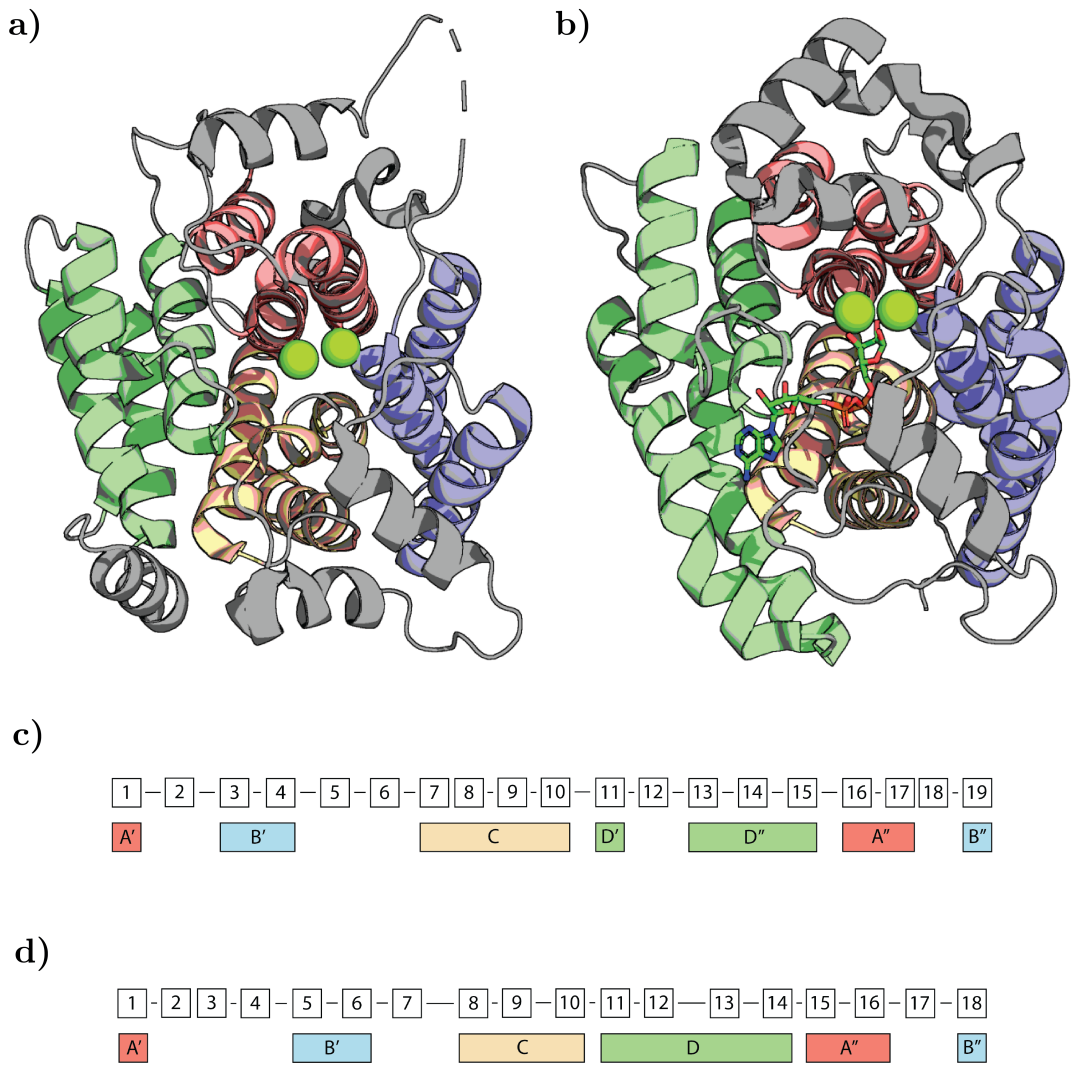


Figure 1.7: *Crystal structures and domain separation of* ***(a)****,* ***(c)*** *hARH3 (PDB: 2FP0) and* ***(b)****,* ***(d)*** *hARH1 (PDB: 6G28).* The quasidomains were colored in *salmon* (quasidomain A), *lightblue* (quasidomain B), *wheat* (quasidomain C) and *palegreen* (quasidomain D). **a)** Of the nineteen α-helices of ARH3, thirteen arrange into four quasidomains (A, B, C and D). The α-helices bundles of quasidomains A and C form opposite sides of the proteins centre, with quasidomains B and D positioned at either side of the interface between quasidomain A and C. **b)** hARH1, here shown with bound ADP-ribose, possesses a very similar α-helical arrangement to hARH3, containing 18 α-helices, of which 12 are arranged into the four quasidomains. **c)** Quasidomain structure of hARH3. **d)** Quasidomain structure of hARH1.

ADP-ribose hydrolases

The ARH family of ADP-ribose hydrolases (ARH) consists of three members in mammals: ARH1, ARH2 and ARH3. Of these, only ARH1 and ARH3 have so far been shown to harbour catalytic activity . Although very different in their primary sequence, both proteins are of similar (around 39 kilodaltons (kDA)) size and structure (Figure 1.7). Resolution of human ARH3 (hARH3) crystal structure identified it to be an all α-helical protein. The domain core is composed of thirteen α-helices organised into four quasidomains (A-D) surrounded by a variable number of auxiliary α-helices (e.g. human ARH3 contains a total of nineteen α-helices (Mueller-Dieckmann et al. (2006)) (Figure 1.7a and c). A very similar domain structure was later shown for the crystal structure of human ARH1 (hARH1) (Figure 1.7b and d) (Rack et al. (2018)).

All active ARH family members contain a binuclear metal centre crucial for the catalytic reaction. For ARH1 and ARH3 this centre is populated by two Mg^{2+} ions (Mg_I and Mg_{II})with each ion octahedrally coordinated in the resting state (Figure 1.7). The coordinating motifs, although highly similar, are distinctive: E$\cdots$**SDD**T$\cdots$*D*S**D***S* for ARH1 and E$\cdots$**[T/S]DD**T$\cdots$*D*T**D***T* for ARH3, where the amino acids in **bold** are coordinating the first and the amino acids in *italics* are coordinating the second Mg^{2+} ion (Rack et al. (2018)). Additional coordination is provided by water molecules and bound ADP-ribose (Figure 1.7b). Both Mg^{2+} ions are required for catalytic activity and mutation of a single coordinating amino acid results in catalytic inactivity of the protein (Rack et al. (2018)). Despite their structural similarity, ARH1 and ARH3 have different substrate specificities. While both are primarily mono-ADP-ribosylhydrolases and possess only much weaker activity against PAR, ARH1 hydrolyses ADP-ribosyl-arginine and ARH3 hydrolyses ADP-ribosyl-serine (Abplanalp et al. (2017), Fontana et al. (2017), O'Sullivan et al. (2019), Rack et al. (2021, 2020)). This distinction in their function has been attributed to differences in adenosine and pyrophosphate binding between the two proteins (Rack et al. (2018, 2020)). While the exact catalytic mechanism remains elusive for hARH1, the basis of hARH3 catalytic function has recently been resolved (Rack et al. (2021)). In its unbound state, the catalytic glutamate (E41) of hARH3 interacts with Mg_{II}, leaving it highly inflexible in a so called *closed* conformation. Serine-ADP-ribose (of e.g. histone H2B MARylated on S7) binding relieves this interaction, allowing E41 flexibility and an

open active site. Additionally, the substrate breaks up an interaction between Mg_{II} and Y137 and places Mg_{II} in a high energy state. Displaced E41 helps in the activation of a water molecule involved in Mg_I coordination, which then attacked C1" of the distal ribose, leading to the break of the glycosidic bond between n ribose and serine. The resultant oxocarbenium ion is stabilized by another water molecule that is able to enter the active site after cleavage. Finally, serine is displaced from Mg_{II} coordination by E41 and the original closed confirmation of hARH3 assumed again (Rack et al. (2021)).

While humans have redundant activity for the hydrolysis of glutamate and aspertate ADP-ribosylation with MacroD1, MacroD2 and TARG1, it is interesting to note that ARH1 and ARH3 are the only known proteins to carry out their specific subtype of mono(ADP-ribossyl)hydrolase reaction in humans. Consequently, aberrations in these proteins have serious phenotypic consequences. ADP-ribosyl-arginine hydrolase activity of ARH1 is, for example, crucial in the defence against the *Vibrio cholerae* bacterial toxin and ART cholera toxin, which MARylate proteins on arginine residues. Loss of ARH1 has thus been shown to render mice sensitive to cholera toxin-induced disease states. (Ishiwata-Endo et al. (2020), Mashimo et al. (2014)). ARH1 deficiency has also been shown to be associated with tumorigenesis and cell proliferation (Ishiwata-Endo et al. (2020), Kato et al. (2015), Mashimo et al. (2014)). Finally, targets of ARH1 include proteins involved in wound healing, stress response and processes in heart and skeletal tissue (Ishiwata-Endo et al. (2020), Leutert et al. (2018)). As a result, mutation or loss of ARH1 affects muscle performance and heart tissue repair. A similar situation is true for the ADP-ribosyl-arginine hydrolase activity of ARH3. This is particularly relevant in the DNA damage response (DDR), where serine-linked ADPr is the predominant form of ADP-ribosylation (Palazzo et al. (2018)). To prevent the formation of excessive PAR, the dangers of which I highlighted under *Macrodomains* in *1.1.4 Erasers of ADP-ribosylation*, ARH3 assists PARG in its hydrolysis (Mashimo & Moss (2016)). More crucially however, it removes serine-linked mono-ADP-ribose that cannot be removed by PARG (Palazzo et al. (2018)). As described in more detail in *1.2.3 PARP1 in DNA damage repair*, the repair of DNA single strand breaks involves PARP1-catalyzed PARylation of histones on serines sites. Absence or catalytic inactivity of ARH3 leaves these histones MARylated, causing transcriptional deregulation (Hanzlikova et al. (2020)). As a result, patients carrying bi-allelic loss of

function mutations in ARH3 suffer from neurodegeneration associated with the role of ARH3 in DDR (Danhauser et al. (2018)).

1.2 DNA repair PARPs

One of the five clades of human PARPs are DNA repair PARPs, which encompass the proteins PARP1, PARP2 and PARP3. Of these, PARP1 and PARP2 have been shown to carry PARylation activity and PARP3 MARylation activity. In the following, I will mainly focus on the function and ascribed roles of the most prominent member of this clade, PARP1, and subsequently also briefly summarize certain functions ascribed to PARP2 and PARP3.

1.2.1 PARP1 catalytic activation

A graphic representation of the beads-on-a-string catalytically inactive confirmation of PARP1 is shown in Figure 1.8 (Mansoorabadi et al. (2014). In this relaxed, pre-DNA binding state, the different domains of PARP1 show little interaction, However, the six α-helices of the HD are folded onto the ART domain and partially covers the active sites, thus inhibiting catalytic activity (Figure 1.8). Langelier and colleagues were the first to show that DNA damage recognition by ZnF1, ZnF3 and WGR leads to an intramolecular signal transduction cascade that activates PARP1 catalytic activity (Langelier et al. (2012)). To achieve crystallisation of the activated PARP1, the authors had to delete the ZnF2 and BRCT domains, yet the structural data together with extensive biochemical characterisation of the protein showed that both regions are dispensable for catalytic activity. The two zinc finger motifs essential for DNA binding, ZnF1 and ZnF3, both make contact with the WGR domain, which is separated from the ART domain by the HD. The described signal transduction cascade was later shown to achieve catalytic activation by effecting a compact form of PARP1, in which the HD is unfolded (Dawicki-McKenna et al. (2015), Steffen et al. (2016)).

In its DNA-bound form, several inter-domain contacts confer the signal of DNA binding by the N-terminal portion of PARP1 to its C-terminus and HD, triggering a conformation change that opens the active site, thus activating the enzyme. Generally, these contacts can be divided into being of the nature ZnF1-WGR-HD and ZnF1-ZnF3-WGR-HD (Langelier & Pascal (2013), Spiegel et al. (2021)). A critical set of contacts in the ZnF1-WGR-HD interface is between D45 of ZnF1, R591 of the WGR domain, hydrophobic contact points in αE of the HD. In ZnF1-ZnF3-WGR-HD signalling, residues R78 and W79 in

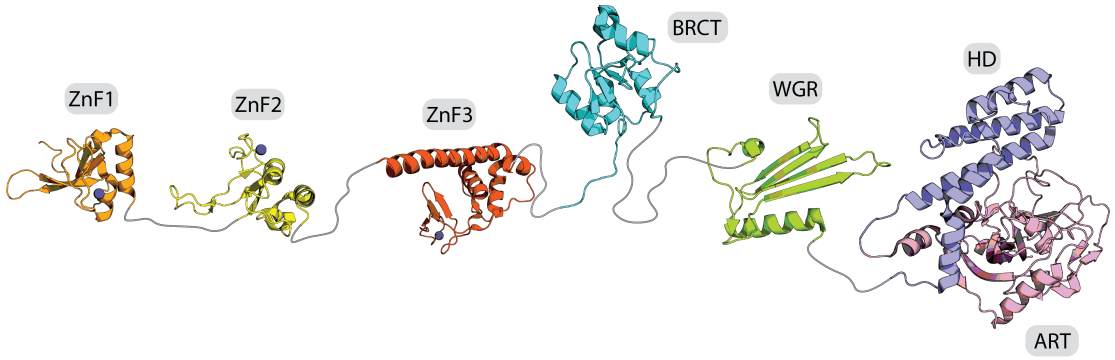


Figure 1.8: Illustration of beads-on-a-string conformation of catalytically inactive, unbound PARP1. The HD and ART domains of the PARP1 catalytic domain are already in contact and the HD is preventing the ART domain from binding NAD^+. The WGR domain is also already in close proximity to the CAT domain, while the other domains are more flexibly connected with each other. The length of the strings between the separate *beads*, i.e. domains, is not representative of the actual number of unstructured amino acids between the domains.

the C-terminal α-helix of ZnF1 form an interface with residues K238 and W246 of the N-terminal ZnF3 α-helix near their contact with DNA (Langelier et al. (2012)). W318 of ZnF3 interacts both with Lys633 of the WGR and Arg735 of the HD (Langelier et al. (2012)). ZnF2, on the other hand, is not involved in catalytic activation owing to the properties of its base-stacking loop, which does not contain an equivalent residue to D45 of ZnF1, and to the specifics of its location on DNA in relation to the other domains, described in *1.2.2 DNA binding of PARP1* (Langelier et al. (2011)).

On the other, C-terminal, end, these newly formed interactions lead to the breaking up of a different interface, that between the HD and ART domain. The HD blocks PARP1 catalytic activity by preventing the binding of NAD^+ to the catalytic fold (Figure 1.9). This occurs at two points. Firstly, αF of the HD interacts with residues of the active site loop (ASL or D-loop). Secondly, the C-terminal portion of αF of the HD interacts with the fourth α-helix of the ART domain, αJ, labelled so in continuation of the α-helix numbering in the HD. Both contacts are being disrupted in the compacting of PARP1 upon DNA binding. The loss of these contacts is the result of unfolding events (Figure 1.9). This includes unfolding to various degrees of the α-helices αB, αC, αD and αF (Spiegel et al. (2021)). Unfolding of αC could be attributed to the eviction of two conserved residues of the HD, L698 and L701 (*leucin switch*), from the hydrophobic core in the initial structure of PARP1 bound to DNA (Langelier et al. (2012)) (Figure 1.9). The magnitude

of helix unfolding in the HD was only later discovered with the use of hydrogen/deuterium exchange-mass spectrometry (HXMS) (Dawicki-McKenna et al. (2015)). The fact that mutations of any of the above mentioned inter-domain contact points abolished DNA-dependent catalytic activation of PARP1 points to their indispensable role in the unfolding of the HD. Similarly, mutation of L698 or L701 results in mild catalytic activity of unbound PARP1, which is not restored to wildtype levels in the presence of DNA (Langelier et al. (2012)).

Together, these findings establish PARP1 as a protein that is activated upon binding to a DNA substrate through a a series of N- to C-terminal intramolecular signalling events. While PARP2 and PARP3 lack zinc finger binding motifs, the existence of both an HD and WGR domain in both proteins indicates that a sequence of interaction events as a results of DNA binding might also be taking place for their activation. Further understanding of the functions of PARP1 is provided by findings identifying which DNA substrates PARP1 specifically binds to. This is outlined in the section below.

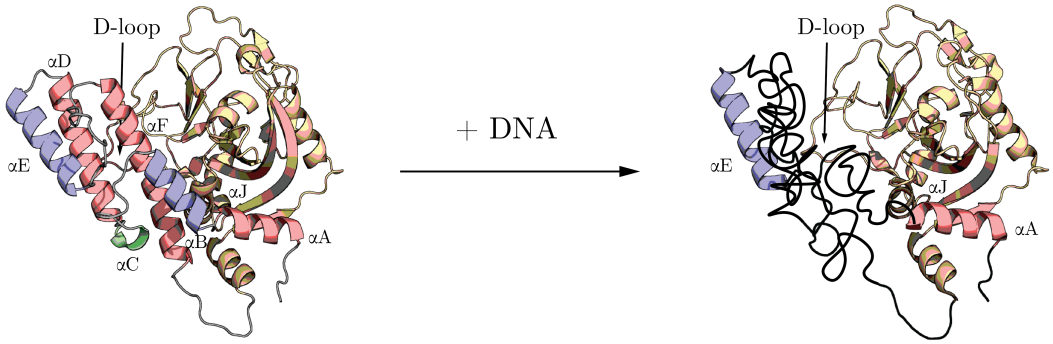


Figure 1.9: *Graphical illustration of HD unfolding.* The illustration is based off the crystal structure of unbound PARP1 catalytic domain (PDB: 1A26, left) and the crystal structure of DNA bound PARP1 catalytic domain (PDB: 4dqy). HD helices αB, αC, αD and αF have been replaces by visual representations of unfolded regions (*black* ribbons). The ART domain is shown in *wheat* and the α-helices of the HD are coloured in *salmon* (αA, αC, αE) and *lightblue* (αB, αD, αF).

1.2.2 DNA binding of PARP1

Almost as important as understanding PARP1 catalytic activation is the nature of its binding to DNA. PARP1 can be catalytically activated by binding to a number of different DNA substrates. Studies that specifically investigated the binding of ZnF1 and ZnF2

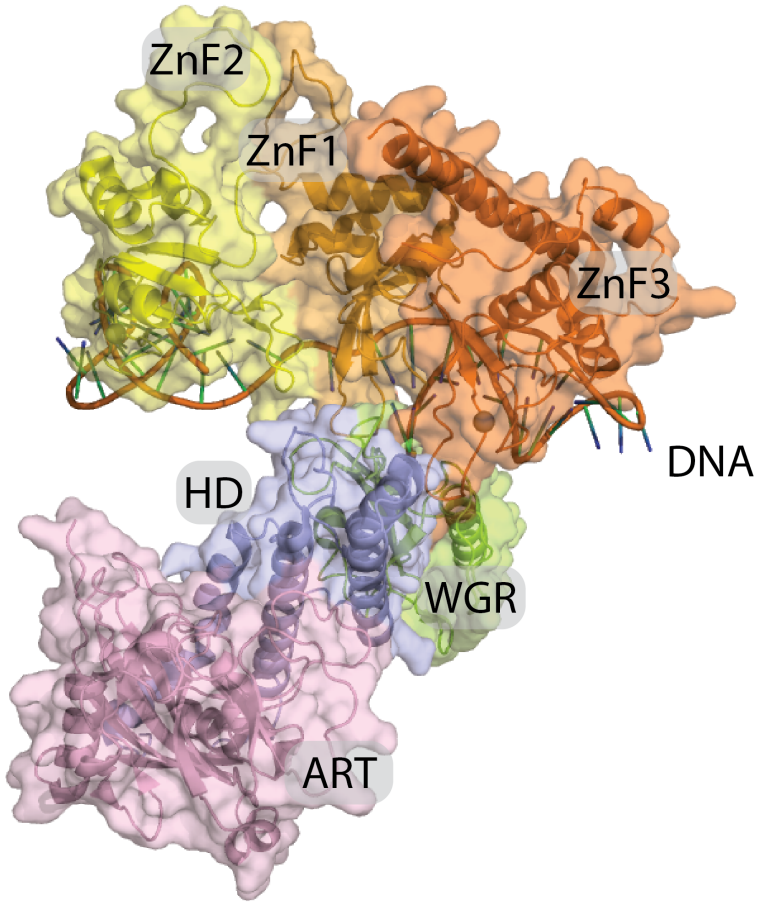


Figure 1.10: Composite model of the ZnF1-ZnF2 fragment bound to a single-strand break (PDB: 2N8A) superimposed on the structure of ZnF1-ZnF3-WGR-CAT (PDB: 4DQY) as seen in the publication of the Neuhaus lab (Eustermann et al. (2015)). ZnF2 is labelled in *yellow*, ZnF1 in*lightorange*, ZnF3 in *orange*, the WGR domain in limon, the HD in *lightblue* and the ART domain in *lightpink*.

to DNA have helped to complete the picture of PARP1 binding: ZnF1 and ZnF2 are each themselves able to bind the end of a DNA double-helix through sequence-independent interactions (Langelier et al. (2011)) (Figure 1.10). The positively charged concave surfaces of ZnF1 and ZnF2 form hydrophobic interfaces with the phosphate backbone of the major and minor grove (phosphate backbone grip), respectively, with residues reaching into the helix to form hydrogen bonds with base pair edges (base stacking loops)(Ali et al. (2012), Langelier et al. (2011)). Loss of ZnF2, but not ZnF1, alone reduces the binding ability of a ZnF1-ZnF2 fragment 3-fold, indicating that ZnF2 is more important for DNA binding (Langelier et al. (2011)).In addition, ZnF3 makes contact with the DNA on the minor grove adjacent to ZnF1 and the WGR domain interacts with the 5' end of the DNA

through W589 stacking against the sugar of the terminal nucleotide.
In line with functions attributed to PARP1 in the DNA damage response (outlined below), PARP1 is able to bind DNA single-strand breaks (SSB) (Figure 1.10). This process is guided and mostly accomplished by ZnF2, whereas ZnF1 binds more weakly (Eustermann et al. (2011)). A model was proposed whereby ZnF2 first recognizes SSBs, binds at the more easily accessible 3' side and directs the positioning of ZnF1 on DNA. A flexible linker region between ZnF1 and ZnF2 allows binding of ZnF1 on the opposite, 5' side of the single-stranded DNA gap in the fashion of a *fly-casting* mechanism. A similar process could also be imagined for double-strand break (DSB) binding of PARP1, if the two ends of the break are in close proximity to each other (Eustermann et al. (2011)). ZnF1-ZnF2 binding to DNA sets in motion the subsequent steps enabling catalytic activation. Due to their positioning on opposite ends of the DNA break, only the top of the ZnF1, but not the ZnF2, base-stacking loop shares an interface with the WGR domain (Figure 1.10). Additionally, ZnF3, which is connected with ZnF2 through another flexible linker region and contacts the WGR domain through its extended loop, is located behind ZnF1 on the 5' end of the DNA break (Eustermann et al. (2015), Langelier et al. (2012)) (Figure 1.10). Consequently, PARP1 catalytic activation is orchestrated from ZnF1, but not ZnF2.

Interestingly, ZnF1 and ZnF2 do not directly interact with the 3' and 5' end of the DNA, making PARP1 recognition of DNA damage sites independent at least of small-chemical-group modifications (Eustermann et al. (2015)). This is in line with findings that PARP1 binds equally well to a DNA dumbbell with a nick, 3'-phosphorylated and 5'-phosphorylated double-stranded DNA (dsDNA) . Only binding to blunt dsDNA alone was slightly lower (Krüger et al. (2020)). In contrast, PARP2 and PARP3 were shown to be selectively activated by 5'-phosphorylated DNA substrates and PARP2 reported to mainly detect DNA nicks (Langelier et al. (2014), Sukhanova et al. (2016)). Finally, even a mechanism by which PARP1 searches the genome for DNA damage sites has been proposed, suggesting a mode of PARP1 finding and binding to its preferred DNA substrates in the first place (Rudolph et al. (2018)). Having established the mode of DNA binding by PARP1, the following sections will highlight how this translates to the protein's function in the human DNA damage response.

1.2.3 PARP1 in DNA damage repair

PARP1 contributes to multiple DDR pathways in the repair of a large number of lesions. Below I will highlight several repair pathways in human cells that PARP1 is involved in. I will give a brief summary of the keys stages and players of each pathway and will describe how PARP1 fits into that picture. PARP1 contributes to DDR in multi-faceted ways difficult to delineate in experimental set-ups. The herein highlighted functions of PARP1 therefore represent a non-exhaustive list of its activities in some of the most well-studied human DNA repair pathways. The following section engages less with the impact of PARP1 on the ability of cells to repair certain types of DNA damage, since these findings often do not reveal the mechanistic basis behind the reported phenotypes. Rather, it focuses on the timely occurrence and nature of PARP1 engagement in the pathways highlighted below.

While PARP1 fulfils certain roles in the DNA repair pathways outlined below, it should be highlighted that some of its functions, such as auto-ADP-ribosylation, concern the players of multiple pathways and others promote DNA repair only indirectly. Two of the main targets of PARP1-catalyzed poly-ADP-ribosylation, PARP1 itself and histones, are prime examples that support this statement. PARP1 auto-modification is important both for the recruitment of different DNA repair factors, discussed below, and for the release of PARP1 from DNA (Pascal (2018)). The attachment of negatively charged ADP-ribose units onto histones is thought to result in the electrostatic repulsion from DNA and this enable chromatin de-condensation (Messner & Hottiger (2011), Strickfaden et al. (2016), Tallis et al. (2014)). Chromatin de-condensation strongly facilitates the accumulation of DDR proteins at DNA damage (Ray Chaudhuri & Nussenzweig (2017)). PARP1 also promotes DNA damage site accessibility by recruiting or ADP-ribosylating chromatin remodellers such as amplified in liver cancer 1 (ALC1) and SMARCA5/SNF2H, or the histone chaperons Aprataxin, APLF and facilitates chromatin transcription (FACT) (Ahel et al. (2009), Huang et al. (2006), Mehrotra et al. (2011), Pines et al. (2012), Smeenk et al. (2013)). Other ways in which PARP1 assists chromatin stability is by influencing transcription. The tumour-suppressor protein and transcription factor p53 is one of the most important responders to cellular stress, impacting DNA repair, cell cycle progression, senescence and cell death (Hafner et al. (2019)). P53 can bind auto-modified PARP1, is functionally im-

paired in the absence of PARP1, and its ADP-ribosylation was shown to prevent its export from the nucleus (Kanai et al. (2007), Malanga & Althaus (2005), Malanga et al. (1998), Mendoza-Alvarez & Alvarez-Gonzalez (2001)). Beyond p53, PARP1 affects transcription by recruiting transcriptional silencers such as the NuRD and polycombe complexes in a PAR-dependent manner, reportedly to produce a transcriptionally repressive state at sites of DNA damage (Chou et al. (2010), Tallis et al. (2014)). In addition, the NuRD and polycombe complexes are themselves directly involved in DNA repair through signalling of histone ubiquitylation (Gieni et al. (2011), Smeenk et al. (2010)). However, CHD3 and CHD4, two subunits of the NuRD complex, were later shown to accumulate at DNA damage sites due to PARP1-dependent chromatin decondensation rather than through PAR binding, highlighting the complexities of discerning the different functions of PARP1 in DDR (Smith et al. (2018)). Finally, in the presence of DNA damage levels that trigger PARP1 catalytic overactivation, excessive PAR formation invokes parthanatos, a form of cell death (see *1.1.4 Macrodomains*). Having illustrated some of the general functions of PARP1 in response to DNA damage, I will now address how these translate to specific roles in some of the major DNA repair pathways.

PARP1 in base excision repair

Base excision repair (BER) processes many different types of DNA lesions including altered (deaminated, some alkylated or oxidated) bases, SSBs and abasic (apuric/apyrimidinic or AP) sites (Spiegel et al. (2021)). Removal of a damaged base is catalyzed by a group of enzymes collectively known as DNA glycosylases. Subsequently, AP-endonuclease 1 (APE1) excises the DNA backbone 5' of the remaining deoxyribose, leaving a nicked DNA containing a one-base gap. A central factor in the continuation of the repair process is XRCC1, which serves as a platform for many downstream DNA synthesis, ligation and stimulating factors including polymerase β, PNKP, DNA ligase 1 and 3 and proliferating cell nuclear antigen (PCNA) (Caldecott (2003, 2019)). Ultimately, repair is completed by either single-nucleotide / short-patch BER or, where ligation is not immediately possible, by long-patch BER (Beard et al. (2019). Short-patch BER employs polymerase β for gap-filling and predominantly ligase 3 for ligation. Long-patch BER includes strand-displacement DNA synthesis of 2-12 nucleotides by polymerase β, δ and/or ϵ, cleavage by flap endonuclease 1 (FEN1), both stimulated by PCNA, and ligation predominantly by

DNA ligase 1 (Caldecott (2008), Gary et al. (1999), Jónsson & Hübscher (1997)). PARP1 recognizes the nicked DNA species produced by APE1 and as a result is catalytically activated. Its main role upon activation stems from its ability to recruit core members of BER (Figure 1.11). In line with this, the recruitment of XRCC1 to DNA damage sites is dependent on PARP1 catalytic activity (Reynolds et al. (2015)). However, the mechanistic basis for XRCC1 recruitment is unclear. While XRCC1 possesses two BRCT domains and could act as reader of auto-modified PARP1, four potential serine ADP-ribosylation sites on XRCC1 have also appeared in a mass spectrometry screen (Larsen et al. (2018)). Conversely, the loss of XRCC1 has been associated with PARP1 hyperactivity and was shown to coincide with the persistence or *trapping* of PARP1 at DNA damage sites (see *1.2.6 PARP1/2 inhibition*, indicating a tight interplay between the two proteins (Demin et al. (2021), Hoch et al. (2017), Shao et al. (2020)).

PARP1 in nucleotide excision repair

Bulky DNA lesions are repaired by nucleotide excision repair (NER) (Kusakabe et al. (2019)). This type of DNA helix-distorting lesion includes base adducts such as DNA-protein crosslinks (DPC) caused by metabolic by-products and chemotherapeutic agents as well as intra-strand crosslinks (ICL), such as 6-4 photoproducts (6-4PP), caused by UV irradiation (Gillet & Schärer (2006), Kusakabe et al. (2019)). Ironically, a subset of DPCs, enzymatic DPCs, can also be formed by PARP1, especially following protein stalling at AP sites in BER as a result of PARP1 inhibition (Prasad et al. (2020)). NER is divided into two sub-pathways, global genome nucleotide excision repair (GG-NER) and transcription-coupled nucleotide excision repair (TC-NER). PARP1 supports GG-NER, the dominant of the two sub-pathways (Ray Chaudhuri & Nussenzweig (2017)). One central repair factor in GG-NER is Xeroderma Pigmentosum C (XPC), which scans DNA for non-hydrogen-bonded nucleotides and forms a dimer with UV excision repair protein RAD23 homolog B (RAD23B) (Clement et al. (2010), Sugasawa et al. (1998), Volker et al. (2001)). However, a subset of UV-induced lesions is not recognized by XPC itself and requires initial detection by the UV-DDB ligase complex (Sugasawa (2010)). The XPC/RAD23B dimer directs the subsequent repair step of DNA unwinding, which is followed by strand incision, gap filling and DNA ligation (Schärer (2013)). Research suggests that XPC forms a complex with PARP1 before binding to damage sites and that this complex favours its deposition at sites

already harbouring the UV-DDB ligase complex of DNA damage binding protein 1 and 2 (DDB1 and DDB2), E3 ubiquitin-protein ligase RBX1 and the E3-regulating, auxiliary protein Cullin-4A (Robu et al. (2017)). Additionally and independently of its role in XPC deposition, PARP1 is capable of binding to UV-based DNA lesions and directly interacts with and ADP-ribosylates DDB2 (Purohit et al. (2016), Robu et al. (2013)). Ubiquitylation activity of the UV-DDB ligase complex in turn promotes chromatin decondensation and XPC stabilization (Robu et al. (2013)). The described roles of PARP1 in NER thus highlight its significance in supporting the initiation of this repair pathway.

PARP1 in homologous recombination

Homologous recombination (HR) is the main repair pathways of DSBs in S-phase cells. Similar to other DNA repair pathways, HR consists of several steps, mainly presynapsis, synapsis and postsynapsis (Heyer et al. (2010)). Presynapsis involves the recruitment of the MRN (MRE11-RAD50-NBS1) complex, which resects DNA and reveals ssDNA overhangs on both sides of the DSB, and subsequent binding of replication protein A (RPA). In synapsis, the DNA repair protein RAD51 binds and replaces RPA at ssDNA stretches and searches for and invades their homologous DNA regions on the intact sister chromatid (Sun et al. (2020)). Finally, DNA synthesis and ligation occur in postsynapsis. This process is again divided in several sub-pathways, of which two major ones are the synthesis-dependent strand annealing (SDSA) and the double-Holliday junction (dHJ) sub-pathways (Prakash et al. (2015)). They deviate firstly in the set of proteins employed, where the dHj sub-pathway requires a specific set of nucleases for the resolution of the repair intermediate (Castor et al. (2013), Rass et al. (2010)). Secondly, they result in different end products, with the dHj sub-pathways allowing for crossover products (Heyer et al. (2010)). Two essential proteins of the HR pathway are Breast cancer type 1 (BRCA1) and 2 (BRCA2) . Although BRCA1 and BRCA2 come together in a complex also containing Partner And Localizer of BRCA2 (PALB2) and RAD51, they carry out different roles in HR (Wu et al. (2020). While BRCA2 is responsible for loading RAD51 onto ssDNA, BRCA1 promotes HR and another double-strand break repair pathway, single strand annealing (SSA), by encouraging DNA end resection at DSBs (Chen, Feng, Lim, Kass & Jasin (2018), Prakash et al. (2015)). As their names suggest, deleterious mutations in BRCA1 and/or BRCA2 are associated with a range of cancers, especially

breast and ovarian cancer (Heeke et al. (2018), Iqbal et al. (2012), Mersch et al. (2015), Moran et al. (2012), Petrucelli et al. (2010)). As a result, HR is deficient in these cancers (Ladan et al. (2021), Nguyen et al. (2020)). PARP1 trapping at DNA damage sites strongly increases the load of DSBs in a cell, which remain insufficiently or unfaithfully repaired in BRCA1/2-mutated and other HR-deficient cells. Following the development and FDA approval of the PARP inhibitor Olaparib (AstraZeneca, Lynparza) in late 2014, PARP inhibition has thus been exploited to trigger genome instability and cell death in HR-deficient tumours (Kim et al. (2015), O'Connor (2015)). While this strategy targets PARPs PARP1 and PARP2, it is believed to exploit not the inhibition of their functions in HR, but rather the contribution of PARP1 to BER (Figure 1.11). The basis for this consideration is outlined in *1.2.6 PARP1/2 inhibition*.

The role of PARP1 in HR again resembles that in NER and BER described above. Mainly, PARP1 has been reported to facilitate the recruitment of BRCA1 to sites of DSBs (Ray Chaudhuri & Nussenzweig (2017)). Interestingly, PARP1 also helps to prevent excessive HR by PARylating BRCA1, weakening its DNA-binding capacity and stabilizing a complex of PARP1, BRCA1 and the ubiquitin-binding protein receptor-associated protein 80 (RAP80) (Hu et al. (2014)). A second example of both a supporting and limiting role for PARP1 is in DNA end resection. On the one hand, PARP1 facilitates DNA end resection by recruiting MRE11 of the MRN complex (Bryant et al. (2009)). On the other, PARP1 has been reported to limit DNA end resection in HR by binding to DNA ends and promoting loading of the repair factor Ku80, a protagonist in the rivalling DSB repair pathway NHEJ (Caron et al. (2019)).

PARP1 in non-homologous end-joining

Outside of S/G2 phase, where a repair template in form of a sister chromatid does not exist, cells preferably repair DSBs through NHEJ. Given the nature of NHEJ to *seal* a DSB rather than copy a repair template such as in HR, the first step in the pathway, called synapsis, is to bring the two DNA ends in close proximity of each other. The first proteins to bind to the ends are the two DNA helicases Ku70 and Ku80, originally X-ray repair cross-complementing protein 6 (XRCC6) and 5 (XRCC5), respectively, which bind each end as a dimer. In the case of two compatible blunt ends, NHEJ can then join the DSB in a ligation step performed by a dimer of the DNA-binding scaffold protein X-ray repair

cross-complementing protein 4 (XRCC4) and DNA Ligase IV. In most cases, however, the DNA ends are incompatible and their repair occurs through the subsequent reaction steps of resection, polymerase reaction and ligation (Zhao et al. (2020)). Resection is designed to remove incompatible 5' and 3' ends and generally reveals only ≤ 4 nucleotide long regions of microhomology between the two ends of the DSB. These are substantially shorter than the ssDNA stretches of ≤ 20 nucleotides laid bare in HR-directed end resection (Chang et al. (2017)). Resection is carried out by the endonuclease Artemis in complex with DNA-dependent protein kinase catalytic subunit (DNA-PKcs), which acts as a sensor of DNA damage and is strongly enhanced in DNA binding by formation of the looping DNA-PK complex with Ku70 and Ku80 (Ma et al. (2002), Yin et al. (2017)). Where end resection does not reveal a microhomology region, the DNA polymerases Polμ and Polλ are able to extend DNA ends in the presence or absence of a complementary sequence to generate compatible ends (Chang et al. (2017), Pryor et al. (2015)). Finally, the processed DNA ends are ligated again primarily by the XRCC4-DNA ligase IV dimer, together with additional stabilizing factors such as XRCC4-like factor (XLF) (Chang et al. (2017)).

Similar to HR, PARP1 contributes to NHEJ at multiple stages. More than 20 years ago already, ADP-ribosylation of DNA-PKcs by PARP1 was shown to promote its kinase activity, which auto-phosphorylates DNA-PKcs, resulting in the activation of Artemis (Ruscetti et al. (1998)). In an example highlighting the complexity of the fine balance between different DNA repair pathways, the observation of PARP1 promoting the loading of Ku80 appears to stand in contradiction to well-established previous claims that PARP1 competes with Ku80 for DNA ends and promotes a back-up pathway of NHEJ, alternative NHEJ (a-NHEJ), in the absence of Ku80 (Chiruvella et al. (2013), Ray Chaudhuri & Nussenzweig (2017), Spiegel et al. (2021), Wang et al. (2006)). Finally, recruitment of the PAR-binding helicase and chromatin remodeller chromodomain-helicase-DNA-binding protein 2 (CHD2) by PARP1 has also been shown to promote the assembly of the NHEJ repair machinery (Luijsterburg et al. (2016)).

In summary, PARP1 directly contributes to several repair pathways including, but not limited to sensing of different types of DNA damage, recruiting proteins through direct or PAR-directed interaction, modifying proteins through PARylation and competing with

DNA repair factors to favor one type of repair over another. Additionally, PARP indirectly supports DNA repair by these pathways through chromatin remodelling and transcription regulation. Functions of the other two DNA repair PARPs, PARP2 and PARP3 are also emerging, but have so far been less extensively described than PARP1. They are outlined in brief in their own, separate sections below.

1.2.4 PARP2 in DNA damage repair

PARP2 strongly resembles PARP1 in its domain architecture, but lacks the N-terminal region including ZnF1, ZnF2 and ZnF3 (Figure 1.3). Despite this, PARP2 was, similar to PARP1, also reported to be involved in both BER and HR, binds DNA DSBs as a dimer and is catalytically activated upon binding of DNA damage sites by its WGR domain (Bilokapic et al. (2020), Kutuzov et al. (2014), Obaji et al. (2021)). Additionally, its N-terminal regions (NTR) contributes to the recognition of SSBs by PARP2 and the proteins consequent activation, providing a molecular basis for its recruitment to sites of DNA damage in BER (Riccio et al. (2016)). Further specifics of DNA binding by PARP2 include a shared preference with PARP3 for 5'-phosphorylated DNA breaks suitable for ligation and for DNA repair intermediates such as flap-containing structures, which arise in long-batch BER (Kutuzov et al. (2013), Langelier et al. (2014)). While earlier research attributed a timely delayed and less significant role in BER to PARP2 compared to PARP1, later findings have reported a functional redundancy for PARP1 and PARP2 in BER, with XRCC1 and PNKP recruitment only impaired in PARP1 PARP2 double KO cells (De Vos et al. (2012), Hanzlikova et al. (2017), Kutuzov et al. (2014), Ronson et al. (2018)). Interestingly, a similar observation was made for the roles of PARP1 and PARP2 in HR-directed repair of stalled replication forks, where only the combined loss of PARP1 and PARP2 triggered a strong reduction of RAD51 foci formation in cells (Ronson et al. (2018)). This observation could be the downstream effect of aborted PARP1/2-dependent MRN complex recruitment (De Vos et al. (2012)). The illustrated overlap between PARP1 and PARP2 functions in BER and HR presents PARP2 as an important player in the DNA damage response. It can also be hypothesized that certain roles of PARP1 and/or PARP2 in the DNA damage response have so far remained masked when examined in single KO cells due to the two proteins sharing several tasks in the DDR.

1.2.5 PARP3 in DNA damage repair

The domain architecture of PARP3 strongly resembles that of PARP2, which is reflected in both their shared affinity for certain DNA substrates and catalytic activation (Figure 1.3) This follows the same pattern as that of PARP1 while not involving the DNA-binding motifs ZnF1, ZnF2 and ZnF3 (Langelier et al. (2014)). The role of PARP3 in the DNA damage response has mainly been attributed to NHEJ, also named classic NHEJ (c-NHEJ) in distinction to a-NHEJ. More precisely, in one of its functions PARP3 is thought to promote NHEJ by recruiting Ku70/Ku80 to sites of DNA damage and limiting strand resection, a vital step in HR (Beck et al. (2014), De Vos et al. (2012), Rodriguez-Vargas et al. (2019)). Additionally, PARP3 has also been suggested to promote the phosphorylation and presence at DSB of the NHEJ factor Aprataxin and APLF, which recruits the XRCC4-DNA ligase IV dimer (Fenton et al. (2013), Rulten et al. (2011)). While past research has centred around NHEJ, the role of PARP3 in DNA repair is not limited to that pathway. In line with this, PARP3 was also reported to detect DNA nicks at nucleosomes and consequently mono-ADP-ribosylate H2B (Grundy et al. (2016)).

In conclusion, all three human DNA repair PARPs have been implicated in the repair of DNA single- and double-strand breaks, with often at least partially overlapping and at times competing functions that operate on multiple levels including protein recruitment and modifying functions, chromatin remodelling and others. As a result, the inhibition particularly of PARP1 and PARP2 has been exploited in the treatment of DNA damage repair-deficient tumours. Below I provide an up-do-date understanding of how these PARP1/2 inhibitors operate on a molecular level.

1.2.6 PARP1/2 inhibition

In 2005, it was first shown that BRCA1/2-deficient human cancer cells are 1000-fold more sensitive to PARP inhibition than their wildtype counterparts, opening the door to a new therapeutic strategy for the treatment of BRCA1/2-mutated tumours (Bryant et al. (2005), Farmer et al. (2005)). By 2008, a group of inhibitors had been found which showed high potency towards the two PARPs responsible for almost all ADP-ribosylation in cells, PARP1 and PARP2 (Menear et al. (2008)). Only one year later, one of the inhibitors,

Olaparib, was tested in the first phase 1 clinical trial for the treatment of different advanced solid tumours carrying BRCA1 or BRCA2 mutations (Fong et al. (2009)). It subsequently became the first PARP inhibitor to be granted Marketing Authorization by the European Commission for the treatment of advanced BRCA-mutated ovarian cancer based on data from a phase 2 clinical trial (Ledermann et al. (2014)). Since then, Olaparib, marketed by AstraZeneca under the name Lynparza, has been approved for the treatment of several other cancers and in combination with other inhibitors (Boussios et al. (2019), de Bono et al. (2020), Golan et al. (2019), Moore et al. (2018), Robson et al. (2017)). In the meantime, further inhibitors, which all bind to the ADP-ribose binding pocket in the catalytic ART domain, have been developed (Shen et al. (2015)). These have been shown to carry even higher potency for inhibiting PARP1 and PARP2, albeit without completely losing cross-reactivity with the structurally nearly identical ART domains of other PARPs such as PARP3, PARP4 and TNK1 and 2 (Carney et al. (2018), Kirby & Cohen (2019), Steffen et al. (2013)). Some of them, however, were demonstrated to carry dramatically increased PARP1/2 selectivity, with the two inhibitors Veliparib and Niraparib being the most selective due to their ability to form a water-mediated hydrogen bond with a PARP1-specific residue of the catalytic pocket (Slade (2020), Wahlberg et al. (2012)).

Despite the incredible discovery of PARP inhibition as a form of treatment for BRCA1/2-mutated cancers, the debate over the molecular basis behind the toxicity of PARP1/2 inhibitors in these cells remains. The now most commonly accepted notion is that toxicity stems from a plurality of factors, all of which result in the accumulation of DSBs at replication forks or transcription sites (Figure 1.11). PARP1/2 inhibitors therefore exploit what has been referred to as the *Achilles heel* of BRCA1/2-mutated cancers: their reduced ability to repair DSBs by HR at a stage of the cell cycle, when cells predominantly rely on HR. (O'Connor (2015)). The fact that PARP1/2 inhibitors have successfully been used both in maintenance treatment as well as in combination with chemotherapy points to two means by which they are thought to exert their toxicity. These means are i) the disruption of the repair of SSBs and ii) the trapping of PARP1/2 on DNA (Figure 1.11) (Helleday (2011), Lord & Ashworth (2012), Murai et al. (2012, 2014)). More recent literature on this topic has focused increasingly on the PARP1/2 trapping aspect, particularly since PARP1 has also been shown to play a role in replication fork reversal, Okazaki fragment ligation and the HR-mediated restart of replication forks (Figure 1.11) (Bryant et al.

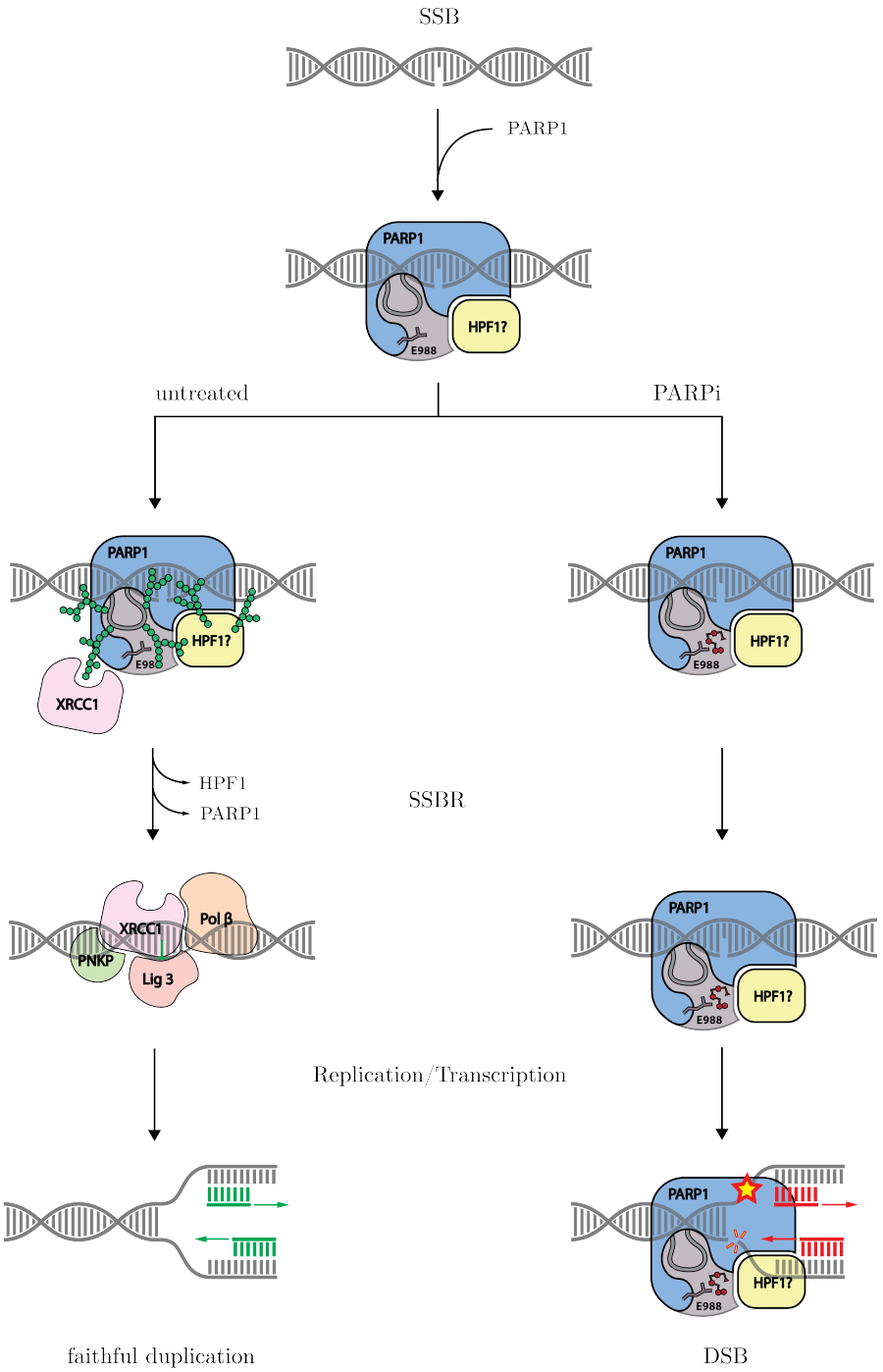


Figure 1.11: *Model to illustrate potential mechanistic basis of HPF1-PARP1 complex-directed serine ADP-ribosylation in SSBR and its inhibition by PARP inhibitors (PARPi).* HPF1 enables PARP1-catalyzed serine auto- and trans-ADP-ribosylation, including possibly HPF1 ADP-ribosylation. One of the central functions of PARP1 in BER - XRCC1 recruitment - is highlighted in the model. PARP inhibition blocks the catalytic activity of DNA-bound PARP1. Consequently, XRCC1 recruitment is prevented. Additionally, PARP1 is trapped at the site of DNA damage. As a result, both the unrepaired SSB and trapped PARP1 present obstacles to DNA transcription and replication, triggering DSB formation.

(2009), Hanzlikova et al. (2018), Slade (2020)). As a result, studying the ability of PARP inhibitors to retain PARP1/2 on DNA has become a particular topic of interest. In addition to the inhibition of the PARP1/2 catalytic site, PARP inhibitor toxicity also stems from the inhibitors' allosteric effects on PARP1/2 binding to DNA. Most strikingly, it has been shown that PARP inhibitors can act on the intramolecular signal transduction cascade for PARP1 compaction and in this way either weaken or strengthen DNA binding of PARP1 (Zandarashvili et al. (2020)). This is referred to as *reverse allostery* and PARP inhibitors that exert a positive allosteric effect on DNA binding are generally regarded as better PARP1 *trappers* than PARP inhibitors having none or a negative allosteric effect. Although it is not clear to what extent reverse allostery determines the ability of PARP inhibitors to be good trappers, reportedly good PARP1 trappers, such as Talazoparib, carry higher toxicity than PARP inhibitors with weaker trapping ability, such as Rucaparib (Hopkins et al. (2019, 2015), Zandarashvili et al. (2020)). A better understanding of the basis of PARP1 trapping, not only regarding PARP inhibition, but also the mechanistic basis of PARP1 dissociation from DNA, will be beneficial for future PARP inhibitor designs and is explored in this thesis.

1.2.7 PARP1/2 and HPF1

One essential contributor to the poly-ADP-ribosyltransferase activity of PARP1 and PARP2 in DNA repair and beyond has so far remained unmentioned. This protein, which is a co-factor, has been termed histone PARylation factor 1 (HPF1) and lies at the centre of the findings described in *3 Results*. Below, I will outline the state of the research at the start of my DPhil course.

In 2016, Ian Gibbs-Seymour and others first described a protein of previously unknown function, C4orf27, with an approximate weight of 35 kDA. This discovery emerged from the search of PBZ-containing proteins following the discovery of the PBZ domain as an ADP-ribose binding domain particularly present in DDR proteins (Ahel et al. (2008)). While human HPF1 itself does not carry a PBZ domain, its orthologues in other species do. The protein was described as binding directly to the ART catalytic domain of PARP1/2 via its C-terminal region (Figure 1.11) (Gibbs-Seymour et al. (2016)). *In vitro* findings showed that HPF1 promotes both PARP1-directed histone trans-ADPr as well as PARP1 auto-ADPr. However, results from cell extracts showed that auto-modified PARP1 under DNA

damage conditions in 293T HPF1$^{-/-}$ contained higher molecular weight fractions, suggesting that HPF1 limits PARP1 hypermodification. The results from PARP1-directed histone trans-ADPr were later also confirmed for PARP2 (Bonfiglio et al. (2017b)). Furthermore, GFP-PARP1 recruitment to sites of laser microirradiation persists in the absence of HPF1 and the loss of HPF1 drives sensitivity to the methylating agent methyl methanesulfonate (MMS) and PARP inhibition (Gibbs-Seymour et al. (2016)). A year later, Bonfiglio et al. found that HPF1 is essential for a novel type of ADP-ribosylation, serine ADPr. While up to this point, ADP-ribosylation was thought to occur only on glutamate and aspartate sites as well as potentially on lysine sites, adding HPF1 to PARP1/2-driven *in vitro* ADPr reactions switched the acceptor residue to serine (Blessing & Ladurner (2020), Bonfiglio et al. (2017b), Vyas et al. (2014)). ADP-ribosylation on serine as well as ADP-ribose chain elongation creates an O-glycosidic bond (Bonfiglio et al. (2017a)). This suggested that the addition of HPF1 to PARP1/2 suspends with the requirement of an nucleophile in form of a hydroxyl group provided by the target amino acid for catalysis of ADPr. Finally, a year later serine was reported to be the main target residue for DNA damage-dependent ADPr in cells (Palazzo et al. (2018)). Interestingly, HPF1 in cells exists at a vastly lower level than PARP1, leading to speculations that it might only be important for initiating serine ADPr following PARP1 activation at sites of DNA damage, since ADP-ribose chain elongation is identical in aspartate/glutamate and serine ADPr (Hein et al. (2015)).

Despite these remarkable first findings, at the start of my DPhil course very little was known about how PARP1 and PARP2 in combination with HPF1 bring about serine ADP-ribosylation. The aim of my project from the onset of my course was therefore to explore the mechanistic basis of PARP1/2-HPF1 directed serine-ADP-ribosylation. Additionally, I also wanted to explore how this relates to PARP inhibition, particularly in the context of HPF1 loss or overexpression. As a result, the most recently published findings on this subject are not summarized here, but rather introduced in *3 Results*.

Materials & Methods

Outlined below are the materials and methods used for the experiments described in the *Results* section.

2.1 Cell biology

The following encompasses all aspects of cell culture including cell growth, CRISPR Cas9, cell lysis and the Flp-In system.

2.1.1 Cell lines

Cell culture work was undertaking in human osteosarcoma (U2OS), embryonic kidney (HEK293T), retinal epithelial (RPE-1), breast cancer (SUM159PT) and osteosarcoma modified with the Flp-In T-Rex system (U2OS Flp-In) cells. U2OS (HTB-96, ATCC) HEK293T (CRL-3216, ATCC) cells were acquired from ATCC. U2OS HPF1 KO, U2OS PARP1 KO, U2OS HPF1/PARP1 KO, 293T HPF1 KO and 293T HPF1/PARP1 KO cells were generated previously (Gibbs-Seymour et al. (2016)). HEK293T PARP1 KO cells were generated as part of this thesis using CRISPR Cas9 (see below). RPE-1 cells (ATCC; CRL-4000) were a generous gift from Keith Caldecott of the University of Sussex. U2OS Flp-In cells were a generous gift from Fumiko Esashi of the University of Oxford and originate from the lab of Daniel Durocher of the University of Toronto. Generation of the U2OS Flp-In cells was originally mentioned in Al-Hakim et al. (2012). SUM159PT cells were a generous gift by Ian Gibbs-Seymour of the University of Oxford (RRID:CVCL_5423, BioIVT).

U2OS and HEK293T cells were grown in DMEM (D6429, Sigma Aldrich or 31966-021, Gibco) supplemented with 10% FBS (F9665-500ML, Merck Millipore). RPE-1 cells were grown in Ham's F-12 Nutrient Mix (21765029, Thermo Fisher) media supplemented with

10% FBS. SUM159PT cells were grown in Ham's F-12 Nutrient Mix (21765029, Thermo Fisher) media supplemented with 5% FBS, 10 mM HEPES (H0887-100ML, Sigma Aldrich), 1 μg/mL hydrocortisone (H0396, Sigma Aldrich) and 5 μg/mL insulin (I9278, Sigma Aldrich). Prior to recombination of the target gene into the genome, U2OS Flp-In cells are grown in DMEM (D6429, Sigma Aldrich or 31966-021, Gibco) supplemented with 10% FBS, 4 μg/mL Blasticidin (ant-bl-1, Invivogen) and 50 μg/mL Zeocin (R25001, Thermo Fisher). Following recombination of the target gene into the genome U2OS Flp-In cells are grown in DMEM (D6429, Sigma Aldrich or 31966-021, Gibco) supplemented with 10% FBS, 4 μg/mL Blasticidin (ant-bl-1, Invivogen) and 200 μg/mL Hygromycin (ant-hg-2, Invivogen). Cells were cultivated in 10 cm dishes (430167, Corning), 15 cm dishes (430599, Corning) or T75 flasks (430825, Corning). Cells were split at least twice a week for now more than four weeks at a time. Cells were usually split 1:10 by first aspirating the media, washing the cells with 5 mL (10 cm dish/T75 flask) or 15 mL (15 cm dish) 1x PBS (D8537-500ML, Sigma Aldrich) and adding 2 mL (10 cm dish/T75 flask) or 8 mL (15 cm dish) TrypLE Express(12604013, Gibco). Following 5 - 10 minutes of incubation (depending on the cell line) cell were resuspended in 8 mL (10 cm dish/T75 flask) or 12 mL (15 cm dish) fresh media, spun down for 5 minutes at 1,000 rpm (U2OS) or 3 minutes at 800 rpm (HEK293T) and then resuspended in fresh media. Finally, 1:10 of the new cell suspension was added to a fresh dish containing media to make up 10 mL (10 cm dish/T75 flask) or 15 mL (15 cm dish).

2.1.2 DNA damage and cell lysis

For hydrogen peroxide treatment, cells were washed once with 1x DPBS containing calcium and magnesium (14040133, Gibco) and subsequently treated with 2mM H_2O_2 (H1009-100ML, Sigma Aldrich). The cells were then incubated for the duration of the DNA damage treatment. 1x DPBS was aspirated, cells placed on ice and and lysis buffer added to the dishes. Finally, the cells were scraped into the lysis buffer using a cell scraper (541070, Greiner Bio-One). For MMS treatment, media was aspirated and cells incubated with 0.1% MMS (129925-5G, Sigma Aldrich)in fresh media for 30 minutes. Subsequently, cells were washed twice with ice-cold 1x PBS, lysis buffer added to dishes on ice and cells scraped into the lysis buffer solution.

Cells were lysed in 1% TritonX-100 (100 mM NaCl, 50 mM Tris-HCl pH 8.0) lysis

buffer supplemented with 250 units/mL benzonase (E1014-25KU, Sigma Aldrich), protease inhibitor (P2714-1BTL, Sigma Aldrich, 1 tablet per 50 mL), phosphatase inhibitor (4906837001, Sigma Aldrich, 1 tablet per 10 mL), the PARP inhibitor Olaparib (04402, LKT Labs) and PARG inhibitor (PD00017273, Selleck Chemicals). PARP and PARG inhibitors were added to prevent non-physiological ADP-ribosylation or ADP-ribose hydrolysis during lysis. U2OS cells were lysed using 1 μg/mL Olaparib and PARG inhbitor (PARGi), while HEK293T cells were lysed using 2 μg/mL Olaparib and PARGi.
Following resuspension in lysis buffer, the cell suspension was transferred into Eppendorf tubes and left to rotate for 30 minutes at 4°C and 20 rpm. Subsequently, the lysate was spun down for 15 minutes at 4°C and 15,000 rpm, separating the lysate into a soluble and an insoluble fraction. The protein concentration of the soluble fraction, in the text referred to as whole cell extract (WCE), was measured by spectroscopy. The concentrations of the different soluble fractions were adjusted to either 3μg/μL or the concentration of the lowest concentrated sample (in case the concentration of that sample was below 3 μg/μL). WCEs were mixed with 4x LDS (NP0008, NuPAGE) buffer at 3:1 before being incubated at 95°C for 5 minutes and spun down for 30 seconds at 15,000 rpm. Complete cell lysates were stored at -20°C.

2.1.3 CRISPR Cas9

Knock-out cell lines of PARP1 and HPF1 were generated through CRISPR Cas9. 5x 10^5 cells of either HEK293T or U2OS Flp-In cells were seeded in two wells of a 6-well plate. 24 hours after seeding the cells, one well was left untransfected and one co-transfected with either of the two following sets of plasmids containing the Cas9 gene sequence and separate guide RNAs (gRNAs):

- PARP1 CRISPR CAS9 plasmids
  - 90 PX462-sg2.1 PARP-1 PX462 pSpCas9n(BB)-2A-Puro (PX462) V2.0 Stbl3 Amp
  - 91 PX462-sg2.2 PARP-1 PX462 pSpCas9n(BB)-2A-Puro (PX462) V2.0 Stbl3 Amp
- HPF1 CRISPR CAS9 plasmids

  - A88 PX462-sg94 HPF1 PX462 pSpCas9n(BB)-2A-Puro (PX462) V2.0 Stbl3 Amp
  - A89 PX462-sg75 HPF1 PX462 pSpCas9n(BB)-2A-Puro (PX462) V2.0 Stbl3 Amp

For transfection conditions, see *2.1.3 Transfections*. The sequence of the guide RNAs was as follows:

- PARP1 gRNAs
  - sg2.1: CCACCTCAACGTCAGGGTGC
  - sg2.2: TGGGTTCTCTGAGCTTCGGT
- HPF1 gRNAs
  - sg94: CAGCAGAATTCCCCGATCCG
  - sg75: TCGGCGGTGGCGGGAAGCGC

24 hours after transfection, cells were trypsinized, resuspended in 10 mL media containing 3 μg/mL Puromycin and transferred into a 10 cm dish. 36 hours after the start of the Puromycin selection, cells were released from the selection, if all control cells were dead or dying. Both 10cm dishes were washed twice with media and 10 mL fresh media were placed back into each dish. Three days later, 6 plates were plated with 0.25, 0.5, 1, 2.5, 5 and 10 cells per well. The cells in the plates were left to grow for two weeks. After two weeks, cells from a confluent colony were transferred into the well of a 24-well plate. Confluent colonies in a 24-well plate were further transferred to 6-well plates. Finally, each colony was split into two 6 cm dishes, of which one was used for the preparation of a cell lysate to test protein expression levels.

2.1.4 Transfections

HEK293T cells were transfected using Polyfect Transfection Reagent (301107, Qiagen) and U2OS cells using Mirus TransIT-LT1 (MIR 2305, Cambridge Bioscience). The different transfection protocols are described below.

Polyfect Transfection Reagent

The day before transfection, cells were seeded at 30 - 40% confluency. On the following morning, cells were transfected at a confluency of 40 - 80%. Depending on the size of the dish, transfection volumes varied:

- **10cm dish:** For each dish, 8 μg of DNA were mixed with Opti-MEM (31985070, Gibco) to a total volume of 300 μL. 80 μL of Polyfect transfection reagent were added, the solution mixed and incubated at RT for 5 - 10 minutes. In the meantime the media in the dish was replaced with 7 mL fresh media. 1 mL of media was added to the transfection mixture and the solution added dropwise to the dish.

- **6cm dish:** For each dish, 4 μg of DNA were mixed with Opti-MEM (31985070, Gibco) to a total volume of 300 μL. 40 μL of Polyfect transfection reagent were added, the solution mixed and incubated at RT for 5 - 10 minutes. In the meantime the media in the dish was replaced with 3 mL fresh media. 1 mL of media was added to the transfection mixture and the solution added dropwise to the dish.

Cells were incubated for 24 hours following transfection and prior to DNA damage treatment and cell lysis.

Mirus TransIT-LT1

The day before transfection, U2OS cells were seeded to achieve at least 50%confluency at point of transfection on the next morning (e.g. 1x 10^5 for a 35mm dish and 2.5x 10^5 for a 6cm dish). Depending on the size of the dish, transfection volumes varied:

- **35mm dish or 6-well plate:** 250 μL of Opti-MEM were mixed with1.25 μg plasmids and 3.75 μL transfection reagent and the mixture incubated at RT for 15 - 30 minutes. During incubation, the media in the dish was replaced with 2 mL fresh media. Following incubation, the transfection mixture was added dropwise to the dish, the dish rocked lightly and the cells incubated for 24 hours.

- **6cm dish:** 500 μL of Opti-MEM were mixed with2.5 μg plasmids and 7.5 μL transfection reagent and the mixture incubated at RT for 15 - 30 minutes. During incubation, the media in the dish was replaced with 4 mL fresh media. Following

incubation, the transfection mixture was added dropwise to the dish, the dish rocked lightly and the cells incubated for 24 hours.

Cells were incubated for 24 hours following transfection and prior to DNA damage treatment and cell lysis.

2.1.5 Recombination in U2OS Flp-In cells

Following the generation of PARP1 and HPF1 KO cell lines in U2OS cells, N-YFP tagged PARP1 WT or mutants or N-YFP tagged HPF1 WT or mutants were introduced into the recombination site of the respective knock-out strain to complement the strain. The vector used was the Flp-In compatible pDEST YFP vector (see *2.2 Materials*). For each protein variant I wanted to express, 80,000 U2OS Flp-In cells were seeded in one well of a 6-well plate 24 hours before transfection in DMEM supplemented with 10% FBS, 4 μg/mL Blasticidin and 50 μg/mL Zeocin. For each transfection, 100 μL Opti-MEM were mixed with 3 μL Mirus TransIT-LT1 transfection reagent. 900 ng of a DEST YFP construct and 900 ng of pOG44 (vector containing the gene for the recombinase, see *2.2 Materials*) were added and the mixed solution incubated at RT for 15 - 30 minutes. The media in the well was replaced with 2 mL fresh media and the transfection mixture added dropwise to the well. One well was left untransfected as a control that the antibiotics work and one well was transfected with pDEST YFP empty vector as a negative control in experiments. Cells were incubated for 24 hours. Subsequently, cells were trypsinized, resuspended in DMEM supplemented with 10% FBS only and transferred into a 15cm dish. At this point it was crucial that cells would be well dispersed across the 15cm dish to allow for colony formation. Following another 24 hours of incubation, the media in each well was replaced with DMEM supplemented with 10% FBS, 4 μg/mL Blasticidin and 200 μg/mL Hygromycin. Hygromycin treatment was expected to induce substantial cell death in untransfected cells 3 - 4 days after the start of the treatment. Single cells were left to grow in the 15cm dish and the media was replaced every 2 - 3 days. Colonies started appearing at 7 - 10 days after the start of Hygromycin treatment and single colonies were transferred into wells of a 24-well plate.

To transfer colonies, the 15cm dish was first washed twice with 1x PBS and colonies covered with cloning discs (Z374431-100EA, Sigma Aldrich) soaked in TrypLE. Cells were incubated for 15 - 20 minutes to allow for the colonies to detach from the dish and adhere

to the cloning discs. Each dish was transferred into the well of a 24-well plate. Colonies not collected with cloning discs were trypsinized, pooled together and grown in a 10cm dish(control *pool*). Single clones were screened similar to potential CRISPR Cas9 knock-out clones, but in two stages:

- **First stage:** Cells were seeded in a 6cm dish at roughly 25% confluency. On the following day, the media was replaced with fresh media containing 1 μg/mL doxycycline (D9891-1G, Sigma Aldrich). Cells were induced for 24 hours before being washed twice with 1x PBS at RT and lysed on ice. Expression levels of the protein of interest were tested by Western Blotting. Expression levels of the clones complemented with the various PARP1 and HPF1 variants was compared with the expression levels of endogenous HPF1 and PARP1 of the U2OS Flp-In WT control cell line. Where possible, three independent clones were collected with different (lower/middle/higher) expression levels at the same doxycycline concentration.

- **Second stage:** A doxycycline titration was carried out to achieve endogenous expression levels. Single clones of different PARP1 and HPF1 variants showing similar expression levels were seeded at roughly 25% confluency in several 6cm dishes. For each dish of the same clone, cells were giving a different doxycycline concentration along a titration gradient (e.g. 0.01/0.1/1 μg/mL doxycycline). Cells were induced for 24 hours before being washed twice with 1x PBS at RT and lysed on ice. Expression levels of the protein of interest were tested by Western Blotting and compared to U2OS Flp-In WT control cells to determine the doxycycline concentration closest to endogenous expression levels of the protein of interest.

2.1.6 Survival assay

For each condition, 1,400 U2OS or RPE-1 cells were seeded in each of 6 wells of three technical replicate 6-well plates. For each plate, cells were seeded in media containing increasing amounts of Olaparib with each well (starting at 0). Since Olaparib is dissolved in DMSO, the negative control contained the same amount of DMSO as the Olaparib treated samples (1:1,000 of the media volume). The media containing Olaparib was replaced every 3 - 4 days. Survival assays using U2OS Flp-In cells slightly deviated from this protocol. In addition to different Olaparib concentrations, the media also contained the appropriate

doxycycline concentration to induce the correct expression levels of the gene of interest. The media containing Olaparib and doxycycline was changed every 3 days. Cells were grown for 11 days. On the 11th day, the media in the places was removed, the wells washed once with 1x PBS and then covered in a 0.5% crystal violet (115940, Sigma Aldrich) in 25% methanol solution and left at RT for 30 minutes. The crystal violet solution was removed and the plates washed in regular water until only the colonies in the wells remained stained. The plates were left to dry overnight. Subsequently, the bottom of each dish was photographed against a white background and the images analyzed in Fiji (Schindelin et al. (2012)). The survival in percent was calculated from the area occupied by the colonies in each well against the DMSO treated control well.

2.1.7 Cell line storage

For storage, 1x 10^6 U2OS or RPE-1 cells, or 2x 10^6 HEK293T or SUM159PT cells were resuspended in 1 mL FBS (F9665, Thermo Fisher) supplemented with 10% DMSO (BP231-100, Fisher Bioreagents), transferred into cryotubes (377267, Thermo Fisher) and placed into a Mr. Frosty Freezing Container (5100-0001, Thermo Fisher) containing 70% 2-propanol (34863-2.5L, Sigma Aldrich) to slow the freezing process. Cell lines were frozen in -80C freezers and kept there for short-term storage (up to 6 months). For long-term storage (¿ 6 months), cells were stored in liquid nitrogen. Cell lines were defrosted again rapidly by placing the cryotubes in a -37°C water bath, resuspending the thawed cell suspension with 9 mL media, spinning the cells down at 1,000 rpm for 5 minutes and resuspending the cell pellet in fresh media for seeding into a 10cm dish.

2.1.8 YFP-tagged protein recruitment to microirradiation sites

For experiments requiring either transfection or 24 hour doxycycline induction, 100,000 U2OS or U2OS Flp-In cells were seeded in a 35mm glass bottom dish (P35G-Q14-C, MatTek). Prior to imaging the media in the dish is replaced with fresh media containing 1 μg/mL or 0.15 μg/mL Hoechst (H3570, Life Technologies). For 1 μg/mL Hoechst, dye incubation time was 20 - 30 minutes and for 0.15 μg/mL Hoechst it was 1 hour. Different Hoechst concentrations affected the accessibility of the DNA and the strength and persistence at sites of DNA damage of the tagged protein of interest. Following sensitization of the cells with Hoechst, the dish was washed once with 1x PBS and 1 - 2 mL imaging

media added to the cells. Imaging media consisted of high-glucose, HEPES-buffered, no phenol-red DMEM (21063029, Gibco) supplemented with 10% FBS, 100 U/mL Pen/Strep solution (15140122, Gibco) and 1 mM sodium pyruvate (11360070, Gibco). Following addition of imaging media, the dish was taken for imaging. Imaging was carried out on the Olympus Sora spinning disc microscope. The objective used was a UPlanApo 1.5NA 60x. The dish was kept at 37°C by a chamber surrounding the objective. No CO_2 was added to the chamber. DNA damage induction was carried out with a 405 nm laser at 100% laser power (amounting to roughly 220 μWatts) and with a cycle number of 80. 405 nm laser power was measured once with the S175C Thorlabs slide laser power meter, although the absolute laser power was subject to variation at 100% laser power set on the system. N-terminally YFP-tagged proteins were excited with a 488 nm laser. Five images were taken immediately before laser microirradiation at the minimal possible time interval between images. Images acquisition immediately after DNA damage was carried out at 10 second intervals. Images were taken with a 95B from Photometrics camera. The software used to drive the microscope was CellSense V3.2. Signal quantification was carried out manually in Fiji and data visualization carried out in Prism 9 (Schindelin et al. (2012)). Fold increase of the fluorescence signal was measured as the signal strength of the tagged protein at the site of DNA damage induction against the same area prior to microirradiation.

2.2 Co-IPs and Western Blotting

This section encompasses all protocols involved in co-immunoprecipitation and Western Blotting procedures of cell lysates.

2.2.1 Co-immunoprecipitation

Depending on the tag (FLAG or YFP), two different co-immunoprecipitation (co-IP) protocols were carried out. Both are given below. For co-IPs, 10 cm dishes of HEK293T cells were grown and lysed in 600 μL lysis buffer containing all supplements described in the subsection *DNA damage and cell lysis*.

FLAG co-IP

Simultaneous to cell lysis, FLAG co-IP columns were prepared. M2 FLAG Affinity Gel (A2220-5ML, Thermo Scientific) was removed from the -20°C freezer, thawed on ice and homogenized by inverting. 1 mL Micro Bio-Spin Chromatography Columns (7326204, Bio-Rad) were pre-wet with 900 μL TritonX-100 lysis buffer (see subsection *DNA damage and cell lysis*) once, the bottom of the columns sealed and 200 μL TritonX-100 lysis buffer added to each column. 100 μL M2 FLAG Affinity Gel were reverse pipetted into each column (using a cut-off 200 μL pipette tip to avoid friction) and the columns subsequently washed 3 times with 900 μL TritonX-100 lysis buffer. At the end of the third wash step, the columns are sealed again, leaving ca. 200 μL lysis buffer in the column to prevent the M2 FLAG Affinity Gel from drying. The columns were stored at 4°C until the cell lysates were ready to be used.

Following Bradford assay, WCEs were prepared from a small fraction of each of the cell lysates (*input* samples). Subsequently, the concentration of the cell lysates was adjusted to that of the lowest concentrated cell lysate and the same volume of each lysate added to a separate column. Columns were left to rotate for 2 hours at 4°C. Subsequently, the columns were allowed to drain and washed 5 times with 900 μL TritonX-100 lysis buffer. Columns were again sealed at the bottom, 200 μL TritonX-100 lysis buffer added and the M2 FLAG Affinity Gel from each column transferred into a separate Eppendorf tube using a cut-off 200 μL pipette tip. The affinity gel was then spun down for 2 minutes at 4°C and 1,000 xg. Lysis buffer was aspirated and the affinity gel resuspend in 100 μL 1x LDS sample buffer (diluted from a 4x LDS buffer with lysis buffer containing all supplements described in the subsection *DNA damage and cell lysis*). Finally, the samples were incubated at 95C for 5 minutes, spun down for 30 seconds at 15,000 rpm and stored at -20°C.

GFP co-IP

Similar to FLAG co-IPs, GFP-Trap Magnetic Agarose (gtma-20, Chromotek) was prepared simultaneously to cell lysis. For each sample, 20 μL of homogenized GFP-Trap Magnetic Agarose were reverse pipetted into an Eppendorf tube and the agarose washed three times with with 900 μL TritonX-100 lysis buffer. The agarose was separated from

the lysis buffer using a DynaMag-2 Magnet (12321D, Thermo Fisher) and the lysis buffer aspirated after every wash step. After preparation of WCEs, the concentration of the cell lysates was adjusted to that of the lowest concentrated cell lysate and the same volume of each lysate added to a separate Eppendorf tube. The tubes were left to rotate for 2 hours at 4°C. Subsequently, the cell lysates were aspirated and the tubes washed for another 3 times with 900 μL TritonX-100 lysis buffer. After the third wash step, the agarose is again resuspended in fresh 900 μL TritonX-100 lysis buffer and the solution transferred into a fresh Eppendorf tube. The lysis buffer was again aspirated and the agarose beads washed a final two times before being resuspended in 100 μL 1x LDS sample buffer (diluted from a 4x LDS buffer with lysis buffer containing all supplements described in the subsection *DNA damage and cell lysis*). Finally, the samples were incubated at 95°C for 5 minutes, spun down for 30 seconds at 15,000 rpm and stored at -20°C.

2.2.2 Western Blotting

For their first use following freezing, samples stored at -20°C were incubated at 95°C for 5 minutes, then spun down for 30 seconds at 15,000 rpm. For subsequent uses, samples were only defrosted on ice and spun down for 30 seconds at 15,000 rpm. Cell lysates were first run on 4-12% Bis-Tris 12-well (NP0322BOX, Invitrogen) or 20-well (WG1402A, Invitrogen) gradient gels in 1x MOPS buffer. The samples were run at 120 Volts for the first 5-10 minutes and then at 150 Volts until the dye front reached the bottom of the gel. Gels were transferred onto the membranes of Trans-Blot Turbo Mini (1704156, Bio-Rad) or Midi (1704159, Bio-Rad) 0.2 μm Nitrocellulose Transfer Packs and transfer was carried out using the 30 minutes Standard SD transfer programme of the Trans-Blot Turbo Transfer System (1704150, Bio-Rad). Membranes were stained with Ponceau S staining solution (P7170-1L, Sigma Aldrich), washed three times with MilliQ water and scanned. The membranes were then blocked in 5% milk in PBS-T for 30-60 minutes. Primary antibody treatment in 5% milk in PBS-T was carried out overnight at 4°C on a rocking shaker. Subsequently, membranes were washed four times in PBS-T over the course of 30 minutes and treated with secondary antibody in 5% milk in PBS-T for two hours at RT on a rocking shaker thereafter. Membranes were again washed four times in PBS-T over the course of 30 minutes before removing excess PBS-T from them using Gel Blot paper (3030-917, VWR International) and covering them in standard (32106, Thermo

Scientific) or strong (34095, Thermo Scientific) ECL Western Blotting Substrate solution for 5 minutes at RT. Excess PBS-T was again removed from the membranes using Gel Blot paper. The chemiluminescent signal from the membranes was transferred onto hyperfilms (28-9068-37, VWR International) and the films developed using a Konica Minolta SRX-101A tabletop processor. Finally, the developed films were scanned and figures assembled using Photoshop Illustrator.

2.3 Cloning and mutagenesis PCR

This section deals with the procedures for Gateway cloning, site-directed mutagenesis PCR and plasmid propagation.

2.3.1 E.coli strains

Lab-grown DH5α cells were used for cloning and XL10-Gold Ultracompetent Cells (200315, Agilent) for site-directed mutagenesis PCR. DH5α cells were made chemically competent. A 1:10,000 to 1:100,000 dilution of 1 μLof DH5α cells was plated on an LB-Agar plate and incubated for 14 - 18 hours at 37°C. A single colony was picked and grown in 2 mL LB media for 14 - 18 hours at 37°C at 200 rpm and 37°C. 1 mL of the suspension was inoculated in 100 mL LB media and grown at 37C shaking at 200 rpm to an OD value of 0.25 - 0.3 (reached after 1.5 to 2 hours). The culture was chilled on ice for 15 minutes and subsequently cells were spun down for 10 minutes at 3300 xg at 4°C. The supernatant was discarded and the cell pellet resuspended in 40 mL ice-cold 01. M $CaCl_2$ solution. The cell suspension was kept on ice for 30 minutes and cells centrifuged as above. Again, the supernatant was removed and the cell pellet resuspended in 01. M $CaCl_2$ solution containing 15 % glycerol. The cell suspension was transferred into PCR tubes in 150 μL aliquots and the tubes snap-frozen in liquid nitrogen and stored at -80°C.

2.3.2 Gateway Cloning

Gateway cloning was used to clone a gene of interest from a Kanamycin-resistant *donor* vector (in this case pDONR221) to a Ampicillin-resistant (in this case pDEST YFP, pDEST FLAG CMV, pDEST12.2) *destination* vector that often carries a tag and is used for transient overexpression of the gene of interest in mammalian cells. Gateway cloning

from the *donor* vector to the *destination* vector was carried out according to the protocol for the Gateway LR Clonase II Enzyme mix (11791-020, Invitrogen). Gateway cloning from the *destination* vector to the *donor* vector, was carried out according to the protocol for the Gateway BP Clonase II Enzyme mix (11789-020, Invitrogen). Subsequently, 5 μL of reaction product were transformed with 50 μL DH5α cells, incubated on ice for 30 minutes, heat shocked 42°C for 45 seconds, incubated on ice again for 2 minutes and mixed with 145 μL pre-warmed S.O.C. medium (15544034, Life Technologies). Finally, the cell suspension was incubated for 1 hour at 37C and 200 rpm and then plated either on a Kanamycin plate (containing 30 μg/mL Kanamycin) or on an Ampicillin plate (containing 50 - 100 μg/mL Ampicillin). The plate was left o/n in a 37C incubator.

2.3.3 Site-directed mutagenesis PCR

Site-directed mutagenesis PCR was carried out using the QuikChange Site-directed Mutagenesis Kit (210519, Agilent). Site-directed mutagenesis PCR was carried out according to the protocol, but scaling down the size of the reaction volume and all its components to 20% of the suggested volume. Primers were designed according to the online primer design tool for the QuikChange Site-directed Mutagenesis Kit. In each reaction, 0.5 μL of a 10 μM solution of each the forward and the reverse primer were used. 3 μL reaction product were transformed with 30 μL XL10-Gold Ultracompetent Cells, incubated on ice for 30 minutes, heat shocked 42C for 45 seconds, incubated on ice again for 2 minutes and mixed with 145 μL pre-warmed S.O.C. medium (15544034, Life Technologies). Finally, the cell suspension was incubated for 1 hour at 37°C and 200 rpm and then plated either on a Kanamycin plate (containing 30 μg/mL Kanamycin) or on an Ampicillin plate (containing 50 - 100 μg/mL Ampicillin). The plate was left o/n in a 37°C incubator.

2.3.4 Plasmid propagation

For plasmid propagation, no more than 25 μg of plasmid were mixed with 50 μL DH5α cells at a ratio of no less than 1:10. The mixture was incubated on ice for 30 minutes, heat shocked 42°C for 45 seconds, incubated on ice again for 2 minutes and mixed with 145 μL pre-warmed S.O.C. medium (15544034, Life Technologies). Finally, the cell suspension was incubated for 1 hour at 37C and 200 rpm and then plated either on a Kanamycin plate (containing 30 μg/mL Kanamycin) or on an Ampicillin plate (containing 50 - 100

μg/mL Ampicillin). The plate was left o/n in a 37°C incubator. Depending on whether a MiniPrep, MidiPrep orMaxiPrep was made, the consecutive steps varied:

MiniPreps

On the next day, a colony was picked, placed in 3 mL LB media with 100 μg/mL Ampicillin or 30 μg/mL Kanamycin and the mixture left shaking at 37C and 200 rpm for 14 - 18 hours. The suspension was spun down for 3 minutes at 4,500 xg and the supernatant discarded. A plasmid MiniPrep was prepared from the cell pellet using the QIAprep Spin Miniprep Kit (27104, Qiagen).

MidiPreps

On the next day, a colony was picked into 300 mL LB media with 100 μg/mL Ampicillin or 30 μg/mL Kanamycin and incubated for 14 - 18 hours at 37C and 200 rpm. On the next day, The liquid culture was spun down for 10 minutes at 4,500 rpm and 4C and the supernatant discarded. A plasmid MaxiPrep was prepared from the cell pellet using the PureLink HiPure Plasmid Midiprep Kit (K210004, Invitrogen).

MaxiPreps

On the next day, a colony was picked, placed in 3 mL LB media with 100 μg/mL Ampicillin or 30 μg/mL Kanamycin and the mixture left shaking at 37°C and 200 rpm for 6 - 8 hours. The suspension was transferred into 300 mL LB media with 100 μg/mL Ampicillin or 30 μg/mL Kanamycin and incubated for 14 - 18 hours at 37°C and 200 rpm. The liquid culture was spun down for 10 minutes at 4,500 rpm and 4°C and the supernatant discarded. A plasmid MaxiPrep was prepared from the cell pellet using the PureLink HiPure Plasmid Maxiprep Kit (K210006, Invitrogen).

2.4 Genotyping

Where the identity of a cell line was unclear from Western Blotting, genotyping was used to sequence certain parts of the cell line's genome.

2.4.1 Genomic DNA purification

Cells were grown in a T25 flask until confluent. The media was aspirated, the cells washed once with 1x PBS and 1000 μL genomic DNA lysis buffer (100 mM Tris Base, 5 mM EDTA, 200 mM NaCl, 0.2% SDS) supplemented with 100 μg/mL Proteinase K (P2308, Sigma Aldrich) added to the flask. The flask was incubated at 37°C in cell culture incubator for at least 48 hours (max. 8 days), at 65°C for 4 hours or at 55°C overnight. The lysate was transferred into a clean 2 mL Eppendorf tube and one volume of ice-cold isopropanol added. The solution was shaken in a Thermomixer at RT for 20 minutes, then centrifuge for 5 minutes at 880 xg in an Eppendorf centrifuge to pellet the DNA. The supernatant was discarded, leaving a white DNA pellet behind. Tubes were dried by placing them upside down on a piece of tissue paper. The DNA pellet was washed by adding 2 mL 70% ethanol (32221-2.5L-M, Sigma Aldrich) to the Eppendorf tube, again centrifuging for 5 minutes at 880 xg, discarding the supernatant and drying the cell pellet. to prevent excessive drying, 1000 μL of TE buffer were immediately added to the tube and the DNA redissolved at 60°C for 2 hours at top speed in a Thermomixer. Genomic DNA solutions were stored at -20C.

2.4.2 Sequencing

Genomic DNA solutions were subsequently used to sequence certain genomic regions, which were amplified from the genomic DNA solutions using the correct primer pairs. PCR amplification was carried out using either Q5 High-Fidelity DNA polymerase (M0491S, New England Biolabs) or DreamTaq Hot Start Green PCR Master Mix (K9021, Thermo Scientific). PCR products were cleaned up by either running the product on an agarose gel and performing agarose gel extraction using the QIAquick Gel Extraction Kit (28706X4, Qiagen) or the QIAquick PCR Purification Kit (28104, Qiagen). PCR amplification and clean-up was carried out as described in the respective manufacturer's protocols. PCR samples were sent for sequencing with the same set of primers use for PCR amplification or with a set of primers set further inward into the product.

2.5 Materials

This section comprises all antibodies and plasmids used in the *Results* section as well as any chemical compounds not already described in the text above.

2.5.1 Antibodies

A list of primary antibodies is shown below. Secondary antibodies against both rabbit (P0399) and mouse (P0447) primary antibodies were purchased from Agilent and used at a dilution of 1:2,000 in 5% milk in PBS-T.

HPF1 was detected using a custom-made rabbit polyclonal antibody produced by DC Biosciences. Antibodies of rabbit 117 raised against the epitope RELPETDADLKRIC were used. The first round of two purification rounds yielded 9 fractions (1.1 - 1.9) In this thesis, only fractions 1.5 and 1.6 were used in Western Blotting at a dilution of 1:500. All antibodies were diluted in 5% milk (S0942, Marvel) in PBS-T.

target	**name**	**manufacturer**	**dilution**	**species**
β-Tubulin	ab6046	Abcam	1:50,000	rabbit
FLAG	A8592	Sigma Aldrich	1:50,000	mouse
γ-H2AX (ser139)	9718S	Cell Signalling	1:1,000	rabbit
GFP	ab290	Abcam	1:5,000	rabbit
Histone H2B	ab1970	Abcam	1:50,000	rabbit
Histone H3	07-690	Merck Millipore	1:50,000	rabbit
mono/poly-ADP-ribose	83732S	Cell Signalling	1:1,000	rabbit
pan-ADPr	MABE1016	Sigma Aldrich	1:1,500	rabbit
PARP1	ab32138	Abcam	1:5,000	rabbit
PARP2	ALX-804-639-L001	Enzo Life Sciences	1:500	mouse

Table 2.1: List of commercially available primary antibodies used in the *Results* section of this thesis.

2.5.2 Buffer solutions and media

Below are outlined the compositions of buffer solutions and different types of growth media:

1x PBS-T (10 L)

- 500 mL 10x PBS (D1408-500ML, Sigma Aldrich), 2x
- TWEEN 20 viscous liquid (P1379, Sigma Aldrich), 10 mL (0.1%)
- 9 L MilliQ water

Triton X-100 lysis buffer (500 mL)

- NaCl (S9888-25KG, Honeywell), 100 mM (2.922 mg)
- 1M Tris-HCl pH 8.0 (51238, Lonza), 50 mM (25 mL)
- Triton X-100 (X100-500ML), 1% (5 mL)
- MilliQ water

U2OS cell lysis buffer (5 mL)

- Triton X-100 lysis buffer, 1.5 mL
- 5x phosphatase inhibitor (4906837001, Sigma Aldrich) in Triton X-100 lysis buffer solution, 1x (1 mL)
- 2x protease inhibitor (P2714-1BTL, Sigma Aldrich) in Triton X-100 lysis buffer solution, 1x (2.5 mL)
- 250,000 units/mL benzonase (E1014-25KU, Sigma Aldrich), 250 units/mL (5 μL)
- 10 mM Olaparib (04402, LKT Labs), 1 μg/mL (0.5 μL)
- 10 mM PARG inhibitor (PD00017273, Selleck Chemicals), 1 μg/mL (0.5 μL)

HEK293T cell lysis buffer (5 mL)

- Triton X-100 lysis buffer, 1.5 mL
- 5x phosphatase inhibitor (4906837001, Sigma Aldrich) in Triton X-100 lysis buffer solution, (1x) 1 mL

- 2x protease inhibitor (P2714-1BTL, Sigma Aldrich) in Triton X-100 lysis buffer solution, 1x (2.5 mL)
- 250,000 units/mL benzonase (E1014-25KU, Sigma Aldrich), 250 units/mL (5 μL)
- 10 mM Olaparib (04402, LKT Labs), 2 μg/mL (1 μL)
- 10 mM PARG inhibitor (PD00017273, Selleck Chemicals), 2 μg/mL (1 μL)

1x MOPS buffer (10 L)

- 20x NuPAGE MOPS SDS Running Buffer (B000102, Invitrogen), 1x (500 mL)
- MilliQ water, 9.5 L

U2OS and HEK293T growth media (550 mL)

- DMEM (D6429, Sigma Aldrich or 31966-021, Gibco), 1x (500 mL
- FBS (F9665-500ML, Merck Millipore), 10% (50 mL)

U2OS Flp-In growth media (550 mL)

- DMEM (D6429, Sigma Aldrich or 31966-021, Gibco), 1x (500 mL
- FBS (F9665-500ML, Merck Millipore), 10% (50 mL)
- Blasticidin (ant-bl-1, Invivogen), 4 μg/mL (220 μL)
- Zeocin (R25001, Thermo Fisher), 50 μg/mL (275 μL)

Complemented U2OS Flp-In growth media (550 mL)

- DMEM (D6429, Sigma Aldrich or 31966-021, Gibco), 1x (500 mL)
- FBS (F9665-500ML, Merck Millipore), 10% (50 mL)
- Blasticidin (ant-bl-1, Invivogen), 4 μg/mL (220 μL)

- Hygromycin (ant-hg-2, Invivogen), 200 μg/mL (1,100 μL)

RPE-1 growth media (550 mL)

- Ham's F-12 Nutrient Mix (D8062-500ML, Sigma Aldrich or 21765-029, Gibco), 1x (500 mL)
- FBS (F9665-500ML, Merck Millipore), 10% (50 mL)

SUM159PT growth media (550 mL)

- Ham's F-12 Nutrient Mix (D8062-500ML, Sigma Aldrich or 21765-029, Gibco), 1x (500 mL)
- FBS (F9665-500ML, Merck Millipore), 5% (25 mL)
- HEPES (H0887-100ML, Sigma Aldrich), 10 mM (500 μL)
- insulin (I9278, Sigma Aldrich), 5 μg/mL (265 μL)
- hydrocortisone (H0396, Sigma Aldrich), 1 μg/mL (137.5 μL)

Imaging media (550 mL)

- phenol red-free DMEM (21063029, Gibco), 1x (500 mL)
- FBS (F9665-500ML, Merck Millipore), 10% (50 mL)
- Pen/Strep solution (15140122, Gibco), 100 U/mL (5.5 mL)
- sodium pyruvate (S8636-100ML, Sigma Aldrich), 1 mM (5.5 mL)

Genomic DNA lysis buffer (100 mL)

- NaCl (S5886-10KG), 200 mM (1.1688 mg)
- EDTA (15575, Gibco), 5 mM (1 mL of 0.5 M stock)
- Proteinase K (P2308, Sigma Aldrich), 100 μg/mL (500 μL)
- Tris-HCl pH 8.0 (51238, Lonza), 1M (25 mL)
- SDS (442444H, VWR Chemicals), 0.2% (2 mL)

2.5.3 Expression vectors

For expression in human cells, mammalian expression vectors pDEST YFP and pDEST FLAG CMV were used. pDEST YFP and pDEST FLAG CMV were previously used in Gibbs-Seymour et al. (2016). Additionally, pDONR221 was used in the generation of mutants and in transferring a construct from one of the two mammalian expression vector to the through a BP and subsequent LR Clonase reaction. pDONR221 is a commercially available antibody (12536017, Thermo Fisher). The vector maps of pDEST YFP and pDEST FLAG CMV are shown in Figure 2.1.

PARP1 only possesses one, full-length, isoform, which is cloned into pDEST YFP and as such transiently overexpressed or expressed as part of the Flp-In T-Rex system in human cells in the experiments given in *Results*. PARP2, however, has two isoforms. For all experiments studying PARP2, I used isoform 2, which is the commonly used isoform in the field and can be considered the main one. PARP2 isoform 2 differs from isoform 1 in the absence of amino acids 68-80, part of an unstructured region downstream of the nuclear localization signal and upstream of the DNA-binding WGR domain. PARP2 isoform 2 is clones into pDEST YFP and as such transiently overexpressed or expressed as part of the Flp-In T-Rex system in human cells in the experiments given in *Results*. HPF1 has only one isoform and is cloned into pDEST YFP and pDEST FLAG CMV and as such transiently overexpressed or expressed as part of the Flp-In T-Rex system in human cells in the experiments given in *3 Results*.

All commercially available plasmids used in this thesis are highlighted in Figure 2.2.

name	**product code**	**manufacturer**
Gateway pDONR221	12536017	Thermo Fisher
pOG44	V6005-20	Thermo Fisher
pSpCas9n(BB)-2A-Puro (PX462) V2.0	62987	Addgene

Table 2.2: List of commercially available plasmids used in the *Results* section of this thesis.

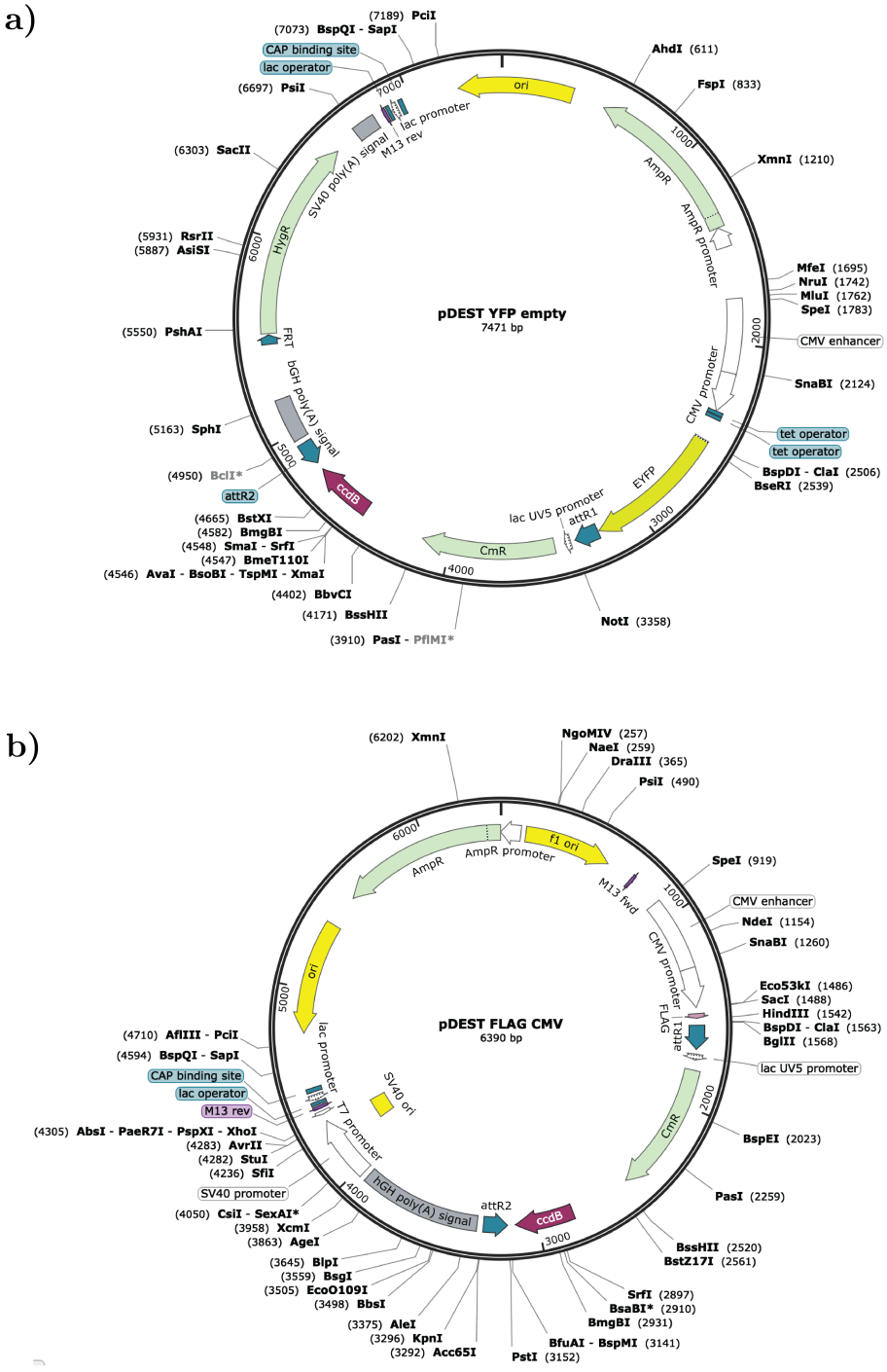


Figure 2.1: Vector maps of pDEST YFP and pDEST FLAG CMV. **a)** Vector map of pDEST YFP. **b)** Vector map of pDEST FLAG CMV.

Results

PARP1 has been shown to bring about serine ADP-ribosylation, the predominant form of ADP-ribosylation (ADPr) in response to DNA damage, only in the simultaneous presence of HPF1. However, prior to the start of this study, little was known of how HPF1 switches PARP1 from glutamate/aspartate-specific to serine-specific ADPr, what is the nature of PARP1/HPF1 complex formation and what are the phenotypic consequences of impairing or losing elements or even the entirety of PARP1/HPF1-catalyzed serine ADP-ribosylation. In this thesis, I attempted to draw a comprehensive picture of the mechanistic basis of PARP1/HPF1 complex formation and its catalysis of serine ADPr.

3.1 A system to study cellular ADPr

In order to explore amino acid sites crucial to the proteins' function, I decided to study DNA damage-induced ADPr patterns in human cell lines by Western Blotting (WB) . Three commonly used cell lines, the human bone osteosarcoma cell line U2OS, the human embryonic kidney cell line HEK293T (293T) and the human hTERT-immortalized retinal pigment epithelial cell line RPE-1, were used to this end. DNA damage-induced ADPr was studied in response to a 10 and 120 minute continuous hydrogen peroxide (H_2O_2) treatment or a 30 minute treatment of MMS followed by 0, 30 or 60 minutes of *recovery* time in MMS-free media (Figure 3.1). The signal was expected to be the strongest directly following DNA damage induction and to revert back to background levels after two hours, as was later reported (Palazzo et al. (2018)). While hydrogen peroxide has been shown to oxidate DNA, MMS methylates bases. Both types of DNA damage are predominantly repaired in base excision repair (BER), in which both PARP1 and PARP2 play a crucial role (see *1.1 DNA repair PARPs*). The impact of the loss of HPF1, PARP1 or PARP2 was examined by comparing wildtype (WT) U2OS and 293T cell lines with their respective

PARP1, PARP2 or HPF1 knock-out cell lines previously generated by Ian Gibbs-Seymour.

3.1.1 PARP1/HPF1-dependence of ADPr levels in U2OS cells

In a first step, whole cell lysates (WCEs) of cells were prepared immediately after H_2O_2 treatment and ADP-ribosylation blotted for using a His-tagged recombinant ADP-ribose binding protein conjugated with a rabbit Fc tag (MABE1016, Sigma-Aldrich). In WB, use of this antibody is referred to as pan-ADPr in comparison to a monocloncal antibody raised against keyhole limpet hemocyanin ADP-ribosylated on lysine (83732S, Cell Signalling) referred to as mono/poly-ADPr. Induction of DNA damage in U2OS cells using hydrogen peroxide generated a strong, transient ADPr (ADPr) signal with particularly pronounced regions at the molecular level of PARP1 (116 kDA; pan-ADPr and mono/poly-ADPr antibody) and of histones (11 kDa for H4, 13 kDA for H3; pan-ADPr antibody only) (Figure 3.1a). This agrees with the observation that PARP1 catalytic activity is largely directed at histones, triggering chromatin de-condensation, and at itself, resulting in the recruitment of PAR-binding DNA repair factors and ultimately PARP1 release from DNA. Loss of PARP1 abolished the overwhelming majority of cellular ADPr, in line with PARP1 being the main driver of ADPr in cells (Amé et al. (1999), Chen, Kassab, Dantzer & Yu (2018)). Only at 120 minutes H_2O_2 treatment could histone ADPr (pan-ADPr antibody) and ADPr of many other substrates be observed (Figure 3.1a). These ADPr events are likely the result of PARP2-catalyzed ADP-ribosylation in the absence of PARP1. Similarly to PARP1, loss of HPF1 in U2OS cells largely abolishes H_2O_2-induced ADPr. While histone ADPr is completely lost, some degree of PARP1 auto-modification remains, suggesting that PARP1 can modify itself, but not histones, as was previously shown by Ian Gibbs-Seymour and others (Figure 3.1a) (Gibbs-Seymour et al. (2016)). Interestingly, PARP1 auto-modification measured by the pan-ADPr antibody in U2OS *HPF1*Δ cells, albeit reduced, reaches a higher molecular weight, signifying longer PAR chains. This corroborates findings that HPF1 limits PARP1 hypermodification (Gibbs-Seymour et al. (2016)).

To confirm that the observed findings were the result of H_2O_2-induced DNA damage rather than the consequence of other oxidation events by hydrogen peroxide, cells were also treated with the methylating agent MMS for 30 minutes and ADPr levels monitored at different time points following the end of the treatment. Cellular fractionation was carried

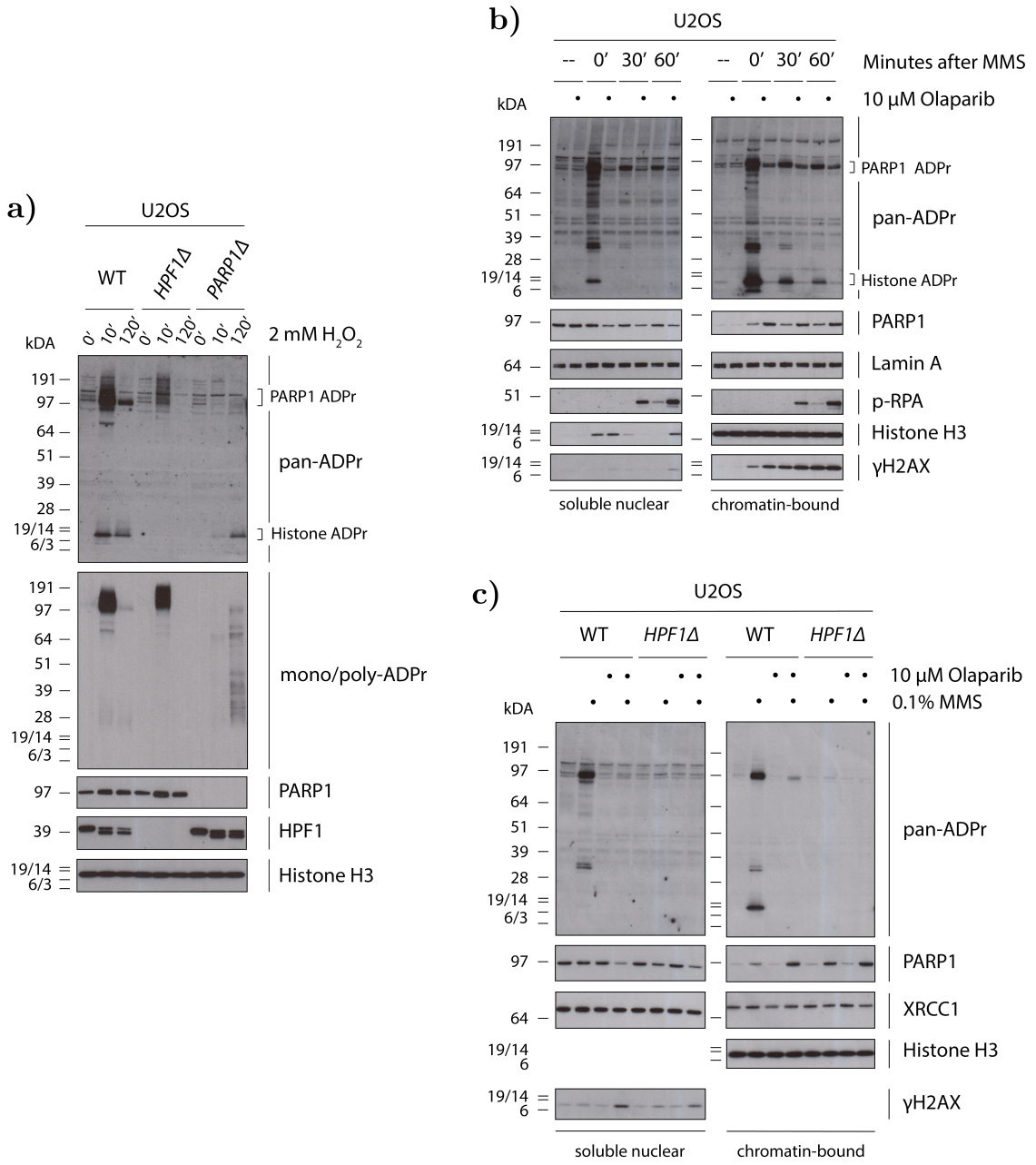


Figure 3.1: *Loss of HPF1 or PARP1 abolishes DNA damage-induced ADPr in U2OS cells.* **a)** The loss of PARP1 or HPF1 abolishes the majority of ADPr in response to hydrogen peroxide-induced DNA damage. **b)** MMS in U2OS cells induces a similar ADPr pattern as H_2O_2, which can be prevented by the use of the PARP1/2 inhibitor Olaparib. **c)** Loss of HPF1 abolished MMS-induced ADPr in 293T cells. Experiments were repeated at least two times.

out and two nuclear fractions (soluble nuclear and chromatin-bound) analyzed by WB to obtain a more detailed impression of nuclear ADPr (Figure 3.1b). Similar to Figure 3.1a, MMS treatment in U2OS cells induced a strong ADPr signal immediately after the end of the treatment in the soluble nuclear fraction, which was strongly decreased following 30

minutes of recovery in MMS-free media. In line with ADPr occurring on chromatin as a direct consequence of DNA damage, observed ADPr levels were substantially stronger in the chromatin-bound fraction, although the signal followed the same pattern as for the soluble nuclear fraction. Dependence of the ADPr signal on the catalytic activity of PARP1 and PARP2 was confirmed by the use of the PARP1/2 inhibitor Olaparib. Treatment of cells with Olaparib 30 minutes prior to DNA damage induction as well as throughout MMS treatment and recovery period reduced the ADPr signal to background levels in all time points. Additional information was provided by blotting for PARP1 (ab32138, Abcam). Induction of DNA damage lead to a mild decrease in PARP1 levels of the soluble nuclear fraction and a respective increase in PARP1 levels of the chromatin-bound fraction, in line with PARP1 recruitment to sites of DNA damage (Figure 3.1b). This shift was drastically enhanced by Olaparib pre-treatment, confirming previous observations that Olaparib acts by *trapping* PARP1 at sites of DNA damage. Induction of DNA damage was confirmed by the rising levels of γ-H2AX, a hallmark of DNA double-strand breaks.

Finally, I also wanted to explore the dependence of cellular ADPr levels on HPF1. To this end, ADPr levels in the soluble nuclear and chromatin-bound fraction of U2OS WT and *HPF1*Δ cells were studied (Figure 3.1c). Indeed, loss of HPF1 abolished ADPr in absence of PARP inhibition in both fractions immediately following MMS treatment. As in Figure 3.1b, PARP1 is recruited to chromatin in response to DNA damage, an effect which is expectedly strongly enhanced in the presence of Olaparib. The absence of HPF1 also appeared to increase PARP1 recruitment levels to chromatin, albeit not beyond Olaparib-induced levels of PARP1 trapping.

To conclude, the induction of either hydrogen peroxide or MMS in U2OS cells leads to similarly rapid induction of ADPr levels following treatment, which subsequently decline strongly as early as 30 minutes following the end of MMS treatment (Figure 3.1). Given the rapid turnover of hydrogen peroxide, no recovery period was given. However, ADP-ribosylation was still approaching untreated levels at 120 minutes of treatment (Figure 3.1a). Additionally, the immediate ADPr response to DNA damage was overwhelmingly dependent on PARP1 and HPF1, with loss of either resembling ADPr levels in undamaged cells. These findings prove that the impact of either HPF1 or PARP1 mutants on DNA damage-dependent cellular ADP-ribosylation can be studied in the background of *HPF1*Δ and *PARP1*Δ cells. However, I first wanted to confirm the initial findings in

other cell lines.

3.1.2 DNA damage induced ADP-ribosylation in 293T and RPE-1 cells

Similar to U2OS cells, DNA damage was induced in 293T and RPE-1 cells by adding hydrogen peroxide (Figure 3.2). 293T cells displayed an almost identical ADPr pattern, albeit with low PARP1 auto-modification levels already present in untreated cells (Figure 3.2a). As before, I wanted to study the effect of knocking out PARP1 and HPF1 on the DNA damage-dependent ADPr pattern of the respective cell lines. 293T *HPF1*$^{-/-}$ cells were previously generated by Ian Gibbs-Seymour, while I generated 293T PARP1$^{-/-}$ cells using CRISPR Cas9. As previously observed with U2OS cells, loss of HPF1 in 293T cells abolished most ADPr apart from low levels of PARP1 auto-modification, while loss of PARP1 lead to a weaker, delayed signal that can be attributed to PARP2 auto- and trans-modification (Figure 3.2a). In RPE-1 cells, hydrogen peroxide treatment triggered lower, but equally clear ADPr at the molecular weight of histones and of PARP1 (Figure 3.2b). Additionally, the effect of knocking-out HPF1 in this cell line was tested using RPE-1 *HPF1*$^{-/-}$ cells generously provided by Keith Caldecott. Again, histones ADPr was entirely lost and PARP1 auto-modification strongly reduced in the knock-out cell lines compared to RPE-1 WT cells.

Having established HPF1 and PARP1 knock-out backgrounds to be suitable for investigating the impact of different HPF1 and PARP1 mutants on DNA damage-dependent ADP-ribosylation in human cells, I wanted to see if I could successfully complement knock-out cells and restore ADPr levels of the WT cell lines using transient overexpression (Figure 3.2c). Given their high efficiency for plasmid transfections, 293T cells were chosen. As before, wildtype and *HPF1*$^{-/-}$ cells were either left untreated or treated with hydrogen peroxide for 10 or 120 minutes. 24 hours prior to DNA damage treatment, cells were transfected with a plasmid containing either FLAG tag alone or N-terminally FLAG-tagged HPF1 (Figure 3.2a) . Both WT and *HPF1*$^{-/-}$ cells expressing FLAG tag alone showed comparable ADPr levels as in Figure 3.2b. Transient overexpression of FLAG-HPF1, however, substantially boosted ADPr signals in both cell lines beyond levels observed in the WT cell line transfected with only FLAG (Figure 3.2c).

As a result of these findings, I established that HPF1 and PARP1 are the main driving factors in DNA damage-dependent ADPr in human cells and that their loss provides a

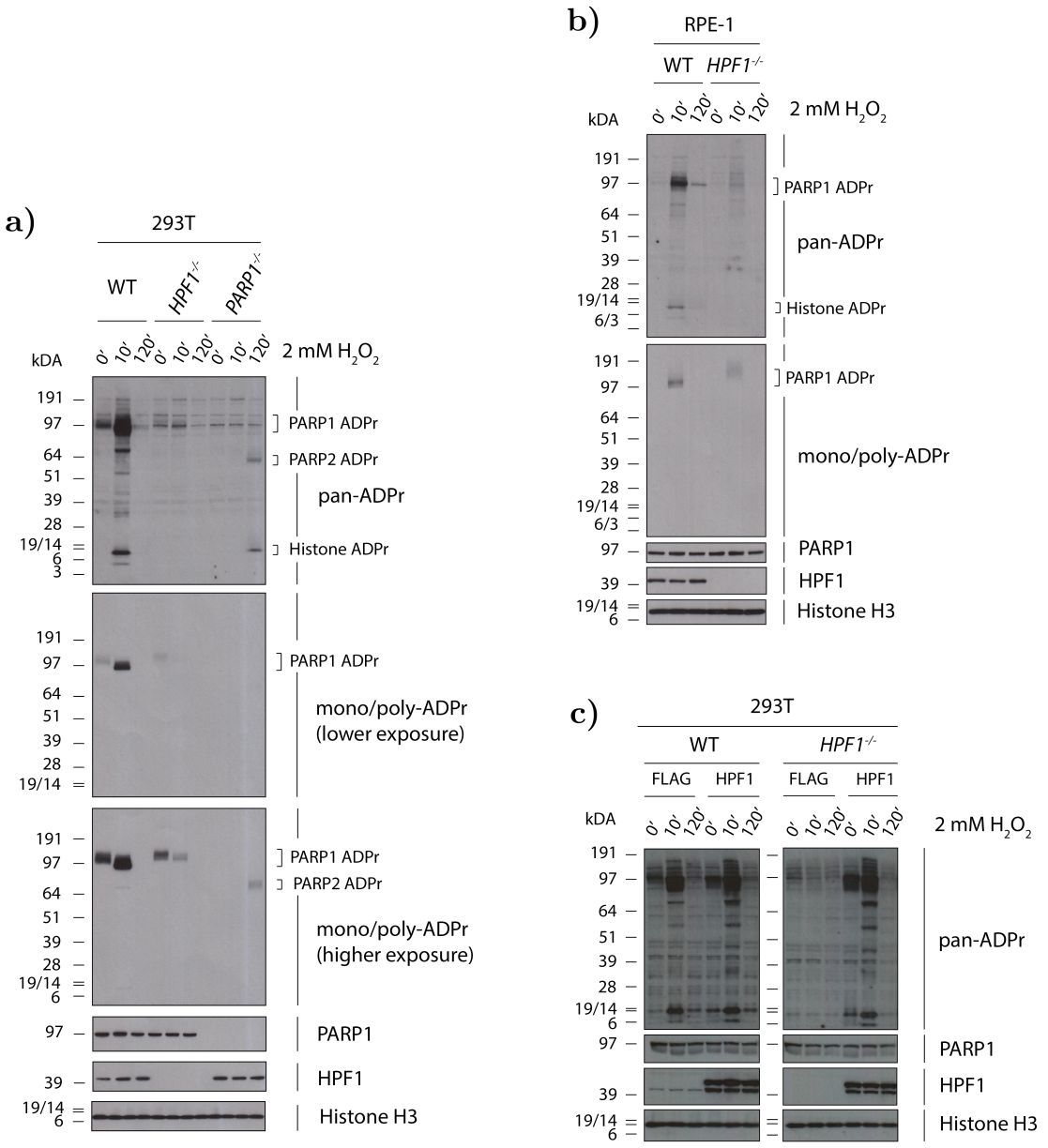


Figure 3.2: *Loss of DNA damage-induced ADP-ribosylation in HPF1$^{-/-}$ cells can be restored by transient HPF1 overexpression.* **a)** The absence of PARP1 and HPF1 lead to the loss of the majority of ADPr in response to hydrogen peroxide-induced DNA damage in 293T cells. **b)** The absence of HPF1 leads to the loss of the majority of ADPr in response to hydrogen peroxide induced DNA damage in RPE-1 cells. **c)** Overexpression of HPF1 restores DNA damage-dependent ADPr in 293T *HPF1$^{-/-}$* cells and drives up ADP-ribosylation under both DNA damage and undamaged conditions. Experiments were repeated at least two times.

background for exploring the effect of HPF1 and PARP1 mutants on DNA damage directed ADP-ribosylation. Additionally, I showed that following DNA damage ADPr levels can successfully be restored in 293T HPF1$^{-/-}$ cells through transient overexpression of FLAG-HPF1. In fact, HPF1 overexpression elevated the ADPr signal beyond wildtype

levels. Most strikingly, this was true not only for hydrogen peroxide treated cells, but also untreated 293T cells, which showed substantial histone and PARP1 ADP-ribosylation as a result of HPF1 overexpression in both the WT and *HPF1*$^{-/-}$ background. In case of the latter, the ADP-ribosylation pattern strongly resembled the one observed for DNA damage-induced ADPr, particularly with regards to PARP1 auto-modification and trans-modification of histones. I therefore established that overexpression of HPF1 in 293T WT or *HPF1*$^{-/-}$ cells can be used as a system to study the consequences of HPF1 mutants of PARP1 auto-modification and histone trans-modification even in the absence of DNA damage.

3.2 Characterizing HPF1 surface mutants

Following the establishment of a system to study phenotypically relevant PARP1 and HPF1 mutants, this chapter explores a series of surface amino acids that contribute to the overall function of HPF1 as an essential co-factor for PARP1 and PARP2 directed serine-ADP-ribosylation.

3.2.1 HPF1 ADP-ribosylation sites

The Ahel lab first reported the significance of the C-terminal portion of HPF1, and particularly the residues Y238 and R239, for PARP1 interaction in 2016 (Gibbs-Seymour et al. (2016)). Additionally, Y238 was discovered to be a potential site of HPF1 modification (Bartlett et al. (2018), Leslie Pedrioli et al. (2018)). I wanted to investigate if the mutation of either Y238 or another potential HPF1 modification site, S97, affects the ADP-ribosylation status of HPF1 in response to DNA damage. To this end I overexpressed N-terminally FLAG-tagged HPF1 in 293T cells and performed FLAG co-immunoprecipitation (co-IP) (Figure 3.3a). Mutation of S97 to acceptor hydroxyl group-lacking alanine or the HPF1-independent ADPr target residue glutamate affected HPF1 overexpression-boosted ADPr levels of histones only mildly. Interaction with endogenous PARP1 remained unchanged in both mutants. Y238 was mutated to either alanine, glutamate or phenylalanine, which - similar to alanine with regards to serine - lacks the potential ADP-ribose acceptor C4 hydroxyl group of tyrosine. While both the mutation of Y238 to alanine or to glutamate abolished HPF1 overexpression-dependent histone ADPr, this was not the case for the phenylalanine mutant. Interestingly, while both Y238A and Y238E completely lost interaction with PARP1, Y238F retained residual levels of PARP1 interaction (Figure 3.3a). As described in *1.2 DNA repair PARPs*, it has previously been shown that i) serine ADPr is the overwhelmingly dominant form of ADPr in response to DNA damage and ii) that HPF1 is required to bring about PARP1/2-catalyzed serine ADPr (Bonfiglio et al. (2017b), Palazzo et al. (2018)). On this basis, the data indicates that weak PARP1 interaction is enough for HPF1 to confer serine ADPr activity onto PARP1. Additionally, if S97 and Y238 are indeed HPF1 modification sites, the loss of HF1 modification does not affect the ability of HPF1 to confer serine trans-ADP-ribosylation in complex with PARP1.

To explore if S97 and Y238 are crucial HPF1 modification sites, FLAG-HPF1 WT and mutants were overexpressed in 293T cells and the cells left either untreated or exposed to hydrogen peroxide (Figure 3.3b). While overexpression of HPF1 S97A and Y238F did not affect the overall ADPr pattern in response to DNA damage, HPF1 Y238A and Y238E suppressed ADP-ribosylation, possibly by exerting a dominant negative effect and out-competing the much lower expressed endogenous HPF1 (Figure 3.3b). FLAG co-IP of the whole cell lysates showed that overexpressed HPF1 was modified both under non-DNA damage (basal) and DNA damage conditions, but that at 2 hours following the start of H_2O_2 treatment ADP-ribosylation of HPF1 had been reversed. Modification levels of HPF1 were similar between FLAG-HPF1 WT, S97A and Y238F. In contrast, HPF1 ADP-ribosylation was almost entirely lost in case of the FLAG-HPF1 Y238A and Y238E mutants (Figure 3.3b). These results suggest that S97 and Y238 are not major HPF1 ADPr modification sites, although Y238 was shown to be ADP-ribosylated *in vitro* (Bartlett et al. (2018), Leslie Pedrioli et al. (2018)). Rather, only the mutants that also abolish PARP1 binding in Figure 3.3a - HPF1 Y238A and Y238E - decrease overall ADPr levels and loose modification of HPF1 itself. Interaction of HPF1 with PARP1 is therefore essential for DNA damage-dependent ADPr overall as well as for HPF1 specifically.

To confirm these findings in the absence of endogenous HPF1, FLAG-HPF1 WT, Y238A and Y238F were overexpressed in both 293T parental (subsequently wildtype or WT) and *HPF1*$^{-/-}$ cells and either left untreated or treated with H_2O_2 for 10 or 120 minutes (Figure 3.3c). Similar to the previous observation in Figure 3.3b, overexpressed FLAG-HPF1 Y238A reduced DNA damage-dependent ADP-ribosylation in 293T WT cells. In 293T *HPF1*$^{-/-}$ cells, FLAG-HPF1 WT overexpression restored ADPr levels observed for 293T WT cells (Figure 3.3c). Restoration of DNA damage-dependent ADP-ribosylation was incomplete in the presence of overexpressed FLAG-HPF1 Y238F . Given that this mutant strongly reduces binding to PARP1 but does not affect modification levels of HPF1, its limited PARP1 binding capacity is most likely the reason for incomplete ADP-ribosylation (Figure 3.3a, c). Finally, overexpression of the PARP1 interaction mutant FLAG-HPF1 Y238A saw an even more drastic decrease in, albeit not complete loss of DNA damage-dependent ADPr compared to FLAG-HPF1 WT. Persistence of low histone and PARP1 modification levels, which are not present in FLAG control-treated 293T *HPF1*$^{-/-}$ cells, points to an incomplete loss of interaction with PARP1 and possibly further conserved

PARP1 interaction residues on the surface of HPF1.

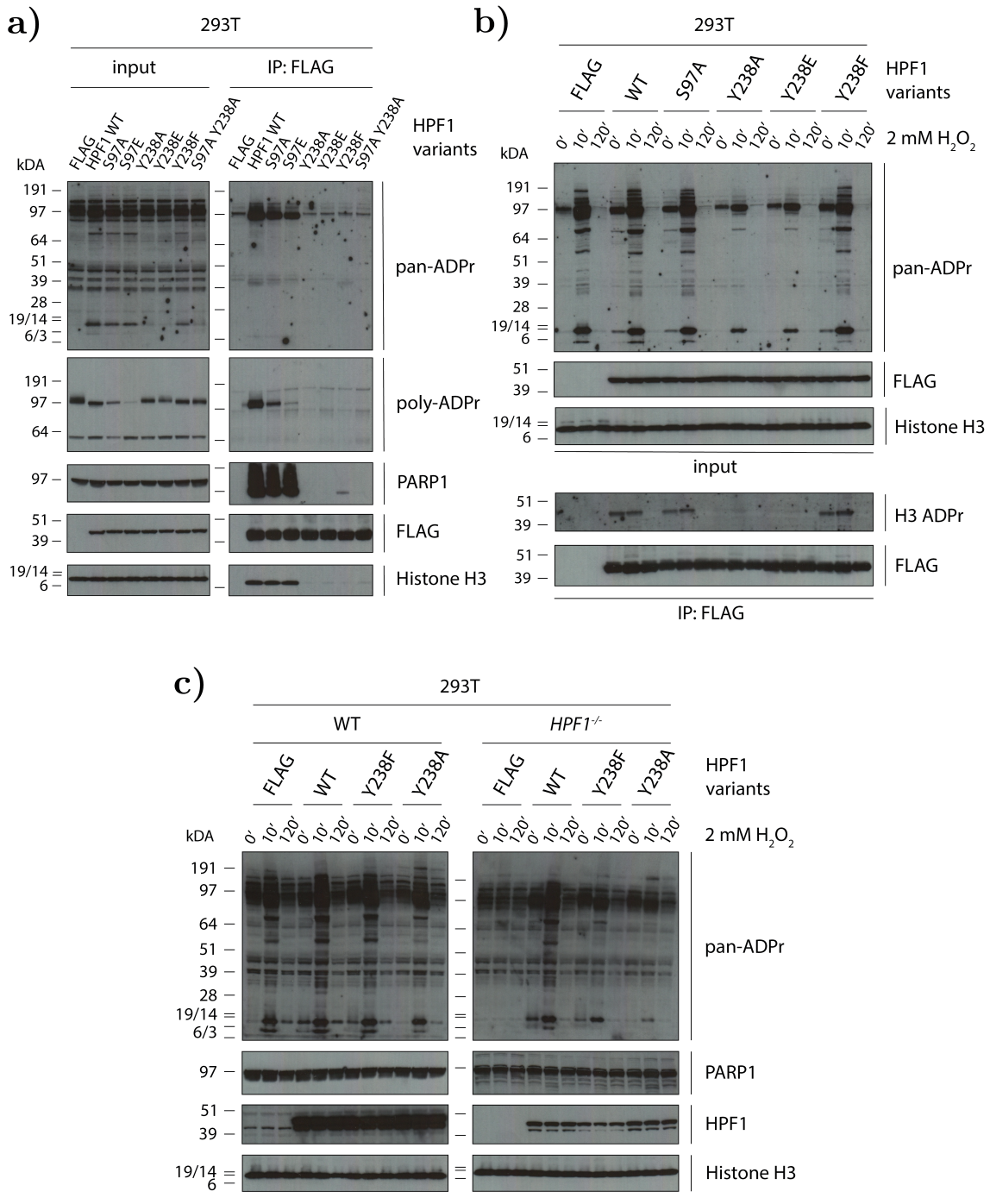


Figure 3.3: *Loss of PARP1 interaction in HPF1 abolishes HPF1 modification and DNA damage-dependent ADP-ribosylation.* **a)** HPF1 mutants that retain PARP1 binding also retain histone ADP-ribosylation as a result of HPF1 overexpression under basal levels. **b)** While S97 and Y238 are not HPF1 modification sites, the PARP1 interaction mutations Y238A and Y238E abolish HPF1 ADPr modification and compromise overall ADP-ribosylation in response to DNA damage. **c)** Confirmation of findings from **b)** in 293T *HPF1*$^{-/-}$ cells. Experiments were repeated two times.

3.2.2 HPF1 sequence conservation

Y238 and R239 were initially identified as important interaction sites for their sequence conservation across species (Gibbs-Seymour et al. (2016)). I order to further study the mechanistic basis of HPF1 function, I aimed to identify additional conserved residues. To achieve that, I carried out ClustalW2 protein sequence alignment of *Hs*HPF1 and its homologs in several different model organisms, namely *Mus musculus*, *Danio rerio*, *Drosophila melanogaster* and *Xenopus tropicalis*. The result of the sequence alignment is shown in Figure 3.4.

Sequence alignment highlighted several single as well as clusters of conserved residues across the five species (Figure 3.4). At the time of its identification as a switch of PARP1 and PARP2 to serine-ADP-ribosylation, no crystal structure of HPF1 was available. It was therefore difficult to determine which conserved residues could be surface-facing. Solution of the *Hs*HPF1 crystal structure by a formed PhD student of the Ivan Ahel lab, Pietro Fontana, solved this problem. Subsequently, sequence conservation calculated with *Consurf* multiple sequence alignment (default settings) was mapped onto the HPF1 structure through B-factor color assignment in *PyMOL*, carried out by Marcin Suskiewicz. This allowed the identification of conserved surface residues (Figure 3.5).

The sequence conservation map highlighted the fact that the majority of conserved residues in *Hs*HPF1 are not surface-facing (Figure 3.5). Rather, they most likely contribute to the overall stability and folding of the protein. An example of this is provided later in this chapter with residue D111, which is part of a cluster of highly conserved residues in the centre of HPF1. Among the patches of conserved surface residues, one comparatively large corner of the HPF1 was particularly striking. This corner included the previously identified residues Y238 and R239. Further conserved surface amino acids in close spatial, but not sequential, proximity of Y238 and R239 included F280, D283, E284 and D286A. An APBS Electrostatics map of HPF1 also revealed that this conserved corner of HPF1 also carried substantial negative charge, mainly resulting from residues D283, E284 and D286. This is highlighted in Figure 3.6.

As a result of these initial observations, I decided to mutate the conserved surface residues highlighted above as well as the internal residue D111 to generate single site mutants of FLAG-HPF1 (Figure 3.7). HPF1 WT and the mutants were subsequently overexpressed in

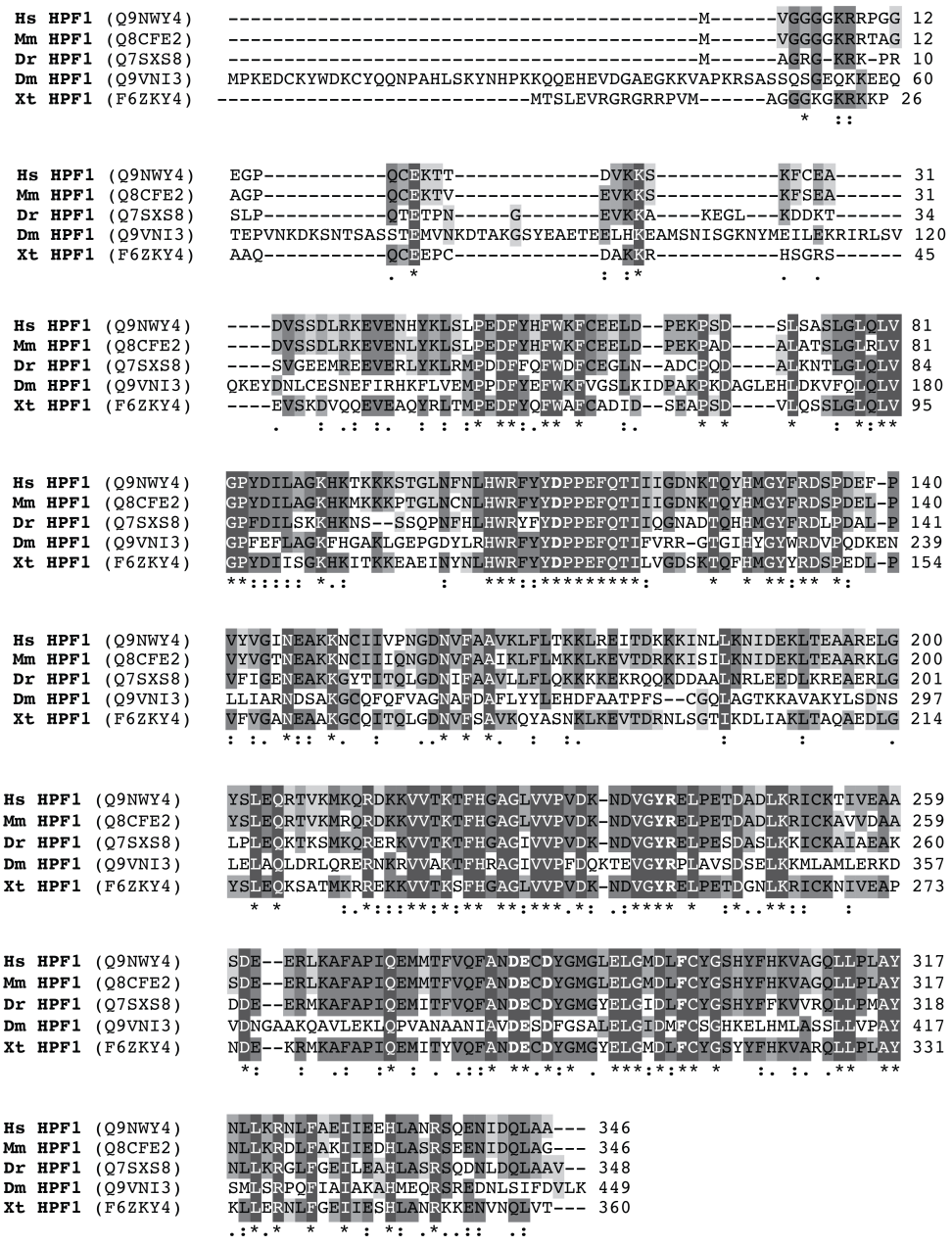


Figure 3.4: *Sequence alignment of the protein sequences from HsHPF1, MmHPF1, DrHPF1, DmHPF1 and XtHPF1.* Conservation between sequences is marked in shades of gray with the darkest shade signifying strongest sequence conservation, while unmarked residues are not conserved. An *asterisk* signifies a set of identical amino acids, a *colon* a case of at least one conserved substitution and a *dot* at least one semi-conserved substitution.

293T WT and *HPF1*$^{-/-}$ cells and co-IP carried out on the cell lysates (Figure 3.7a). Of the overexpressed constructs, only HPF1 WT and HPF1 Y238F were able to trigger low levels of PARP1 auto-modification and histone trans-ADP-ribosylation both in 293T WT and *HPF1*$^{-/-}$ cells. Mutation of either Y238, R239, D283, E284 or D286A to alanine did not restore ADPr levels in either cell line. Interestingly, ADPr status of FLAG-HPF1 WT and

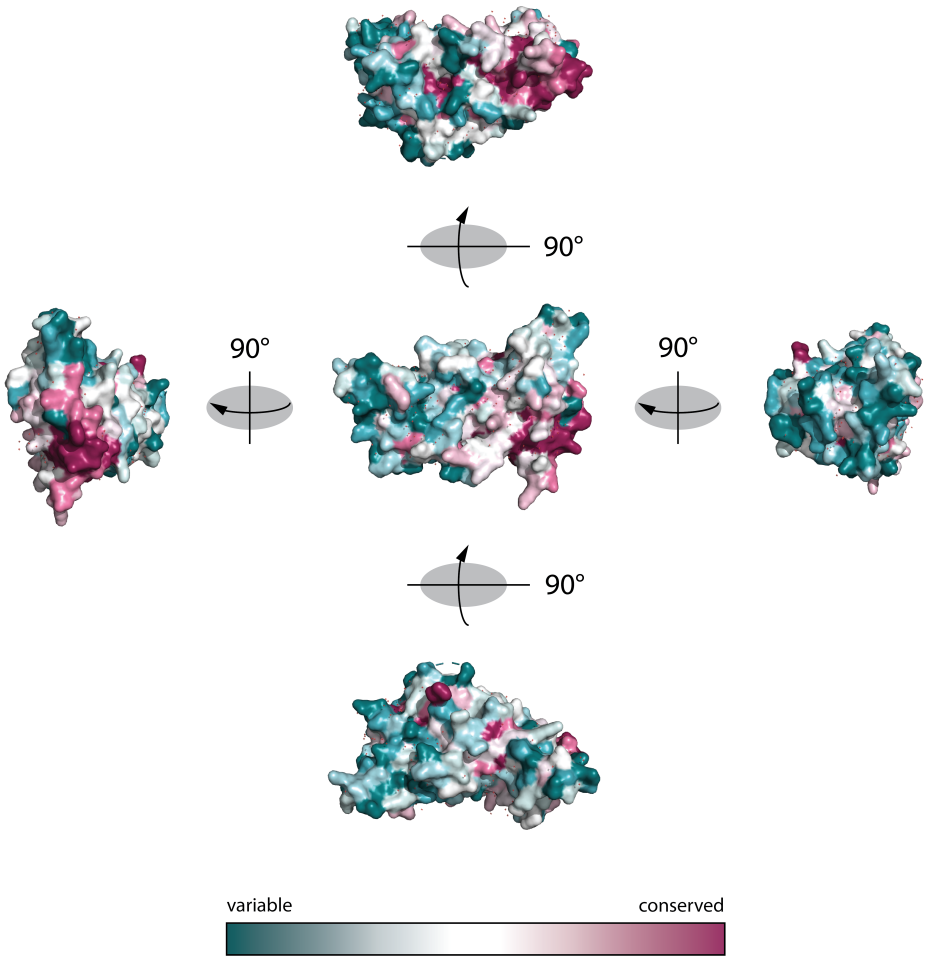


Figure 3.5: *Structure of Consequence conservation of HsHPF1 (PDB: 6M3I) visualized by Marcin Suskiewicz. Seance purple* indicates the strongest, *white* intermediate and *eden green* the weakest sequence conservation. Highest sequence conservation is visible for a corner of HPF1 which also contains Y238 and R239.

the mutants as tested in the co-IPs did not correlate with histone ADPr levels upon HPF1 overexpression. Rather, only the mutation of Y238 and E284 to alanine triggered loss of HPF1 ADP-ribosylation. While HPF1 ADPr levels were low in the case of both HPF1 WT and Y238F, both the mutation R239A and even more strongly so D286A appeared to boost HPF1 ADPr (Figure 3.7a).

In order to gain a better understanding of the mechanistic source behind the observed effects, I decided to test the binding abilities to histones, PARP1 and PARP2 of the HPF1 mutants R239A, D283A, E284A and D286A (Figure 3.7b). Loss of PARP1 binding in the HPF1 Y238A mutant has already been covered in the previous subchapter, while HPF1 D111A is an internal residue and therefore expected to impact PARP1 binding not

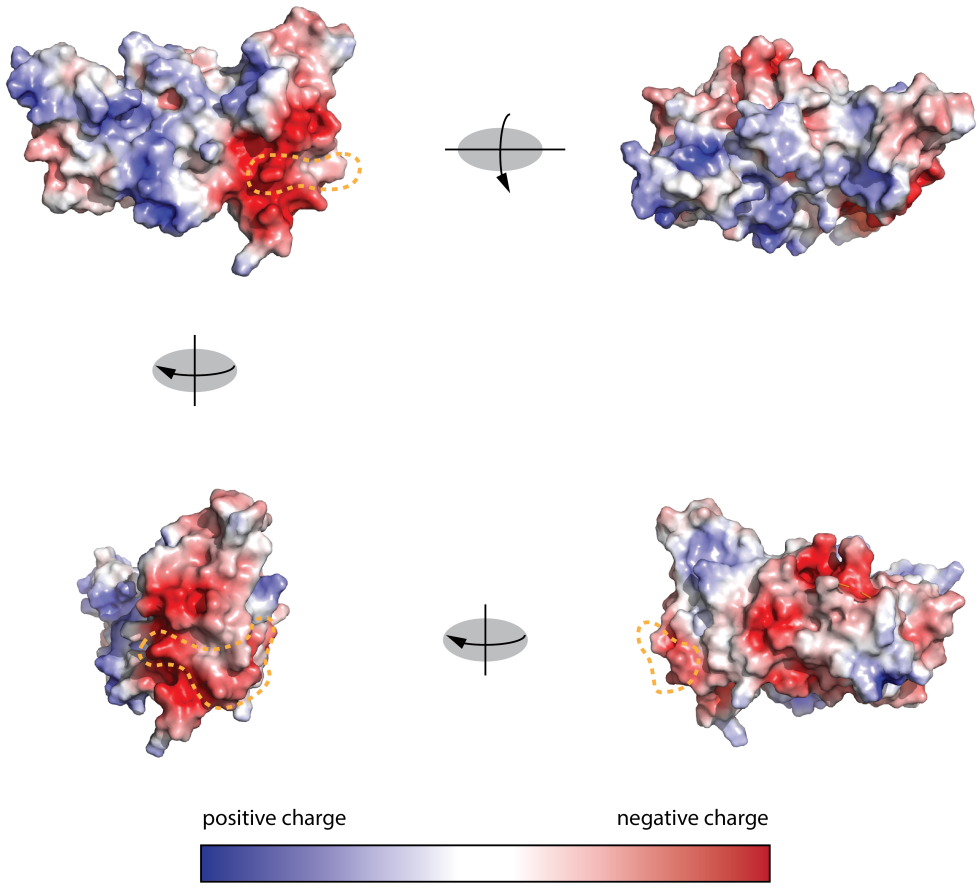


Figure 3.6: *Electrostatic map of HPF1 highlighting the charges of HPF1 surface residues.* The map was generated using the APBS Electrostatics plugin of *PyMOL*, where *red* signifies the strongest negative, *white* neutral and *blue* the strongest positive charge.

through the loss of an interaction site but rather loss of protein stability. Induction of DNA damage through hydrogen peroxide for 10 minutes triggered the expected ADPr signal in both 293T WT and FLAG-HPF1 complemented 293T *HPF1*$^{-/-}$ cells, but not in 293T *HPF1*$^{-/-}$ cells transfected with FLAG only. While both the D283A and E284A mutant abolished DNA damage-dependent cellular ADPr entirely, low levels of histone and PARP1 ADPr remained in cells complemented with FLAG-HFP1 D286A (Figure 3.7b). Even more substantial ADPr levels were retained in FLAG-HFP1 R239A complemented 293T HPF1$^{-/-}$ cells. However, an experiment using site-specific antibodies provided by the research group of Ivan Matic indicated that mutation of R239 to alanine results in a seperation-of-function mutant that abolished histone H3 S10 ADPr levels, but not histone H4 S1 ADP-ribosylation (see Figure A.1 in *A Appendix*).

FLAG-HPF1 co-IPs compared these observations with the ability of the HPF1 mutants

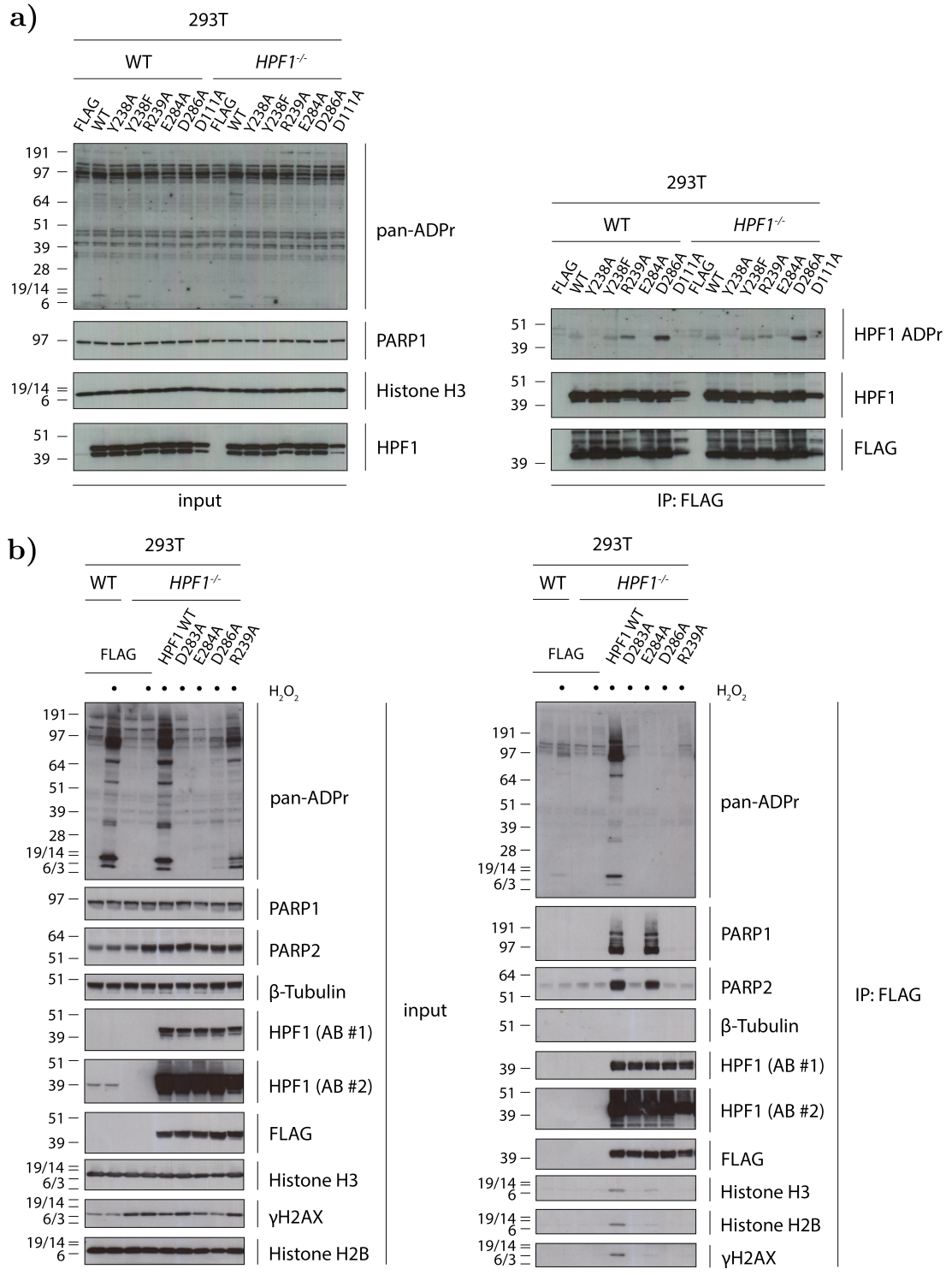


Figure 3.7: *Identifying characteristics of residues belonging to a highly conserved, negatively charged corner of HPF1.* **a)** HPF1 mutants D111A, Y238A, R239A, D283A, E284A and D286A are unable to trigger PARP1 auto- and histone trans-modification under basal conditions. **b)** HPF1 mutants D283A, E284A, D286A and R239A affect the ability of 293T cells to form ADP-ribosylation in response to DNA damage to varying degrees. FLAG co-IPs of the HPF1 variants compared this observation against their ability to bind histones, PARP1 and PARP2. Experiments were repeated at least two times.

to bind histones, PARP1 and PARP2. Unsurprisingly, the co-IP of FLAG-HPF1 WT produces a robust WB signal for PARP1, PARP2, histone H3, histone H2B and histone γH2AX. These signals were reduced to baseline levels in the FLAG-HPF1 D283A mutant, indicating that D283 is essential for interaction with PARP1, PARP2 and histones (Figure 3.7b). Most surprisingly, although HPF1 E284A did not reconstitute ADP-ribosylation in 293T *HPF1*$^{-/-}$ cells, the mutant was able to bind PARP1 and PARP2 to the same extent and showed reduced binding only towards histone H3, H2B and γH2AX. This indicates that E28A is not involved in the binding of PARP1 and PARP2. One possibility could be that E284 contributes to substrate binding, which would be in line with its reduced affinity for histones. However, given that the HPF1 E284A mutant also does not restore PARP1 ADPr and that the predominant form of ADP-ribosylation in response to DNA damage is serine ADPr, it is more likely that E284 is essential to the ability of HPF1 to switch PARP1-catalyzed ADP-ribosyltion from glutamate/aspartate to serine sites. Finally, HPF1 D286A and R239A, similar to HPF1 D283A, appear to lose interaction with PARP1, PARP2 and histones (Figure 3.7b). A possibly very faint remnant of a signal in the PARP1 blot might point to dissappearingly low levels of residual interaction between these two HPF1 mutants and PARP1, which could explain their limited capacity to restore low levels of ADP-ribosylation.

One unexpected conclusion from comparison between the findings of Figure 3.7a and Figure 3.7b is the apparent inverse correlation between binding capacity of HPF1 and levels of DNA damage-induced ADPr on the one hand and its ability to be modified on the other. While HPF1 Y238A loses HPF1 modification, the reduced ability of HPF1 R239A, and even more so of HPF1 D286A, to bind PARP1 and restore DNA damage-induced ADPr appears to increase the modification levels of both mutants. If E284 is indeed essential for HPF1 to confer serine ADPr capacity onto PARP1, this would also translate to HPF1 modification occurring on serine residues, since HPF1 ADPr levels are absent in co-IPs of FLAG-HPF1 E284A (Figure 3.7a).

The side chains of the conserved PARP1 interaction residues Y238, R239, D283 and D286 are highlighted in another (*ribbon*) representation of HPF1 (Figure 3.8). Together they constitute the majority of highly conserved residues in the negatively charged, conserved corner of HPF1 and can rightfully be thought of as the PARP1 interaction motif on HPF1. The sequence of this motif would be of the nature of YR[43-45x]DxxD. This cluster

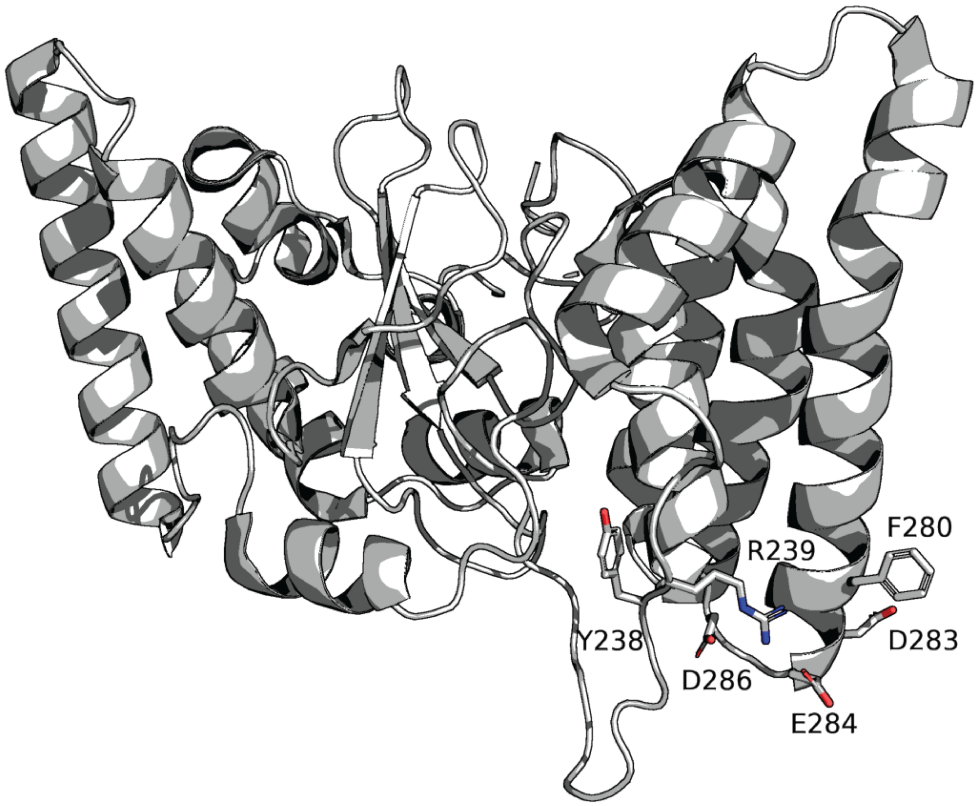


Figure 3.8: *Structure of HPF1 highlighting the side chains of residues belonging to the conserved, negatively charged corner of HPF1.* Oxygens are marked in *red* and nitrogens in *blue*.

does not contained E284, which, albeit equally important for PARP-driven DNA damage-dependent ADPr and possibly an essential factor in HPF1 switching of PARP1/2-directed glutamate/aspartate ADPr to serine sites, is not a PARP1 interaction residue (Figure 3.8). Its position is therefore also marked as *x*. One more highly conserved HPF1 corner residue - F280 - remained uncharacterized in the initial identification of PARP1 interaction sites on HPF1. Structural insights show this residue as stacking with Y460 of PARP2 or Y907 of PARP1, which in turn stack with the adenine of bound ADP-ribose. However, the consequences of mutating this residue on PARP1/PARP2 catalytic activity remain to be elucidated.

3.2.3 HPF1 in complex with PARP2 ART domain

With the resolution of a crystal structure showing HPF1 in complex with the PARP1 ART (CAT ΔHD) domain solved by Marcin Suskiewicz, he was able to visualize how the conserved, negatively charged corner of HPF1 interacted with the catalytic portion of PARP2. Given that the ART domain of PARP1 and PARP2 are virtually identical,

many of the findings from the crystal structure can be translated to the situation in the HPF1-PARP1 complex (Figure 3.9a). Specifically, the structure shows full length HPF1 in complex with the C-terminal portion of PARP2. This portion starts just after the WGR domain at residue R197 and contains the entire ART domain. Of the HD domain it contains only the αA helix, which remains folded in the catalytically active form of the catalytic domain. Bound to the PARP2 fragment is an NAD^+ analogue called benzamide adenine dinucleotide (BAD) (Figure 3.9a).

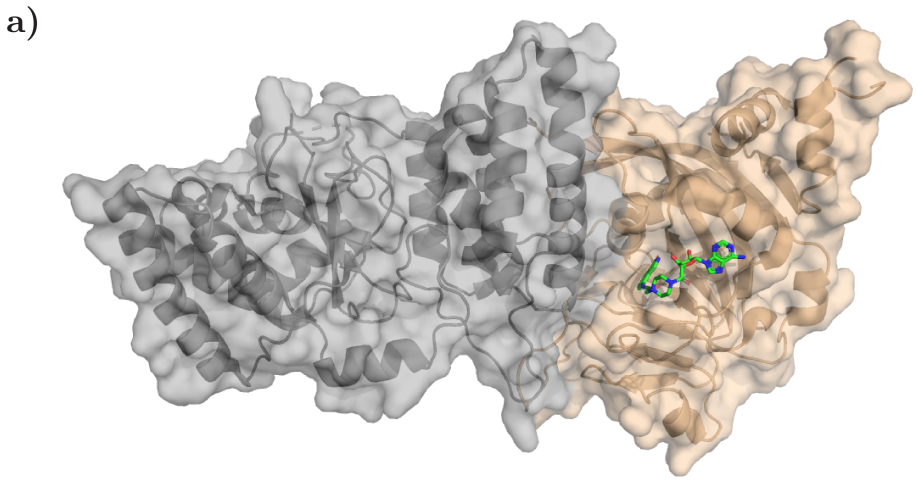


Figure 3.9: *Crystal structure of HPF1 in complex with the ART domain of PARP2 binding the NAD^+ analogue BAD.* **a)** HPF1 is colored in *wheat* and the ART domain of PARP2 in *grey*. **b)** Highlighted are the interaction residues Y238, R239, D283 and D286, the HPF1 catalytic residue E284 and the PARP2 catalytic triad H415, Y460 and E545.

A close-up of the interface between HPF1 and PARP2 reveals the positions of the identified PARP1/2 interaction residues on HPF1 as well as the catalytic triad (H415, Y460 and E545) of PARP2 (Figure 3.9b). HPF1 binds PARP2 in immediate vicinity of the active site, although only E284 and D283 appear to be reaching into the PARP2 catalytic fold. Y238, R239 and D286 in the structure are too far away from any counterpart residues to be directly interacting with PARP2, suggesting that their contribution to binding is indirect, possibly through the coordination of other residues. D283 reaches into αK of the ART domain, pointing towards a direct contact of this residue with PARP2. Interestingly, E284 is located in close proximity to the catalytic glutamate E545 of PARP2 (Figure 3.9b). This provides further evidence that E284, rather than contributing to PARP2 binding, contributes to its catalytic activity.

For the catalysis of glutamate and aspartate ADP-ribosylation by PARP1/2 only one catalytic glutamate residue, E988 in PARP1 and E545 in PARP2, is required (Figure 3.10a. The reason for this is that the side chains of aspartate and glutamate are already ionized at neutral pH and therefore do not require catalytic activation by PARP1/2. Rather, they are themselves able to lead a nucleophilic attack on C1' (of the adenosine-distal ribose), while E988/E545 facilitates the reaction by hydrogen-bonding and positioning the substrate residue or by hydrogen-bonding the hydroxyl-group of C2' and thus stabilizing the oxocarbenium reaction intermediate resulting from weakening of the C1'-nicotinamide bond (Alemasova & Lavrik (2019), Kleine et al. (2008), Marsischky et al. (1995*a*), Ruf et al. (1998, 1996)) (Figure 3.10a). Interestingly, E988 has been shown to be altogether dispensable for the initiation reaction, but not the elongation reaction of ADP-ribosylation, rendering PARP1 E988 mutants mono-ADP-ribosyl-transferases (Aberle et al. (2020), Marsischky et al. (1995*b*), Rank et al. (2016), Rolli et al. (1997)).

In contrast to glutamate/aspartate ADP-ribosylation, no ionized substrate residue exists for serine and arginine ADPr. In the latter case, cholera-toxin-like ADP-ribosyltransferases that catalyze arginine ADP-ribosylation harbour two catalytic glutamate residues as part of a conserved R-S-ExE motif (Laing et al. (2011)). Similarly, the combination of results from the HPF1-PARP2 ART domain crystal structure and biochemical assays (both carried out by Marcin Suskiewicz) as well as my cell biology results presented above lead Marcin and I to propose that E284 of HPF1 works together with PARP1 E988

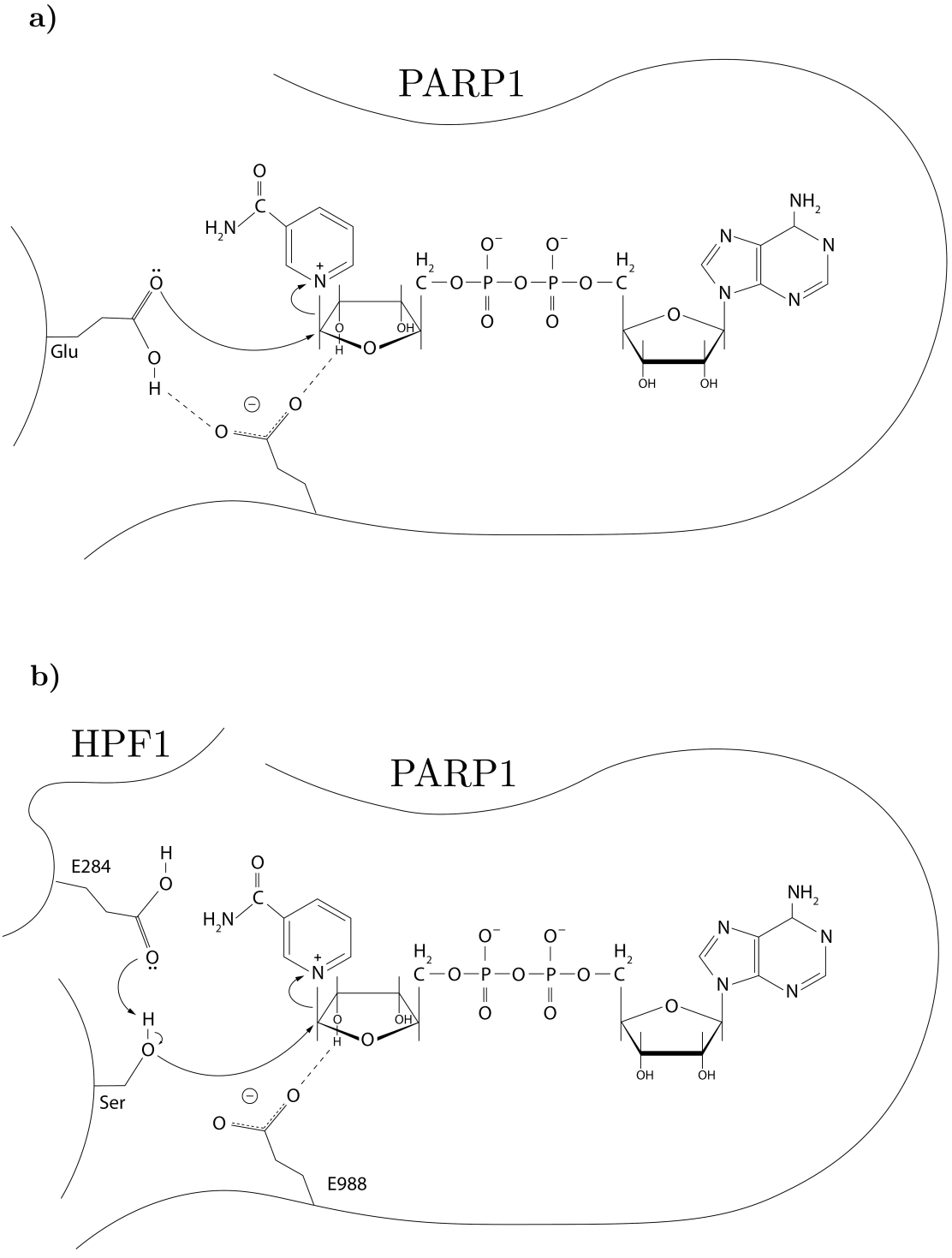


Figure 3.10: *Reaction mechanism of glutamate ADP-ribosylation (**a**)) and serine ADP-ribosylation (**b**)).* **a)** E988 of PARP1 forms a hydrogen bond with the hydroxyl group of the substrate glutamate side chain or with C2' of the adenine-proximal ribose of NAD^+ and the negatively charged oxygen of the substrate glutamate carries out a nucleophilic attack on C1'. **b)** E988 of PARP1 forms a hydrogen bond with the C2' hydroxy group of the adenine-proximal NAD^+ ribose, E284 of HPF1 deprotonates the serine residue of the substrate and the deprotonated serines makes a nucleophilic attack on C1'.

or PARP2 E545 to enable PARP1/2-catalysed serine ADPr (Figure 3.10b). The findings were published in 2020 (Suskiewicz et al. (2020)). They propose a mechanism in which HPF1 E284 is required to deprotonate serine, allowing the latter to carry out a nucleophilic attack on C1', while E988/E545 forms a hydrogen bond to stabilize the oxocarbenium reaction intermediate (Figure 3.10b).

3.3 HPF1 interaction sites on PARP1

The solution of the HPF1-PARP2 ART domain crystal structure by Marcin Suskiewicz provided further insight into the mechanism of the PARP1/2 ART domain catalytic priming for serine ADP-ribosylation. In addition, it also lent some insight into potential HPF1 interaction sites on PARP1/2, which are explored in this subchapter.

3.3.1 Structure of HPF1-PARP1 complex

In subchapter *2.2.1 PARP1 catalytic activation*, I introduced a PARP1 composite model constructed from two different structures (PDB: 4DQY, PDB: 2N8A) by alignment on the shared ZnF1 domain. This model presents PARP1 ZnF1-ZnF2-ZnF3-WGR-HD-ART bound to a single-strand break. Only the BRCT domain, which has not been crystallized due to its in large parts unstructured nature, is missing. Given that one of the main roles of PARP1 in the DNA damage response is in SSBR, this composite model can be expected to represent the main configuration of active PARP1 in the nucleus. Superimposing the HPF1-PARP2 ART domain crystal structure onto the composite model by alignment of the PARP1 and PARP2 ART domains might give an impression of what an HPF1-PARP1 complex bound to a SSB could look like (Figure 3.11).

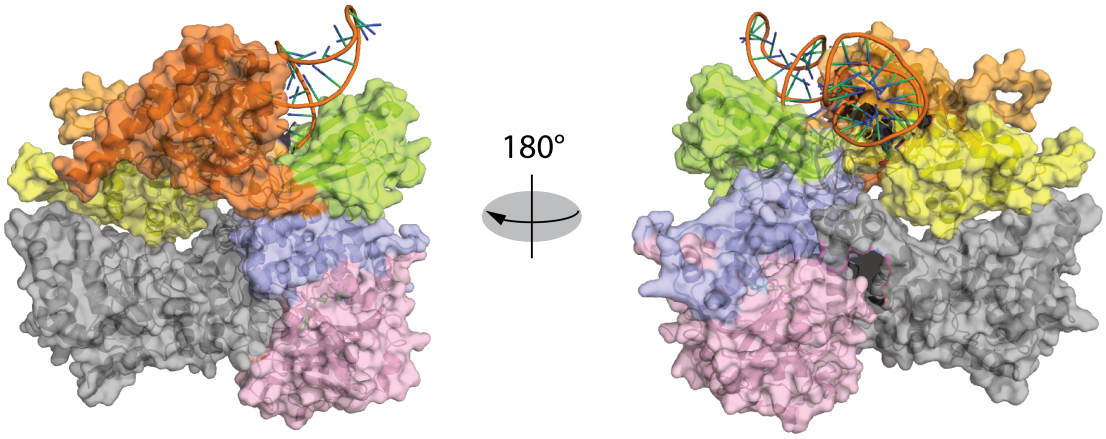
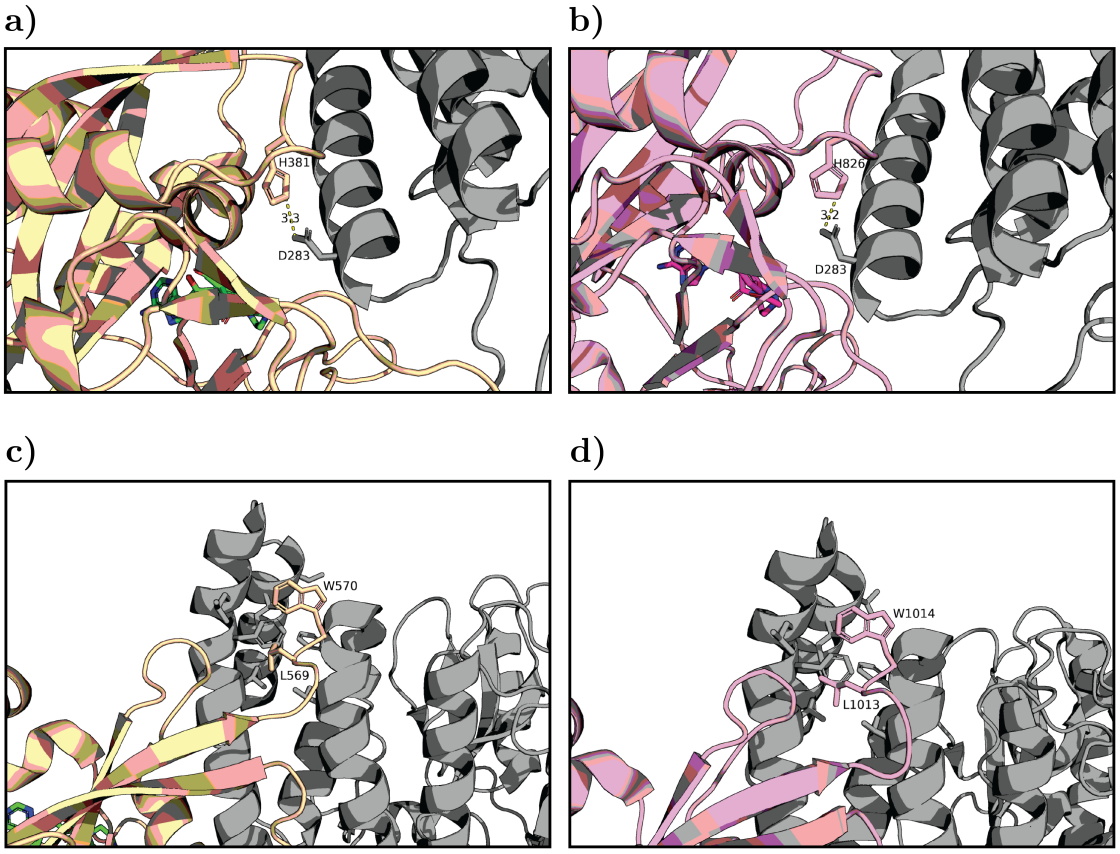


Figure 3.11: *Superimposition of the HPF1-PARP2 ART domain crystal structure (6TX3) onto the composite model from the introduction subchapter 1.2.1 PARP1 catalytic activation.* HPF1 is labelled in *grey*. The PARP1 domains are lablled as follows: ZnF2 in *yellow*, ZnF1 in *lightorange*, ZnF3 in *orange*, the WGR domain in lemon, the HD in *lightblue* and the ART domain in *lightpink*.

Beyond that, the HPF1-PARP2 ART domain crystal structure highlights PARP2 residues

that could be important for interaction with HPF1 among residues previously identified by Marcin Suskiewicz through sequence alignment as being conserved between PARP1 and PARP2, but not PARP3 (Figure 3.11). Since PARP3 is a mono-ADP-ribosyltransferase and has not been described to catalyze serine ADPr or interact with HPF1, any residues conserved between PARP1 and PARP2, but not PARP3, in the shared regions between the three proteins are likely to be either responsible for the poly-ADP-ribosyltransferase activity or HPF1-binding ability of PARP1 and PARP2. Superimposition of the HPF1-PARP2 ART domain crystal structure onto the composite model from the introduction



e)

	PARP2	PARP1
D283 interaction	H381	H826
C-terminus	L569, W570	L1013, W1014

Figure 3.12: *Identification of potential HPF1 interaction sites on PARP1/2.* **a)** and **b)** show the H381 of PARP2 and H826 of PARP1, respectively, forming a hydrogen bond with D283 of HPF1. **c)** and **d)** illustrate the three C-terminal residues of PARP2 and PARP1, respectively, which could be forming hydrophobic interactions with HPF1. **e)** presents a table highlighting the respective potential HPF1 interaction residues on PARP1 and PARP2.

subchapter *1.2.1 PARP1 catalytic activation* illustrates the position of equivalent residues on PARP1 to the ones highlighted on PARP2. One candidate residue for HPF1 interaction on PARP2 that is visualized by the crystal structure is residue H381 (Figure 3.12a). The Nθ of histidine can form an N-H...O=C hydrogen bond with D283 of the HPF1 negative charged corner introduced in *3.2.2 HPF1 sequence conservation* and this interaction is likely to possess an electrostatic component as well. Superimposition of the PARP1 structure reveals that the equivalent PARP1 residue, H826, is similarly positioned and its Nθ equally suited to form the same bond (Figure 3.12b).

Strikingly, one potential reason for the previous absence of HPF1 crystal structures with the PARP1/2 catalytic domain is the fact that some, albeit not all, previously crystallized PARP1 fragments were missing C-terminal residues to facilitate crystallization. The PARP1/2 C terminus is flexible in the absence of HPF1, but the HPF1-PARP2 ART structure shows that in particular its last two residues are involved in HPF1 binding (Figure 3.12c and d). On PARP2 these are L569 and W570. Both residues are hydrophobic, opening up the question whether they might form hydrophobic contacts with HPF1 that are crucial for its ability to bind the protein. Indeed, HPF1 harbours several hydrophobic residues on its α-helices αH, αI, and αK (Figure 3.12c). The equivalent residues to the two PARP2 C-terminal residues on PARP1 are L1013 and W1014 (Figure 3.12d). The lack of conservation between residue Q568 of PARP2 and S1014 of PARP1 and the fact that both are not hydrophobic amino acids further suggests that only the last two amino acids in PARP1 and PARP2 might be essential for HPF1 binding. Following the 2020 publication for the Ahel lab, which already presented NMR interaction data between PARP1 and HPF1, a similar study has been published in 2021 revealing the crystal structure of HPF1 in complex with the ART domain of PARP1 (Sun et al. (2021), Suskiewicz et al. (2020)). This novel crystal structure contains the last three C-terminal residues of PARP1. Similar to the situation observed for H381 of PARP2 and H826 of PARP1, their localization in relation to HPF1 mimics the situation observed for the HPF1-PARP2 ART domain complex (Figure 3.12d).

3.3.2 HPF1 interaction sites on PARP1

In order to visualize PARP1-HPF1 interaction in cells and determine its nature through putative interaction mutants, I was first required to establish conditions reliably showing

PARP1-HPF1 binding. Since HPF1 is thought to bind only catalytically active PARP1, one aspect of seeking the correct conditions was to maximize the amount of active PARP1 molecules in cells. While FLAG-HPF1 overexpression was able to pull down considerable levels of endogenous PARP1, only very low levels of endogenous HPF1 could be detected in co-IPs of YFP-PARP1 (Figure 3.13a). Expressing a constitutively active PARP1 mutant lacking the HD (YFP-PARP1 ΔHD), did initially not overcome this obstacle, due its low expression levels (Figure 3.13a). These were likely a consequence of constitutive PARP1 activity being toxic to cells. Catalytically impairing YFP-PARP1 ΔHD by combining it with a E988Q mutation (lane 5) did not affect its expression levels, but drastically improved its binding to simultaneously overexpressed FLAG-HPF1 compared to the YFP-

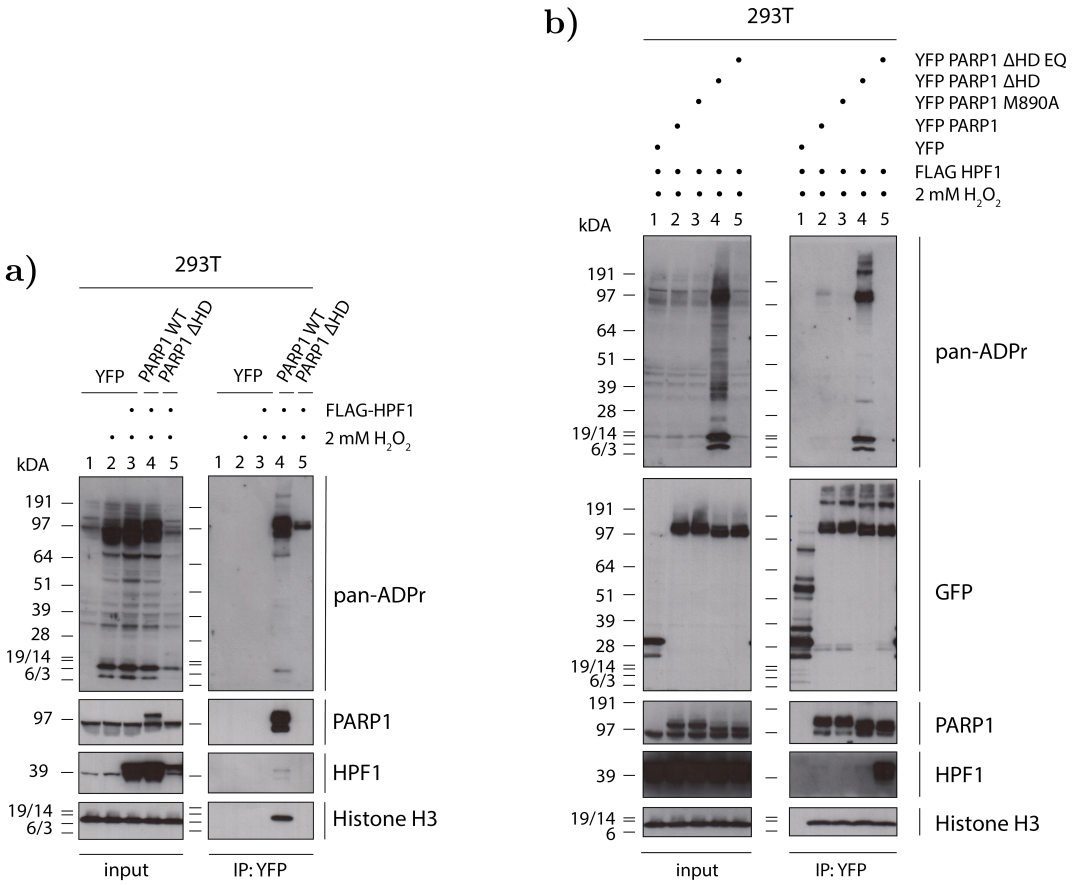


Figure 3.13: *Catalytically impaired PARP1 ΔHD binds detectable levels of FLAG-HPF1.* **a)** Transiently overexpressed YFP-PARP1 can bind barely detectable levels of overexpressed FLAG-HPF1. Deletion of HD in YFP-PARP1 almost eliminates expression of the mutant. **b)** A catalytically impaired PARP1 ΔHD E988Q double mutant further inhibited by Olaparib, but not the inhibited PARP1 ΔHD single mutant, was able to bind robust levels of transiently overexpressed FLAG-HPF1. Experiments were repeated at least two times.

PARP1 ΔHD single mutant (lane 4) (Figure 3.13b). Finally, in a tentative first, single-repeat experiment, I was able to show that additional catalytic inhibition through Olaparib pretreatment allowed the observation of robust endogenous HPF1 levels in a co-IP of YFP-PARP1 ΔHD (lane 4) (Figure 3.14a).

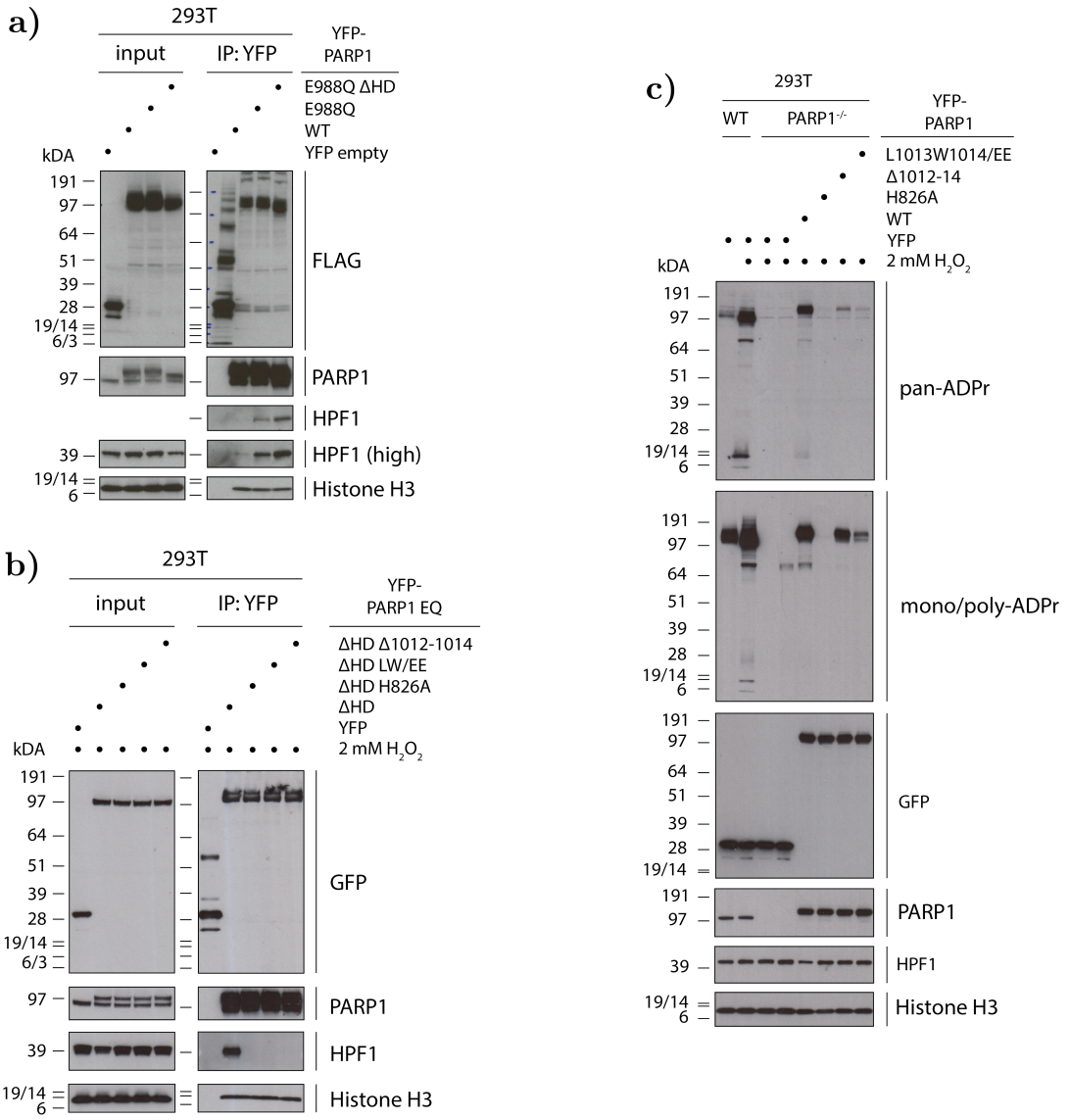


Figure 3.14: *The C-terminus and H826 of PARP1 are essential for PARP1 interaction with HPF1.* **a)** E988Q mutation of full-length PARP1 encourages FLAG-HPF1 binding, while additional deletion of the HD shows further, cumulatively enhanced binding.**b)** Mutation of H826 or L1013/W1014 of PARP1 abolishes interaction with HPF1. **c)** HPF1 interaction mutants of PARP1 are unable to complement DNA damage-induced ADPr lost in 293T *PARP1*$^{-/-}$ cells. In **a)** and **c)**, experiments were carried out once In **b)**, the experiment was repeated at least two times.

Following the generation of conditions for observing PARP1-HPF1 interaction in cells, I decided to use the enhanced HPF1 binding mutant YFP-PARP1 ΔHD E988Q to test the

effect of the potential interaction mutations H826A, Δ1012-1014 and L1013E/W1014E on the ability of PARP1 to bind endogenous HPF1 (Figure 3.14b). The same experimental set-up as previously used for the experiments in Figure 3.14a was also used in this case. None of the additional mutations affected PARP1 expression levels, with all constructs being expressed to the same extent as endogenous PARP1. Co-IP also revealed equal levels of precipitated YFP-PARP1 between all variants (Figure 3.14b). However, only YFP-PARP1 ΔHD E988Q was able to bind HPF1. All of the additional mutations abolished the interaction with HPF1. The results illustrate that the last two C-terminal residues of PARP1, which are both conserved between PARP1 and PARP2, are both required for the interaction with FLAG-HPF1. Similarly, residue H826 of PARP1 is also essential for HPF1 interaction (Figure 3.14b). Interestingly, H826 in the above mentioned crystal structure of the PARP1 catalytic fragment with Carba-NAD (PDB: 1A26) makes contact with the phosphates of the acceptor ADP-ribose in a configuration mimicking the

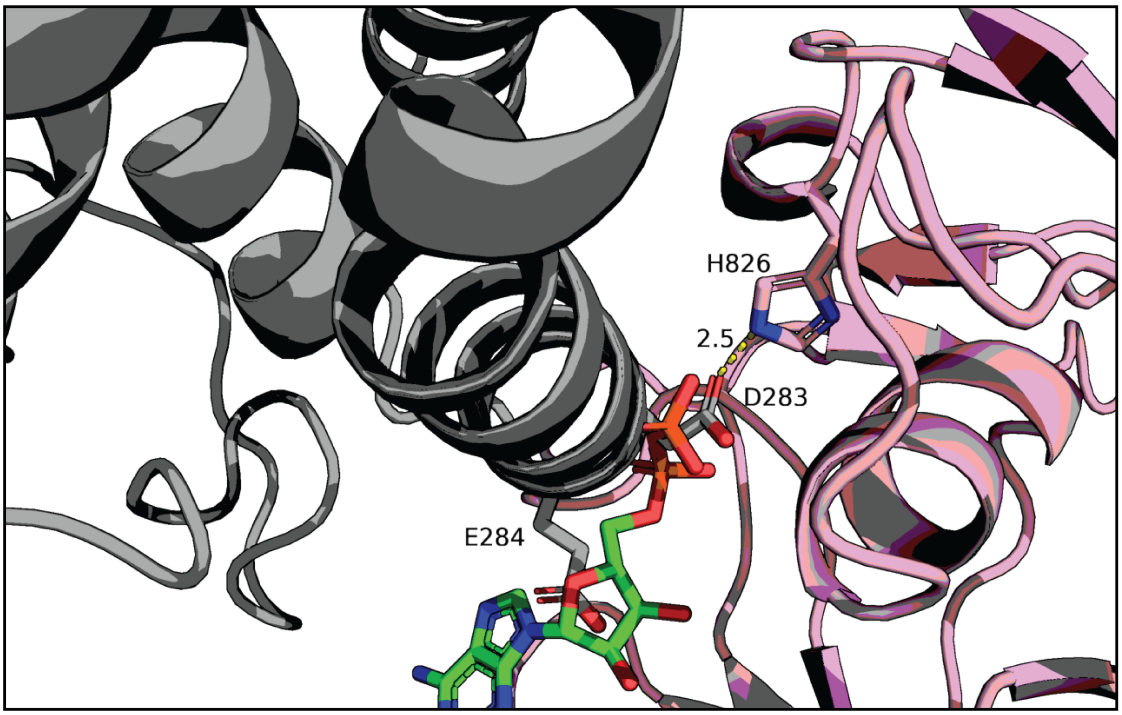


Figure 3.15: *Composite model of the HPF1-PARP2 ART domain structure (PDB: 6TX3) superimposed on the structure of the catalytic fragment of PARP1 bound to Carba-NAD (PDB: 1A26).* HPF1 is shown in *gray* and PARP1 in *pink*. The hydrogen bond between the nitrogen of H826 and the carboxyl group of D283 is shown. The oxygen-coordinating, nicotinamide-proximal phosphate of Carba-NAD sits in close proximity to δC of E284. The nicotinamide cyclopentane portion of Carba-NAD, which is flexible in the crystal structure, is not shown.

elongation reaction (Figure 3.15). This indicates that the residue is important not only for HPF1 interaction in the initiation reaction, but also for the binding of the acceptor ADP-ribose in the elongation reaction.

Finally, I also wanted to test if the previously identified HPF1 interaction mutants of PARP1 are able to complement 293T *PARP1*$^{-/-}$ cells (Figure 3.14c). I carried out a tentative first, single-repeat complementation assay overexpressing full-length YFP-PARP1 WT, H826A, Δ1014-1012 and L1013E/W1014E in 293T *PARP1*$^{-/-}$ cells and introducing DNA damage with hydrogen peroxide. While 293T WT cells showed robust induction of PARP1 auto- and histone trans-ADPr, the signal was lost in *PARP1*$^{-/-}$ cells. All YFP-PARP1 constructs were expressed to similar levels and substantially higher than endogenous PARP1 in 293T WT cells. Unsurprisingly, only YFP-PARP1 WT was able to reconstitute ADP-ribosylation. While histone ADPr was lost in all mutants, residual levels of PARP1 auto-modification remained in cells complemented with either PARP1 Δ1014-1012 or L1013E/W1014E (Figure 3.14c). This points further towards the essential role of H826 in PARP1-catalyzed ADPr and also provides evidence that PARP1 auto-modification is overwhelmingly coupled to its ability to bind HPF1. PARP1 auto-modification is discussed more in the following chapter.

3.4 PARP1 auto-modification

As indicated in the previous subchapter, one observation from studying HPF1 interaction mutants of PARP1 was the fact that the loss of HPF1 binding to PARP1 correlates with the loss of PARP1 auto-modification. This prompts the question, if PARP1 auto-modification as a result of DNA damage or under basal conditions is dependent on HPF1. I therefore decided to study the identity of the principal putative PARP1 auto-modification sites in human cells, their dependence on HPF1, and the consequences of their loss for the ability of PARP1 to resist inhibition by PARP inhibitors (PARPi).

3.4.1 PARP1 auto-modification sites

Previous mass spectrometry results have identified various putative glutamate and serine sites as targets of PARP1 auto-modification, while other sites can be predicted (Bonfiglio et al. (2017b), Larsen et al. (2018), Martello et al. (2016), Sharifi et al. (2013)). 6 such glutamate and 3 serine sites are located downstream of the BRCT domain in an region that is part of a bigger domain long known to be the main acceptor of PARP1 auto-modification (D'Amours et al. (1999)) (Figure 3.16). Given that this auto-modification region is highly flexible and is so far not part of the crystal structure of any PARP1 fragment, its location within the compacted, catalytically active PARP1 protein remains elusive. The proximity of the sites to the protein-interaction BRCT domain suggests that the sites could be trans-modified by another protein. However, two aspects of PARP1 ADPr make this unlikely: PARP1 auto-modification is both largely dependent on i) HPF1-binding (as shown earlier) and ii) PARP1 catalytic activity (as shown later in this chapter). This leaves only the option of PARP1 being modified by another PARP-HPF1 complex. Recently, the Halic lab has shown that two PARP2-HPF1 complexes can bridge the gap in a double strand break (Bilokapic et al. (2020)). Similarly, it has long been suggested that PARP1 binds SSBs as a dimer and there is also evidence to suggest that PARP1 dimerization positively impacts both PARP1 catalytic activity and its ability to be auto-modified (Alemasova & Lavrik (2019), Mendoza-Alvarez & Alvarez-Gonzalez (1993), Pion et al. (2005)). However, other more recent findings propose the notion of both monomeric DNA binding by PARP1 as well as intra- rather than intermolecular PARP1 auto-modification (Eustermann et al. (2015), Steffen et al. (2016)). Structural flexibility of the auto-modification domain cer-

tainly supports the possibility of a single PARP1 molecular modifying itself. Determining the nature of PARP1 modification sites could help ultimately resolve any uncertainties regarding the mechanism of its auto-ADP-ribosylation. An illustration of the potential modification sites and their approximate location on PARP1 is shown in Figure 3.16.

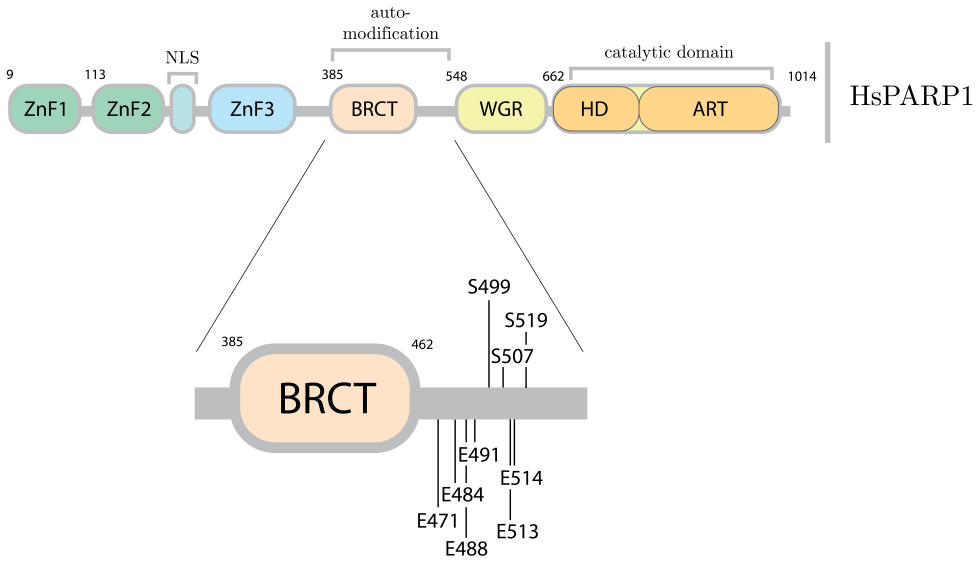


Figure 3.16: *Domain structure of PARP1 highlighting potential auto-modification sites.* The sites are located C-terminal of the protein-interaction BRCT domain in the auto-modifcation region. All of the potential serine sites (S499, S507 and S519) are preceded by a lysine in agreement with serine modification sites often appearing in a KS motif (Larsen et al. (2018)).

To identify the nature of PARP1 auto-modification in cells I first decided to test PARP1 auto-modification levels of different PARP1 mutants under DNA damage conditions (Figure 3.17). To this extent, I complement U2OS PARP1 KO cells with either YFP-PARP1 WT, a S499A/S507A/S519A (3x S/A) mutant or a E471A/E484A/E488A/E491A/E513A/E514A (6x E/A mutant) previously generated by Ian Gibbs-Seymour (Figure 3.17a). All three variants were expressed at comparable degrees above endogenous PARP1 expression levels, allowing direct comparison between them. Similar to 293T cells, hydrogen peroxide treatment of wildtype cells triggered robust PARP1 auto-modification, which was lost in PARP1 KO cells and restored by PARP1 WT and PARP1 6x E/A. However, no significant levels of PARP1 auto-modification was observed with PARP1 3x S/A overexpression (Figure 3.17a). This points towards S499, S507 and S519 being the main sites of PARP1 auto-modification in response to DNA damage. Unfortunately, only low levels of histone ADPr could be observed in U2OS WT cells. Additionally, following loss of

histone ADPr levels in U2OS PARP1 KO cells, none of the YFP-PARP1 variants reconstituted histone ADPr levels in this experiment, leaving open the question of how PARP1 auto-modification levels might affect PARP1-catalyzed trans-ADPr.

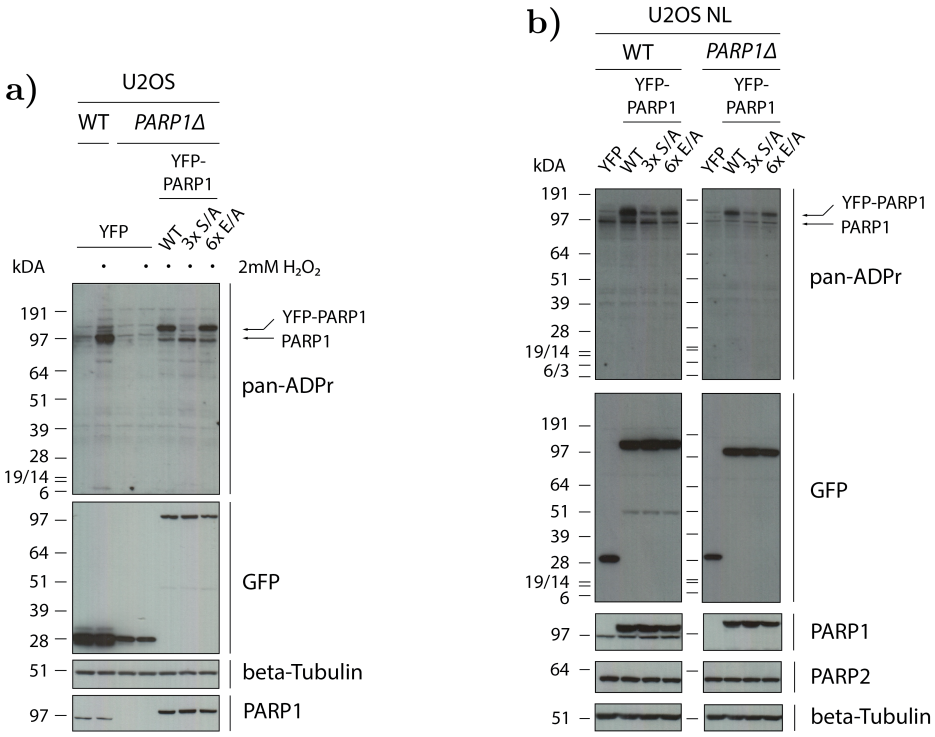


Figure 3.17: *The serine sites S499, S507 and S519 are the predominant targets of PARP1 auto-modification.* **a)** The influence of mutating three potential serine or six potential glutamate ADP-ribosylation sites on PARP1 auto-modification is tested under DNA damage conditions. **b)** Under basal conditions, mutation of the three potential serine sites still leads to the loss of the majority of PARP1 ADP-ribosylation, while a smaller fraction appears of ADP-ribosylated PARP1 appears to depend on glutamate. In **a)**, the experiment was repeated twice. In **b)**, the experiment was carried out once in the particular cell lines.

Subsequently, I wanted to see if a similar situation was true for basal conditions. Additionally, given that the overexpression of YFP-PARP1 in the U2OS cells shown in Figure 3.17a triggered the appearance of an additional ADPr band of unknown identity at a slightly lower molecular weight than endogenous PARP1, I decided to observe PARP1 auto-modification levels under basal conditions in U2OS WT and PARP1 KO cells received from Nick Lakin (U2OS NL) (Figure 3.17b). Overexpression of YFP-PARP1 in these cells in a tentative, single-repeat experiment also exceeded that of endogenous PARP1 and was sufficient to result in ADP-ribosylated YFP-PARP1 WT even in the absence of DNA damage. Similarly to Figure 3.17a, while low levels of endogenous PARP1 auto-modification

could be observed in WT cells, this signal was absent in U2OS PARP1 KO cells. In U2OS WT cells, auto-modified YFP-PARP1 appeared as an additional band above ADP-ribosylated endogenous PARP1 (Figure 3.17b). Again, mutation of the three potential serine auto-modification sites had the strongest effect on YFP-PARP1 auto-modification both in WT and PARP1 KO cells. However, in U2OS WT cells it did not fully abolish YFP-PARP1 ADPr. Additionally, a less substantial reduction in YFP-PARP1 ADP-ribosylation could also be observed for the 6x E/A mutant. This indicates that, under basal conditions, while serine might still be the predominant type of acceptor amino acid for PARP1 auto-modification, a smaller fraction can also be attributed to glutamate (Figure 3.17b). To confirm the findings I repeated the previous complementation experiment from Figure 3.17a in 293T *PARP1*$^{-/-}$ cells. Additionally, I generated single and double mutants of the three serine auto-modification sites S499, S507 and S519 to determine which of the sites has the strongest impact on PARP1 auto-modification. The results are shown in Figure 3.18.

They broadly confirm the initial findings made in U2OS WT and PARP1 KO cells. Treatment of cells with hydrogen peroxide induced a robust ADPr signal, particularly of histones and PARP1 (Figure 3.18). Loss of PARP1 abolished that signal and YFP-PARP1 overexpression in 293T *PARP1*$^{-/-}$ cells mostly restored PARP1 auto-modification but only to a small degree histone ADPr. Of the PARP1 S499A, S507A and S519A single mutants, S499A appeared to leave PARP1 auto-modification levels unaffected, if not even slightly increased, while PARP1 S507A and PARP1 S519A showed similarly reduced ADPr levels. Intriguingly, it was the combination of the S499A and S507A mutations that resulted in loss of most PARP1 ADPr, while PARP S499A/S519A and PARP1 S507A/S519A showed similarly reduced ADPr levels to PARP1 S507A and PARP1 S519A single mutants (Figure 3.18). This points towards a more complicated mechanism of PARP1 auto-modification that could involve cross-talk between the three sites. In such a scenario it is possible to imagine that a certain mutation might affect PARP1 auto-modification not just through the loss of a target site, but also because this site's absence might impact - for example in a compensatory or inhibitory manner- the extend to which the other target sites nearby can be modified. While S499 and S519 might therefore not necessarily be the two main PARP1 auto-modification target sites, their combined mutation certainly abolishes the bulk of PARP1 auto-ADPr - possibly also by preventing modification on S507. Mutation

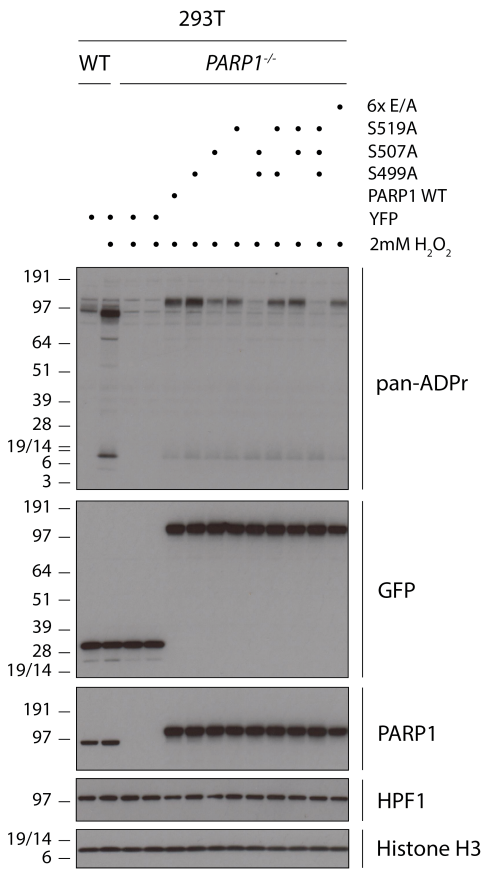


Figure 3.18: *PARP1 is predominantly dependent on serine sites for auto-modification in 293T PARP1$^{-/-}$ cells following DNA damage induction.* Mutation of S499 and S507 to alanine is sufficient to abolish almost all ADP-ribosylation on PARP1. The mutation of six glutamate sites also affect PARP1 auto-modification levels, albeit to a much lesser degree. The experiment was repeated at least two times.

of the six putative glutamate ADPr sites also affected ADP-ribosylation of PARP1, albeit to a much lower extent (Figure 3.18). Their combined mutation to alanine prompted the same reduction in PARP1 auto-modification as either the PARP1 S507A or the PARP1 S519A mutant.

Altogether, these findings point to a role of both serine and glutamate sites in PARP1 auto-modification (Figure 3.18). The results also identified S499, S507 and S519 as the major serine target sites. Given that serine has been described to be the predominant form of ADPr under DNA damage conditions, it is unsurprising that mutation of the three tested serine sites would abolish the majority of H_2O_2-induced PARP1 ADPr. However, the above findings provide evidence that this is also true for basal conditions. Given that in both cases mutation of putative glutamate ADP-ribosylation sites also affects PARP1

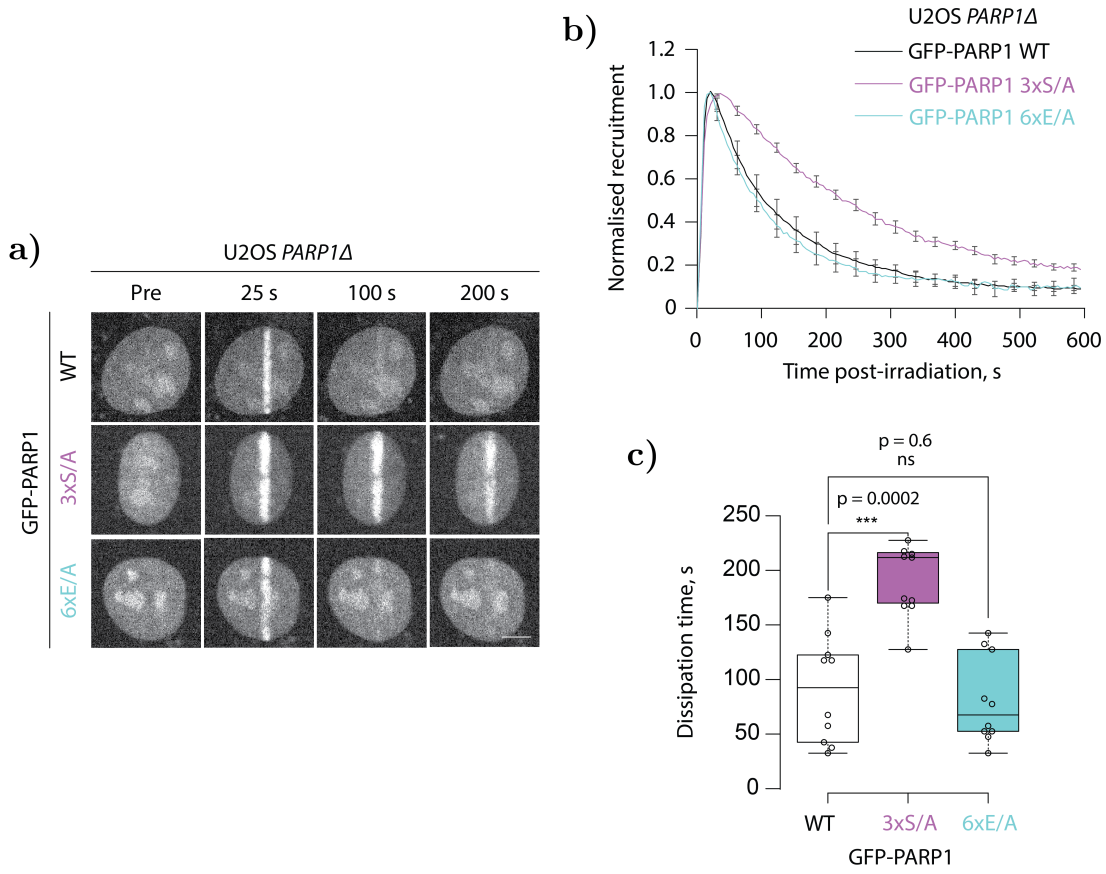


Figure 3.19: *YFP-PARP1 auto-modification status determines dissipation rates from sites of laser-induced DNA damage in U2OS PARP1Δ cells.* **a)** Snapshots highlighting the difference in laser stripe recruitment between YFP-PARP1 WT and the two mutants at 0, 25, 100 and 200 seconds after DNA damage induction. **b)** Recruitment dynamics of YFP-PARP1 WT, 3x S/A and 6x E/A at sites of laser induced DNA damage normalized to the strongest value of fluorescence intensity at the DNA damage site for each of the three variants. **c)** Difference in dissipation times from laser induced DNA damage sites between YFP-PARP1 WT, 3x S/A and 6x E/A. In b), data points are shown as mean ± SEM from the analysis of at least 10 nuclei. In c), the box limits correspond to the 25th and 75th percentiles and the bold line indicates the median value; the whiskers extend 1.5 times the interquartile range. *p $<$ 0.05; **p $<$ 0.01; ***p $<$ 0.001 (two-tailed Student's t-test).

ADPr levels leaves the question whether serine and glutamate target sites on PARP1 serve partially redundant roles. To explore how the loss of serine and/or glutamate ADPr on PARP1 affects the protein's recruitment to and its dissociation from sites of DNA damage, our collaborators from Université de Rennes 1 in France - Rebecca Smith, Siham Zentout and Sébastien Huet - transiently transfected the YFP-PARP1 WT, 3x S/A and 6x E/A constructs used in the above experiments into U2OS PARP1 KO cells and tested their

recruitment to sites of laser-induced DNA damage (Figure 3.19). DNA damage was induced in cells with a 405 nm laser at 125 μW. Laser microirradiation was performed along a 16 μm line. Figure 3.19a illustrates the fluorescence intensity of YFP-PARP1 WT, 3x S/A and 6x E/A at the site of laser-induced damage at 0, 25, 100 and 200 seconds after DNA damage induction. YFP-PARP1 WT and 6x E/A recruitment behaved very similar, with a fluorescent signal appearing 25 seconds after DNA damage induction and rapidly disappearing again at 100 seconds after microirradiation. In contrast, YFP-PARP1 3x S/A appeared to show stronger fluorescence signal at 25 seconds after microirradiation, which persisted even at 200 seconds after damage induction (Figure 3.19a).

Images from different time points between 0 and 600 seconds were quantified using R software and fluorescence intensity of each time point was normalized to the time point of highest fluorescence intensity (Figure 3.19b). While YFP-PARP1 WT and 6x E/A recruitment peaked almost immediately after microirradiation, the highest level of YFP-PARP1 3xS/A was achieved slightly later. Dissipation of YFP-PARP1 WT and 6x E/A occurred almost as rapidly as association, resembling a spike. Following its more gradual increase in fluorescence intensity, YFP-PARP1 3xS/A, on the other hand, showed a much slower decrease of the fluorescence signal at sites of microirradiation. Only at 600 seconds after laser stripe treatment was the fluorescence signal in YFP-PARP1 3x S/A expressing cells again converging on that of YFP-PARP1 WT and 6x E/A expressing cells (Figure 3.19b). This much slower dissipation of the PARP 3x S/A mutant from the site of laser-induced DNA damage was further reflected in the average dissipation time between the three variants (Figure 3.19c). Dissipation time was measured as the time required for the fluorescence signal to have decreased to 50% of its maximum value. Again YFP-PARP1 WT and 6x E/A behaved almost identical, with differences between the two proteins being not statistically significant. Dissipation time for YFP-PARP1 3x S/A was markedly increased with the average at more than double the average dissipation for YFP-PARP1 WT (Figure 3.19c).

These results connect the observations on PARP1 auto-modification with that of PARP1 dissociation from sites of DNA damage. In addition to the observations of Figure 3.17 and Figure 3.18 that the loss of the three putative target sites of serine ADP-ribosylation on PARP1 - S499, S507 and S519 - abolishes the majority of PARP1 ADPr in cells, the findings from Figure 3.19 illustrate that the absence of these sites also drastically delays

the dissociation of YFP-PARP1 from sites of laser-induced DNA damage. Together, these results indicate i) that PARP1 auto-modification is required for the efficient release of PARP1 from sites of DNA damage and ii) that PARP1 serine, but not glutamate, auto-modification is seminal for the release of PARP1 from sites of DNA damage. Therefore, it can be speculated that although glutamate ADPr does constitute a minority fraction of PARP1 auto-modification its loss in the presence of the serine auto-modification sites has no significant effect on the release of PARP1 from sites of DNA damage. It is, however, likely that in the case of loss of HPF1 and consequent absence of serine ADPr, glutamate ADP-ribosylation of PARP1 could allow its release from DNA. This idea is further illuminated in the next subchapter.

3.4.2 PARP1 auto-modification and PARPi resistance

One possibility for both serine and glutamate ADP-ribosylation sites to co-exist on PARP1 could be a *fall-back* mechanism under which auto-modification of PARP1 could still take place in cells that have lost HPF1 or carry a non-functional mutant of the protein. Following induction of DNA damage, PARP1 auto-modification is crucial for the protein's subsequent release from DNA. Most PARP inhibitors used in the clinic do not strengthen the binding of PARP1 to DNA (see *1.2.6 PARP1/2 inhibition* on PARP1 inhibition. Rather, it is thought that they trap PARP1 on DNA by disallowing it to be released from sites of DNA damage through through a mechanism dependent on auto-ADP-ribosylation. This could involve direct steric and/or electrostatic repulsion between negatively charged poly-ADP-ribose and DNA but could also proceed via auto-ADPr-dependent recruitment of additional anti-trapping factors (e.g. ALC1 or XRCC1) (Demin et al. (2021)). In line with the importance of auto-ADP-ribosylation the absence of HPF1 in cells and the resulting loss of serine ADP-ribosylation might lead to the trapping of PARP1 on DNA. No co-factor, however, is required for glutamate ADP-ribosylation, which could still allow for PARP1 auto-modification and its release from DNA in the absence of serine ADP-ribosylation.

However, the above data suggests that serine ADPr on PARP1 is substantially more abundant than glutamate ADPr. If glutamate auto-ADPr on PARP1, by nature of being a fall-back mechanism, is less efficiently catalyzed than serine auto-ADP-ribosylation, the lack of HPF1 in cells could affect the amount of PARP inhibitor required to suppress

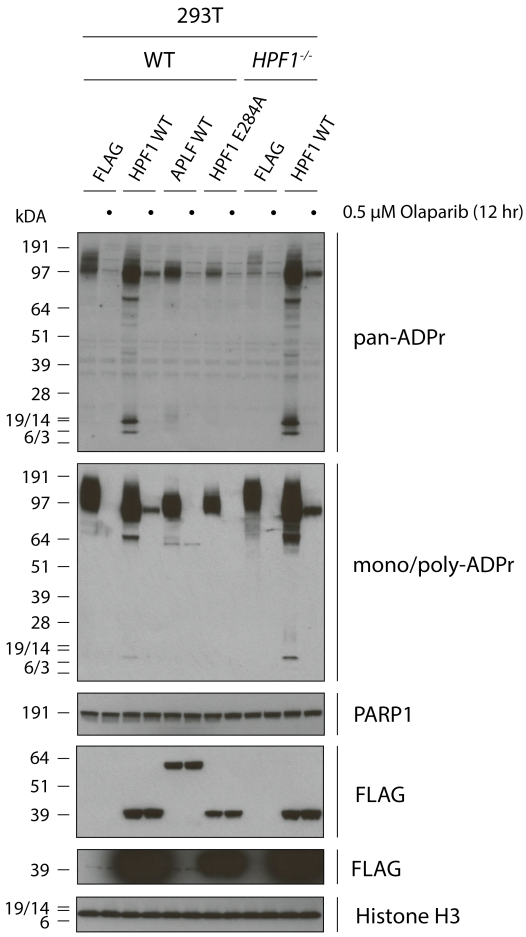


Figure 3.20: *HPF1 overexpression in 293T cells confers PARP1 auto-modification resistance to the PARP1/2 inhibitor Olaparib.* This effect is directly linked to the catalytic activity of HPF1, since the catalytically inactive mutant HPF1 E284A is not able to confer resistance. FLAG-APLF is used as a negative control. The experiment was repeated two times.

PARP1 auto-modification and therefore achieve PARP1 trapping. Conversely, given the much lower abundance of HPF1 compared to PARP1, overexpression of HPF1 in cells could allow PARP1 auto-modification to persist in the presence of PARP inhibitor concentrations that would suppress PARP1 auto-modification under wildtype conditions. In other words, HPF1 overexpression could confer some level of PARP inhibitor resistance. To test these hypotheses, I first transfected 293T WT and *PARP1*$^{-/-}$ cells with FLAG-HPF1 WT and E284A for 24 hours before treating the cells with 0.5 μM of the PARP1/2 inhibitor Olaparib for 12 hours (Figure 3.20). FLAG-HPF1 WT was strongly overexpressed in 293T WT and HPF1$^{-/-}$ cells. FLAG-HPF1 E284A was expressed at a lower level in 293T WT cells than FLAG-HPF1 WT, albeit still by many factors more than endogenous HPF1. Expression levels of FLAG-APLF, which was used as a negative control, lay between that

of FLAG-HPF1 WT and FLAG-HPF1 E284A. As previously observed, FLAG-HPF1 WT overexpression triggered substantial PARP1 auto-modification and histone ADPr as well as ADPr of several other substrates both in 293T WT and HPF1$^{-/-}$ cells (Figure 3.20). Overexpression of FLAG-APLF, on the other hand, did not affect ADPr levels and FLAG-HPF1 E284A overexpression exerted a dominant negative effect, suppressing basal PARP1 ADPr levels. This is in agreement with a previously reported increased affinity of FLAG-HPF1 E284 for PARP1 (Rudolph et al. (2021), Sun et al. (2021)). While the overwhelming majority of ADPr under FLAG-HPF1 WT overexpression conditions was suppressed in the presence of Olaparib, residual levels of auto-modified PARP1 remained. This was not the case for either FLAG-APLF or FLAG-HPF1 E284A overexpression (Figure 3.20). Consequently, HPF1 overexpression is able to confer resistance to the inhibition of PARP1 auto-modification by Olaparib in 293T cells.

In the clinic, PARP inhibitor treatment for cancer therapy, if not used as maintenance treatment, is often used in combination with DNA damaging agents. I wanted to test whether the resistance of PARP1 auto-modification to PARP inhibition was also dependent on HPF1 and therefore serine ADP-ribosylation under DNA damage conditions. Glutamate ADP-ribosylation, on the other hand, depends on the catalytic activity of PARP1 alone. I therefore also studied whether overexpression of YFP-PARP1 WT or its constitutively active ΔHD mutant in cells is able to confer PARP1 auto-modification resistance to PARP inhibitors. To this end I overexpressed YFP-PARP1 WT or ΔHD with or without FLAG-HPF1 in 293T WT cells. and treated the cells with 1 μM Olaparib at the point of transfection. 24 hours following the start of transfection, the cells were treated with 2 mM H_2O_2 for 10 minutes or left untreated (Figure 3.21a).

Hydrogen peroxide induced robust ADP-ribosylation, which was suppressed in cells pre-treated with Olaparib for 24 hours (lanes 1 to 4). Given the already much higher concentration of PARP1 compared to HPF1 in cells, PARP1 overexpression could be expected to encourage HPF1-independent PARP1-catalyzed glutamate auto-ADPr. However, overexpression of YFP-PARP1 WT or ΔHD alone did not lead to the formation of Olaparib-resistant PARP1 auto-ADPr (lanes 7 and 8). This indicates that glutamate auto-ADPr is unlikely to overcome PARP1 inhibition by Olaparib in these conditions. Interestingly, the overexpression of HPF1 alone in 293T WT cells was sufficient to form a low level of PARP1 auto-modification in the presence of Olaparib (lane 6) (Figure 3.21a). In a sim-

ilar fashion, the overexpression of YFP-PARP1 WT together with FLAG-HPF1 resulted in auto-ADPr of YFP-PARP1 as well as endogenous PARP1 (lane 9). Co-IP of YFP-PARP1 ΔHD and FLAG-HPF1 even achieved ADPr levels similar to that of uninhibited 293T WT cells under DNA damage conditions, restoring not just PARP1 auto-ADPr but also histone trans-ADPr and boosting both in the absence of DNA damage (lane 10 and 11) (Figure 3.21a). However, Olaparib-resistant ADPr as a result of YFP-PARP1 ΔHD overexpression under basal and DNA damage conditions was observed only in the presence of co-overexpressed FLAG- HPF1. This supports the notion that the ability of PARP1 to overcome inhibition by Olaparib is closely tied to its serine ADPr catalytic activity and regulated by HPF1 expression levels. To confirm that the identity of the ADPr band observed in lane 6 of Figure 3.21a is indeed auto-modified PARP1, the experiment was repeated in in a tentative, single-repeat experiment in 293T *PARP1*$^{-/-}$ cells (Figure 3.21b).

As expected, FLAG-HPF1 overexpression alone in 293T *PARP1*$^{-/-}$ did not produce any type of ADPr signal at or around the molecular weight of PARP1 (lane 6) (Figure 3.21b). Again, the overexpression of YFP-PARP1 WT and ΔHD only in combination with FLAG-HPF1 were able to restore PARP1 auto-modification under DNA damage conditions (lanes 8 and 9). Interestingly, the use of the mono/poly-ADPr antibody (Cell signalling, 83732) revealed that, while PARP1 auto-modification following hydrogen peroxide treatment under uninhibited conditions took the shape of a wide smear, PARP ADPr levels in YFP-PARP1 and FLAG-HPF1 co-expressing cells under Olaparib-treated conditions showed very concise bands. The signal was even more narrow than auto-modified PARP1 under basal conditions (Figure 3.21b). This indicated that HPF1 overexpression, while reconstituting PARP1 auto-ADP-ribosylation, limits chains elongation, possibly due to its higher presence in the cell nucleus and therefore its higher degree of complex formation with PARP1. This agrees with previous observations that FLAG-HPF1 overexpression limits PARP1 hypermodification as well as with the composite model from *3.3.2 HPF1 interaction sites on PARP1*, which illustrates the steric incompatibility between the HPF1-PARP1 ADPr initiation and the PARP1 ADP-ribose chain elongation steps (Gibbs-Seymour et al. (2016)). Consequently, the nature of the Olaparib-resistant band from Figure 3.21b is likely the result of more serine ADP-ribosylation initiation events, but reduced chain elongation resulting from HPF1 overexpression.

Since several types of tumours have been shown to possess overexpressed levels of HPF1,

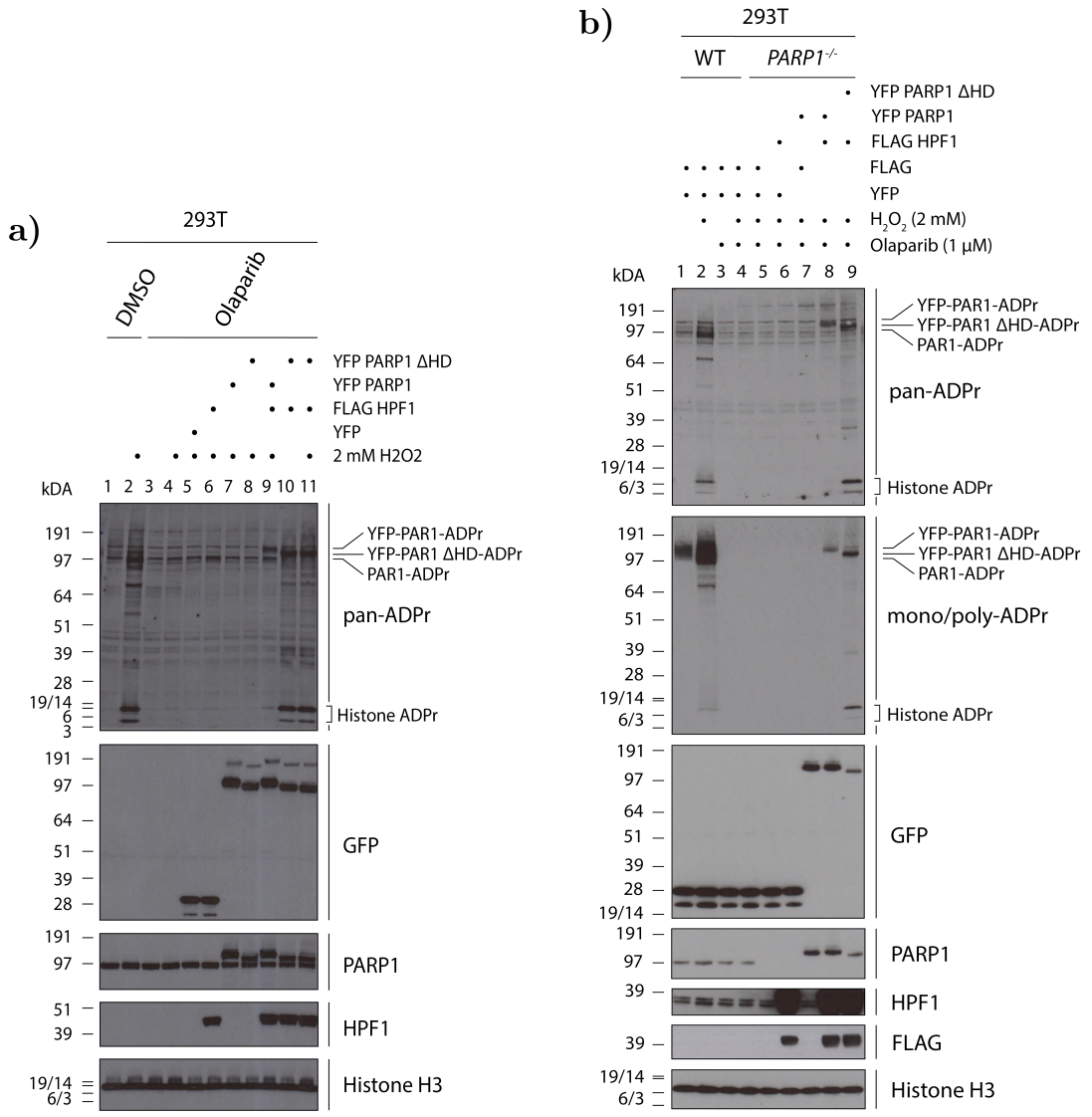


Figure 3.21: *Resistance of PARP1 auto-modification to PARP inhibition depends on HPF1 overexpression.* **a)** Overexpression of PARP1 WT or ΔHD in combination with FLAG-HPF1 overexpression, but not alone, confers PARP1 auto-modification resistance to the PARP1/2 inhibitor Olaparib. **b)** Similar to **a)** complementation of 293T *PARP1*$^{-/-}$ cells with PARP1 WT or ΔHD restores PARP1 ADP-ribosylation levels following PARP1/2 inhibitor treatment only in the presence of FLAG-HPF1 overexpression. Experiments were repeated at least two times.

it would be interesting to observe how the molecular weight distribution of auto-modified PARP1 correlates with HPF1 overexpression levels. It might be possible that a certain degree of HPF1 overexpression, which is lower than that of FLAG-HPF1 overexpression shown in Figure 3.20, confers a sufficient resistance to PARP inhibitors while being less limiting on chain elongation. Depending on whether the chain length of PARP1 auto-modification impacts its ability to leave sites of DNA damage or not, this could determine

which degree of HPF1 overexpression maximally benefits PARP inhibitor resistance.

3.4.3 HPF1 expression and PARP inhibitor resistance

While at the time of the experiments a cellular system to fine-tune HPF1 expression levels was lacking, I wanted to study the consequences of either HPF1 loss or overexpression on the concentration of PARP inhibitor required to suppress PARP1 auto-modification. To this extent I decided to test a titration of concentrations of Olaparib and another, more potent PARP1/2 inhibitor - Talazoparib - in 293T WT and *HPF1*$^{-/-}$ cells as well as 293T *HPF1*$^{-/-}$ cells overexpressing FLAG-HPF1 (Figure 3.22).

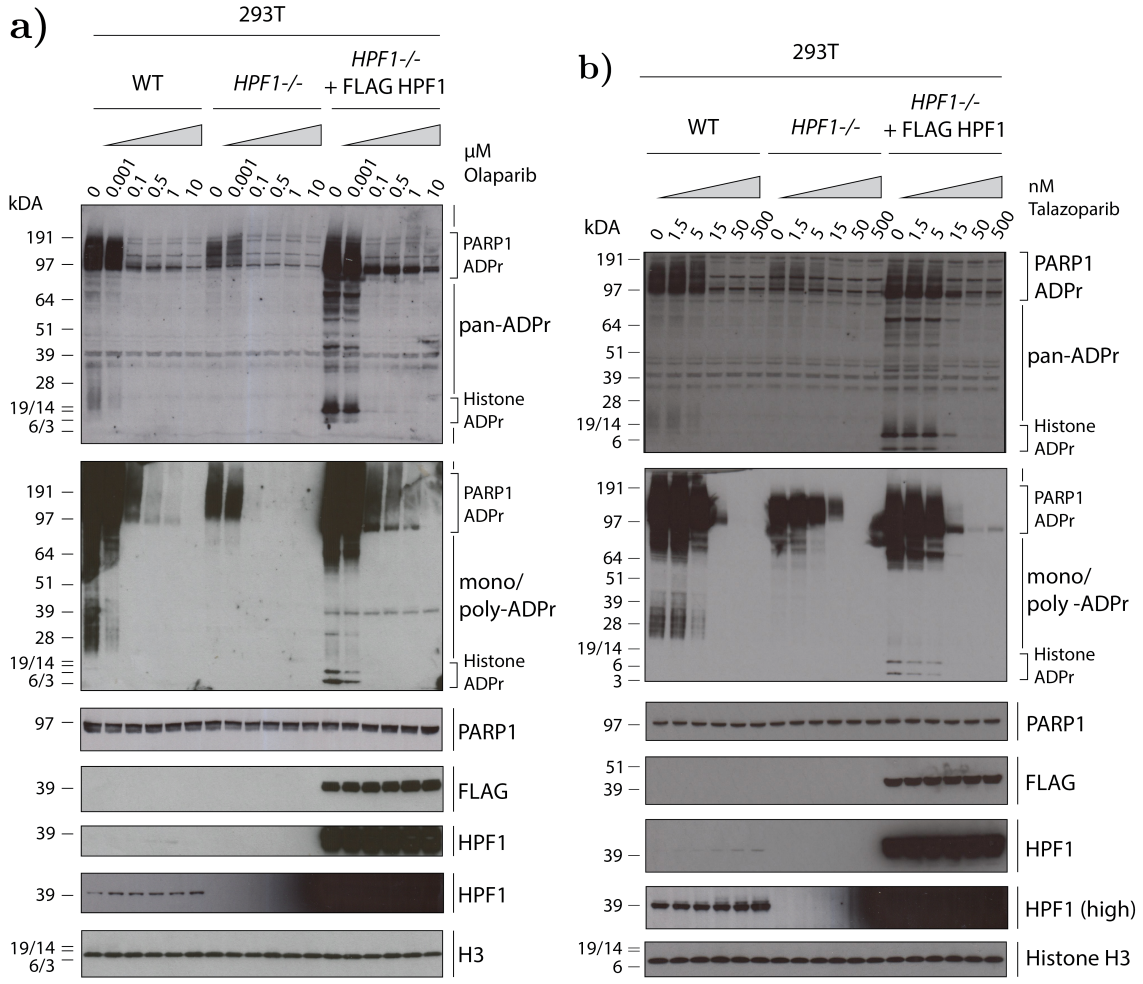


Figure 3.22: *FLAG-HPF1 overexpression increases the concentrations of different PARP inhibitors required to suppress PARP1 auto-modification in 293T cells.* **a)** Overexpression of HPF1 resists PARP1 auto-modification inhibition by Olaparib while loss of HPF1 further potentiates inhibition. **b)** A similar effect as achieved with Olaparib can be observed for equivalently potent concentrations of the PARP1/2 inhibitor Talazoparib. Experiments were repeated at least two times.

Cells were first treated with either DMSO alone or 0.001, 0.1, 0.5, 1 or 10 μM Olaparib under basal conditions (Figure 3.22a). In 293T WT cells, the majority of PARP1 auto-modification was suppressed at 0.5 μM Olaparib, while residual levels of PARP1 ADPr still persisted up to 1 μM Olaparib in the pan-ADPr blot. In the mono/poly-ADPr only a very faint smear of ADP-ribosylated PARP1 still persisted at 0.5 and 1 μM Olaparib. It should be noted that the pan-ADPr antibody carries a relatively high background signal, as evident from previous experiments. Residual signals in 293T WT cells inhibited with 10 μM Olaparib can therefore be attributed to the background signal of the pan-ADPr antibody. As expected, loss of HPF1 in 293T *HPF1*$^{-/-}$ cells further potentiated the inhibition of PARP1 auto-modification by Olaparib (Figure 3.22a). In line with my previous observation that PARP1 auto-modification occurs predominantly on serine sites, PARP1 ADPr levels are greatly reduced in untreated 293T *HPF1*$^{-/-}$ cells even under non-DNA damage conditions. While 0.001 μM Olaparib only mildly inhibits the remaining amount of modified PARP1, no ADPr signal can be observed at 0.1 μM Olaparib or above. However, when FLAG-HPF1 was overexpressed in 293T *HPF1*$^{-/-}$ cells, PARP1 auto-modification, histone trans-ADPr and ADPr of many substrates in between was strongly enhanced. Interestingly, in the absence of PARP inhibition, HPF1 overexpression did not abolish the higher molecular weight fraction of the PARP1 ADPr signal that corresponds to long chains, although it might have led to shorter average length of chains as indicated by the more pronounced band of the lower molecular fraction of the PARP1 ADPr signal around 97 kDa. Similar to the situation in 293T WT cells, Olaparib concentrations of as little as 0.1 μM abolished the largest fraction of the PARP1 ADPr signal as well as histone ADPr levels (Figure 3.22a). However, PARP1 modified by short chains persisted in 293T *HPF1*$^{-/-}$ cells complemented with FLAG-HPF1 to a much stronger extent and up to much higher Olaparib concentrations than in 293T WT cells.

To consolidate my findings, I repeated the experiment in a tentative, single-repeat experiment with the PARP1/2 inhibitor Talazoparib, which is substantially more potent than Olaparib (Figure 3.22b). While Olaparib and Talazoparib both do not significantly affect binding of PARP1 to DNA, the increased potency of Talazoparib could be derived from it lower binding constant K_D and especially slower dissociation rate constant k_{off} (Ogden et al. (2021), Rudolph et al. (2020), Zandarashvili et al. (2020)). Just as before, cells were treated under basal conditions with either DMSO alone or 1.5, 5, 15, 50 or 500 nM

Talazoparib (Figure 3.22b). PARP1 ADP-ribosylation levels in 293T WT cells were fully suppressed at 15 nM Talazoparib. In contrast to Olaparib, 293T WT cells did not show residual levels of PARP1 ADPr at or above 15 nM Talazoparib in line with its increased potency. 293T *HPF1*$^{-/-}$ cells again showed lower basal levels of PARP1 ADPr in the absence of Talazoparib, which decreased at as similar rate to that observed for 293T WT cells and were fully suppressed at 15 nM Talazoparib. As observed in Figure 3.21 and Figure 3.22a, FLAG-HFP1 overexpression in 293T *HPF1*$^{-/-}$ cells decreased the strength of the higher molecular weight portion of the PARP1 ADPr signal and increased the signal strength of the lower molecular weight fraction in the pan-ADPr blot (Figure 3.22b). At the same time, low levels of PARP1 auto-modification were able to resist 15 nM Talazoparib and PARP1 ADPr was only fully suppressed at 50 nM Talazoparib treatment. This confirms the findings from the Olaparib titration experiment.

The above observations agree with the notion that serine ADP-ribosylation, when promoted through elevated HPF1 concentration, can overcome PARP1 inhibition to enable detectable levels of PARP1 auto-modification. However, both glutamate ADP-ribosylation and ADP-ribose chain elongation are dependent on PARP1 alone. With regards to the latter, The strong limitation of ADP-ribose chain length under PARP1 inhibitor conditions in both 293T WT cells and 293T HPF1-/- cells complemented with FLAG-HPF1 suggests a preference of PARP1 for its HPF1-bound serine ADPr initiation state over it ADP-ribose chain-bound ADPr elongation state (Figure 3.22). The cause of chain elongation reduction is therefore to be sought in an HPF1 abundance in cells rather than the efficiency of the reaction, particularly since ADP-ribose chain elongation is known to occur at a much faster rate than at least glutamate/aspartate ADPr initiation (Mendoza-Alvarez & Alvarez-Gonzalez (1999)). The limited contribution of glutamate ADP-ribosylation to overall PARP1 auto-modification as well as the sensitivity of HPF1-independent ADP-ribosylation to Olaparib in 293T *HPF1*$^{-/-}$ cells indicates that glutamate/asparatate PARP1 auto-ADP-riboslyation initiation catalyzed by PARP1 alone is less efficient than that on serine and in complex with HPF1 (Figure 3.22).

To test how the above observations affect the ability of PARP1 to be released from sites of DNA damage, our collaborators from Université de Rennes 1 in France - Rebecca Smith, Siham Zentout and Sébastien Huet - tested the recruitment of YFP-PARP1 to sites of laser microirradiation-induced DNA damage in U2OS WT and *HPF1*Δ cells (Figure 3.23). As

in the experiment of Figure 3.19, DNA damage was induced in cells with a 405 nm laser at 125 μW along a 16 μm line. Figure 3.23a contains representative images depicting the fluorescence intensity of YFP-PARP1 along the site of microirradiation in U2OS WT and *HPF1*$^{-/-}$ cells at 0, 60, 180 and 300 seconds after microirradiation. Noticeably, while YFP-PARP1 shows the previously observed typical rapid dissociation from the site of laser-induced damage in U2OS WT, this was not the case for U2OS *HPF1*Δ cells. In U2OS WT cells, almost all of the fluorescence signal from YFP-PARP1 recruitment to the DNA damage site had disappeared at 180 seconds after microirradiation, while in U2OS *HPF1*Δ cells, most the YFP-PARP1 signal remained and was still detectable even at 300 seconds (Figure 3.23a). At 30 nM Olaparib treatment, YFP-PARP1 started to persist at the microirradiated site, but was substantially decreased at 180 seconds and had again mostly faded at 300 seconds after microirradiation.

In U2OS *HPF1*Δ cells, on the other hand, signal persistence of YFP-PARP1 appeared to be elevated against that in U2OS WT cells at both 180 and 300 seconds after microirradiation. Only at 30 μM Olaparib was the persistence of YFP-PARP1 at sites of laser-induced damage comparable between U2OS WT and *HPF1*Δ (Figure 3.23a). At the same time, this concentration of Olaparib also resulted in only mildly noticeable differences in the intensity of the fluorescent signal between the different time points. This observation was confirmed in the YFP-PARP1 dissipation curves, where images from different time points between 0 and 600 seconds were quantified using R software and fluorescence intensity of each time point was normalized to the time point of highest fluorescence intensity (Figure 3.23b). While in U2OS WT cells the YFP-PARP1 fluorescence signal at sites of microirradiation rapidly fell, a much more gradual decline could be observed in U2OS *HPF1*Δ cells, with the two signals only starting to converge again at 400 seconds after microirradiation. 30 nM Olaparib treatment resulted in YFP-PARP1 dissociation being delayed in both U2OS WT and *HPF1*Δ cells and narrowing the initial difference in relative fluorescence intensity of YFP-PARP1 between both cell lines. However, in contrast to untreated conditions the two signal curves remained diverged up to the last time point just under 600 seconds after laser stripe induction (Figure 3.23b). At every point following the peak of fluorescence intensity, the relative amount YFP-PARP1 judged by the strength of the fluorescence signal remained higher in U2OS *HPF1*Δ cells than U2OS WT cells. This indicates that even endogenous HPF1 levels in cells are sufficient to promote PARP1

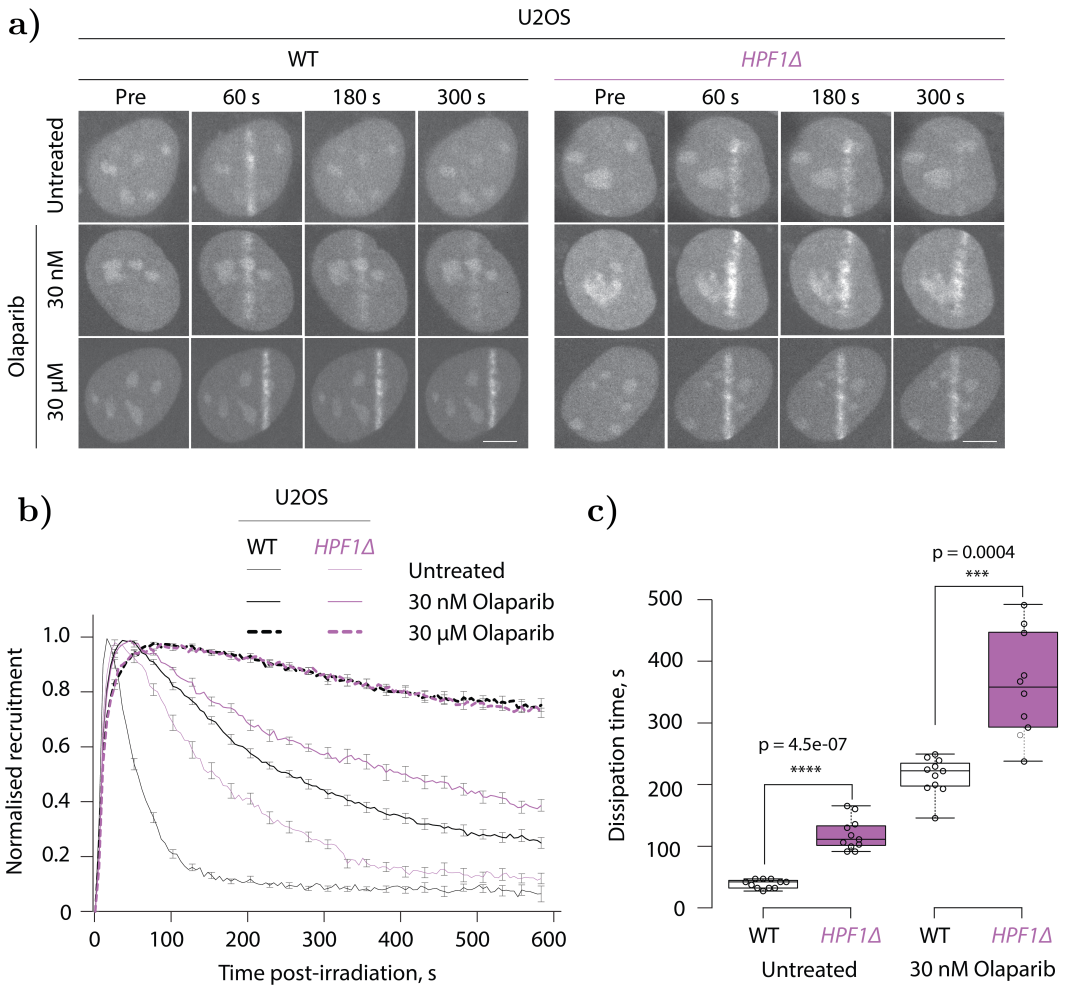


Figure 3.23: *YFP-PARP1 recruitment and dissipation times at sites of laser microirradiation in the presence or absence of the PARP1/2 inhibitor Olaparib depends on HPF1.* **a)** Representative images of YFP-PARP1 fluorescent signal at different time point following microirradiation in U2OS WT and *HPF1*Δ cells under different Olaparib concentrations. **b)** Quantification of YFP-PARP1 recruitment to and dissipation from sites of laser-induced damage as relative fluorescence intensity measurements at the sites of microirradiation. **c)** Calculation of YFP-PARP1 dissipation times in U2OS WT and *HPF1*Δ cells under untreated or 30 nM Olaparib-treated conditions. In **b)**, data points are shown as mean ± SEM from the analysis of at least 10 nuclei. In **c)**, the box limits correspond to the 25th and 75th percentiles and the bold line indicates the median value; the whiskers extend 1.5 times the interquartile range. *p < 0.05; **p < 0.01; ***p < 0.001 (two-tailed Student's t-test).

dissociation from DNA under PARP inhibitor treatment. Only at 30 μM Olaparib did the YFP-PARP1 fluorescent signals in U2OS WT and *HPF1*Δ cells follow an identical pattern in response to microirrdiation. At such a high PARP inhibitor concentration, YFP-PARP1 persistence at sites of DNA damage still constituted over 70% of peak re-

cruitment levels at just under 600 seconds as judged by fluorescence intensity, over 30% more than in U2OS *HPF1*Δ cells treated with 30 nM Olaparib (Figure 3.23b). Finally, dissipation times were calculated for each condition, with that of YFP-PARP1 in U2OS *HPF1*Δ cells being approximately twice as long as that of YFP-PARP1 in U2OS WT cells (Figure 3.23c). This difference was somewhat smaller in cells treated with 30 nM Olaparib, but nevertheless constituted a significant variation between U2OS WT and *HPF1*Δ cells. Under these conditions, the dissociation time of YFP-PARP1 in U2OS *HPF1*Δ cells was nevertheless 50% higher than in U2OS WT cells. No dissociation times were given for the 30 μM Olaparib condition, since the YFP-PARP1 signal curve was virtually identical in U2OS WT and *HPF1*Δ cells (Figure 3.23b).

The findings confirm the notion that the presence of HPF1 is required for efficient release of PARP1 from DNA. Additionally, endogenous HPF1 also confers a certain level of PARP inhibitor resistance, leading to a faster PARP1 dissipation from sites of microirradiatiton in U2OS WT over *HPF1*Δ cells (Figure 3.23). This is in line with Olaparib titration experiments from Figure 3.22, where residual levels of PARP1 auto-modification could be observed at 100 nM Olaparib treatment under basal conditions in U2OS WT, but not *HPF1*Δ cells. Between the two findings, this could further suggest that short chain PARP1 auto-modification, as it also appears in FLAG-HPF1 overexpressing 293T *HPF1*$^{-/-}$ cells, is sufficient to achieve PARP1 dissipation. Together, the results from the titration assay and the laser stripe experiment connect PARP inhibitor resistance of PARP1 auto-modification with the ability of PARP1 to efficiently leave sites of DNA damage, identifying PARP1 auto-modification as the mechanism of PARP1 release from DNA. Unfortunately, the effect of HPF1 overexpression on PARP1 recruitment to and dissipation from sites of laser-induced DNA damage was not tested in the experiments from the collaborators (Figure 3.23). It remains a fascinating prospect whether HPF1 overexpression, particularly limited HPF1 overexpression as found in certain types of tumours, can accelerate PARP1 dissipation from sites of microirradiation in line with the observation that FLAG-HPF1 overexpression in 293T HPF1$^{-/-}$ confers the ability of PARP inhibitor resistant short chain auto-ADPr on PARP1. To study phenotypic consequences of the absence of PARP1 serine auto-modification through different PARP1 and HPF1 mutants in a more expression-regulated manner, I therefore decided to make use of the Flp-In T-REx system in U2OS cells, which is described in the following subchapter.

3.5 PARP1/HPF1 mutant phenotypes

Already slightly touched upon in the previous subchapter by the laser stripe experiments from our collaborators Rebecca Smith, Siham Zentout and Sébastien Huet (Figure 3.22 and 3.26), I also wanted to explore if the observed effects of the previously described PARP1 and HPF1 mutants on ADP-ribosylation have any consequence on the sensitivity of human cells to PARP inhibitor treatment. Such a connection between HPF1 expression levels or mutations in HPF1 or PARP1 and cellular PARP inhibitor sensitivity could potentially be exploited in cancer treatment, given the common use of PARP inhibitors to that end in the clinic (Grudem & Hendrickson (2020), Mateo et al. (2019), Slade (2020)).

3.5.1 The Flp-In T-REx system

As illustrated in Figure 3.17 and 3.18, serine ADPr is the main type of PARP1 auto-modification under both basal and DNA damage conditions in two independent cell lines (U2OS and RPE-1 cells). Additionally, I showed that in the absence of HPF1, which helps catalyze serine ADP-ribosylation, PARP1 auto-modification is fully repressed at a lower PARP inhibitor concentration than in the equivalent wildtype cells, and that overexpression of HPF1 conferred a certain degree of resistance to the inhibition of PARP1 auto-modification by PARP inhibitors (Figure 3.25). Finally, the absence of PARP1 serine auto-ADPr sites, but not of putative glutamate ADPr sites, was shown by our collaborators to lead to the prolonged presence of YFP-PARP1 at sites of laser induced damage (Figure 3.22). The latter findings can be seen as indicative of extended PARP1 retention at DNA damage sites as a result of its inability to be released through auto-modification. Altogether, the highlighted data open up the question whether this difference in PARP inhibitor response between wildtype or auto-modification impaired PARP1 translates to differences in cellular survival under PARP inhibitor treatment.

Until this point, PARP1 and HPF1 mutants have been studied through transfection of cells with expression vectors, resulting in the transient overexpression of protein variants. Since this method does not allow to regulate protein expression levels or to monitor the effects of protein expression over more than two days, I decided to use a different expression system, the Flp-In T-REx system. This is system, as described under *2 Materials & Methods*, allows for both the stable expression and the regulation of expression levels of

a, in this case, N-terminally YFP-tagged GOI. I therefore decided to use this system to study the PARP1 and HPF1 mutants described in previous chapters to negatively affect either PARP1 auto-ADPr or overall cellular ADPr in the presence of DNA damage.

3.5.2 Stable YFP-PARP1 expression

My first interest was to study differences in Olaparib inhibitor response between cells constitutively expressing YFP-PARP1 WT, 3x S/A and another PARP1 mutant carrying the 3x S/A auto-modification domain mutations and substitutions of three additional serine sites, S104A, S204A and S224A, that are not located in the auto-modification domain. Albeit S499, S507 and S519 together being responsible for the overwhelming majority of ADPr on PARP1 (see *3.4.1 PARP1 auto-modification sites*), these latter three sites might be important for PARP1 auto-modification given their presence in ZnF1 (S104), ZnF2 (S204) and just C-terminal of ZnF2 (S224). The mutant containing the original three serine auto-modification site substitutions and the three additional N-terminal serine site substitutions is subsequently referred to as PARP1 6x S/A. To first generate a background in which I would be able to specifically study phenotypic consequences of the two mutants, PARP1 3x S/A and PARP1 6x S/A, I generated U2OS Flp-In *PARP1*Δ cells using CRISPR Cas9 technology according to the protocol described in *2 Materials & Methods* for generating PARP1 and *HPF1*Δ cells lines. 35 putative *PARP1*Δ single clones were tested for their PARP1 levels using Western Blotting. Cell lines with no detectable PARP1 levels are marked in **bold** (Figure 3.24). Of those candidates, three single clones of similar growth rate to U2OS Flp-In WT cells were selected and tested for residual levels of PARP1 or its potential fragments (Figure 3.24).

All three cell lines did not show any levels of either full-length PARP1 or PARP1 fragments. The PARP1 antibody used to detect PARP1 expression levels - ab32138 by Abcam - recognizes full-length PARP1 as well as the 58 kDA and 42 kDA proteolysis fragments and the 25 kDA caspase-3 cleavage fragment. Although no epitope is given by the manufacturer, the antibody's ability to detect the 25 kDA N-terminal cleavage product, which includes only ZnF1, ZnF2 and part of the nuclear localization signal, makes the nuclear presence of any PARP1 fragment, let alone a functioning one, very unlikely (Castri et al. (2014), Langelier et al. (2008)). HPF1 levels appeared to be uninfluenced by the lack of PARP1 in the three single clones (labelled 43A, 25 and 11) (Figure 3.24). Both U2OS

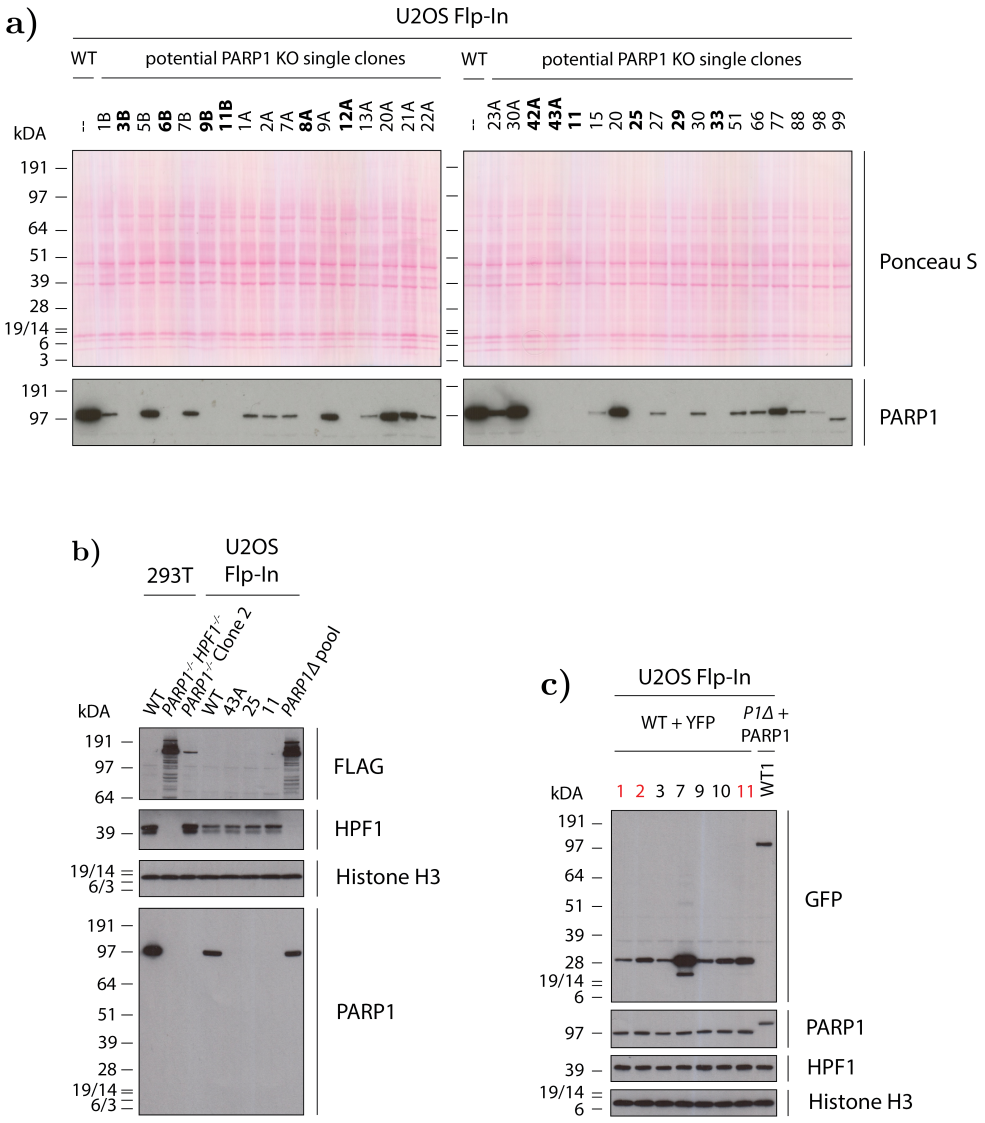


Figure 3.24: *Generation of U2OS Flp-In PARP1Δ cells.* **a)** Putative U2OS Flp-In *PARP1Δ* single clones were screened for their PARP1 expression levels. **b)** Three putative U2OS Flp-In *PARP1Δ* single clones were selected and the expression of full-length PARP1 or fragments thereof as well as FLAG-Cas9 integration into the genome tested. **c)** Complementation of U2OS Flp-In WT cells with YFP alone. Selected single clones are marked in red. Experiments were carried out once.

Flp-In WT and the pool of potential *PARP1Δ* cells (*PARP1Δ* pool) were used as controls. Additional controls for comparison included 293T WT, *PARP1*$^{-/-}$ and *PARP1*$^{-/-}$ *HPF1*$^{-/-}$ cells. No residual PARP1 levels could be observed for 293T *PARP1*$^{-/-}$ and *PARP1*$^{-/-}$ *HPF1*$^{-/-}$cells (Figure 3.24). Interestingly, 293T WCEs of the same protein concentration as U2OS Flp-In cells (as judged by the histone H3 loading control) contained higher levels of PARP1 and HPF1. Additionally, FLAG was blotted for to test the stable integration

of the Cas9 plasmid into the newly generated cell lines. Both 293T *PARP1*$^{-/-}$ *HPF1*$^{-/-}$ as well as U2OS Flp-In *PARP1*Δ pool cells showed a strong signal at the molecular weight of Cas9 (163 kDA), suggesting integration of its plasmid into the genome. A weaker signal of the same molecular weight could also be observed in 293T *PARP1*$^{-/-}$ clone (Clone 2), which was not used for any experiments in this thesis (Figure 3.24). The problem around the use of cell lines with stable integration of the vector containing Cas9 is that its integration into the genome might be dirsuptive depending on its location of integration and that it confers Puromycin resistance onto cells, excluding that antibiotic as a selection marker. No FLAG signal could be observed U2OS Flp-In WT cells or either of the U2OS Flp-In *PARP1*Δ single clones, pre-empting this problem.

Following the generation of U2OS Flp-In *PARP1*Δ cells, I decided to complement one of the single clones (Clone 25) with different YFP-PARP1 constructs, namely PARP1 WT, the auto-ADPr mutants PARP1 3x S/A and 6x S/A, the mono-ADP-ribosyltransferase mutant PARP1 E988Q and the catalytically dead PARP1 mutant H862A E988Q Figure 3.25). As a control cell line, U2OS Flp-In WT cells were complemented with YFP alone (Figure 3.24c). Generation of complemented single clones was carried out according to the respective protocol in *2 Materials & Methods*. YFP only (YFP) expression in U2OS Flp-In WT cells was tested following 24 hours of 1 μg/mL doxycycline treatment. Three single clones expressing YFP (YFP1, YFP2 and YFP11) at three different levels were kept and compared to a single clone of each YFP-PARP1 WT (WT1), YFP-PARP1 3x S/A (3x S/A4) or YFP-PARP1 6x S/A (6x S/A1) complemented U2OS Flp-In *PARP1*Δ cells (Figure 3.24c). YFP-PARP1 expression was induced by adding either 0.1 or 1 μg/mL doxycycline to the growth media for 24 hours. Cells were subsequently lysed and YFP-PARP1 expression levels compared to that of endogenous PARP1 in U2OS Flp-In WT cells by Western Blotting (Figure 3.25).

As exemplified above, single clones were identified through a nomenclature stating the name of their cell line (e.g. U2OS WT) and an abbreviation of the complemented construct (e.g. 3x S/A to stand for YFP-PARP1 3xS/A) followed by a clone-specific number. Where there can be no ambiguity about the nature of the cell line based off the complemented construct (e.g. only U2OS *PARP1*Δ cells having been complemented with YFP-PARP1 constructs), the cell line name is subsequently often omitted. This nomenclature is used in all subsequent experiments in this subchapter.

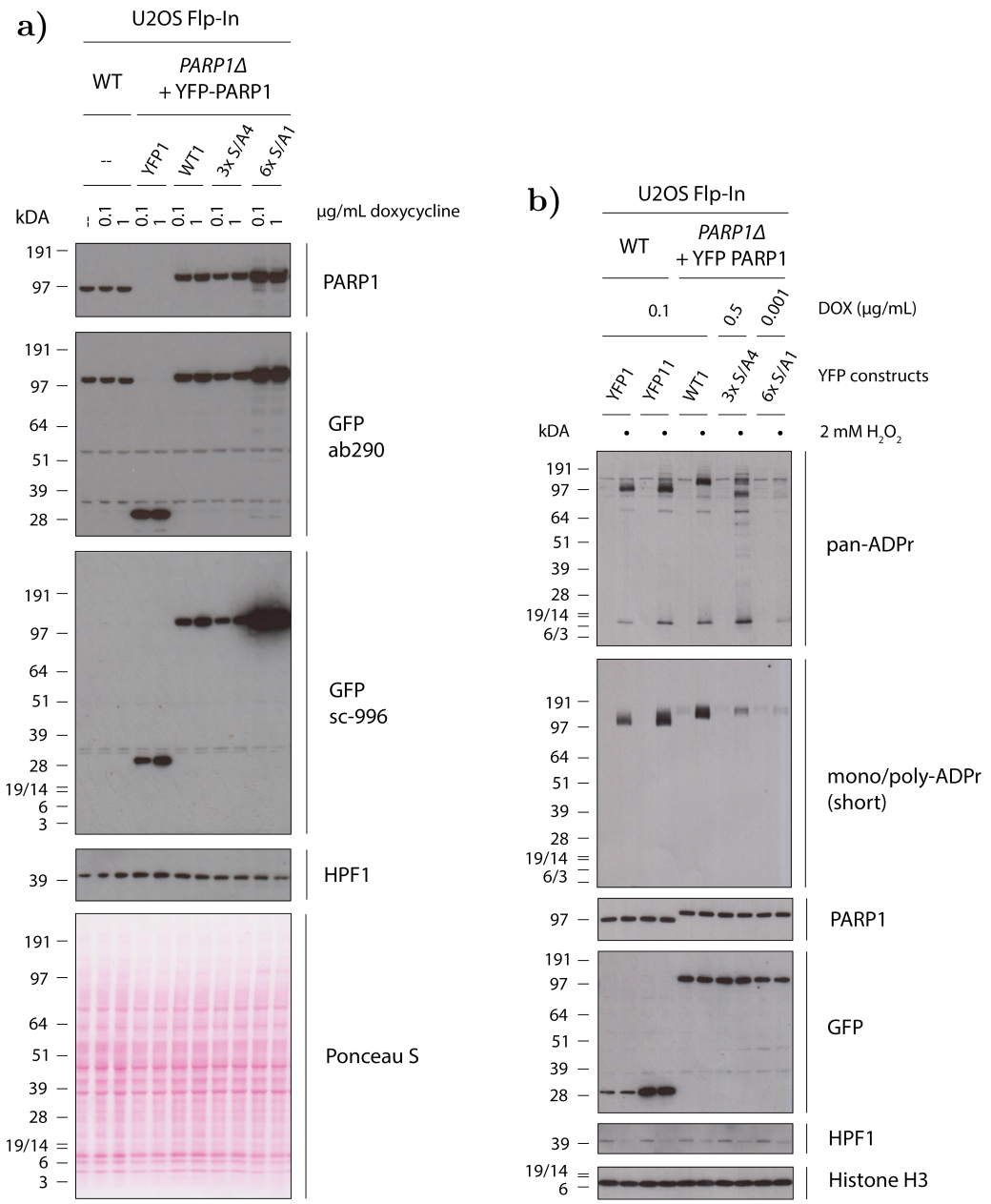


Figure 3.25: *Stable complementation of U2OS Flp-In PARP1Δ cells with YFP (**a**)), or YFP-PARP1 WT (**b**)), 3x S/A (**c**)) or 6x S/A (**d**)).* **a)** U2OS Flp-In *PARP1*Δ Clone 25 were stably complemented with YFP-PARP1 WT, 3x S/A or 6x S/A and their expression induced with either 0.1 or 1 μg/mL doxycycline. **b)** ADPr pattern in complemented cells following DNA damage induction with hydrogen peroxide. Experiments were carried out once.

YFP-PARP1 WT, YFP-PARP1 3x S/A4 and YFP-PARP1 6x S/A1 expression levels initially tested at 0.1 μg/mL doxycycline in Figure 3.25a were optimized to resemble those of endogenous PARP1 (0.5 μg/mL, 0.5 μg/mL and 0.001 μg/mL doxycycline, respectively) (Figure 3.25b). A YFP-expressing control cell line was induced with 0.1 μg/mL doxycycine. A signal observed at above the 97 kDA band in the GFP blot, when blotting with

the Abcam antibody ab290, is likely a cross-reaction of that antibody with lacZ-Zeocin and was not reproduced in a different antibody, sc-996 (Figure 3.25a). In a preliminary, first-repeat experiment, treatment of cells with H_2O_2 induced PARP1 and histone ADPr in YFP expressing U2OS Flp-In WT cells (YFP1 and YFP11) (Figure 3.25b). Comparable levels were observed for YFP-PARP1 complemented U2OS Flp-In PARP1 KO cells (WT1) (Figure 3.25b). PARP1 auto-modification was reduced in YFP-PARP1 3x S/A4 expressing cells (3x S/A4), but lead to the emergence of a different ADPr band previously observed in U2OS cells (Figure 3.17). In comparison, YFP-PARP1 6x S/A1 expressing cells (6x S/A1) lost almost all PARP1 auto-modification in the absence and presence of DNA damage (Figure 3.25b). Interestingly, this also coincided with reduced histone ADPr levels in that cell line. These findings indicate that outside of the serine target sites in the classic auto-modification domain, residues S104, S204 and S224 also contribute to PARP1 auto-modification, albeit to a lesser extent. This hints at glutamate ADPr making up an even smaller fraction of overall PARP1 auto-modification than suggested in the previous results subchapter.

3.5.3 Consequences of impaired PARP1 auto-modification

Following the findings from the results chapter *PARP1 auto-modification*, I wanted to use the stably complemented U2OS Flp-In *PARP1*Δ cells to explore their response to persistent PARP inhibitor treatment. Experiments were carried out by Evgeniia Prokhorova from Ivan Ahel's lab, who performed a 6-day Olaparib γH2AX and a 11-day Olaparib survival assay with U2OS Flp-In *PARP1*Δ YFP1, WT1 and 3x S/A4 cells (Figure 3.26). Doxycycline concentrations were again adjusted by Evgeniia Prokhorova to achieve equal expression levels between YFP1 (0.1 μg/mL), YFP-PARP1 WT1 (0.1 μg/mL) and YFP PARP1 3x S/A4 (0.5 μg/mL) expression levels to correspond to each other (Figure 3.26a). The experiment also confirmed absence of expression in samples lacking doxycycline. To test differences in DNA damage levels, Evgeniia grew the complemented cell lines for 6 days in the presence of either DMSO alone, 1 μM or 3.8 μM Olaparib and with the doxycycline levels determined in Figure 3.26a (Figure 3.26b). Growth media was replaced once after three days. YFP and YFP-PARP1 expression levels were stable across all samples and were not impacted by Olaparib treatment (Figure 3.26a). Accumulation of DNA damage in the cells was measured by blotting for γH2AX levels, an established

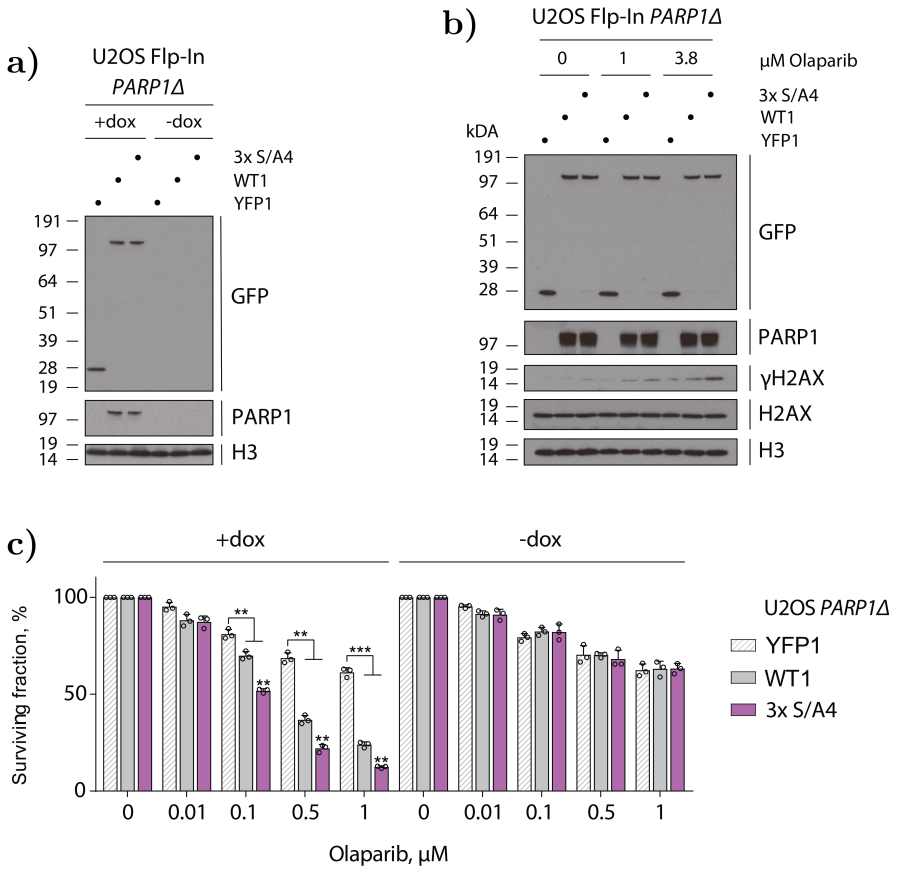


Figure 3.26: *Impaired PARP1 auto-modification raises DNA damage levels in Olaparib-treated cells.* **a)** Doxycycline concentrations were adjusted to produce equal YFP1, YFP-PARP1 WT1 and YFP PARP1 3x S/A4 expression levels. **b)** Impaired PARP1 serine auto-modification resulted in elevated γH2AX levels following a 6-day Olaparib treatment. **c)** PARP1 serine auto-modification impairment sensitized cells to Olaparib in an 11-day survival assay. in **a)** and **b)**, experiments were repeated at least twice. In **c)**, data are shown as mean ± SEM of three independent experiments.

marker of DNA double strand breaks (Mah et al. (2010)). Interestingly, γH2AX levels of U2OS Flp-In *PARP1*Δ 3x S/A4 cells were elevated over those of U2OS Flp-In *PARP1*Δ WT1 cells in all conditions, with U2OS Flp-In *PARP1*Δ YFP1 cells showing the lowest levels (Figure 3.26b). This is in agreement with the loss of PARP1 conferring resistance to PARP inhibitors and impaired PARP1 auto-modification negatively impacting the ability of PARP1 to de-trap (Gibbs-Seymour et al. (2016)). In order to test cellular survival, Evgeniia grew colonies of the three different complemented U2OS Flp-In *PARP1*Δ cell lines over 11 days in colony survival assays as described in the protocol in *2 Materials & Methods* (Figure 3.26c). In the presence of the respective doxycycline concentrations, cells were treated either with DMSO only or 0.01, 0.1, 0.5 or 1 μM Olaparib. Growth media with

the respective DMSO/Olaparib and doxycycline concentrations was replaced every 3 days. As expected, no difference in survival was observed between U2OS Flp-In *PARP1*Δ YFP1, WT1 and 3x S/A4 cells in the absence of doxycycline induction (Figure 3.26c). However, in the presence of doxycycline both U2OS Flp-In *PARP1*Δ WT1 and 3x S/A4 cells were more sensitive than YFP1 cells. The most severe phenotype could be observed in U2OS Flp-In *PARP1*Δ 3x S/A4 cells, with the PARP1 auto-modification mutant sensitizing cells more to Olaparib than the wildtype protein (Figure 3.26c). These findings are in line with the observations from Figure 3.26b.

Together, the data from the complemented U2OS Flp-In *PARP1*Δ cells i) confirms the importance of serine ADP-ribosylation sites on PARP1 for PARP1 auto-modification and ii) highlights the significance of PARP1 auto-modification for its tolerance to the PARP1/2 inhibitor Olaparib. The combined mutation of six serine ADP-ribosylation sites on PARP1 - S104, S204, S224, S499, S507 and S519 - in U2OS Flp-In cells abolished PARP1 auto-modification in response to DNA damage, cementing serine as the essential target amino acid for PARP1 auto-modification (Figure 3.26). This loss of PARP1 auto-modification, which in its majority is already achieved in the auto-modification mutant YFP-PARP1 3x S/A, has serious consequences for the ability of cells to tolerate PARP1/2 inhibition. While the loss of PARP1 in cells prevents its trapping on DNA by PARP inhibitors, a central factor of their toxicity, the presence even of PARP1 WT in cells results in increased sensitivity (Figure 3.26c). This effect is further aggravated in cells expressing the auto-modification impaired mutant PARP1 3x S/A. These observations add to the findings from *3.4.2 PARP1 auto-modification and PARPi resistance*, which illustrate the importance of HPF1 and consequentially of serine ADP-ribosylation for Olaparib-resistant PARP1 auto-modification (Figure 3.21 and Figure 3.22). Furthermore, YFP-PARP1 3x S/A was shown to be delayed in its dissipation from laser stripe-induced DNA damage compared to YFP-PARP1 WT, providing further evidence for the importance of PARP1 serine auto-ADP-ribosylation for its release from sites of DNA damage (Figure 3.19). This data together with the findings from the 6-day Olaparib treatment assay and the 11-day Olaparib survival assay from Figure 3.26 make a compelling case that it is PARP1 serine auto-modification which is the main mechanism for PARP1 release following recruitment to DNA damage sites and that the loss of this modification severely impairs the ability of PARP1 to modify itself under both basal and particularly PARP1/2 inhibitor conditions,

rendering these cells sensitive to PARP inhibitor treatment.

3.5.4 Stable YFP-HPF1 expression

Following the successful generation of stably YFP-PARP1 expressing U2OS Flp-In *PARP1*Δ cells, I decided to use the same Flp-In TREx system for first generating U2OS Flp-In *HPF1*Δ cell lines and then complementing a knock-out cell line with YFP-HPF1 WT and mutants, specifically the catalytic mutant HPF1 E284A and the PARP1-interaction mutant HPF1 D286A. Generation of U2OS Flp-In *HPF1*Δ cells is outlined in Figure 3.27.

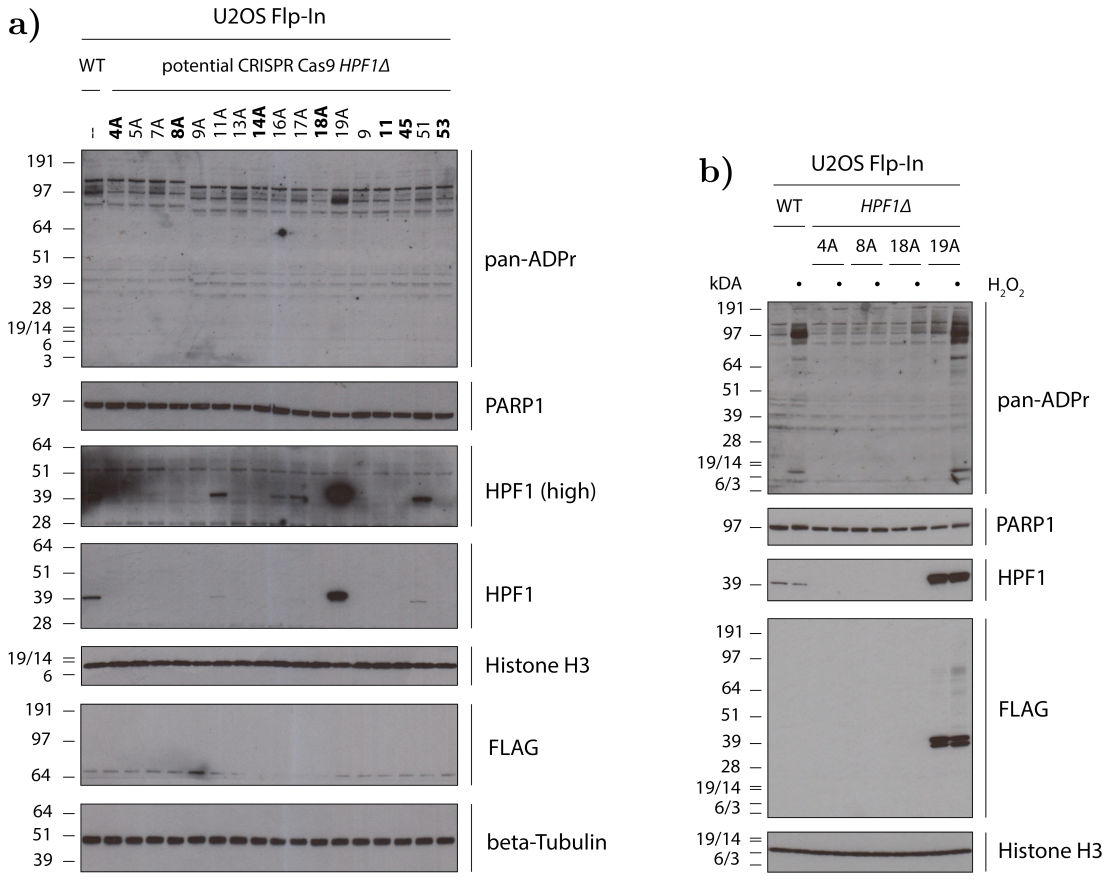


Figure 3.27: *Generation of U2OS Flp-In HPF1*Δ *cells.* **a)** A selection of 17 potential U2OS Flp-In *HPF1*Δ single clones. Clones not expressing detectable levels of HPF1 are highlighted in **bold**. **b)** ADPr pattern of three U2OS Flp-In *HPF1*Δ single clones and one HPF1 overexpression clone in response to DNA damage. Experiments were carried out once.

Generation of U2OS Flp-In *HPF1*Δ cells was carried out using CRISPR Cas9 technology according to the protocol in *2 Materials & Methods*. A screen of 17 putative *HPF1*Δ single clones is shown in Figure 3.27a. I tested both HPF1 expression levels as well as basal ADP-riboxylation levels in the cells compared to a U2OS Flp-In WT control. The

rabbit polyclonal HPF1 antibody used was raised against the C-terminal HPF1 peptide RELPETDADLKRIC by DC Biosciences. Given that the two HPF1 CRISPR Cas9 gRNAs (see *2 Materials & Methods*) target the HPF1 gene for cleavage within exon 1, the possibility of an undetected truncated HPF1 protein in candidate U2OS Flp-In *HPF1*Δ single clones exists. However, the peptide against which the HPF1 antibody is raised begins at amino acid R239, one of the residues involved in PARP1 binding previously identified by Ian Gibbs-Seymour (Gibbs-Seymour et al. (2016)). A truncated version of HPF1 in a putative U2OS Flp-In *HPF1*Δ is therefore highly unlikely to contain the downstream interaction residues D283 and D284, the mutation of which to alanine abolished interaction with PARP1. Whether such a HPF1 fragment, however, might still retain the ability to bind to sites of DNA damage independent of PARP1 interaction remains questionable, but not impossible. Nonetheless, the potential presence of a serine ADPr competent HPF1 portion can be tested by examining the candidate clone's ADP-ribosylation pattern in response to DNA damage. This was done for three single candidate clones (4A, 8A and 18A) chosen based on the resemblance of their growth rate with that of U2OS Flp-In WT cells, their absence of any detectable HPF1 signal and their lack of an ADPr signal under basal conditions (Figure 3.27b). While H_2O_2 treatment of U2OS Flp-In WT cells resulted in a robust ADP-ribosylation signal, no signal induction could be observed in clones 4A and 8A, in agreement with previous findings for 293T and U2OS *HPF1*Δ cells highlighted in *3.1 A system to study cellular ADPr*. Only in clone 18A, a weak ADPr signal could be observed at the molecular weight of PARP1 (Figure 3.27b). This signal suggests remaining auto-modification activity of PARP1, conferred either by the presence of an HPF1 fragment or HPF1-independent glutamate ADP-ribosylation activity of PARP1. However, the latter is highly unlikely, given that glutamate ADPr would otherwise also had been observed in clones 4A and 8A (Figure 3.27b). Ultimately, clone 8A was taken forward for complementation by YFP-HPF1 variants.

Similar to the complementation of U2OS Flp-In WT with YFP alone (Figure 3.24c), I was able to collect and test the expression of 8 single clones for U2OS Flp-In *HPF1*Δ cells complemented either with YFP alone, YFP-HPF1 WT, YFP-HPF1 E284A or YFP-HPF1 D286A (Figure 3.28a-d). Just as before, expression of YFP or one of the YFP-HPF1 variants was induced over 24 hours with 1μg/mL doxycycline and expression levels examined by Western Blotting. In addition, endogenous PARP1 expression levels were also

studied to test the consequence of different YFP-HPF1 expression levels on endogenous PARP1 expression. WCEs of single clones were blotted for HPF1 and YFP and three single clones of each YFP, YFP-HPF1 WT, YFP-HPF1 E284A or YFP-HPF1 D286A expressing cells were selected (clones marked in red) (Figure 3.28a-d). The single clones were selected to constitute one low-, one medium-, and one high-expressing clone and were labelled according to the same nomenclature used for YFP-expressing U2OS Flp-In WT clones. The three selected clones from each complemented U2OS Flp-In *HPF1*Δ cells are therefore subsequently named U2OS Flp-In *HPF1*Δ YFP1/YFP5/YFP8 (Figure 3.28a), WT2/WT5/WT8 (Figure 3.28b), E284A3/E284A4/E284A8 (Figure 3.28c) and D286A5/D286A7/D286A8 (Figure 3.28d).

The choice of clones with different YFP or YFP-HPF1 expression levels together with changes in doxycycline concentrations allows for the coverage of a large range of expression levels. As a result, these single clones can be used not only to study the phenotypic impact of the selected HPF1 mutants on cells, but also to explore the consequences of different degrees of both HPF1 overexpression and reduced expression. Between each other, the single clones of each complementation did not appear to differ in endogenous PARP1 expression levels (Figure 3.28). However, in each case they showed higher PARP1 expression than U2OS Flp-In WT YFP11. Given the similarly elevated levels of endogenous PARP1 between single clones for each type of complementation, lower endogenous PARP1 expression levels in U2OS Flp-In WT EV11 cells are more likely to be a characteristic of that specific clone than the result of YFP or YFP-HPF1 WT, E284A, or D286A expression in U2OS Flp-In *HPF1*Δ cells.

Following the generation of U2OS Flp-In *HPF1*Δ YFP, WT, E284A and D286A cells, I wanted to see if complementation with YFP-HPF1 also restored DNA damage-dependent ADP-ribosylation in U2OS Flp-In *HPF1*Δ cells. To this extent I tested in a tentative first, single-repeat experiment U2OS Flp-In *HPF1*Δ clones YFP8, WT8, E284A3 and D286A8, since these clones showed the highest expression levels of their respective complemented constructs and therefore were the most likely to restore or even boost ADPr levels under basal and DNA damage conditions. Following 24 hours of 1 μg/mL doxycycline treatment, cells were either left untreated or treated for 10 minutes with 2 mM H_2O_2 before being lysed and subjected to Western Blotting analysis of ADPr levels (Figure 3.29).

YFP-HPF1 expression levels in U2OS Flp-In *HPF1*Δ WT8, E284A3 and D286A8 cells

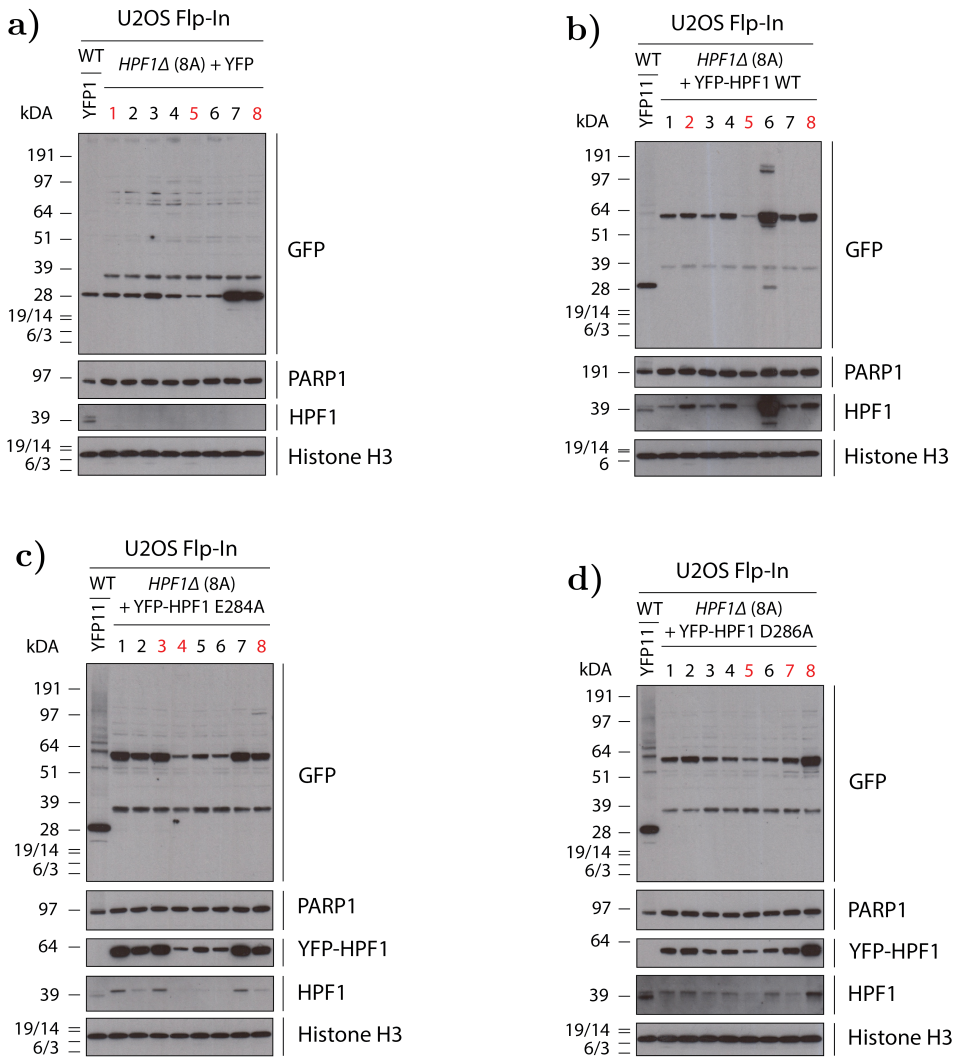


Figure 3.28: *Stable complementation of U2OS Flp-In HPF1Δ cells with YFP (**a**), or YFP-HPF1 WT (**b**), E284A (**c**) or D286A (**d**).* For each type of complementation, three single clones were selected (marked in *red*) **a)** The three single clones kept were YFP1, YFP5 and YFP8. **b)** The three single clones kept were WT2, WT5 and WT8. **c)** The three single clones kept were E284A3, E284A4 and E284A8. **d)** The three single clones kept were D286A5, D286A7 and D286A8. Experiments were carried out once.

were comparable between each other and with the YFP expression levels of U2OS Flp-In WT YFP11 and U2OS Flp-In *HPF1*Δ YFP8 cells (Figure 3.29). PARP1 levels were comparable between all samples with the difference that H_2O_2-induced PARP1 automodification was visible in the PARP1 blot as a region of higher molecular weight above the unmodified PARP1 band. YFP-HPF1 expression levels far exceeded that of endogenous HPF1 in U2OS Flp-In WT YFP11 cells. From the HPF1 blot it appeared as if a small fraction of YFP-HPF1 was cleaved to yield untagged HPF1. Interestingly, this fraction

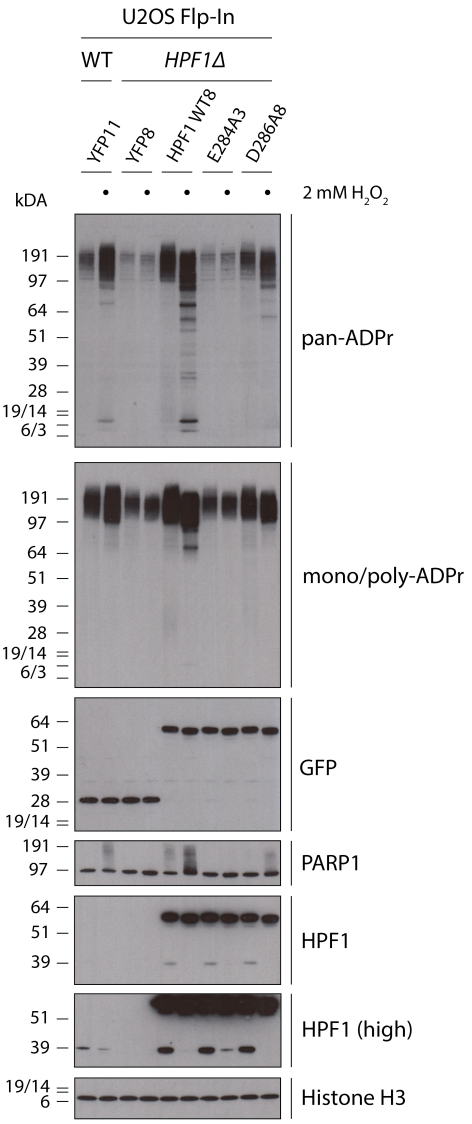


Figure 3.29: *Stable expression of catalytically inactive YFP-HPF1 does not restore DNA-damage dependent ADPr in U2OS Flp-In WT YFP11 and U2OS Flp-In cells.* ADPr levels were tested under basal conditions and following DNA damage induction by hydrogen peroxide following 24 hours of doxycycline treatment. The experiment was carried out once.

was substantially stronger in basal conditions than DNA damage conditions (Figure 3.29). The magnitude of YFP-HPF1 overexpression in U2OS Flp-In *HPF1*Δ cells is highlighted by the magnitude by which even the small fraction of cleaved YFP-HPF1 outweighs endogenous HPF1 expression.

Similar to the observations in Figure 3.25b, U2OS Flp-In WT YFP11 cells showed low levels of PARP1 auto-modification under basal conditions and robust PARP1 auto- and trans-ADP-ribosylation in response to DNA damage. Both basal and DNA damage-induced ADPr were abolished in U2OS Flp-In *HPF1*Δ YFP8 cells (Figure 3.29). ADPr levels in

U2OS Flp-In *HPF1*Δ WT8 cells, on the other hand, were boosted both under basal and DNA damage conditions, particularly enhancing PARP1 auto-ADP-ribosylation under basal and histone and other protein trans-ADPr under DNA damage conditions. In line with previous observations on HPF1 overexpression in cells, chain lengths of PARP1 automodification in U2OS Flp-In *HPF1*Δ WT8 cells appeared to be limited compared to U2OS Flp-In WT YFP11 cells as judged by the molecular weight of the PARP1 ADPr regions in the pan-ADPr and mono/poly-ADPr blots (Gibbs-Seymour et al. (2016)). U2OS Flp-In *HPF1*Δ E284A3 mirrored the observation from U2OS Flp-In *HPF1*Δ YFP8 cells, again confirming the significance of catalytically active HPF1 and therefore serine ADPr for overall cellular ADP-ribosylation under both basal and DNA damage conditions (Figure 3.29). U2OS Flp-In *HPF1*Δ D286A8 cells presented a situation between U2OS Flp-In *HPF1*Δ E284A3 and U2OS Flp-In *HPF1*Δ YFP8 cells, carrying strongly reduced PARP1 automodification and histone trans-modification levels but falling short of complete absence of ADPr under basal and DNA damage conditions. Since D286 of HPF1 is less directly involved in PARP1 interaction than D283, it can be speculated whether this is the reason for residual ADPr levels in *HPF1*Δ D286A8 cells. However, in previous experiments, such as that of Figure 3.7b in *3.2.1 HPF1 ADP-ribosylation sites*, HPF1 D286A proved to be no less efficient in abolishing DNA damage-induced ADPr than HPF1 D283A. It therefore remains unclear whether the expression YFP-HPF1 D283A would have achieved any lower ADPr levels, especially given that all tested YFP-HPF1 variants are strongly overexpressed in U2OS Flp-In *HPF1*Δ cells (Figure 3.29). One explanation for the observation in U2OS Flp-In *HPF1*Δ D286A8 cells is therefore that under overexpressed YFP-HPF1 conditions binding-impaired HPF1 molecules could achieve sufficient transient contact with PARP1 molecules to enable residual levels of cellular ADPr.

Complementation of *HPF1*Δ cells with overexpressed HPF1 has already been shown to restore DNA damage-dependent ADPr even under transient transfection conditions in 293T cells (see *3.2.1 HPF1 ADP-ribosylation sites*). The result confirmed restoration of ADPr for U2OS Flp-In *HPF1*Δ cells complemented with overexpressed YFP-HPF1 (Figure 3.29). One goal of generating complemented U2OS Flp-In *HPF1*Δ cells was to study the phenotypic consequences of stable HPF1 WT and mutants expression at the level of endogenous HPF1. A similar aim regarding PARP1 resulted in the observation of increased γH2AX levels and decreased survivals in U2OS Flp-In *PARP1*Δ 3x S/A4 cells

(Figure 3.26). To carry out these assays in complemented U2OS Flp-In *HPF1*Δ cells, I performed a doxycycline titration on the low-expressing clones U2OS Flp-In *HPF1*Δ YFP5, WT5, E284A4 and D286A5 using U2OS Flp-In WT YFP1 cells as a control. The clones were treated with 0.003, 0.01, 0.03, 0.1 or 0.3 μg/mL doxycycline for 24 hours or left untreated for the same duration to control for any YFP or YFP-HPF1 expression in the absence of doxycycline induction. Cells were lysed and expression levels of YFP and YFP-HPF1 variants tested by Western Blotting (Figure 3.30).

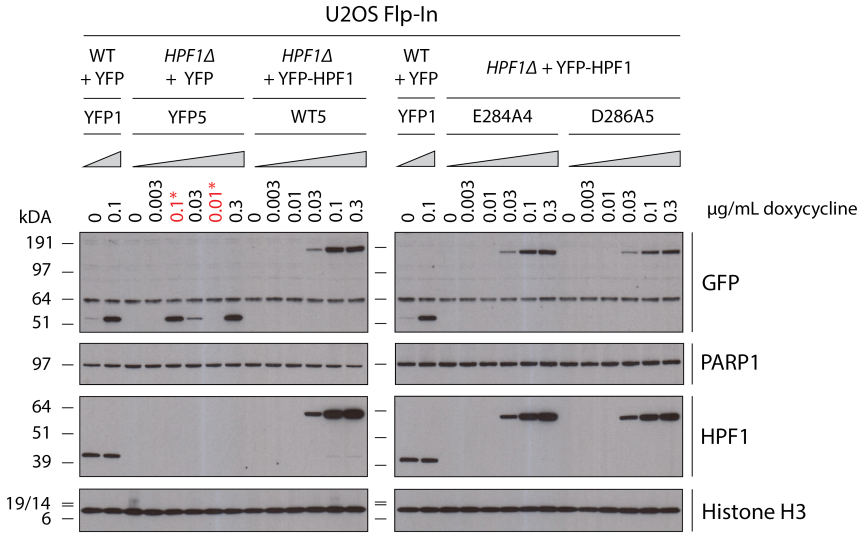


Figure 3.30: *Doxycycline titration adjusting low-expressing clones U2OS Flp-In HPF1*Δ *YFP5, WT5, E284A4 and D286A5 to endogenous HPF1 levels.* Treatment was carried out over 24 hours and U2OS Flp-In WT YFP1 used control cell line. No YFP or YFP-HPF1 expression was detectable in the absence of doxycycline in the *HPF1*Δ cell lines or the WT control cell line. The experiment was carried out once.

In the absence of doxycycline no YFP or YFP-HPF1 expression could be observed in complemented U2OS Flp-In *HPF1*Δ cells. A low degree of YFP expression was visible in not induced U2OS Flp-In WT YFP1 cells, suggesting that another YFP complemented U2OS Flp-In WT clone might be better suited as a control in future experiments (Figure 3.30). The two samples of lane 5 and 7 coloured in red and marked with an asterisk were swapped. The experiment established the comparable doxycycline concentrations for U2OS Flp-In *HPF1*Δ YFP5, WT5, E284A4 and D286A5 at 0.03 μg/mL and for Flp-In WT YFP1 cells at 0.1 μg/mL (Figure 3.30). YFP-HPF1 levels also compared to the expression levels of endogenous HPF1 in U2OS Flp-In WT YFP1 cells. The experiment showed that 0.1 μg/mL doxycycline could be used to induce comparable GFP expression

between U2OS Flp-In WT YFP1 and U2OS Flp-In *HPF1*Δ YFP5 cells. Subsequently, the experiment of Figure 3.29 was repeated to confirm whether ADPr in the above clones behaved as expected and were a suitable model for phenotypic studies (Figure 3.31a and b and Figure 3.32).

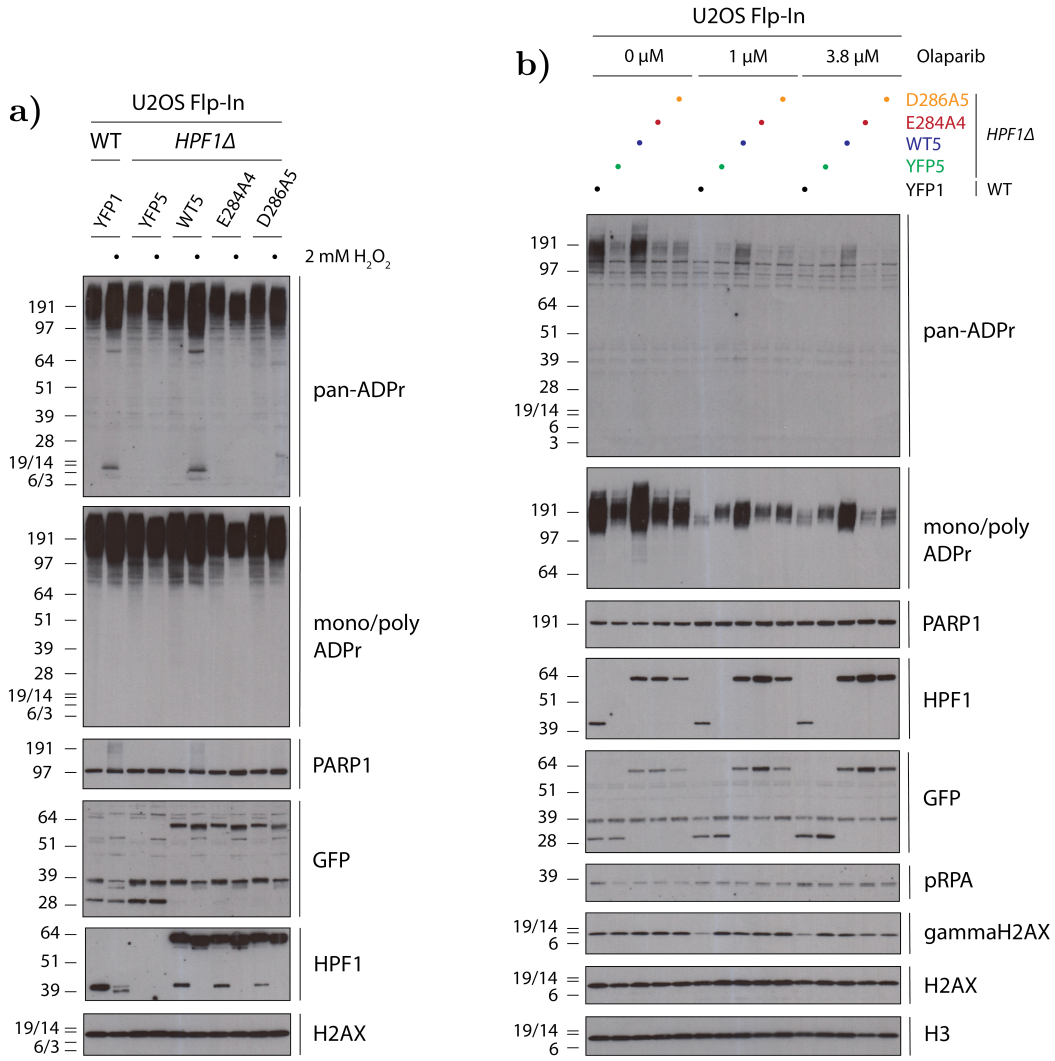


Figure 3.31: *ADPr complementation assay and 6-day Olaparib treatment assay of U2OS Flp-In WT YFP1 and U2OS Flp-In HPF1*Δ *YFP5, WT5, E284A4 and D286A5 cells.* **a)** ADPr levels were tested under basal conditions and following DNA damage induction by hydrogen peroxide following 24 hours of doxycycline treatment. **b)** γH2AX levels of cells after 6 days in the presence or absence of continuous Olaparib treatment. In **a)**, the experiment was repeated two times. In **b)**, the experiment was carried out once.

In the ADPr assay, YFP-HPF1 WT and mutants were expressed under elevated, but close-to-endogenous HPF1 expression levels, particularly compared to transient overexpression (Figure 3.29). DNA damage induction had varying effects on YFP-HPF1 expression,

with levels slightly elevated upon DNA damage in *HPF1*Δ WT5 and E284A4 cells, but slightly reduced in *HPF1*Δ D286A5 cells (Figure 3.31a). Despite these variations,YFP-HPF1 WT expression levels in *HPF1*Δ cells were able to imitate control conditions of U2OS Flp-In WT YFP1 cells in the pan-ADPr blot (Figure 3.31a). Meanwhile, DNA damage-induced ADPr was lost in U2OS Flp-In *HPF1*Δ E284A4 cells and only partially retained in *HPF1*Δ D286A5 cells, with histone ADPr absent at the shown exposure while PARP1 auto-modification partially persisted. Results from the mono/poly-ADPr blot, mostly captured PARP1 auto-modification. Here, a substantial reduction in the signal strength following hydrogen peroxide treatment was only observed in *HPF1*Δ YFP5 and E284A4 cells (Figure 3.31a).

YFP expression levels between U2OS Flp-In WT YFP1 and U2OS Flp-In *HPF1*Δ YFP5 remained to be adjusted and DNA damage induction in U2OS Flp-In WT YFP1 cells saw reduced HPF1 levels and a second lower-molecular weight HPF1 band (Figure 3.31a). A similar observation was previously made under basal conditions for U2OS Flp-In WT YFP1 and YFP11 cells (Figure 3.28), but not in an independent repeat of the experiment from Figure 3.31a (see Figure A.2 in *A Appendix*). This aspect of the experiment therefore requires further clarification, despite not appearing to prevent a robust ADPr response to DNA damage in U2OS Flp-In WT YFP1 cells. As a whole, however, the assay showed that based on the previously determined nature of the YFP-HPF1 variant, ADPr levels could be fully, partially or not restored in complemented U2OS Flp-In *HPF1*Δ. The results agree with the effect previously ascribed the tested YFP-HPF1 variants in the preceding chapters and present a more physiological system for studying said variants (Figure 3.31a).

3.5.5 Phenotypes of HPF1 mutants

After establishing that stable, doxycycline-inducible YFP-HPF1 expression can complement U2OS Flp-In *HPF1*Δ cells, I aimed to assess in a 6-day Olaparib treatment assay any differential effects between the cell lines on cellular ADPr levels and DNA damage. Since the experiment was carried out only once, all interpretations of the result are tentative conclusions requiring repetition. As previously in Figure 3.26b, damage was measured by studying cellular γH2AX levels (Figure 3.31b). As the assay conclusively shows, the majority of PARP1 auto-modification under basal conditions is lost in U2OS Flp-In *HPF1*Δ YFP1 cells and restored to slightly above endogenous levels in *HPF1*Δ WT5 cells. Ola-

parib treatment appeared to increase YFP-HPF1 expression, complicating the interpretation of the results. One possible consequence is the resistance of ADPr levels to Olaparib treatment in cells. While PARP1 auto-modification was fully suppressed in WT YFP1 cells at 1 μM Olaparib, this was not the case for *HPF1*Δ WT5 cells, which showed residual PARP1 ADPr even at 3.8 μM Olaparib (Figure 3.31b). However, this could also stem from WT YFP1 potentially being an unreliable cell line, which was later shown to exhibit a visibly impaired growth rate compared to other complemented U2OS Flp-In WT and *HPF1*Δ clones. The latter is plausible particularly in the light that PARP1 auto-ADPr levels were suppressed only at 3.8 μM Olaparib even in the negative control clone lacking HPF1, U2OS Flp-In *HPF1*Δ YFP5 (Figure 3.31b). The overall image from the observed ADPr pattern, however, is one confirming previous findings from the thesis and also providing a few further insights (Figure 3.31b). Most importantly, the result highlights the use of the U2OS Flp-In system for testing different degrees of HPF1 expression. It also further supports the speculation made in *3.4.2 PARP1 auto-modification and PARPi resistance*that HPF1 overexpression confers higher Olaparib resistance at close-to-physiological levels compared higher-order transient overexpression as recored in Figure 3.22.
Unfortunately, no increase in γH2AX levels upon Olaparib treatment could be observed (Figure 3.31b). Differences in γH2AX levels appeared to at least partially coincided with fluctuations in H2AX levels. Phospho-RPA levels, also an indication of DNA damage, showed an almost inverse effect to that of the γH2AX blot, further complicating any interpretation. The result, however, stands in contrast to strongly reduced survival of U2OS Flp-In *HPF1*Δ E284A4 and enlarged, apoptotic-looking U2OS Flp-In *HPF1*Δ YFP5 and D286A5 cells at 3.8 μM Olaparib at the end of the 6-day Olaparib treatment. OD values of the collected samples reflect this observation and are documented in Figure 3.32a. Further repetitions of the assay are required to explore the basis for the discrepancies between OD values and γH2AX levels.

Strikingly, OD measurements from the 6-day Olaparib treatment experiments found the value reduced to 50% in 3.8μM Olaparib-treated *HPF1*Δ E284A4 cells compared to their DMSO treated counterparts. In *HPF1*Δ WT5 and D286A5 cells the reduction was only roughly 27% (Figure 3.32a). This suggests that cell viability is both affected and dependent on the nature of the expressed YFP-HPF1 construct in *HPF1*Δ cells. I therefore further explored to what extent the sensitivity of U2OS cells to Olaparib is dependent on

a)

	DMSO	1 µM Olaparib	3.8 µM Olaparib
HPF1 KO YFP1	0.275	0.140	0.158
HPF1 KO YFP5	0.428	0.370	0.306
HPF1 KO WT1	0.381	0.306	0.276
HPF1 KO E284A4	0.376	0.282	0.194
HPF1 KO D286A5	0.366	0.323	0.267

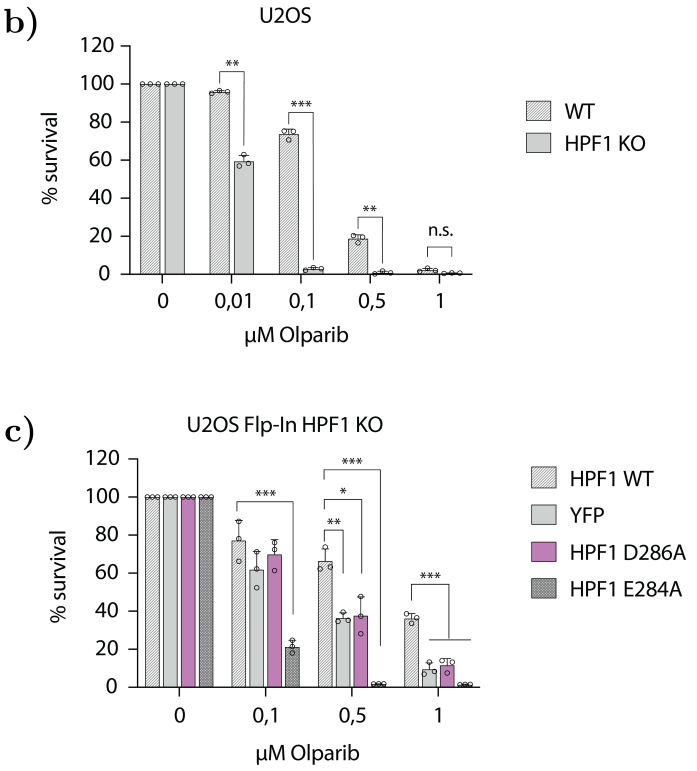


Figure 3.32: *Catalytic inactivation of HPF1 enhances sensitivity of U2OS Flp-In cells to Olaparib over HPF1 loss.* **a)** OD values of U2OS Flp-In WT and *HPF1*Δ cells of 6-day Olaparib treatment experiment from (Figure 3.31b). **b)** Survival of U2OS WT vs. *HPF1*Δ cells in an 11-day Olaparib survival assay (* = $p \leq 0.05$, ** = $p \leq 0.01$, *** = $p \leq 0.001$). **c)** Survival of complemented U2OS Flp-In WT and *HPF1*Δ cells in an 11-day Olaparib survival assay (* = $p \leq 0.05$, ** = $p \leq 0.01$, *** = $p \leq 0.001$). In **b)** and **c)**, data are shown as mean ± SEM of three technical repeats.

HPF1. To test this further, I carried out three technical replicates of a 11-day Olaparib survival assay on U2OS WT and *HPF1*Δ cells according to the corresponding protocol in *2 Materials & Methods* (Figure 3.32b). The results confirmed previous findings by Ian Gibbs-Seymour that the loss of HPF1 strongly sensitizes cells to Olaparib (Gibbs-Seymour et al. (2016)). Even at as little as 0.01 μM Olaparib *HPF1*Δ cells were substantially more sensitive than WT cells ($p \leq 0.01$). The difference was the starkest at 0.1 μM Olaparib, where survival of U2OS *HPF1*Δ was reduced to less than 5% while the survival in U2OS

WT cells on average still lay at more than 70% ($p \leq 0.001$) (Figure 3.32b).
Although U2OS WT YFP1 and *HPF1*Δ WT5 cells showed only non-significant differences in resistance to Olaparib, the U2OS WT YFP1 clone was excluded from the data shown here due to its much weaker levels of colony formations. The full set is shown in Figure A.3 in *A Appendix*. Starting from *HPF1*Δ WT5 cells as a positive control, the loss of HPF1 in *HPF1*Δ YFP5 cells significantly sensitized cells to Olaparib (Figure 3.32c). A similar sensitivity could be observed for *HPF1*Δ cells complemented with the PARP1 interaction mutant YFP-HPF1 D286A, highlighting that it is the loss of PARP1 interaction that drives the Olaparib sensitivity in *HPF1*Δ cells. Strikingly, *HPF1*Δ E32844 cells exceeded *HPF1*Δ YFP5 and *HPF1*Δ D286A cells in sensitivity to Olaparib (Figure 3.32c). This leads to the question whether the expression of catalytically inactive HPF1 encourages PARP1 trapping in U2OS Flp-In cells. To test this, I wanted to explore YFP-HPF1 recruitment to sites of laser-induced microirradiation in U2OS Flp-In *HPF1*Δ WT5, E284A4 and D286A5 cells (Figure 3.33).

As previously done for complementation assays (Figure 3.29 and Figure 3.31a), YFP-HPF1 expression was induced for 24 hours with 0.03 μg/mL doxycycline prior to laser stripe damage. Pre-treatment of cells with Hoechst, use of imaging media and laser microirradiation are described in the respective protocol in *2 Materials & Methods*. Fluorescence intensity was measured before and after microirradiation in the nuclei of 12 individual cells and the fluorescence increase in percent at sites of microirradiation blotted against time. In an initial experiment, recruitment of YFP-HPF1 WT was compared with that of YFP-HPF1 E284A at 0, 30 and 60 seconds after microirradiation following pre-treatment with 1 μg/mL Hoechst for 20-30 minutes (H3570, Thermo Fisher). Surprisingly, at every time point after microirradiation, fluorescence increase at sites of laser-induced damage was almost twice as strong for YFP-HPF1 E284A expressing cells than YFP-HPF1 WT expressing cells (Figure 3.33a). Representative images are shown in Figure 3.33b. From both the graph and the representative images, it also appeared as if the YFP-HPF1 WT, but not the YFP-HPF1 E284A, fluorescence signal was slowly declining at 60 seconds following microirradiation. However, whether this already indicates persistance of YFP-HPF1 E284A at sites of laser-induced damage remains speculation. Although Ian Gibbs-Seymour has previously used the 30 seconds time point as indicator of highest fluorescence signal following microirradiation in time course experiments, the exact peak of YFP-HPF1 recruitment

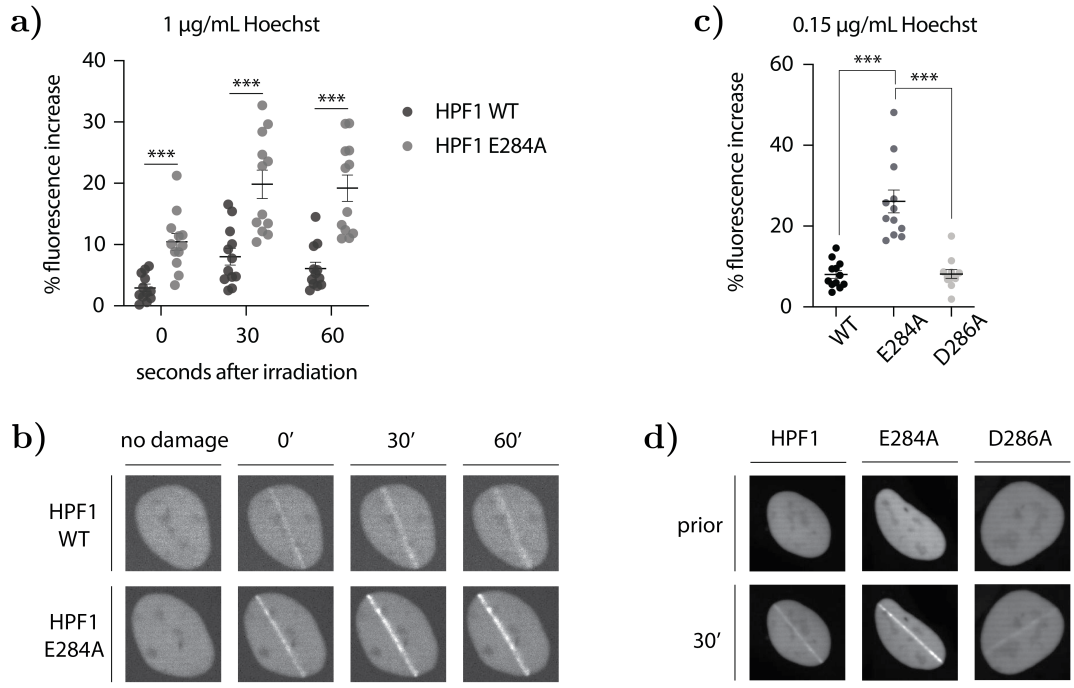


Figure 3.33: *HPF1 E284A shows strongly enhanced recruitment to sites of laser microirradiation-induced DNA damage.* **a)** Increase in GFP fluorescent intensity at sites of laser-induced damage at 0, 30 and 60 seconds following microirradiation in U2OS Flp-In *HPF1*Δ WT5 and E284A4 cells (*** = $p \leq 0.001$) (two-tailed paired t-test). **b)** Representative images of the result from **a)**. **c)** Increase in GFP fluorescent intensity at sites of laser-induced damage at 30 seconds in U2OS Flp-In *HPF1*Δ WT5, E284A4 and D286A5 cells (*** = $p \leq 0.001$) (two-tailed paired t-test). **d)** Representative images of the result from **c)**. In **a)** and **c)**, data points are shown as mean ± SEM from the analysis of 12 nuclei.

to sites of laser-induced damage is unclear and would require an experiment containing both shorter time point intervals and more distant time points (Gibbs-Seymour et al. (2016).

In the initial experiment, values from the nuclei of individual cells were scattered over a substantial range both for YFP-HPF1 and for YFP-HPF1 E284A (Figure 3.33a). One reason for that could be the Hoechst concentration used. Hoechst pre-sensitizes DNA to damage. Therefore, heterogeneity of local Hoechst concentration in a cell population could lead to outliers of YFP-HPF1 recruitment, particularly if a high Hoechst concentration combined with microirradiation results in excessive DNA damage. I therefore also tested YFP-HPF1 WT and E284A recruitment following 0.15 μg/mL Hoechst pre-treatment for 1 hour and extended the list of tested YFP-HPF1 variants to HPF1 D286A (Figure 3.33c). As before, YFP-HPF1 E284A was recruited to sites of laser-induced damage at twice the

strength as YFP-HPF1 WT, while the individual 12 measurements were less scattered within each YFP-HPF1 construct. Interestingly, loss of PARP1 interaction in the YFP-HPF1 D286A mutant did not affect its ability to recruit to sites of laser-induced damage (Figure 3.33c). Both from the graph and representative images of Figure 3.33d, YFP-HPF1 WT and D286A behaved identical following microirradiation. The experiment was carried out independently three time with similar results, whereby in one repeat a small but insignificant reduction in recruitment could be observed for the YFP-HPF1 D286A mutant (see Figure A.4a in *A Appendix*). Another repeat showed an also small, but significant ($p \leq 0.05$) reduction (see Figure A.4b in *A Appendix*). The questions therefore remains, if a different PARP1 binding mutant might paint a clearer picture or whether stronger overall recruitment of YFP-HPF1 WT might reveal a difference in recruitment between YFP-HPF1 WT and D286A. Equally, composite models of PARP1 bound both to a DSB and HPF1 leave open the possibility of HPF1 directly binding DNA. As a result, HPF1 might not require PARP1 binding to recruit to sites of DNA damage, explaining the equal degree of fluorescence intensity increase at microirradiation sites for both YFP-HPF1 WT and the D286A mutant.

The above findings from microirradiation experiments provide a possible explanation for the increased sensitivity of U2OS Flp-In *HPF1*Δ E284A5 cells to Olaparib. Increased recruitment of YFP-HPF1 E284A to sites of laser-induced damage is likely to signify increased HPF1-PARP1 complex formation and fewer not complexed PARP1 molecules at sites of DNA damage. A reason for this could be the stronger affinity of YFP-HPF1 E284A for PARP1, resulting in the variant remaining bound to PARP1 longer than YFP-HPF1 WT (Rudolph et al. (2021), Sun et al. (2021)). Due to its catalytic inactivation, HPF1 E284A does not switch PARP1-catalyzed ADP-ribosylation from glutamate/aspartate ADPr to serine ADPr, the main form of PARP1 auto-modification. However, this does not yet explain the phenotype observed in Figure 3.32c, given that loss of serine ADPr is also the case in *HPF1*Δ or HPF1 D286A expressing cells. Extended HPF1-PARP1 complex formation might impair initiation of PARP1 glutamate auto-modification, although it is not clear whether PARP1-catalyzed glutamate auto-ADPr can take place in its HPF1-bound state. However, as previously described in *3.3.1 HPF1 interaction sites on PARP1* and shown in Figure 3.15, HPF1 binding to PARP1 is irreconcilable with ADP-ribose chain elongation. Extended binding of HPF1 E284A to PARP1 could therefore also mean that,

even if PARP1 auto-modification on glutamate sites could take place in an HPF1-PARP1 complex, chain elongation might be impaired. As a result, PARP1 auto-modification required for its release from DNA might be even more inefficient than in *HPF1*Δ cells or cells expressing HPF1 D286A, further enhancing the susceptibility of PARP1 to be trapped at DNA by PARP1/2 inhibitors. In conclusion, further increased PARP1 trapping at sites of DNA damage could be the basis for the increased Olaparib sensitivity of U2OS Flp-In *HPF1*Δ E284A5 cells (Figure 3.32c).

Discussion

The findings reported above present a new way of thinking about not just ADP-riboslyation, but post-translational modifications (PTMs) in general. Not only do they confirm previous research that HPF1 binds PARP1 and drives serine ADP-ribosylation, the most abundant type of ADP-ribosylation in human cells, both under basal and DNA damage conditions (Bonfiglio et al. (2017b), Palazzo et al. (2018)). They also, and most importantly, for the first time describe the catalytic completion of a PTM-catalyzing protein by a helper protein that provides a catalytic residue. This discovery provides the molecular basis for how HPF1 achieves the shift in PARP1 from glutamate/aspartate to serine ADP-ribosylation. Furthermore, the thesis links PARP1-HPF1 driven serine ADP-ribosylation to an important aspect of PARP1 activity in DNA repair: its release from DNA damage sites. Finally, the data also explores the consequences of losing this catalytic switch in human cells and how this could be clinically exploited in the future.

4.1 PARP1/2-HPF1 interaction

The first goal in gaining a better understanding of the PARP1/2-HPF1 complex was to identify the points of contact between the proteins. Conservation studies of the peptide sequence of different HPF1 homologues together with the mapping of sequence conservation onto the structure of HPF1 by Marcin Suskiewicz revealed a negatively charged corner of conserved residues on the surface of HPF1. Single site mutations of several residues extended the list of PARP1/2-binding sites from the previously reported Y238 and R239 to the two key aspartate residues D283 and D286. Solution of an HPF1-PARP2 ART (CAT ΔHD) domain crystal structure by Marcin Suskiewicz subsequently provided insights into the points of contact of the two residues with PARP2 (Suskiewicz et al. (2020)). NMR interaction data and mutagenesis data from ADP-ribosylation assays con-

firmed these contacts with the equivalent PARP1 residues. In the crystal structures D283 is positioned close to H381 of PARP2 and H826 of a superimposed PARP1 structure, most likely forming a hydrogen bond between the Nθ of H826 and the carboxyl group of D283. Interestingly, although D286 equally abolished PARP1-binding, no such obvious point of contact exists for the residue. Rather, there are multiple hypotheses to how D286 might contribute to the HPF1-PARP1/2 complex. Together with R239 it could coordinate E284, which is in detail described below. However, it is unclear how the loss of that coordination might abolish the ability of HPF1 to bind PARP1/2. Another interesting observation was the discovery that HPF1-PARP2 ART domain crystals revealed a crystal contact between K179 of one HPF1 molecule and D235, Y238 and D286 of another, neighbouring HPF1 in the same crystal lattice. Hydrogen bonds can be drawn between the nitrogen of K179 and the carboxyl groups of D235 and D286 (Figure 4.1a). Given that serine ADP-ribosylation sites on target proteins are in many cases accompanied by a preceding lysine residue, prompting the term *KS motif*, both D235 or D286 could stimulate substrate binding and improve PARP1 substrate specificity by hydrogen-bonding lysine (Hendriks et al. (2019), Larsen et al. (2018)). However, loss of this function in an HPF1 D286A mutant also does not explain the abolition of PARP1 interaction. On the PARP1/2 end of the interaction, the two C-terminal residues on PARP1 and PARP2 form vital hydrophobic contacts with HPF1 residues on the α-helices αH, αI, and αK.

4.2 HPF1 catalytic residue

The third residue in the HPF1 negatively charged corner to disrupt cellular ADP-ribosylation levels is E284A. However, other than in the case of the D283 and D286 mutants, the HPF1 E284 mutant does not lose interaction with PARP1. On the contrary, HPF1 E284 has in fact been shown to bind more strongly to PARP1 *in vitro* than the wildtype protein (Rudolph et al. (2021), Sun et al. (2021)). Overexpression of HPF1 E284A in 293T WT cells even outcompetes endogenous HPF1 to block basal and DNA damage-dependent cellular ADP-ribosylation. Since HPF1 had already been shown to be responsible for bringing about serine ADP-ribosylation, the dominant type of ADP-ribosylation in cells under DNA damage conditions, the E284 residue was speculated to affect the ability of HPF1 to trigger the switch from HPF1-independent glutamate/aspartate ADP-ribosylation. The HPF1-

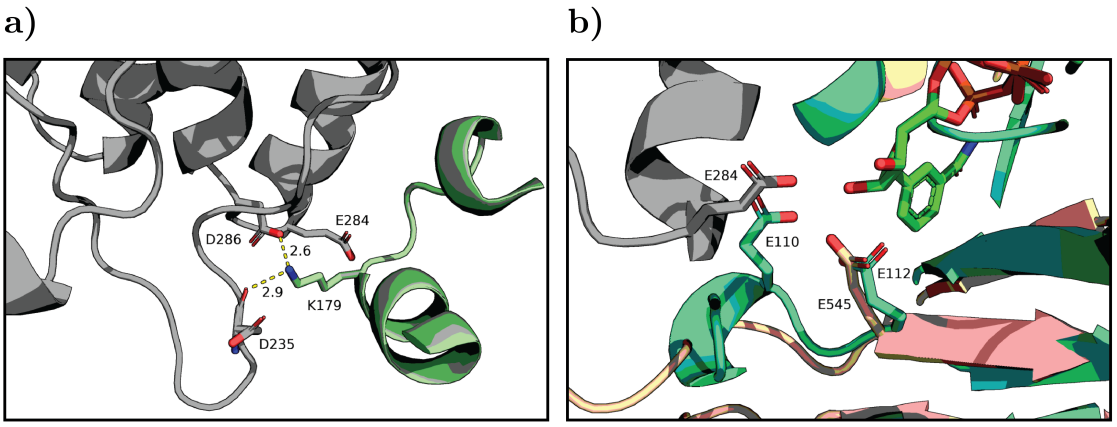


Figure 4.1: Highlights of structural features of the key HPF1 residues D286 and E284. **a)** Structure illustrating the potential role of HPF1 D286 in forming a hydrogen bond with lysine, based the contact between two HPF1 molecules in the same crystal lattice. Lysin often precedes a target serine residue, which is activated by the catalytic E284 shown in close proximity in the background. The two HPF1 molecules are shown in *gray* and *palegreen*. **b)** Superimposition of cholera toxin onto the crystal structure of HPF1-PARP2 ART domain. HPF1 is colored in *gray*, PARP2 ART domain in *wheat* and cholera toxin in *greencyan*.

PARP2 ART domain crystal structure ultimately provided the functional basis for this observation. While the catalytic glutamate of PARP1 or PARP2, E988 and E545 respectively, alone is able to confer ADP-ribose on negatively charged glutamate and aspartate residues due to their nuecleophilic carboxyl side chains, no nucleophile is provided by the ADP-ribosylation substrate in serine ADP-ribosylation. Rather, E284 de-protonates the serine substrate and thus converts it into a nucleophile. This conclusion is supported by the existence of two catalytic glutamate residues in cholera-toxin-like ADP-ribosyltransferases to bring about arginine ADP-ribosylation (Laing et al. (2011)).

Figure 4.1b shows a superimposition of *Vibrio cholerae 569B* cholera toxin and HPF1-PARP2 ART domain crystal structures. Highlighted are the key catalytic residues - E110 and D112 in the case of cholera toxin and HPF1 E284 and PARP2 E545 in the case of the HPF1-PARP2 ART domain structure - in close proximity to the NAD^+ analogue BAD. While E112 of cholera toxin is turned outward in the crystal structure, the amino acid's side change is thought to be flexible in its substrate free state, which is the case here. Therefore, in Figure 4.1b the cholera toxin E112 side chain can be turned while the main chain remains in the same position.This arrangement underlines the similarity in reactive site between a serine ADP-ribosylating HPF1-PARP1/2 complex and a arginine-ADP-

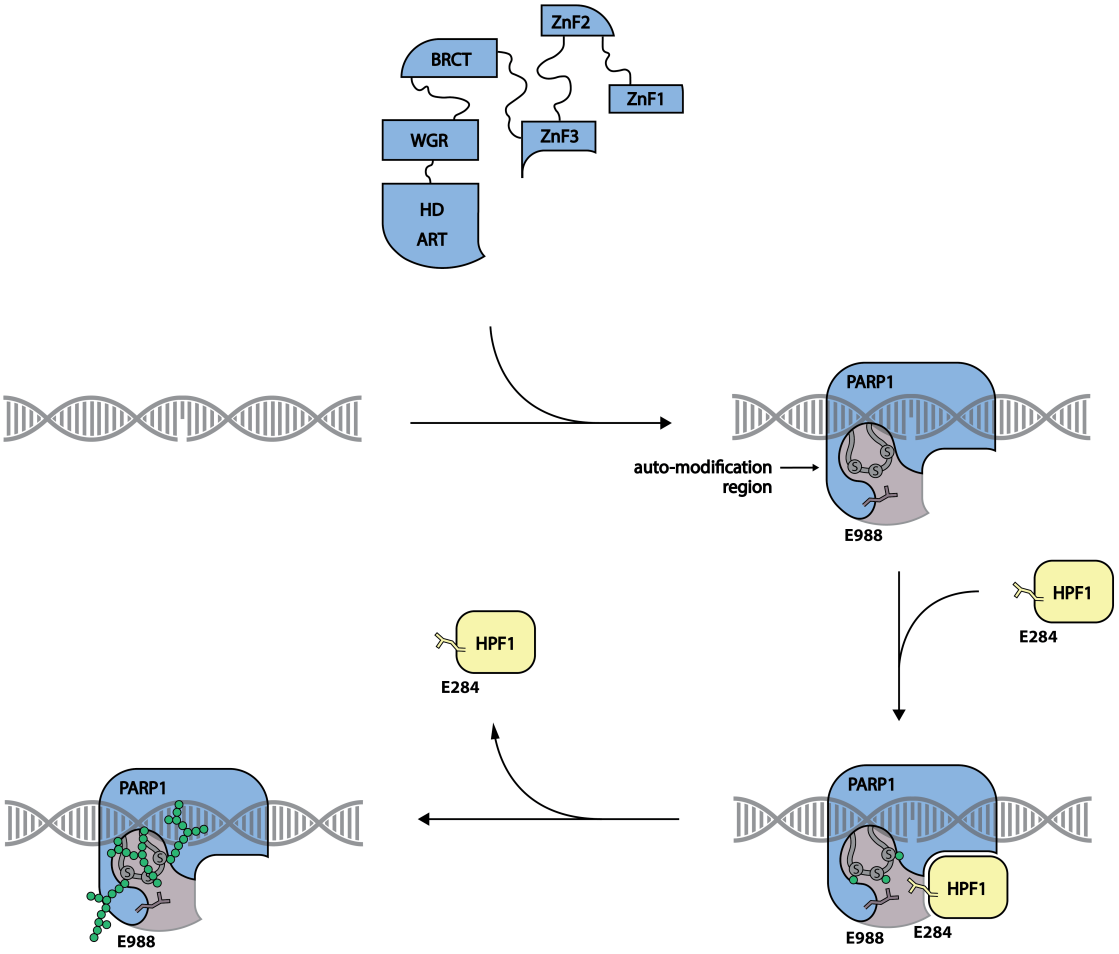


Figure 4.2: Stages of PARP1/HPF1-catalyzed serine ADPr from DNA damage recognition and PARP1 catalytic activation over HPF1-PARP1 complex formation and serine ADPr initiation to HPF1 release and PARP1-directed ADP-ribose chain elongation. Release of PARP1 from DNA following auto-PARylation is not shown.

ribosylation catalyzing cholera toxin.

The discovery that PARP1 and PARP2 are catalytically incomplete without the *glutamate finger* of HPF1 is reminiscent of GTPase catalytic activation by the *arginine finger* of GTPase activating proteins (Kötting et al. (2008)). It also describes the first instance, in which a PTM-catalyzing protein requires a cofactor for catalytic completion. The finding reshapes the way that previous *in vitro* experiments with PARP1/2 alone are viewed, particularly regarding the nature of acceptor amino acids and their significance in DNA damage-dependent ADP-ribosylation. The catalytically complete assembly of PARP1/2-HPF1 together with an activating DNA substrate can therefore be used in the future to accurately display DNA damage-dependent ADP-ribosylation reactions on target proteins.

The findings on the HPF1 catalytic site and PARP1/HPF1 interaction sites also provide vital insights into the spaciotemporal separation of the different steps in PARP1/2-catalyzed ADP-ribosylation. *In vitro* results from Marcin Suskiewicz supported the notion gathered from co-IP data that HPF1 binding to PARP1 only occurs following PARP1 catalytic activation, which was achieved by adding DNA to the reaction or deleting the HD (Figure 4.2) (Suskiewicz et al. (2020)). In a similar way, co-crystallization of the PARP1/2 catalytic domain with HPF1 only occurred when the HD, which is unfolded in catalytically active PARP1, was not present (Sun et al. (2021), Suskiewicz et al. (2020)). Independence of ADP-ribose chain elongation from HPF1 also raised the question of whether the HPF1-PARP1 interaction is required following initiation of serine ADPr. Indeed, HPF1-binding to PARP1 is incompatible with chain elongation, pointing towards a highly transient nature of the HPF1-PARP1 complex (see Figure 3.15). The 50-fold higher PARP1 abundance compared to HPF1 in cells further supports the requirement of HPF1 to be a highly efficient, transient initiator of serine ADPr (Hein et al. (2015)).

4.3 PARP1 auto-modification

PARP1 auto-ADPr, triggering either electrostatic repulsion or auto-ADPr-dependent recruitment of anti-trapping factors, is the mechanism by which PARP1 is thought to be released from DNA damage sites following its initial recruitment (Demin et al. (2021), Palazzo et al. (2021), Pascal (2018)). Given that PARP1 auto-modification relies on PARP1 catalytic activity, PARP1 inhibition does not only prevent many of its functions in the human DNA damage response, but also its timely dissociation from DNA. Loss of HPF1 in cells has been shown to exert a similarly strong sensitivity to PARP inhibitors as seen in BRCA1/2-mutated cells (Fong et al. (2009), Gibbs-Seymour et al. (2016)). We found that three serine sites in the auto-modification domain of PARP1, S499, S507 and S519, are the three most significant sites for PARP1 auto-modification (Figure 4.2) (Prokhorova et al. (2021)). The work of our collaborators (Rebecca Smith, Siham Zentout and Sébastien Huet) subsequently uncovered the recruitment dynamics of such a triple serine to alanine (3x S/A) mutated auto-modification-impaired PARP1 mutant, illustrating its reduced ability to dissipate from sites of laser-induced DNA damage. Evgeniia Prokhorova and I connected these findings with observations on the increased PARP sen-

sitivity of U2OS Flp-In cells carrying 3x S/A PARP1 (Prokhorova et al. (2021)). Further prove came from cells expressing the PARP1-binding mutant HPF1 D286A, which also showed increased sensitivity to PARP inhibition. Mutation of six putative glutamate auto-ADP-ribosylation sites, E471A, E484A, E488A, E491A, E513A, E514A, also impacted PARP1 auto-modification levels, albeit to a smaller extent. While this result reveals partial redundancy between serine and glutamate PARP1 auto-ADPr, the latter likely serves as a less efficient fall-back option (similar to PARP2 in BER). The lack of PARP1 serine auto-modification alone potentiates the trapping effect of PARP inhibitors and is at least one reason for the drastic sensitivity to PARP inhibition observed in HPF1 KO cells. However, it cannot be excluded that the observed sensitivities stem not only from the inability of PARP1 to dissociate from DNA, but also from impaired recruitment of DNA repair factors and chromatin remodellers possibly recognizing and binding PAR chains of auto-modified PARP1 (Ahel et al. (2009), Bryant et al. (2009), Gottschalk et al. (2009), Reynolds et al. (2015), Shao et al. (2020)).

Interestingly, the sensitivity observed in HPF1 D286A expressing cells is further exacerbated in cells expressing the HPF1 E284A catalytic mutant. One explanation for this could be the stronger affinity of HPF1 E284A for PARP1 compared to HPF1 WT (Rudolph et al. (2021), Sun et al. (2021)). This can have two consequences. Firstly, since HPF1-binding to PARP1 and ADP-ribose chain elongation are mutually exclusive, HPF1 E284A could delay PARP1 auto-poly-ADPr. Recent research showed that PARP1 released from DNA is highly modified, indicating that PARP1 mono-ADPr is insufficient for its release from DNA (Krüger et al. (2020)). Stronger binding by HPF1 E284A could therefore impair PAR-mediated dissociation from DNA. Secondly, a prediction on HPF1 positioning in the HPF1-PARP1-DNA complex sees HPF1 closely surrounded by the HD as well as ZnF2 and, at a distance, also ZnF1 and ZnF3 (Figure 3.11). Through this proximity to the zinc finger motifs of PARP1, HPF1 could contribute to tighter PARP1 DNA binding, potentiating the reverse allostery observed for some PARP inhibitors (Zandarashvili et al. (2020)). In light of this, the development of an inhibitor that could trap the HPF1-PARP1 complex on DNA, rather than HPF1 alone, seems an interesting concept.

4.4 Clinical relevance

Over the last seven years, the development of PARP inhibitors for use in the treatment of BRCA1/2-mutated cancers has been shown to be widely successful across different types of cancers and treatment schemes. At the basis of this success lies the synthetic lethality between the inhibition of PARP1/2 and HR deficiency (Bryant et al. (2005), Farmer et al. (2005)). Similarly, I confirm in this thesis the initial finding that loss of HPF1 drastically sensitizes cells to the PARP inhibitor Olaparib, which is also supported in other studies (DeWeirdt et al. (2020), Gibbs-Seymour et al. (2016), Hewitt et al. (2021)). Conversely, I also provide evidence that HPF1 overexpression can confer resistance to the inhibition of PARP1 auto-modification. This effect, however, is less clear than the loss of HPF1. Albeit being responsible for more efficient PARP1 auto-modification, HPF1 both limits chain elongation on PARP1 and promotes trans-ADP-ribosylation (Gibbs-Seymour et al. (2016)). This is particularly visible when HPF1 is transienly overexpressed, allowing the initiation of efficient serine ADP-ribosylation on PARP1 in the presence of PARP inhibitors while strongly limiting chain elongation (see *3.4.3 HPF1 expression and PARP inhibitor resistance*). Both aspects were recently confirmed in two pre-prints. Initiation of HPF1-dependent serine ADPr occurs at a comparable rate to that of the ADP-ribose chain elongation reaction, while glutamate/aspartate ADPr initiation is 250-fold slower than chain elongation (Langelier et al. (2021), Mendoza-Alvarez & Alvarez-Gonzalez (1999)). However, a concentration of 14 μM HPF1 to 1 μM PARP1 was also shown to reduce ADP-ribose chain elongation on a S10 mono-ADP-ribose-modified histone H3 substrate by 50% compared to the absence of HPF1 (Mohapatra et al. (2021)). PARP inhibitor resistance might therefere be limtied to a certain, narrow HPF1 overexpression range, under which sufficient chain elongation can still occur to achieve PARP1 release from DNA.

The impact of HPF1 loss in cells is well illustrated by the loss of cellular ADP-ribosylation levels. Conversely, a situation where ADP-ribosylation initiation of a large number of PARP1 substrates is maximally boosted without strongly limiting ADP-ribose chain length on PARP1 might be a good indicator for identifying the level of HPF1 overexpression that could confer the strongest PARP inhibitor resistance. In conclusion, the above findings identify HPF1 as a biomarker for the treatment of cancer cells with PARP inhibitors, while cellular ADP-ribosylation levels are a good negative predictor of PARP inhibitor sensi-

tivity. Interestingly, the antagonist of HPF1, ARH3, is an equally suitable biomarker, however in reverse fashion to HPF1. While he overexpression of ARH3 confers PARP inhibitor sensitivity to cells, loss of ARH3 results in PARP inhibitor resistance (Prokhorova et al. (2021)).

Altogether, the findings from this thesis make a strong case for extending the use of PARP inhibitors to HPF1-negative cells. Loss of HPF1 even further sensitizes already PARP1/2 inhibitor-sensitive BRCA1/2-mutated cells, suggesting that cancers cells of such a genetic background might respond even better to PARP inhibitor treatment (Prokhorova et al. (2021)). At the same time, the data suggests that the use of PARP inhibitors might be less successful in cells carrying elevated ADP-ribosylation levels as a result of HPF1 overexpression. In a more general sense, the above results have added further traction to finding new combinations for synthetic lethality with PARP inhibitors, as is currently happening in the case of ATM/ATR inhibition and/or loss (Lloyd et al. (2020), Southgate et al. (2020)).

4.5 Future directions

Many cancer cell lines show discrepancies in HPF1 transcription levels, which might translate to elevated or decreased HPF1 protein levels. Using the U2OS Flp-In system, it would be interesting to study different levels of HPF1 expression below and above that of endogenous HPF1 levels to explore how they influence sensitivity to PARP inhibitors. Within that it would be of particular interest to determine the HPF1 concentration at which cells are conferred the maximum resistance to PARP inhibitors. Towards the end of my DPhil course I have also started developing HPF1 D283A, HPF1 E284A and PARP1 3x S/A knock-in cells of RPE-1 and SUM159PT cell lines. The aim of this work was to study the above explored mutants in a more physiological setting. This would underline the significance of serine ADP-ribosylation, PARP1/2-HPF1 interaction and PARP1 auto-modification with regards to cancer therapeutic treatments, for which particularly the triple negative breast cancer cell line SUM159PT is a good model. Unfortunately, at the point of concluding my DPhil course, I was only able to generate heterozygous HPF1 D283A and E284A clones of RPE-1 and SUM159PT cells. The generation of these cell

lines, however, is continued and will hopefully provide further exciting insights towards the prospect of PARP inhibitor use in serine ADP-ribosylation impaired cancer cells.

Bibliography

Aasland, R., Abrams, C., Ampe, C., Ball, L. J., Bedford, M. T., Cesareni, G., Gimona, M., Hurley, J. H., Jarchau, T., Lehto, V. P., Lemmon, M. A., Linding, R., Mayer, B. J., Nagai, M., Sudol, M., Walter, U. & Winder, S. J. (2002), 'Normalization of nomenclature for peptide motifs as ligands of modular protein domains.', *FEBS letters* **513**(1), 141–144.

Aberle, L., Krüger, A., Reber, J. M., Lippmann, M., Hufnagel, M., Schmalz, M., Trussina, I. R. E. A., Schlesiger, S., Zubel, T., Schütz, K., Marx, A., Hartwig, A., Ferrando-May, E., Bürkle, A. & Mangerich, A. (2020), 'PARP1 catalytic variants reveal branching and chain length-specific functions of poly(ADP-ribose) in cellular physiology and stress response', *Nucleic acids research* **48**(18), 10015–10033.

Abplanalp, J., Leutert, M., Frugier, E., Nowak, K., Feurer, R., Kato, J., Kistemaker, H. V. A., Filippov, D. V., Moss, J., Caflisch, A. & Hottiger, M. O. (2017), 'Proteomic analyses identify ARH3 as a serine mono-ADP-ribosylhydrolase.', *Nat Commun* **8**(1), 2055.

Agnew, T., Munnur, D., Crawford, K., Palazzo, L., Mikoč, A. & Ahel, I. (2018), 'MacroD1 Is a Promiscuous ADP-Ribosyl Hydrolase Localized to Mitochondria', *Frontiers in Microbiology* **9**, 114.

Ahel, D., Horejsí, Z., Wiechens, N., Polo, S. E., Garcia-Wilson, E., Ahel, I., Flynn, H., Skehel, M., West, S. C., Jackson, S. P., Owen-Hughes, T. & Boulton, S. J. (2009), 'Poly(ADP-ribose)-dependent regulation of DNA repair by the chromatin remodeling enzyme ALC1.', *Science* **325**(5945), 1240–1243.

Ahel, I., Ahel, D., Matsusaka, T., Clark, A. J., Pines, J., Boulton, S. J. & West, S. C. (2008), 'Poly(ADP-ribose)-binding zinc finger motifs in DNA repair/checkpoint proteins', *Nature* **451**(7174), 81–85.

Al-Hakim, A. K., Bashkurov, M., Gingras, A.-C., Durocher, D. & Pelletier, L. (2012),

'Interaction proteomics identify NEURL4 and the HECT E3 ligase HERC2 as novel modulators of centrosome architecture.', *Molecular & cellular proteomics : MCP* **11**(6), M111.014233.

Alemasova, E. E. & Lavrik, O. I. (2019), 'Poly(ADP-ribosyl)ation by PARP1: reaction mechanism and regulatory proteins.', *Nucleic acids research* **47**(8), 3811–3827.

Ali, A. A. E., Jukes, R. M., Pearl, L. H. & Oliver, A. W. (2009), 'Specific recognition of a multiply phosphorylated motif in the DNA repair scaffold XRCC1 by the FHA domain of human PNK.', *Nucleic acids research* **37**(5), 1701–1712.

Ali, A., Timinszky, G., structural, R. A.-B. N. & 2012 (2012), 'The zinc-finger domains of PARP1 cooperate to recognize DNA strand breaks', *nature.com* .

Alvarez-Gonzalez, R., Biochemistry, M. J. & 1987 (1987), 'Characterization of polymers of adenosine diphosphate ribose generated in vitro and in vivo', *ACS Publications* .

Amé, J. C., Rolli, V., Schreiber, V., Niedergang, C., Apiou, F., Decker, P., Muller, S., Höger, T., Ménissier-de Murcia, J. & de Murcia, G. (1999), 'PARP-2, A novel mammalian DNA damage-dependent poly(ADP-ribose) polymerase.', *J. Biol. Chem.* **274**(25), 17860–17868.

Aravind, L. (2001), 'The WWE domain: a common interaction module in protein ubiquitination and ADP ribosylation.', *Trends in Biochemical Sciences* **26**(5), 273–275.

Aravind, L., Zhang, D., de Souza, R. F., Anand, S. & Iyer, L. M. (2015), 'The natural history of ADP-ribosyltransferases and the ADP-ribosylation system.', *Current topics in microbiology and immunology* **384**(Chapter 414), 3–32.

Barkauskaite, E., Jankevicius, G. & Ahel, I. (2015), 'Structures and Mechanisms of Enzymes Employed in the Synthesis and Degradation of PARP-Dependent Protein ADP-Ribosylation.', *Mol. Cell* **58**(6), 935–946.

Barkauskaite, E., Jankevicius, G., Ladurner, A. G., Ahel, I. & Timinszky, G. (2013), 'The recognition and removal of cellular poly(ADP-ribose) signals.', *Febs J* **280**(15), 3491–3507.

Bartlett, E., Bonfiglio, J. J., Prokhorova, E., Colby, T., Zobel, F., Ahel, I. & Matic, I. (2018), 'Interplay of Histone Marks with Serine ADP-Ribosylation', *Cell Reports* **24**(13), 3488–3502.e5.

Beard, W. A., Horton, J. K., Prasad, R. & Wilson, S. H. (2019), 'Eukaryotic Base Excision Repair: New Approaches Shine Light on Mechanism.', *Annual review of biochemistry* **88**, 137–162.

Beck, C., Boehler, C., Guirouilh Barbat, J., Bonnet, M.-E., Illuzzi, G., Ronde, P., Gauthier, L. R., Magroun, N., Rajendran, A., Lopez, B. S., Scully, R., Boussin, F. D., Schreiber, V. & Dantzer, F. (2014), 'PARP3 affects the relative contribution of homologous recombination and nonhomologous end-joining pathways.', *Nucleic acids research* **42**(9), 5616–5632.

Bell, C. E. & Eisenberg, D. (1996), 'Crystal Structure of Diphtheria Toxin Bound to Nicotinamide Adenine Dinucleotide†', *Biochemistry* .

Berger, W., Steiner, E., Grusch, M., Elbling, L. & Micksche, M. (2009), 'Vaults and the major vault protein: novel roles in signal pathway regulation and immunity.', *Cellular and molecular life sciences : CMLS* **66**(1), 43–61.

Bilokapic, S., Suskiewicz, M. J., Ahel, I. & Halic, M. (2020), 'Bridging of DNA breaks activates PARP2-HPF1 to modify chromatin.', *Nature* **45**(7826), 8129–5.

Blessing, C. & Ladurner, A. G. (2020), 'Tickling PARPs into serine action.', *Nature structural & molecular biology* **31**(4), 101–3.

Boehler, C., Gauthier, L. R., Mortusewicz, O., Biard, D. S., Saliou, J.-M., Bresson, A., Sanglier-Cianferani, S., Smith, S., Schreiber, V., Boussin, F. & Dantzer, F. (2011), 'Poly(ADP-ribose) polymerase 3 (PARP3), a newcomer in cellular response to DNA damage and mitotic progression.', *Proceedings of the National Academy of Sciences of the United States of America* **108**(7), 2783–2788.

Bonfiglio, J. J., Colby, T. & Matic, I. (2017a), 'Mass spectrometry for serine ADP-ribosylation? Think o-glycosylation!', *Nucleic acids research* **45**(11), 6259–6264.

Bonfiglio, J. J., Fontana, P., Zhang, Q., Colby, T., Gibbs-Seymour, I., Atanassov, I.,

Bartlett, E., Zaja, R., Ahel, I. & Matic, I. (2017b), 'Serine ADP-Ribosylation Depends on HPF1.', *Mol. Cell* **65**(5), 932–940.e6.

Boussios, S., Karihtala, P., Moschetta, M., Karathanasi, A., Sadauskaite, A., Rassy, E. & Pavlidis, N. (2019), 'Combined Strategies with Poly (ADP-Ribose) Polymerase (PARP) Inhibitors for the Treatment of Ovarian Cancer: A Literature Review.', *Diagnostics (Basel, Switzerland)* **9**(3), 87.

Brennan, D. F. & Barford, D. (2009), 'Eliminylation: a post-translational modification catalyzed by phosphothreonine lyases.', *Trends in Biochemical Sciences* **34**(3), 108–114.

Bryant, H. E., Petermann, E., Schultz, N., Jemth, A.-S., Loseva, O., Issaeva, N., Johansson, F., Fernandez, S., McGlynn, P. & Helleday, T. (2009), 'PARP is activated at stalled forks to mediate Mre11-dependent replication restart and recombination.', *EMBO J.* **28**(17), 2601–2615.

Bryant, H. E., Schultz, N., Thomas, H. D., Parker, K. M., Flower, D., Lopez, E., Kyle, S., Meuth, M., Curtin, N. J. & Helleday, T. (2005), 'Specific killing of BRCA2-deficient tumours with inhibitors of poly(ADP-ribose) polymerase.', *Nature* **434**(7035), 913–917.

Buch-Larsen, S. C., Hendriks, I. A., Lodge, J. M., Rykær, M., Furtwängler, B., Shishkova, E., Westphall, M. S., Coon, J. J. & Nielsen, M. L. (2020), 'Mapping Physiological ADP-Ribosylation Using Activated Ion Electron Transfer Dissociation.', *Cell Reports* **32**(12), 108176.

Caldecott, K. W. (2003), 'XRCC1 and DNA strand break repair.', *DNA repair* **2**(9), 955–969.

Caldecott, K. W. (2008), 'Single-strand break repair and genetic disease.', *Nature reviews. Genetics* **9**(8), 619–631.

Caldecott, K. W. (2019), 'XRCC1 protein; Form and function.', *DNA repair* **81**, 102664.

Carney, B., Kossatz, S., Lok, B. H., Schneeberger, V., Gangangari, K. K., Pillarsetty, N. V. K., Weber, W. A., Rudin, C. M., Poirier, J. T. & Reiner, T. (2018), 'Target engagement imaging of PARP inhibitors in small-cell lung cancer.', *Nat Commun* **9**(1), 176–13.

Caron, M.-C., Sharma, A. K., O'Sullivan, J., Myler, L. R., Ferreira, M. T., Rodrigue, A., Coulombe, Y., Ethier, C., Gagné, J.-P., Langelier, M.-F., Pascal, J. M., Finkelstein, I. J.,

Hendzel, M. J., Poirier, G. G. & Masson, J.-Y. (2019), 'Poly(ADP-ribose) polymerase-1 antagonizes DNA resection at double-strand breaks.', *Nat Commun* **10**(1), 2954–16.

Castor, D., Nair, N., Déclais, A.-C., Lachaud, C., Toth, R., Macartney, T. J., Lilley, D. M. J., Arthur, J. S. C. & Rouse, J. (2013), 'Cooperative control of holliday junction resolution and DNA repair by the SLX1 and MUS81-EME1 nucleases.', *Mol. Cell* **52**(2), 221–233.

Castri, P., Lee, Y.-J., Ponzio, T., Maric, D., Spatz, M., Bembry, J. & Hallenbeck, J. (2014), 'Poly(ADP-ribose) polymerase-1 and its cleavage products differentially modulate cellular protection through NF-kappaB-dependent signaling.', *Biochimica et biophysica acta* **1843**(3), 640–651.

Catara, G., Corteggio, A., Valente, C., Grimaldi, G. & Palazzo, L. (2019), 'Targeting ADP-ribosylation as an antimicrobial strategy.', *Biochemical pharmacology* **167**, 13–26.

Chang, H. H. Y., Pannunzio, N. R., Adachi, N. & Lieber, M. R. (2017), 'Non-homologous DNA end joining and alternative pathways to double-strand break repair.', *Nature Reviews Molecular Cell Biology* **18**(8), 495–506.

Chen, C.-C., Feng, W., Lim, P. X., Kass, E. M. & Jasin, M. (2018), 'Homology-Directed Repair and the Role of BRCA1, BRCA2, and Related Proteins in Genome Integrity and Cancer.', *Annual review of cancer biology* **2**, 313–336.

Chen, Q., Kassab, M. A., Dantzer, F. & Yu, X. (2018), 'PARP2 mediates branched poly ADP-ribosylation in response to DNA damage.', *Nat Commun* **9**(1), 3233–13.

Chiruvella, K. K., Liang, Z. & Wilson, T. E. (2013), 'Repair of double-strand breaks by end joining.', *Cold Spring Harbor perspectives in biology* **5**(5), a012757.

Chou, D. M., Adamson, B., Dephoure, N. E., Tan, X., Nottke, A. C., Hurov, K. E., Gygi, S. P., Colaiácovo, M. P. & Elledge, S. J. (2010), 'A chromatin localization screen reveals poly (ADP ribose)-regulated recruitment of the repressive polycomb and NuRD complexes to sites of DNA damage.', *Proceedings of the National Academy of Sciences of the United States of America* **107**(43), 18475–18480.

Clapperton, J. A., Manke, I. A., Lowery, D. M., Ho, T., Haire, L. F., Yaffe, M. B. & Smerdon, S. J. (2004), 'Structure and mechanism of BRCA1 BRCT domain recognition

of phosphorylated BACH1 with implications for cancer.', *Nature structural & molecular biology* **11**(6), 512–518.

Clement, F. C., Camenisch, U., Fei, J., Kaczmarek, N., Mathieu, N. & Naegeli, H. (2010), 'Dynamic two-stage mechanism of versatile DNA damage recognition by xeroderma pigmentosum group C protein.', *Mutation research* **685**(1-2), 21–28.

D'Amours, D., Desnoyers, S., D'Silva, I. & Poirier, G. G. (1999), 'Poly(ADP-ribosyl)ation reactions in the regulation of nuclear functions.', *The Biochemical journal* **342 (Pt 2)**(Pt 2), 249–268.

Danhauser, K., Alhaddad, B., Makowski, C., Piekutowska-Abramczuk, D., Syrbe, S., Gomez-Ospina, N., Manning, M. A., Kostera-Pruszczyk, A., Krahn-Peper, C., Berutti, R., Kovács-Nagy, R., Gusic, M., Graf, E., Laugwitz, L., Röblitz, M., Wroblewski, A., Hartmann, H., Das, A. M., Bültmann, E., Fang, F., Xu, M., Schatz, U. A., Karall, D., Zellner, H., Haberlandt, E., Feichtinger, R. G., Mayr, J. A., Meitinger, T., Prokisch, H., Strom, T. M., Płoski, R., Hoffmann, G. F., Pronicki, M., Bonnen, P. E., Morlot, S. & Haack, T. B. (2018), 'Bi-allelic ADPRHL2 Mutations Cause Neurodegeneration with Developmental Delay, Ataxia, and Axonal Neuropathy.', *American journal of human genetics* **103**(5), 817–825.

DaRosa, P. A., Wang, Z., Jiang, X., Pruneda, J. N., Cong, F., Klevit, R. E. & Xu, W. (2015), 'Allosteric activation of the RNF146 ubiquitin ligase by a poly(ADP-ribosyl)ation signal.', *Nature* **517**(7533), 223–226.

Dawicki-McKenna, J. M., Langelier, M.-F., DeNizio, J. E., Riccio, A. A., Cao, C. D., Karch, K. R., McCauley, M., Steffen, J. D., Black, B. E. & Pascal, J. M. (2015), 'PARP-1 Activation Requires Local Unfolding of an Autoinhibitory Domain.', *Mol. Cell* **60**(5), 755–768.

de Bono, J., Mateo, J., Fizazi, K., Saad, F., Shore, N., Sandhu, S., Chi, K. N., Sartor, O., Agarwal, N., Olmos, D., Thiery-Vuillemin, A., Twardowski, P., Mehra, N., Goessl, C., Kang, J., Burgents, J., Wu, W., Kohlmann, A., Adelman, C. A. & Hussain, M. (2020), 'Olaparib for Metastatic Castration-Resistant Prostate Cancer.', *The New England journal of medicine* **382**(22), 2091–2102.

De Vos, M., Schreiber, V. & Dantzer, F. (2012), 'The diverse roles and clinical relevance of PARPs in DNA damage repair: current state of the art.', *Biochemical pharmacology* **84**(2), 137–146.

Demin, A. A., Hirota, K., Tsuda, M., Adamowicz, M., Hailstone, R., Brazina, J., Gittens, W., Kalasova, I., Shao, Z., Zha, S., Sasanuma, H., Hanzlikova, H., Takeda, S. & Caldecott, K. W. (2021), 'XRCC1 prevents toxic PARP1 trapping during DNA base excision repair.', *Mol. Cell* **81**(14), 3018–3030.e5.

Derbyshire, D. J., Basu, B. P., Serpell, L. C., Joo, W. S., Date, T., Iwabuchi, K. & Doherty, A. J. (2002), 'Crystal structure of human 53BP1 BRCT domains bound to p53 tumour suppressor.', *EMBO J.* **21**(14), 3863–3872.

DeWeirdt, P. C., Sangree, A. K., Hanna, R. E., Sanson, K. R., Hegde, M., Strand, C., Persky, N. S. & Doench, J. G. (2020), 'Genetic screens in isogenic mammalian cell lines without single cell cloning.', *Nat Commun* **11**(1), 752–15.

Durocher, D. & Jackson, S. P. (2002), 'The FHA domain.', *FEBS letters* **513**(1), 58–66.

Eustermann, S., Brockmann, C., Mehrotra, P. V., Yang, J.-C., Loakes, D., West, S. C., Ahel, I. & Neuhaus, D. (2010), 'Solution structures of the two PBZ domains from human APLF and their interaction with poly(ADP-ribose).', *Nature structural & molecular biology* **17**(2), 241–243.

Eustermann, S., Videler, H., Yang, J.-C., Cole, P. T., Gruszka, D., Veprintsev, D. & Neuhaus, D. (2011), 'The DNA-binding domain of human PARP-1 interacts with DNA single-strand breaks as a monomer through its second zinc finger.', *Journal of molecular biology* **407**(1), 149–170.

Eustermann, S., Wu, W.-F., Langelier, M.-F., Yang, J.-C., Easton, L. E., Riccio, A. A., Pascal, J. M. & Neuhaus, D. (2015), 'Structural Basis of Detection and Signaling of DNA Single-Strand Breaks by Human PARP-1.', *Mol. Cell* **60**(5), 742–754.

Farmer, H., McCabe, N., Lord, C. J., Tutt, A. N. J., Johnson, D. A., Richardson, T. B., Santarosa, M., Dillon, K. J., Hickson, I., Knights, C., Martin, N. M. B., Jackson, S. P., Smith, G. C. M. & Ashworth, A. (2005), 'Targeting the DNA repair defect in BRCA mutant cells as a therapeutic strategy.', *Nature* **434**(7035), 917–921.

Fatokun, A. A., Dawson, V. L. & Dawson, T. M. (2014), 'Parthanatos: mitochondrial-linked mechanisms and therapeutic opportunities.', *British journal of pharmacology* **171**(8), 2000–2016.

Feldman, J. L., Dittenhafer-Reed, K. E. & Denu, J. M. (2012), 'Sirtuin catalysis and regulation.', *J. Biol. Chem.* **287**(51), 42419–42427.

Fenton, A. L., Shirodkar, P., Macrae, C. J., Meng, L. & Koch, C. A. (2013), 'The PARP3- and ATM-dependent phosphorylation of APLF facilitates DNA double-strand break repair.', *Nucleic acids research* **41**(7), 4080–4092.

Fong, P. C., Boss, D. S., Yap, T. A., Tutt, A., Wu, P., Mergui-Roelvink, M., Mortimer, P., Swaisland, H., Lau, A., O'Connor, M. J., Ashworth, A., Carmichael, J., Kaye, S. B., Schellens, J. H. M. & de Bono, J. S. (2009), 'Inhibition of poly(ADP-ribose) polymerase in tumors from BRCA mutation carriers.', *The New England journal of medicine* **361**(2), 123–134.

Fontana, P., Bonfiglio, J. J., Palazzo, L., Bartlett, E., Matic, I. & Ahel, I. (2017), 'Serine ADP-ribosylation reversal by the hydrolase ARH3.', *Elife* **6**, e28533.

García-Saura, A. G., Zapata-Pérez, R., Hidalgo, J. F. & Sánchez-Ferrer, Á. (2018), 'Comparative inhibitory profile and distribution of bacterial PARPs, using Clostridioides difficile CD160 PARP as a model.', *Scientific Reports* **8**(1), 8056–12.

Gary, R., Kim, K., Cornelius, H. L., Park, M. S. & Matsumoto, Y. (1999), 'Proliferating cell nuclear antigen facilitates excision in long-patch base excision repair.', *Journal of Biological Chemistry* **274**(7), 4354–4363.

Gibbs-Seymour, I., Fontana, P., Rack, J. G. M. & Ahel, I. (2016), 'HPF1/C4orf27 Is a PARP-1-Interacting Protein that Regulates PARP-1 ADP-Ribosylation Activity.', *Mol. Cell* **62**(3), 432–442.

Gibson, B. A. & Kraus, W. L. (2012), 'New insights into the molecular and cellular functions of poly(ADP-ribose) and PARPs', *Nature Reviews Molecular Cell Biology* **13**(7), 411–424.

Gieni, R. S., Ismail, I. H., Campbell, S. & Hendzel, M. J. (2011), 'Polycomb group proteins

in the DNA damage response: a link between radiation resistance and "stemness".', *Cell cycle (Georgetown, Tex.)* **10**(6), 883–894.

Gillet, L. C. J. & Schärer, O. D. (2006), 'Molecular mechanisms of mammalian global genome nucleotide excision repair.', *Chemical reviews* **106**(2), 253–276.

Golan, T., Hammel, P., Reni, M., Van Cutsem, E., Macarulla, T., Hall, M. J., Park, J.-O., Hochhauser, D., Arnold, D., Oh, D.-Y., Reinacher-Schick, A., Tortora, G., Algül, H., O'Reilly, E. M., McGuinness, D., Cui, K. Y., Schlienger, K., Locker, G. Y. & Kindler, H. L. (2019), 'Maintenance Olaparib for Germline BRCA-Mutated Metastatic Pancreatic Cancer.', *The New England journal of medicine* **381**(4), 317–327.

Gottschalk, A. J., Timinszky, G., Kong, S. E., Jin, J., Cai, Y., Swanson, S. K., Washburn, M. P., Florens, L., Ladurner, A. G., Conaway, J. W. & Conaway, R. C. (2009), 'Poly(ADP-ribosyl)ation directs recruitment and activation of an ATP-dependent chromatin remodeler.', *Proceedings of the National Academy of Sciences of the United States of America* **106**(33), 13770–13774.

Gravells, P., Grant, E., Smith, K. M., James, D. I. & Bryant, H. E. (2017), 'Specific killing of DNA damage-response deficient cells with inhibitors of poly(ADP-ribose) glycohydrolase.', *DNA repair* **52**, 81–91.

Grudem, M. & Hendrickson, A. W. (2020), 'Current and Future Directions for PARP Inhibition.', *Journal of the advanced practitioner in oncology* **11**(3), 297–300.

Grundy, G. J., Polo, L. M., Zeng, Z., Rulten, S. L., Hoch, N. C., Paomephan, P., Xu, Y., Sweet, S. M., Thorne, A. W., Oliver, A. W., Matthews, S. J., Pearl, L. H. & Caldecott, K. W. (2016), 'PARP3 is a sensor of nicked nucleosomes and monoribosylates histone H2B Glu2', *Nat Commun* **7**(1), 1–12.

Guarente, L. (2018), *Chapter 1. Sirtuins, NAD+, Aging, and Disease: A Retrospective and Prospective Overview*, Elsevier Inc.

Hafner, A., Bulyk, M. L., Jambhekar, A. & Lahav, G. (2019), 'The multiple mechanisms that regulate p53 activity and cell fate.', *Nature Reviews Molecular Cell Biology* **20**(4), 199–210.

Haikarainen, T., Krauss, S. & Lehtiö, L. (2014), 'Tankyrases: Structure, Function and Therapeutic Implications in Cancer', *Current Pharmaceutical Design* **20**(41), 6472–6488.

Hanukoglu, I. (2015), 'Proteopedia: Rossmann fold: A beta-alpha-beta fold at dinucleotide binding sites.', *Biochemistry and molecular biology education : a bimonthly publication of the International Union of Biochemistry and Molecular Biology* **43**(3), 206–209.

Hanzlikova, H., Gittens, W., Krejcikova, K., Zeng, Z. & Caldecott, K. W. (2017), 'Overlapping roles for PARP1 and PARP2 in the recruitment of endogenous XRCC1 and PNKP into oxidized chromatin.', *Nucleic acids research* **45**(5), 2546–2557.

Hanzlikova, H., Kalasova, I., Demin, A. A., Pennicott, L. E., Cihlarova, Z. & Caldecott, K. W. (2018), 'The Importance of Poly(ADP-Ribose) Polymerase as a Sensor of Unligated Okazaki Fragments during DNA Replication.', *Mol. Cell* **71**(2), 319–331.e3.

Hanzlikova, H., Prokhorova, E., Krejcikova, K., Cihlarova, Z., Kalasova, I., Kubovciak, J., Sachova, J., Hailstone, R., Brazina, J., Ghosh, S., Cirak, S., Gleeson, J. G., Ahel, I. & Caldecott, K. W. (2020), 'Pathogenic ARH3 mutations result in ADP-ribose chromatin scars during DNA strand break repair.', *Nat Commun* **11**(1), 3391–13.

Hawse, W. F. & Wolberger, C. (2009), 'Structure-based mechanism of ADP-ribosylation by sirtuins.', *J. Biol. Chem.* **284**(48), 33654–33661.

Hayashi, K., Tanaka, M., Shimada, T., and, M. M. B. & 1983 (1983), 'Size and shape of poly (ADP-ribose): examination by gel filtration, gel electrophoresis and electron microscopy', *Elsevier* .

He, F., Tsuda, K., Takahashi, M., Kuwasako, K., Terada, T., Shirouzu, M., Watanabe, S., Kigawa, T., Kobayashi, N., Güntert, P., Yokoyama, S. & Muto, Y. (2012), 'Structural insight into the interaction of ADP-ribose with the PARP WWE domains.', *FEBS letters* **586**(21), 3858–3864.

Heeke, A. L., Pishvaian, M. J., Lynce, F., Xiu, J., Brody, J. R., Chen, W.-J., Baker, T. M., Marshall, J. L. & Isaacs, C. (2018), 'Prevalence of Homologous Recombination-Related Gene Mutations Across Multiple Cancer Types.', *JCO precision oncology* **2018**.

Hein, M. Y., Hubner, N. C., Poser, I., Cox, J., Nagaraj, N., Toyoda, Y., Gak, I. A., Weisswange, I., Mansfeld, J., Buchholz, F., Hyman, A. A. & Mann, M. (2015), 'A human interactome in three quantitative dimensions organized by stoichiometries and abundances.', *Cell* **163**(3), 712–723.

Helleday, T. (2011), 'The underlying mechanism for the PARP and BRCA synthetic lethality: clearing up the misunderstandings.', *Molecular oncology* **5**(4), 387–393.

Hendriks, I. A., Larsen, S. C. & Nielsen, M. L. (2019), 'An Advanced Strategy for Comprehensive Profiling of ADP-ribosylation Sites Using Mass Spectrometry-based Proteomics.', *Molecular & cellular proteomics : MCP* **18**(5), 1010–1026.

Hewitt, G., Borel, V., Segura-Bayona, S., Takaki, T., Ruis, P., Bellelli, R., Lehmann, L. C., Sommerova, L., Vancevska, A., Tomas-Loba, A., Zhu, K., Cooper, C., Fugger, K., Patel, H., Goldstone, R., Schneider-Luftman, D., Herbert, E., Stamp, G., Brough, R., Pettitt, S., Lord, C. J., West, S. C., Ahel, I., Ahel, D., Chapman, J. R., Deindl, S. & Boulton, S. J. (2021), 'Defective ALC1 nucleosome remodeling confers PARPi sensitization and synthetic lethality with HRD.', *Mol. Cell* **81**(4), 767–783.e11.

Heyer, W.-D., Ehmsen, K. T. & Liu, J. (2010), 'Regulation of homologous recombination in eukaryotes.', *Annual review of genetics* **44**, 113–139.

Hoch, N. C., Hanzlikova, H., Rulten, S. L., Tétreault, M., Komulainen, E., Ju, L., Hornyak, P., Zeng, Z., Gittens, W., Rey, S. A., Staras, K., Mancini, G. M. S., McKinnon, P. J., Wang, Z.-Q., Wagner, J. D., Care4Rare Canada Consortium, Yoon, G. & Caldecott, K. W. (2017), 'XRCC1 mutation is associated with PARP1 hyperactivation and cerebellar ataxia.', *Nature* **541**(7635), 87–91.

Holbourn, K. P., Shone, C. C. & Acharya, K. R. (2006), 'A family of killer toxins. Exploring the mechanism of ADP-ribosylating toxins.', *Febs J* **273**(20), 4579–4593.

Hopkins, T. A., Ainsworth, W. B., Ellis, P. A., Donawho, C. K., DiGiammarino, E. L., Panchal, S. C., Abraham, V. C., Algire, M. A., Shi, Y., Olson, A. M., Johnson, E. F., Wilsbacher, J. L. & Maag, D. (2019), 'PARP1 Trapping by PARP Inhibitors Drives Cytotoxicity in Both Cancer Cells and Healthy Bone Marrow.', *Molecular cancer research : MCR* **17**(2), 409–419.

Hopkins, T. A., Shi, Y., Rodriguez, L. E., Solomon, L. R., Donawho, C. K., DiGiammarino, E. L., Panchal, S. C., Wilsbacher, J. L., Gao, W., Olson, A. M., Stolarik, D. F., Osterling, D. J., Johnson, E. F. & Maag, D. (2015), 'Mechanistic Dissection of PARP1 Trapping and the Impact on In Vivo Tolerability and Efficacy of PARP Inhibitors.', *Molecular cancer research : MCR* **13**(11), 1465–1477.

Hopp, A.-K., Teloni, F., Bisceglie, L., Gondrand, C., Raith, F., Nowak, K., Muskalla, L., Howald, A., Pedrioli, P. G. A., Johnsson, K., Altmeyer, M., Pedrioli, D. M. L. & Hottiger, M. O. (2021), 'Mitochondrial NAD+ Controls Nuclear ARTD1-Induced ADP-Ribosylation.', *Mol. Cell* **279**(D1), 11521–354.e5.

Houl, J. H., Ye, Z., Brosey, C. A., Balapiti-Modarage, L. P. F., Namjoshi, S., Bacolla, A., Laverty, D., Walker, B. L., Pourfarjam, Y., Warden, L. S., Babu Chinnam, N., Moiani, D., Stegeman, R. A., Chen, M.-K., Hung, M.-C., Nagel, Z. D., Ellenberger, T., Kim, I.-K., Jones, D. E., Ahmed, Z. & Tainer, J. A. (2019), 'Selective small molecule PARG inhibitor causes replication fork stalling and cancer cell death.', *Nat Commun* **10**(1), 5654–15.

Hu, Q.-D., Lu, H., Huo, K., Ying, K., Li, J., Xie, Y., Mao, Y. & Li, Y.-Y. (2003), 'A human homolog of the yeast gene encoding tRNA 2'-phosphotransferase: cloning, characterization and complementation analysis.', *Cellular and molecular life sciences : CMLS* **60**(8), 1725–1732.

Hu, X. & Zheng, W. (2018), Chapter one - chemical probes in sirtuin research, *in* W. Zheng, ed., 'Sirtuins in Health and Disease', Vol. 154 of *Progress in Molecular Biology and Translational Science*, Academic Press, pp. 1–24.

Hu, Y., Petit, S. A., Ficarro, S. B., Toomire, K. J., Xie, A., Lim, E., Cao, S. A., Park, E., Eck, M. J., Scully, R., Brown, M., Marto, J. A. & Livingston, D. M. (2014), 'PARP1-driven poly-ADP-ribosylation regulates BRCA1 function in homologous recombination-mediated DNA repair.', *Cancer discovery* **4**(12), 1430–1447.

Huang, D., Camacho, C. V., Setlem, R., Ryu, K. W., Parameswaran, B., Gupta, R. K. & Kraus, W. L. (2020), 'Functional Interplay between Histone H2B ADP-Ribosylation and Phosphorylation Controls Adipogenesis.', *Mol. Cell* **79**(6), 934–949.e14.

Huang, J.-Y., Chen, W.-H., Chang, Y.-L., Wang, H.-T., Chuang, W.-t. & Lee, S.-C. (2006), 'Modulation of nucleosome-binding activity of FACT by poly(ADP-ribosyl)ation.', *Nucleic acids research* **34**(8), 2398–2407.

Iqbal, J., Ragone, A., Lubinski, J., Lynch, H. T., Moller, P., Ghadirian, P., Foulkes, W. D., Armel, S., Eisen, A., Neuhausen, S. L., Senter, L., Singer, C. F., Ainsworth, P., Kim-Sing, C., Tung, N., Friedman, E., Llacuachaqui, M., Ping, S., Narod, S. A. & Hereditary Breast Cancer Study Group (2012), 'The incidence of pancreatic cancer in BRCA1 and BRCA2 mutation carriers.', *British journal of cancer* **107**(12), 2005–2009.

Ishiwata-Endo, H., Kato, J., Stevens, L. A. & Moss, J. (2020), 'ARH1 in Health and Disease.', *Cancers* **12**(2), 479.

Iwata, H., Goettsch, C., Sharma, A., Ricchiuto, P., Goh, W. W. B., Halu, A., Yamada, I., Yoshida, H., Hara, T., Wei, M., Inoue, N., Fukuda, D., Mojcher, A., Mattson, P. C., Barabási, A.-L., Boothby, M., Aikawa, E., Singh, S. A. & Aikawa, M. (2016), 'PARP9 and PARP14 cross-regulate macrophage activation via STAT1 ADP-ribosylation.', *Nat Commun* **7**(1), 12849.

Jankevicius, G., Ariza, A., Ahel, M. & Ahel, I. (2016), 'The Toxin-Antitoxin System DarTG Catalyzes Reversible ADP-Ribosylation of DNA.', *Mol. Cell* **64**(6), 1109–1116.

Jankevicius, G., Hassler, M., Golia, B., Rybin, V., Zacharias, M., Timinszky, G. & Ladurner, A. G. (2013), 'A family of macrodomain proteins reverses cellular mono-ADP-ribosylation.', *Nature structural & molecular biology* **20**(4), 508–514.

Jaspers, P., Blomster, T., Brosché, M., Salojärvi, J., Ahlfors, R., Vainonen, J. P., Reddy, R. A., Immink, R., Angenent, G., Turck, F., Overmyer, K. & Kangasjärvi, J. (2009), 'Unequally redundant RCD1 and SRO1 mediate stress and developmental responses and interact with transcription factors.', *The Plant journal : for cell and molecular biology* **60**(2), 268–279.

Jaspers, P., Overmyer, K., Wrzaczek, M., Vainonen, J. P., Blomster, T., Salojärvi, J., Reddy, R. A. & Kangasjärvi, J. (2010), 'The RST and PARP-like domain containing SRO protein family: analysis of protein structure, function and conservation in land plants.', *BMC genomics* **11**(1), 170–20.

Jónsson, Z. O. & Hübscher, U. (1997), 'Proliferating cell nuclear antigen: more than a clamp for DNA polymerases.', *BioEssays : news and reviews in molecular, cellular and developmental biology* **19**(11), 967–975.

Joo, W. S., Jeffrey, P. D., Cantor, S. B., Finnin, M. S., Livingston, D. M. & Pavletich, N. P. (2002), 'Structure of the 53BP1 BRCT region bound to p53 and its comparison to the Brca1 BRCT structure.', *Genes Dev.* **16**(5), 583–593.

Kanai, M., Hanashiro, K., Kim, S.-H., Hanai, S., Boulares, A. H., Miwa, M. & Fukasawa, K. (2007), 'Inhibition of Crm1-p53 interaction and nuclear export of p53 by poly(ADP-ribosyl)ation.', *Nature cell biology* **9**(10), 1175–1183.

Karras, G. I., Kustatscher, G., Buhecha, H. R., Allen, M. D., Pugieux, C., Sait, F., Bycroft, M. & Ladurner, A. G. (2005), 'The macro domain is an ADP-ribose binding module.', *EMBO J.* **24**(11), 1911–1920.

Kato, J., Vekhter, D., Heath, J., Zhu, J., Barbieri, J. T. & Moss, J. (2015), 'Mutations of the functional ARH1 allele in tumors from ARH1 heterozygous mice and cells affect ARH1 catalytic activity, cell proliferation and tumorigenesis.', *Oncogenesis* **4**(6), e151–e151.

Kato-Murayama, M., Bessho, Y., Shirouzu, M. & Yokoyama, S. (2005), 'Crystal structure of the RNA 2'-phosphotransferase from Aeropyrum pernix K1.', *Journal of molecular biology* **348**(2), 295–305.

Kickhoefer, V. A., Siva, A. C., Kedersha, N. L., Inman, E. M., Ruland, C., Streuli, M. & Rome, L. H. (1999), 'The 193-kD vault protein, VPARP, is a novel poly(ADP-ribose) polymerase.', *The Journal of cell biology* **146**(5), 917–928.

Kim, G., Ison, G., McKee, A. E., Zhang, H., Tang, S., Gwise, T., Sridhara, R., Lee, E., Tzou, A., Philip, R., Chiu, H.-J., Ricks, T. K., Palmby, T., Russell, A. M., Ladouceur, G., Pfuma, E., Li, H., Zhao, L., Liu, Q., Venugopal, R., Ibrahim, A. & Pazdur, R. (2015), 'FDA Approval Summary: Olaparib Monotherapy in Patients with Deleterious Germline BRCA-Mutated Advanced Ovarian Cancer Treated with Three or More Lines of Chemotherapy.', *Clinical cancer research : an official journal of the American Association for Cancer Research* **21**(19), 4257–4261.

Kim, I.-K., Kiefer, J. R., Ho, C. M. W., Stegeman, R. A., Classen, S., Tainer, J. A. & Ellenberger, T. (2012), 'Structure of mammalian poly(ADP-ribose) glycohydrolase reveals a flexible tyrosine clasp as a substrate-binding element.', *Nature structural & molecular biology* **19**(6), 653–656.

Kim, M. K. (2018), 'Novel insight into the function of tankyrase (Review)', *Oncology Letters* **16**(6), 6895–6902.

Kirby, I. T. & Cohen, M. S. (2019), 'Small-Molecule Inhibitors of PARPs: From Tools for Investigating ADP-Ribosylation to Therapeutics.', *Current topics in microbiology and immunology* **420**, 211–231.

Kleine, H., Poreba, E., Lesniewicz, K., Hassa, P. O., Hottiger, M. O., Litchfield, D. W., Shilton, B. H. & Lüscher, B. (2008), 'Substrate-assisted catalysis by PARP10 limits its activity to mono-ADP-ribosylation.', *Mol. Cell* **32**(1), 57–69.

Kötting, C., Kallenbach, A., Suveyzdis, Y., Wittinghofer, A. & Gerwert, K. (2008), 'The GAP arginine finger movement into the catalytic site of Ras increases the activation entropy.', *Proceedings of the National Academy of Sciences of the United States of America* **105**(17), 6260–6265.

Kraus, W. L. (2015), 'PARPs and ADP-Ribosylation: 50 Years ... and Counting.', *Mol. Cell* **58**(6), 902–910.

Krüger, A., Bürkle, A., Hauser, K. & Mangerich, A. (2020), 'Real-time monitoring of PARP1-dependent PARylation by ATR-FTIR spectroscopy.', *Nat Commun* **11**(1), 2174–15.

Kusakabe, M., Onishi, Y., Tada, H., Kurihara, F., Kusao, K., Furukawa, M., Iwai, S., Yokoi, M., Sakai, W. & Sugasawa, K. (2019), 'Mechanism and regulation of DNA damage recognition in nucleotide excision repair.', *Genes and environment : the official journal of the Japanese Environmental Mutagen Society* **41**(1), 2–6.

Kutuzov, M. M., Khodyreva, S. N., Amé, J.-C., Ilina, E. S., Sukhanova, M. V., Schreiber, V. & Lavrik, O. I. (2013), 'Interaction of PARP-2 with DNA structures mimicking DNA repair intermediates and consequences on activity of base excision repair proteins.', *Biochimie* **95**(6), 1208–1215.

Kutuzov, M. M., Khodyreva, S. N., Schreiber, V. & Lavrik, O. I. (2014), '[The role of PARP2 in DNA repair].', *Molekuliarnaia biologiia* **48**(4), 561–572.

Ladan, M. M., van Gent, D. C. & Jager, A. (2021), 'Homologous Recombination Deficiency Testing for BRCA-Like Tumors: The Road to Clinical Validation.', *Cancers* **13**(5), 1004.

Laing, S., Unger, M., Koch-Nolte, F. & Haag, F. (2011), 'ADP-ribosylation of arginine.', *Amino acids* **41**(2), 257–269.

Langelier, M.-F., Billur, R., Sverzhinsky, A., Black, B. E. & Pascal, J. M. (2021), 'HPF1 dynamically controls the PARP1/2 balance between initiating and elongating ADP-ribose modifications', *bioRxiv* p. 2021.05.19.444852.

Langelier, M.-F. & Pascal, J. M. (2013), 'PARP-1 mechanism for coupling DNA damage detection to poly(ADP-ribose) synthesis.', *Current opinion in structural biology* **23**(1), 134–143.

Langelier, M.-F., Planck, J. L., Roy, S. & Pascal, J. M. (2011), 'Crystal structures of poly(ADP-ribose) polymerase-1 (PARP-1) zinc fingers bound to DNA: structural and functional insights into DNA-dependent PARP-1 activity.', *J. Biol. Chem.* **286**(12), 10690–10701.

Langelier, M.-F., Planck, J. L., Roy, S. & Pascal, J. M. (2012), 'Structural basis for DNA damage-dependent poly(ADP-ribosyl)ation by human PARP-1.', *Science* **336**(6082), 728–732.

Langelier, M.-F., Riccio, A. A. & Pascal, J. M. (2014), 'PARP-2 and PARP-3 are selectively activated by 5' phosphorylated DNA breaks through an allosteric regulatory mechanism shared with PARP-1.', *Nucleic acids research* **42**(12), 7762–7775.

Langelier, M.-F., Servent, K. M., Rogers, E. E. & Pascal, J. M. (2008), 'A third zinc-binding domain of human poly(ADP-ribose) polymerase-1 coordinates DNA-dependent enzyme activation.', *J. Biol. Chem.* **283**(7), 4105–4114.

Langelier, M.-F., Zandarashvili, L., Aguiar, P. M., Black, B. E. & Pascal, J. M. (2018), 'NAD+ analog reveals PARP-1 substrate-blocking mechanism and allosteric communication from catalytic center to DNA-binding domains.', *Nat Commun* **9**(1), 844.

Larsen, S. C., Hendriks, I. A., Lyon, D., Jensen, L. J. & Nielsen, M. L. (2018), 'Systems-wide Analysis of Serine ADP-Ribosylation Reveals Widespread Occurrence and Site-Specific Overlap with Phosphorylation.', *Cell Reports* **24**(9), 2493–2505.e4.

Lawarée, E., Jankevicius, G., Cooper, C., Ahel, I., Uphoff, S. & Tang, C. (2020), 'DNA ADP-Ribosylation Stalls Replication and Is Reversed by RecF-Mediated Homologous Recombination and Nucleotide Excision Repair', *Cell Reports* **30**(5), 1373–1384.e4.

Lebeaupin, T., Smith, R., Huet, S. & Timinszky, G. (2017), 'Poly(ADP-Ribose)-Dependent Chromatin Remodeling in DNA Repair.', *Methods in molecular biology (Clifton, N.J.)* **1608**, 165–183.

Ledermann, J., Harter, P., Gourley, C., Friedlander, M., Vergote, I., Rustin, G., Scott, C. L., Meier, W., Shapira-Frommer, R., Safra, T., Matei, D., Fielding, A., Spencer, S., Dougherty, B., Orr, M., Hodgson, D., Barrett, J. C. & Matulonis, U. (2014), 'Olaparib maintenance therapy in patients with platinum-sensitive relapsed serous ovarian cancer: a preplanned retrospective analysis of outcomes by BRCA status in a randomised phase 2 trial.', *The Lancet. Oncology* **15**(8), 852–861.

Lee, M. S., Edwards, R. A., Thede, G. L. & Glover, J. N. M. (2005), 'Structure of the BRCT repeat domain of MDC1 and its specificity for the free COOH-terminal end of the gamma-H2AX histone tail.', *Journal of Biological Chemistry* **280**(37), 32053–32056.

Leslie Pedrioli, D. M., Leutert, M., Bilan, V., Nowak, K., Gunasekera, K., Ferrari, E., Imhof, R., Malmström, L. & Hottiger, M. O. (2018), 'Comprehensive ADP-ribosylome analysis identifies tyrosine as an ADP-ribose acceptor site.', *EMBO reports* **19**(8).

Leung, A. K. L. (2014), 'Poly(ADP-ribose): an organizer of cellular architecture.', *The Journal of cell biology* **205**(5), 613–619.

Leung, C. C. Y. & Glover, J. N. M. (2011), 'BRCT domains: easy as one, two, three.', *Cell cycle (Georgetown, Tex.)* **10**(15), 2461–2470.

Leutert, M., Menzel, S., Braren, R., Rissiek, B., Hopp, A.-K., Nowak, K., Bisceglie, L., Gehrig, P., Li, H., Zolkiewska, A., Koch-Nolte, F. & Hottiger, M. O. (2018), 'Proteomic Characterization of the Heart and Skeletal Muscle Reveals Widespread Arginine ADP-Ribosylation by the ARTC1 Ectoenzyme.', *Cell Reports* **24**(7), 1916–1929.e5.

Li, G.-Y., McCulloch, R. D., Fenton, A. L., Cheung, M., Meng, L., Ikura, M. & Koch, C. A. (2010), 'Structure and identification of ADP-ribose recognition motifs of APLF and role in the DNA damage response.', *Proceedings of the National Academy of Sciences of the United States of America* **107**(20), 9129–9134.

Li, M., Lu, L.-Y., Yang, C.-Y., Wang, S. & Yu, X. (2013), 'The FHA and BRCT domains recognize ADP-ribosylation during DNA damage response.', *Genes Dev.* **27**(16), 1752–1768.

Lloyd, R. L., Wijnhoven, P. W. G., Ramos-Montoya, A., Wilson, Z., Illuzzi, G., Falenta, K., Jones, G. N., James, N., Chabbert, C. D., Stott, J., Dean, E., Lau, A. & Young, L. A. (2020), 'Combined PARP and ATR inhibition potentiates genome instability and cell death in ATM-deficient cancer cells.', *Oncogene* **60**(25), 547–15.

Loeffler, P. A., Cuneo, M. J., Mueller, G. A., DeRose, E. F., Gabel, S. A. & London, R. E. (2011), 'Structural studies of the PARP-1 BRCT domain.', *BMC structural biology* **11**(1), 37–11.

Lord, C. J. & Ashworth, A. (2012), 'The DNA damage response and cancer therapy.', *Nature* **481**(7381), 287–294.

Luijsterburg, M. S., de Krijger, I., Wiegant, W. W., Shah, R. G., Smeenk, G., de Groot, A. J. L., Pines, A., Vertegaal, A. C. O., Jacobs, J. J. L., Shah, G. M. & van Attikum, H. (2016), 'PARP1 Links CHD2-Mediated Chromatin Expansion and H3.3 Deposition to DNA Repair by Non-homologous End-Joining.', *Mol. Cell* **61**(4), 547–562.

Luo, X., Ryu, K. W., Kim, D.-S., Nandu, T., Medina, C. J., Gupte, R., Gibson, B. A., Soccio, R. E., Yu, Y., Gupta, R. K. & Kraus, W. L. (2017), 'PARP-1 Controls the Adipogenic Transcriptional Program by PARylating C/EBPβ and Modulating Its Transcriptional Activity.', *Mol. Cell* **65**(2), 260–271.

Lüscher, B., Ahel, I., Altmeyer, M., Ashworth, A., Bai, P., Chang, P., Cohen, M., Corda, D., Dantzer, F., Daugherty, M. D., Dawson, T. M., Dawson, V. L., Deindl, S., Fehr, A. R., Feijs, K. L. H., Filippov, D. V., Gagné, J.-P., Grimaldi, G., Guettler, S., Hoch, N. C., Hottiger, M. O., Korn, P., Kraus, W. L., Ladurner, A., Lehtiö, L., Leung, A. K. L., Lord, C. J., Mangerich, A., Matic, I., Matthews, J., Moldovan, G.-L., Moss, J., Natoli,

G., Nielsen, M. L., Niepel, M., Nolte, F., Pascal, J., Paschal, B. M., Pawłowski, K., Poirier, G. G., Smith, S., Timinszky, G., Wang, Z.-Q., Yélamos, J., Yu, X., Zaja, R. & Ziegler, M. (2021), 'ADP-ribosyltransferases, an update on function and nomenclature.', *Febs J* .

Lüscher, B., Bütepage, M., Eckei, L., Krieg, S., Verheugd, P. & Shilton, B. H. (2018), 'ADP-Ribosylation, a Multifaceted Posttranslational Modification Involved in the Control of Cell Physiology in Health and Disease.', *Chemical reviews* **118**(3), 1092–1136.

Ma, Y., Pannicke, U., Schwarz, K. & Lieber, M. R. (2002), 'Hairpin opening and overhang processing by an Artemis/DNA-dependent protein kinase complex in nonhomologous end joining and V(D)J recombination.', *Cell* **108**(6), 781–794.

Mach, J. (2019), 'ADP Ribosylation: The Modification Causing a Disease Resistance Sensation.', *The Plant Cell* **31**(11), 2552–2553.

Mah, L.-J., El-Osta, A. & Karagiannis, T. C. (2010), 'gammaH2AX: a sensitive molecular marker of DNA damage and repair.', *Leukemia* **24**(4), 679–686.

Mahajan, A., Yuan, C., Lee, H., Chen, E. S.-W., Wu, P.-Y. & Tsai, M.-D. (2008), 'Structure and function of the phosphothreonine-specific FHA domain.', *Science signaling* **1**(51), re12.

Malanga, M. & Althaus, F. R. (2005), 'The role of poly(ADP-ribose) in the DNA damage signaling network.', *Biochemistry and cell biology = Biochimie et biologie cellulaire* **83**(3), 354–364.

Malanga, M., Pleschke, J. M., Kleczkowska, H. E. & Althaus, F. R. (1998), 'Poly(ADP-ribose) binds to specific domains of p53 and alters its DNA binding functions.', *Journal of Biological Chemistry* **273**(19), 11839–11843.

Mansoorabadi, S. O., Wu, M., Tao, Z., Gao, P., Pingali, S. V., Guo, L. & Liu, H.-w. (2014), 'Conformational activation of poly(ADP-ribose) polymerase-1 upon DNA binding revealed by small-angle X-ray scattering.', *Biochemistry* **53**(11), 1779–1788.

Marsischky, G. T., Wilson, B. A. & Collier, R. J. (1995*a*), 'Role of glutamic acid 988 of human poly-ADP-ribose polymerase in polymer formation. Evidence for active site similarities to the ADP-ribosylating toxins.', *J. Biol. Chem.* **270**(7), 3247–3254.

Marsischky, G. T., Wilson, B. A. & Collier, R. J. (1995*b*), 'Role of glutamic acid 988 of human poly-ADP-ribose polymerase in polymer formation. Evidence for active site similarities to the ADP-ribosylating toxins.', *Journal of Biological Chemistry* **270**(7), 3247–3254.

Martello, R., Leutert, M., Jungmichel, S., Bilan, V., Larsen, S. C., Young, C., Hottiger, M. O. & Nielsen, M. L. (2016), 'Proteome-wide identification of the endogenous ADP-ribosylome of mammalian cells and tissue.', *Nat Commun* **7**(1), 12917.

Mashimo, M., Kato, J. & Moss, J. (2014), 'Structure and function of the ARH family of ADP-ribosyl-acceptor hydrolases.', *DNA repair* **23**, 88–94.

Mashimo, M. & Moss, J. (2016), 'Functional Role of ADP-Ribosyl-Acceptor Hydrolase 3 in poly(ADP-Ribose) Polymerase-1 Response to Oxidative Stress.', *Current protein & peptide science* **17**(7), 633–640.

Mateo, J., Lord, C. J., Serra, V., Tutt, A., Balmaña, J., Castroviejo-Bermejo, M., Cruz, C., Oaknin, A., Kaye, S. B. & de Bono, J. S. (2019), 'A decade of clinical development of PARP inhibitors in perspective.', *Annals of oncology : official journal of the European Society for Medical Oncology* **30**(9), 1437–1447.

Mehrotra, P. V., Ahel, D., Ryan, D. P., Weston, R., Wiechens, N., Kraehenbuehl, R., Owen-Hughes, T. & Ahel, I. (2011), 'DNA repair factor APLF is a histone chaperone.', *Mol. Cell* **41**(1), 46–55.

Mendoza-Alvarez, H. & Alvarez-Gonzalez, R. (1993), 'Poly(ADP-ribose) polymerase is a catalytic dimer and the automodification reaction is intermolecular.', *J. Biol. Chem.* **268**(30), 22575–22580.

Mendoza-Alvarez, H. & Alvarez-Gonzalez, R. (1999), 'Biochemical characterization of mono(ADP-ribosyl)ated poly(ADP-ribose) polymerase.', *Biochemistry* **38**(13), 3948–3953.

Mendoza-Alvarez, H. & Alvarez-Gonzalez, R. (2001), 'Regulation of p53 sequence-specific DNA-binding by covalent poly(ADP-ribosyl)ation.', *Journal of Biological Chemistry* **276**(39), 36425–36430.

Menear, K. A., Adcock, C., Boulter, R., Cockcroft, X.-l., Copsey, L., Cranston, A., Dillon, K. J., Drzewiecki, J., Garman, S., Gomez, S., Javaid, H., Kerrigan, F., Knights, C., Lau, A., Loh, V. M., Matthews, I. T. W., Moore, S., O'Connor, M. J., Smith, G. C. M. & Martin, N. M. B. (2008), '4-[3-(4-cyclopropanecarbonylpiperazine-1-carbonyl)-4-fluorobenzyl]-2H-phthalazin-1-one: a novel bioavailable inhibitor of poly(ADP-ribose) polymerase-1.', *Journal of medicinal chemistry* **51**(20), 6581–6591.

Merritt, E. A., Sarfaty, S., Van Den Akker, F., L'Hoir, C., Martial, J. A. & Hol, W. G. J. (1994), 'Crystal structure of cholera toxin B-pentamer bound to receptor GM1 pentasaccharide', *Protein Science* **3**(2), 166–175.

Mersch, J., Jackson, M. A., Park, M., Nebgen, D., Peterson, S. K., Singletary, C., Arun, B. K. & Litton, J. K. (2015), 'Cancers associated with BRCA1 and BRCA2 mutations other than breast and ovarian.', *Cancer* **121**(2), 269–275.

Messner, S. & Hottiger, M. O. (2011), 'Histone ADP-ribosylation in DNA repair, replication and transcription.', *Trends in cell biology* **21**(9), 534–542.

Michan, S. & Sinclair, D. (2007), 'Sirtuins in mammals: insights into their biological function.', *The Biochemical journal* **404**(1), 1–13.

Mikolčević, P., Hloušek-Kasun, A., Ahel, I. & Mikoč, A. (2021), 'ADP-ribosylation systems in bacteria and viruses.', *Computational and structural biotechnology journal* **19**, 2366–2383.

Minguez, P., Parca, L., Diella, F., Mende, D. R., Kumar, R., Helmer-Citterich, M., Gavin, A.-C., van Noort, V. & Bork, P. (2012), 'Deciphering a global network of functionally associated post-translational modifications.', *Molecular systems biology* **8**(1), 599.

Mohapatra, J., Tashiro, K., Beckner, R. L., Sierra, J., Kilgore, J. A., Williams, N. S. & Liszczak, G. (2021), 'Serine ADP-ribosylation marks nucleosomes for ALC1-dependent chromatin remodeling', *bioRxiv* p. 2021.07.06.449314.

Moore, K., Colombo, N., Scambia, G., Kim, B.-G., Oaknin, A., Friedlander, M., Lisyanskaya, A., Floquet, A., Leary, A., Sonke, G. S., Gourley, C., Banerjee, S., Oza, A., González-Martín, A., Aghajanian, C., Bradley, W., Mathews, C., Liu, J., Lowe, E. S., Bloomfield, R. & DiSilvestro, P. (2018), 'Maintenance Olaparib in Patients with

Newly Diagnosed Advanced Ovarian Cancer.', *The New England journal of medicine* **379**(26), 2495–2505.

Moran, A., O'Hara, C., Khan, S., Shack, L., Woodward, E., Maher, E. R., Lalloo, F. & Evans, D. G. R. (2012), 'Risk of cancer other than breast or ovarian in individuals with BRCA1 and BRCA2 mutations.', *Familial cancer* **11**(2), 235–242.

Mueller-Dieckmann, C., Kernstock, S., Lisurek, M., von Kries, J. P., Haag, F., Weiss, M. S. & Koch-Nolte, F. (2006), 'The structure of human ADP-ribosylhydrolase 3 (ARH3) provides insights into the reversibility of protein ADP-ribosylation.', *Proc National Acad Sci* **103**(41), 15026–15031.

Munir, A., Banerjee, A. & Shuman, S. (2018), 'NAD+-dependent synthesis of a 5'-phospho-ADP-ribosylated RNA/DNA cap by RNA 2'-phosphotransferase Tpt1.', *Nucleic acids research* **46**(18), 9617–9624.

Munnur, D. & Ahel, I. (2017), 'Reversible mono-ADP-ribosylation of DNA breaks.', *Febs J* **284**(23), 4002–4016.

Munnur, D., Bartlett, E., Mikolčević, P., Kirby, I. T., Matthias Rack, J. G., Mikoč, A., Cohen, M. S. & Ahel, I. (2019), 'Reversible ADP-ribosylation of RNA.', *Nucleic acids research* **47**(11), 5658–5669.

Murai, J., Huang, S.-y. N., Das, B. B., Renaud, A., Zhang, Y., Doroshow, J. H., Ji, J., Takeda, S. & Pommier, Y. (2012), 'Trapping of PARP1 and PARP2 by Clinical PARP Inhibitors.', *Cancer research* **72**(21), 5588–5599.

Murai, J., Huang, S.-y. N., Renaud, A., Zhang, Y., Ji, J., Takeda, S., Morris, J., Teicher, B., Doroshow, J. H. & Pommier, Y. (2014), 'Stereospecific PARP trapping by BMN 673 and comparison with olaparib and rucaparib.', *Molecular cancer therapeutics* **13**(2), 433–443.

Nguyen, L., W M Martens, J., Van Hoeck, A. & Cuppen, E. (2020), 'Pan-cancer landscape of homologous recombination deficiency.', *Nat Commun* **11**(1), 5584–12.

Obaji, E., Haikarainen, T. & Lehtiö, L. (2018), 'Structural basis for DNA break recognition by ARTD2/PARP2.', *Nucleic acids research* **46**(22), 12154–12165.

Obaji, E., Maksimainen, M. M., Galera-Prat, A. & Lehtiö, L. (2021), 'Activation of PARP2/ARTD2 by DNA damage induces conformational changes relieving enzyme autoinhibition.', *Nat Commun* **12**(1), 3479–8.

O'Connor, M. J. (2015), 'Targeting the DNA Damage Response in Cancer.', *Mol. Cell* **60**(4), 547–560.

Ogden, T. E. H., Yang, J.-C., Schimpl, M., Easton, L. E., Underwood, E., Rawlins, P. B., McCauley, M. M., Langelier, M.-F., Pascal, J. M., Embrey, K. J. & Neuhaus, D. (2021), 'Dynamics of the HD regulatory subdomain of PARP-1; substrate access and allostery in PARP activation and inhibition.', *Nucleic acids research* **49**(4), 2266–2288.

O'Sullivan, J., Ferreira, M. T., Gagné, J.-P., Sharma, A. K., Hendzel, M. J., Masson, J.-Y. & Poirier, G. G. (2019), 'Emerging roles of eraser enzymes in the dynamic control of protein ADP-ribosylation', *Nat Commun* **10**(1), 1–14.

Otto, H., Reche, P. A., Bazan, F., Dittmar, K., Haag, F. & Koch-Nolte, F. (2005), 'In silico characterization of the family of PARP-like poly(ADP-ribosyl)transferases (pARTs).', *BMC genomics* **6**(1), 139–23.

Palazzo, L., Leidecker, O., Prokhorova, E., Dauben, H., Matic, I. & Ahel, I. (2018), 'Serine is the major residue for ADP-ribosylation upon DNA damage.', *Elife* **7**, 935.

Palazzo, L., Suskiewicz, M. J. & Ahel, I. (2021), 'Serine ADP-ribosylation in DNA-damage response regulation.', *Current opinion in genetics & development* **71**, 106–113.

Pascal, J. M. (2018), 'The comings and goings of PARP-1 in response to DNA damage.', *DNA repair* **71**, 177–182.

Perina, D., Mikoč, A., Ahel, J., Ćetković, H., Zaja, R. & Ahel, I. (2014), 'Distribution of protein poly(ADP-ribosyl)ation systems across all domains of life.', *DNA repair* **23**, 4–16.

Petrucelli, N., Daly, M. B. & Feldman, G. L. (2010), 'Hereditary breast and ovarian cancer due to mutations in BRCA1 and BRCA2.', *Genetics in medicine : official journal of the American College of Medical Genetics* **12**(5), 245–259.

Pines, A., Vrouwe, M. G., Marteijn, J. A., Typas, D., Luijsterburg, M. S., Cansoy, M., Hensbergen, P., Deelder, A., de Groot, A., Matsumoto, S., Sugasawa, K., Thoma, N.,

Vermeulen, W., Vrieling, H. & Mullenders, L. (2012), 'PARP1 promotes nucleotide excision repair through DDB2 stabilization and recruitment of ALC1.', *The Journal of cell biology* **199**(2), 235–249.

Pion, E., Ullmann, G. M., Amé, J.-C., Gérard, D., de Murcia, G. & Bombarda, E. (2005), 'DNA-induced dimerization of poly(ADP-ribose) polymerase-1 triggers its activation.', *Biochemistry* **44**(44), 14670–14681.

Pleschke, J. M., Kleczkowska, H. E., Strohm, M. & Althaus, F. R. (2000), 'Poly(ADP-ribose) binds to specific domains in DNA damage checkpoint proteins.', *J. Biol. Chem.* **275**(52), 40974–40980.

Prakash, R., Zhang, Y., Feng, W. & Jasin, M. (2015), 'Homologous recombination and human health: the roles of BRCA1, BRCA2, and associated proteins.', *Cold Spring Harbor perspectives in biology* **7**(4), a016600.

Prasad, R., Horton, J. K. & Wilson, S. H. (2020), 'Requirements for PARP-1 covalent crosslinking to DNA (PARP-1 DPC).', *DNA repair* **89**, 102824.

Prokhorova, E., Zobel, F., Smith, R., Zentout, S., Gibbs-Seymour, I., Schützenhofer, K., Peters, A., Groslambert, J., Zorzini, V., Agnew, T., Brognard, J., Nielsen, M. L., Ahel, D., Huet, S., Suskiewicz, M. J. & Ahel, I. (2021), 'Serine-linked PARP1 auto-modification controls PARP inhibitor response.', *Nat Commun* **12**(1), 4055–12.

Pryor, J. M., Waters, C. A., Aza, A., Asagoshi, K., Strom, C., Mieczkowski, P. A., Blanco, L. & Ramsden, D. A. (2015), 'Essential role for polymerase specialization in cellular nonhomologous end joining.', *Proceedings of the National Academy of Sciences of the United States of America* **112**(33), E4537–45.

Purohit, N. K., Robu, M., Shah, R. G., Geacintov, N. E. & Shah, G. M. (2016), 'Characterization of the interactions of PARP-1 with UV-damaged DNA in vivo and in vitro.', *Scientific Reports* **6**(1), 19020–11.

Rack, J. G. M., Ariza, A., Drown, B. S., Henfrey, C., Bartlett, E., Shirai, T., Hergenrother, P. J. & Ahel, I. (2018), '(ADP-ribosyl)hydrolases: Structural Basis for Differential Substrate Recognition and Inhibition.', *Cell chemical biology* **25**(12), 1533–1546.e12.

Rack, J. G. M., Liu, Q., Zorzini, V., Voorneveld, J., Ariza, A., Honarmand Ebrahimi, K., Reber, J. M., Krassnig, S. C., Ahel, D., van der Marel, G. A., Mangerich, A., McCullagh, J. S. O., Filippov, D. V. & Ahel, I. (2021), 'Mechanistic insights into the three steps of poly(ADP-ribosylation) reversal.', *Nat Commun* **12**(1), 4581–14.

Rack, J. G. M., Palazzo, L. & Ahel, I. (2020), '(ADP-ribosyl)hydrolases: structure, function, and biology.', *Genes Dev.* **34**(5-6), 263–284.

Rack, J. G. M., Perina, D. & Ahel, I. (2016), 'Macrodomains: Structure, Function, Evolution, and Catalytic Activities.', *Annual review of biochemistry* **85**(1), 431–454.

Rack, J. G., Morra, R., Barkauskaite, E., Kraehenbuehl, R., Ariza, A., Qu, Y., Ortmayer, M., Leidecker, O., Cameron, D. R., Matic, I., Peleg, A. Y., Leys, D., Traven, A. & Ahel, I. (2015), 'Identification of a Class of Protein ADP-Ribosylating Sirtuins in Microbial Pathogens.', *Mol. Cell* **59**(2), 309–320.

Rank, L., Veith, S., Gwosch, E. C., Demgenski, J., Ganz, M., Jongmans, M. C., Vogel, C., Fischbach, A., Buerger, S., Fischer, J. M. F., Zubel, T., Stier, A., Renner, C., Schmalz, M., Beneke, S., Groettrup, M., Kuiper, R. P., Bürkle, A., Ferrando-May, E. & Mangerich, A. (2016), 'Analyzing structure-function relationships of artificial and cancer-associated PARP1 variants by reconstituting TALEN-generated HeLa PARP1 knock-out cells.', *Nucleic acids research* **44**(21), 10386–10405.

Rass, U., Compton, S. A., Matos, J., Singleton, M. R., Ip, S. C. Y., Blanco, M. G., Griffith, J. D. & West, S. C. (2010), 'Mechanism of Holliday junction resolution by the human GEN1 protein.', *Genes Dev.* **24**(14), 1559–1569.

Ray Chaudhuri, A. & Nussenzweig, A. (2017), 'The multifaceted roles of PARP1 in DNA repair and chromatin remodelling.', *Nature Reviews Molecular Cell Biology* **18**(10), 610–621.

Reynolds, P., Cooper, S., Lomax, M. & O'Neill, P. (2015), 'Disruption of PARP1 function inhibits base excision repair of a sub-set of DNA lesions.', *Nucleic acids research* **43**(8), 4028–4038.

Riccio, A. A., Cingolani, G. & Pascal, J. M. (2016), 'PARP-2 domain requirements for

DNA damage-dependent activation and localization to sites of DNA damage.', *Nucleic acids research* **44**(4), 1691–1702.

Ritter, H., Koch-Nolte, F., Marquez, V. E. & Schulz, G. E. (2003), 'Substrate binding and catalysis of ecto-ADP-ribosyltransferase 2.2 from rat.', *Biochemistry* **42**(34), 10155–10162.

Robinson, N., Ganesan, R., Hegedűs, C., Kovács, K., Kufer, T. A. & Virág, L. (2019), 'Programmed necrotic cell death of macrophages: Focus on pyroptosis, necroptosis, and parthanatos.', *Redox biology* **26**, 101239.

Robson, M., Im, S.-A., Senkus, E., Xu, B., Domchek, S. M., Masuda, N., Delaloge, S., Li, W., Tung, N., Armstrong, A., Wu, W., Goessl, C., Runswick, S. & Conte, P. (2017), 'Olaparib for Metastatic Breast Cancer in Patients with a Germline BRCA Mutation.', *The New England journal of medicine* **377**(17), 1700.

Robu, M., Shah, R. G., Petitclerc, N., Brind'Amour, J., Kandan-Kulangara, F. & Shah, G. M. (2013), 'Role of poly(ADP-ribose) polymerase-1 in the removal of UV-induced DNA lesions by nucleotide excision repair.', *Proceedings of the National Academy of Sciences of the United States of America* **110**(5), 1658–1663.

Robu, M., Shah, R. G., Purohit, N. K., Zhou, P., Naegeli, H. & Shah, G. M. (2017), 'Poly(ADP-ribose) polymerase 1 escorts XPC to UV-induced DNA lesions during nucleotide excision repair.', *Proceedings of the National Academy of Sciences of the United States of America* **114**(33), E6847–E6856.

Rodriguez-Vargas, J. M., Nguekeu-Zebaze, L. & Dantzer, F. (2019), 'PARP3 comes to light as a prime target in cancer therapy', *Cell cycle (Georgetown, Tex.)* .

Rolli, V., O'Farrell, M., Ménissier-de Murcia, J. & de Murcia, G. (1997), *Random Mutagenesis of the Poly(ADP-ribose) Polymerase Catalytic Domain Reveals Amino Acids Involved in Polymer Branching*, American Chemical Society.

Ronson, G. E., Piberger, A. L., Higgs, M. R., Olsen, A. L., Stewart, G. S., McHugh, P. J., Petermann, E. & Lakin, N. D. (2018), 'PARP1 and PARP2 stabilise replication forks at base excision repair intermediates through Fbh1-dependent Rad51 regulation.', *Nat Commun* **9**(1), 746–12.

Rosenthal, F., Feijs, K. L. H., Frugier, E., Bonalli, M., Forst, A. H., Imhof, R., Winkler, H. C., Fischer, D., Caflisch, A., Hassa, P. O., Lüscher, B. & Hottiger, M. O. (2013), 'Macrodomain-containing proteins are new mono-ADP-ribosylhydrolases.', *Nature structural & molecular biology* **20**(4), 502–507.

Rudolph, J., Mahadevan, J., Dyer, P. & Luger, K. (2018), 'Poly(ADP-ribose) polymerase 1 searches DNA via a 'monkey bar' mechanism.', *Elife* **7**, 1046.

Rudolph, J., Mahadevan, J. & Luger, K. (2020), 'Probing the Conformational Changes Associated with DNA-Binding to PARP1.', *Biochemistry* p. acs.biochem.0c00256.

Rudolph, J., Roberts, G., Muthurajan, U. M. & Luger, K. (2021), 'HPF1 and nucleosomes mediate a dramatic switch in activity of PARP1 from polymerase to hydrolase.', *Elife* **10**.

Ruf, A., de Murcia, G. & Schulz, G. E. (1998), 'Inhibitor and NAD+ Binding to Poly(ADP-ribose) Polymerase As Derived from Crystal Structures and Homology Modeling†,‡', *J. Mol. Biol.* .

Ruf, A., Mennissier de Murcia, J., de Murcia, G. & Schulz, G. E. (1996), 'Structure of the catalytic fragment of poly(AD-ribose) polymerase from chicken.', *Proc National Acad Sci* **93**(15), 7481–7485.

Rulten, S. L., Fisher, A. E. O., Robert, I., Zuma, M. C., Rouleau, M., Ju, L., Poirier, G., Reina-San-Martin, B. & Caldecott, K. W. (2011), 'PARP-3 and APLF function together to accelerate nonhomologous end-joining.', *Mol. Cell* **41**(1), 33–45.

Ruscetti, T., Lehnert, B. E., Halbrook, J., Le Trong, H., Hoekstra, M. F., Chen, D. J. & Peterson, S. R. (1998), 'Stimulation of the DNA-dependent protein kinase by poly(ADP-ribose) polymerase.', *J. Biol. Chem.* **273**(23), 14461–14467.

Schärer, O. D. (2013), 'Nucleotide excision repair in eukaryotes.', *Cold Spring Harbor perspectives in biology* **5**(10), a012609.

Schindelin, J., Arganda-Carreras, I., Frise, E., Kaynig, V., Longair, M., Pietzsch, T., Preibisch, S., Rueden, C., Saalfeld, S., Schmid, B., Tinevez, J.-Y., White, D. J., Hartenstein, V., Eliceiri, K., Tomancak, P. & Cardona, A. (2012), 'Fiji: an open-source platform for biological-image analysis.', *Nature methods* **9**(7), 676–682.

Schleicher, E. M., Galvan, A. M., Imamura-Kawasawa, Y., Moldovan, G.-L. & Nicolae, C. M. (2018), 'PARP10 promotes cellular proliferation and tumorigenesis by alleviating replication stress.', *Nucleic acids research* **46**(17), 8908–8916.

Schuller, M., Butler, R. E., Ariza, A., Tromans-Coia, C., Jankevicius, G., Claridge, T. D. W., Kendall, S. L., Goh, S., Stewart, G. R. & Ahel, I. (2021), 'Molecular basis for DarT ADP-ribosylation of a DNA base.', *Nature* pp. 1–6.

Shao, Z., Lee, B. J., Rouleau-Turcotte, É., Langelier, M.-F., Lin, X., Estes, V. M., Pascal, J. M. & Zha, S. (2020), 'Clinical PARP inhibitors do not abrogate PARP1 exchange at DNA damage sites in vivo.', *Nucleic acids research* **58**(17), 911–9709.

Sharifi, R., Morra, R., Appel, C. D., Tallis, M., Chioza, B., Jankevicius, G., Simpson, M. A., Matic, I., Ozkan, E., Golia, B., Schellenberg, M. J., Weston, R., Williams, J. G., Rossi, M. N., Galehdari, H., Krahn, J., Wan, A., Trembath, R. C., Crosby, A. H., Ahel, D., Hay, R., Ladurner, A. G., Timinszky, G., Williams, R. S. & Ahel, I. (2013), 'Deficiency of terminal ADP-ribose protein glycohydrolase TARG1/C6orf130 in neurodegenerative disease.', *EMBO J.* **32**(9), 1225–1237.

Shen, Y., Aoyagi-Scharber, M. & Wang, B. (2015), 'Trapping Poly(ADP-Ribose) Polymerase.', *The Journal of pharmacology and experimental therapeutics* **353**(3), 446–457.

Shiozaki, E. N., Gu, L., Yan, N. & Shi, Y. (2004), 'Structure of the BRCT repeats of BRCA1 bound to a BACH1 phosphopeptide: implications for signaling.', *Mol. Cell* **14**(3), 405–412.

Shirai, H., Poetsch, A. R., Gunji, A., Maeda, D., Fujimori, H., Fujihara, H., Yoshida, T., Ogino, H. & Masutani, M. (2013), 'PARG dysfunction enhances DNA double strand break formation in S-phase after alkylation DNA damage and augments different cell death pathways.', *Cell death & disease* **4**(6), e656–e656.

Simon, N. C., Aktories, K. & Barbieri, J. T. (2014), 'Novel bacterial ADP-ribosylating toxins: structure and function.', *Nature reviews. Microbiology* **12**(9), 599–611.

Simonet, N. G., Thackray, J. K., Vazquez, B. N., Ianni, A., Espinosa-Alcantud, M., Morales-Sanfrutos, J., Hurtado-Bagès, S., Sabidó, E., Buschbeck, M., Tischfield, J., De La Torre, C., Esteller, M., Braun, T., Olivella, M., Serrano, L. & Vaquero, A. (2020),

'SirT7 auto-ADP-ribosylation regulates glucose starvation response through mH2A1.', *Science advances* **6**(30), eaaz2590.

Slade, D. (2020), 'PARP and PARG inhibitors in cancer treatment.', *Genes Dev.* **34**(5-6), 360–394.

Slade, D., Dunstan, M. S., Barkauskaite, E., Weston, R., Lafite, P., Dixon, N., Ahel, M., Leys, D. & Ahel, I. (2011), 'The structure and catalytic mechanism of a poly(ADP-ribose) glycohydrolase.', *Nature* **477**(7366), 616–620.

Smeenk, G., Wiegant, W. W., Marteijn, J. A., Luijsterburg, M. S., Sroczynski, N., Costelloe, T., Romeijn, R. J., Pastink, A., Mailand, N., Vermeulen, W. & van Attikum, H. (2013), 'Poly(ADP-ribosyl)ation links the chromatin remodeler SMARCA5/SNF2H to RNF168-dependent DNA damage signaling.', *J Cell Sci* **126**(Pt 4), 889–903.

Smeenk, G., Wiegant, W. W., Vrolijk, H., Solari, A. P., Pastink, A. & van Attikum, H. (2010), 'The NuRD chromatin-remodeling complex regulates signaling and repair of DNA damage.', *The Journal of cell biology* **190**(5), 741–749.

Smith, R., Lebeaupin, T., Juhász, S., Chapuis, C., D'Augustin, O., Dutertre, S., Burkovics, P., Biertümpfel, C., Timinszky, G. & Huet, S. (2019), 'Poly(ADP-ribose)-dependent chromatin unfolding facilitates the association of DNA-binding proteins with DNA at sites of damage.', *Nucleic acids research* **47**(21), 11250–11267.

Smith, R., Sellou, H., Chapuis, C., Huet, S. & Timinszky, G. (2018), 'CHD3 and CHD4 recruitment and chromatin remodeling activity at DNA breaks is promoted by early poly(ADP-ribose)-dependent chromatin relaxation.', *Nucleic acids research* **46**(12), 6087–6098.

Southgate, H. E. D., Chen, L., Tweddle, D. A. & Curtin, N. J. (2020), 'ATR Inhibition Potentiates PARP Inhibitor Cytotoxicity in High Risk Neuroblastoma Cell Lines by Multiple Mechanisms.', *Cancers* **12**(5), 1095.

Spiegel, J. O., Van Houten, B. & Durrant, J. D. (2021), 'PARP1: Structural insights and pharmacological targets for inhibition.', *DNA repair* **103**, 103125.

Steffen, J. D., Brody, J. R., Armen, R. S. & Pascal, J. M. (2013), 'Structural Implications for Selective Targeting of PARPs.', *Frontiers in oncology* **3**, 301.

Steffen, J. D., McCauley, M. M. & Pascal, J. M. (2016), 'Fluorescent sensors of PARP-1 structural dynamics and allosteric regulation in response to DNA damage.', *Nucleic acids research* **44**(20), 9771–9783.

Steffen, J. D., Tholey, R. M., Langelier, M.-F., Planck, J. L., Schiewer, M. J., Lal, S., Bildzukewicz, N. A., Yeo, C. J., Knudsen, K. E., Brody, J. R. & Pascal, J. M. (2014), 'Targeting PARP-1 allosteric regulation offers therapeutic potential against cancer.', *Cancer research* **74**(1), 31–37.

Strickfaden, H., McDonald, D., Kruhlak, M. J., Haince, J.-F., Th'ng, J. P. H., Rouleau, M., Ishibashi, T., Corry, G. N., Ausio, J., Underhill, D. A., Poirier, G. G. & Hendzel, M. J. (2016), 'Poly(ADP-ribosyl)ation-dependent Transient Chromatin Decondensation and Histone Displacement following Laser Microirradiation.', *J. Biol. Chem.* **291**(4), 1789–1802.

Sugasawa, K. (2010), 'Regulation of damage recognition in mammalian global genomic nucleotide excision repair.', *Mutation research* **685**(1-2), 29–37.

Sugasawa, K., Ng, J. M., Masutani, C., Iwai, S., van der Spek, P. J., Eker, A. P., Hanaoka, F., Bootsma, D. & Hoeijmakers, J. H. (1998), 'Xeroderma pigmentosum group C protein complex is the initiator of global genome nucleotide excision repair.', *Mol. Cell* **2**(2), 223–232.

Sukhanova, M. V., Abrakhi, S., Joshi, V., Pastre, D., Kutuzov, M. M., Anarbaev, R. O., Curmi, P. A., Hamon, L. & Lavrik, O. I. (2016), 'Single molecule detection of PARP1 and PARP2 interaction with DNA strand breaks and their poly(ADP-ribosyl)ation using high-resolution AFM imaging.', *Nucleic acids research* **44**(6), e60–e60.

Sun, F.-H., Zhao, P., Zhang, N., Kong, L.-L., Wong, C. C. L. & Yun, C.-H. (2021), 'HPF1 remodels the active site of PARP1 to enable the serine ADP-ribosylation of histones.', *Nat Commun* **12**(1), 1028–10.

Sun, Y., McCorvie, T. J., Yates, L. A. & Zhang, X. (2020), 'Structural basis of homologous recombination.', *Cellular and molecular life sciences : CMLS* **77**(1), 3–18.

Suskiewicz, M. J., Zobel, F., Ogden, T. E. H., Fontana, P., Ariza, A., Yang, J.-C., Zhu, K., Bracken, L., Hawthorne, W. J., Ahel, D., Neuhaus, D. & Ahel, I. (2020), 'HPF1

completes the PARP active site for DNA damage-induced ADP-ribosylation.', *Nature* **579**(7800), 598–602.

Tallis, M., Morra, R., Barkauskaite, E. & Ahel, I. (2014), 'Poly(ADP-ribosyl)ation in regulation of chromatin structure and the DNA damage response.', *Chromosoma* **123**(1-2), 79–90.

Teloni, F. & Altmeyer, M. (2016), 'Readers of poly(ADP-ribose): designed to be fit for purpose.', *Nucleic acids research* **44**(3), 993–1006.

Timinszky, G., Till, S., Hassa, P. O., Hothorn, M., Kustatscher, G., Nijmeijer, B., Colombelli, J., Altmeyer, M., Stelzer, E. H. K., Scheffzek, K., Hottiger, M. O. & Ladurner, A. G. (2009), 'A macrodomain-containing histone rearranges chromatin upon sensing PARP1 activation.', *Nature structural & molecular biology* **16**(9), 923–929.

Tucker, J. A., Bennett, N., Brassington, C., Durant, S. T., Hassall, G., Holdgate, G., McAlister, M., Nissink, J. W. M., Truman, C. & Watson, M. (2012), 'Structures of the Human Poly (ADP-Ribose) Glycohydrolase Catalytic Domain Confirm Catalytic Mechanism and Explain Inhibition by ADP-HPD Derivatives', *PLOS ONE* **7**(12), e50889.

Verheugd, P., Forst, A. H., Milke, L., Herzog, N., Feijs, K. L. H., Kremmer, E., Kleine, H. & Lüscher, B. (2013), 'Regulation of NF-κB signalling by the mono-ADP-ribosyltransferase ARTD10.', *Nat Commun* **4**(1), 1683–11.

Volker, M., Moné, M. J., Karmakar, P., van Hoffen, A., Schul, W., Vermeulen, W., Hoeijmakers, J. H., van Driel, R., van Zeeland, A. A. & Mullenders, L. H. (2001), 'Sequential assembly of the nucleotide excision repair factors in vivo.', *Mol. Cell* **8**(1), 213–224.

Vyas, S., Matic, I., Uchima, L., Rood, J., Zaja, R., Hay, R. T., Ahel, I. & Chang, P. (2014), 'Family-wide analysis of poly(ADP-ribose) polymerase activity.', *Nat Commun* **5**(1), 4426.

Wahlberg, E., Karlberg, T., Kouznetsova, E., Markova, N., Macchiarulo, A., Thorsell, A.-G., Pol, E., Frostell, Å., Ekblad, T., Öncü, D., Kull, B., Robertson, G. M., Pellicciari, R., Schüler, H. & Weigelt, J. (2012), 'Family-wide chemical profiling and structural analysis of PARP and tankyrase inhibitors', *Nature Biotechnology* **30**(3), 283–288.

Wang, M., Wu, W., Wu, W., Rosidi, B., Zhang, L., Wang, H. & Iliakis, G. (2006), 'PARP-1 and Ku compete for repair of DNA double strand breaks by distinct NHEJ pathways.', *Nucleic acids research* **34**(21), 6170–6182.

Wang, Z., Michaud, G. A., Cheng, Z., Zhang, Y., Hinds, T. R., Fan, E., Cong, F. & Xu, W. (2012), 'Recognition of the iso-ADP-ribose moiety in poly(ADP-ribose) by WWE domains suggests a general mechanism for poly(ADP-ribosyl)ation-dependent ubiquitination.', *Genes Dev.* **26**(3), 235–240.

Wilson, V. G. (2017), 'Introduction to Sumoylation.', *Advances in experimental medicine and biology* **963**, 1–12.

Wu, S., Zhou, J., Zhang, K., Chen, H., Luo, M., Lu, Y., Sun, Y. & Chen, Y. (2020), 'Molecular Mechanisms of PALB2 Function and Its Role in Breast Cancer Management.', *Frontiers in oncology* **10**, 301.

Yang, c.-S., Jividen, K., Spencer, A., Dworak, N., Ni, L., Oostdyk, L. T., Chatterjee, M., Kusmider, B., Reon, B., Parlak, M., Gorbunova, V., Abbas, T., Jeffery, E., Sherman, N. E. & Paschal, B. M. (2017), 'Ubiquitin Modification by the E3 Ligase/ADP-Ribosyltransferase Dtx3L/Parp9', *Molecular Cell* **66**(4), 503–516.e5.

Yin, X., Liu, M., Tian, Y., Wang, J. & Xu, Y. (2017), 'Cryo-EM structure of human DNA-PK holoenzyme.', *Cell research* **27**(11), 1341–1350.

Zandarashvili, L., Langelier, M.-F., Velagapudi, U. K., Hancock, M. A., Steffen, J. D., Billur, R., Hannan, Z. M., Wicks, A. J., Krastev, D. B., Pettitt, S. J., Lord, C. J., Talele, T. T., Pascal, J. M. & Black, B. E. (2020), 'Structural basis for allosteric PARP-1 retention on DNA breaks.', *Science* **368**(6486), eaax6367.

Zaveri, A., Wang, R., Botella, L., Sharma, R., Zhu, L., Wallach, J. B., Song, N., Jansen, R. S., Rhee, K. Y., Ehrt, S. & Schnappinger, D. (2020), 'Depletion of the DarG antitoxin in Mycobacterium tuberculosis triggers the DNA-damage response and leads to cell death.', *Molecular microbiology* **73**(1282), mmi.14571.

Zhang, Y., Mao, D., Roswit, W. T., Jin, X., Patel, A. C., Patel, D. A., Agapov, E., Wang, Z., Tidwell, R. M., Atkinson, J. J., Huang, G., McCarthy, R., Yu, J., Yun, N. E., Paessler, S., Lawson, T. G., Omattage, N. S., Brett, T. J. & Holtzman, M. J.

(2015), 'PARP9-DTX3L ubiquitin ligase targets host histone H2BJ and viral 3C protease to enhance interferon signaling and control viral infection.', *Nature immunology* **16**(12), 1215–1227.

Zhao, B., Rothenberg, E., Ramsden, D. A. & Lieber, M. R. (2020), 'The molecular basis and disease relevance of non-homologous DNA end joining.', *Nature Reviews Molecular Cell Biology* **21**(12), 765–781.

Zweifel, M. E., Leahy, D. J. & Barrick, D. (2005), 'Structure and Notch receptor binding of the tandem WWE domain of Deltex.', *Structure (London, England : 1993)* **13**(11), 1599–1611.

Appendix

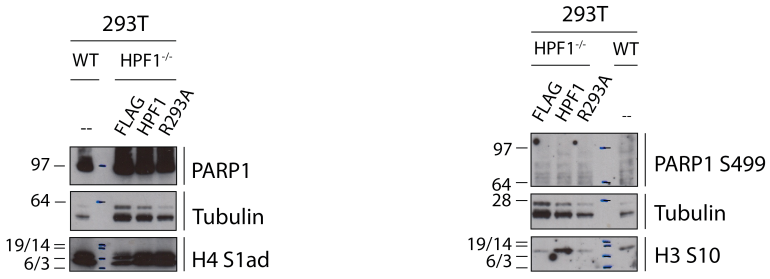


Figure A.1: Transient overexpression of FLAG-HPF1 R293A recovers histone H4 ADPr on S1, but not histone H3 ADPr on S10, indicating a separation of function in how HPF1 enables serine ADP-ribosylation of different substrates. The experiment was carried out once.

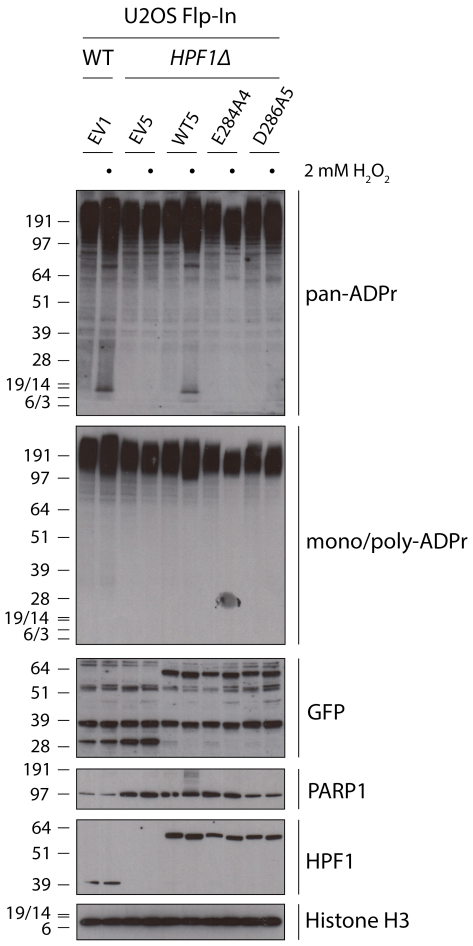


Figure A.2: Independent repeat of Figure 3.31a showing the reconstitution of cellular ADPr levels in U2OS Flp-In *HPF1*Δ cells complemented with different YFP-HPF1 variants. In contrast to Figure 3.31a, not degradation of endogenous HPF1 in U2OS Flp-In WT cells could be observed.

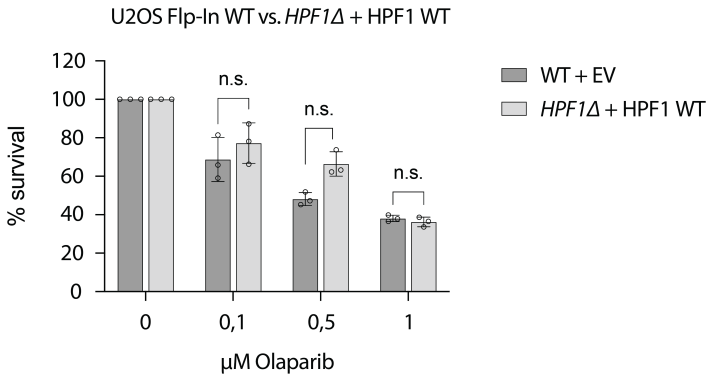


Figure A.3: Survival to Olaparib of U2OS Flp-In WT and U2OS Flp-In *HPF1*Δ WT5 cells. Survival of U2OS Flp-In WT cells to Olaparib was not included in the survival assay shown in Figure 3.32b, since the cell line formed much fewer colonies than any of the complemented U2OS Flp-In *HPF1*Δ clones under untreated conditions. However, comparison of the cell line's survival to that of U2OS Flp-In *HPF1*Δ complemented with FLAG-HPF1 WT (WT5) showed similar survival. Data are shown as mean ± SEM of three technical repeats

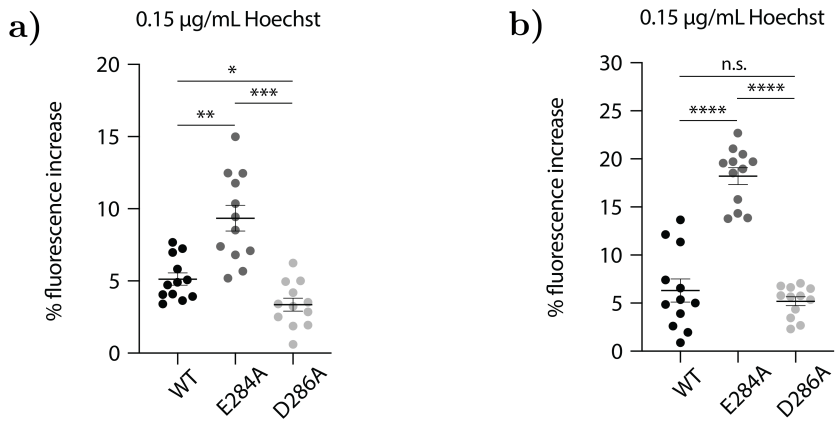


Figure A.4: Two independent repeats of the experiment shown in Figure 3.33b. **a)** While the difference between HPF1 WT and E284A is smaller in this repeat than the one from Figure 3.33b, a small but significant difference in the other direction can be observed between HPF1 WT and D286A (* = $p \leq 0.05$, ** = $p \leq 0.01$). **b)** In the second repeat again no difference in recruitment to sites of laser-induced damage can be observed between HPF1 WT and D286A. On the other hand, a stronger difference was observed between HPF1 WT and E284A than in the experiment in Figure 3.33b (n.s. = not significant, **** = $p \leq 0.0001$). Data points are shown as mean ± SEM from the analysis of 12 nuclei.